

FINAL REPORT TO THE PAUL G. ALLEN FAMILY FOUNDATION ON:

CULTIVATING SEAWEEDS TO MITIGATE OCEAN ACIDIFICATION AND GENERATE HABITAT, FERTILIZER, FOOD, AND FUEL

FOR ACTIVITIES PERFORMED MAY 22, 2015 – DECEMBER 15, 2019



TABLE OF CONTENTS

PROJECT REPORT	13
1. Site Selection	13
2. Permitting.....	14
3. Kelp Seed Propagation.....	16
4. Kelp Farm Development	17
5. Kelp Cultivation	20
6. Kelp Harvest.....	31
7. Chemical assessment of seaweed cultivation array.....	34
8. Biological assessment of seaweed cultivation array	50
9. Modeling the effect of seaweed on ocean acidification.....	57
10. Seaweed Site Evaluator Model.....	80
11. Engagement Activities, Communication Products, and Publicity	81
12. Leveraged Projects.....	83
CONCLUSION.....	84
APPENDIX A.....	88

PROJECT TEAM:

Betsy Peabody (co-lead) – Puget Sound Restoration Fund
Jonathan (Joth) Davis (co-lead) – Hood Canal Mariculture/Puget Sound Restoration Fund
Simone Alin – NOAA, Pacific Marine Environmental Laboratory
Nina Bednarsek – Southern California Coastal Water Research Project
Meg Chadsey – Washington Sea Grant
Richard Feely – NOAA, Pacific Marine Environmental Laboratory
Micah Horwith – Washington Department of Natural Resources (now WA. Department of Ecology)
Dale Kiefer – University of Southern California and System Science Applications, Inc.
John Mickett – University of Washington, Applied Physics Laboratory
Tom Mumford – Marine Agronomics
Jan Newton – University of Washington, Applied Physics Laboratory; Washington Ocean
Acidification Center
Zach Siegrist – System Science Applications, Inc.
Jodie Toft – Puget Sound Restoration Fund

Cover photos: Kelp array and monitoring moorings looking northeast (credit: John Mickett); (inset) sugar kelp cultivated at Hood Head demonstration site (credit: Joth Davis)

EXECUTIVE SUMMARY

In Puget Sound, where the effects of ocean acidification threaten important marine resources, there is a heightened need for investigating mitigation actions. Corrosive conditions associated with acidification are already impacting some calcifiers such as pteropods, crab, and foraminifera¹, and laboratory studies further suggest that oysters, crabs, krill, and salmon are also sensitive to the effects of acidification.² These species are not only important to the health of the marine ecosystem, but some are highly valued culturally and economically as well. According to the Governor's Office,³ in the coming decades, as seawater absorbs increasing amounts of dissolved carbon dioxide, conditions in Washington waters are expected to worsen, with changes occurring "more rapidly in Puget Sound waters than along our coast." In the face of these deteriorating conditions, we are confronted with many questions, one of which is: what can we do locally - in the water - to ameliorate the effects of acidification? The investigation described in this report sought an answer to that question.

In 2012, following several years of detrimental impacts to the Washington State shellfish industry resulting from acidification, former Governor Christine Gregoire convened the Washington State Blue Ribbon Panel on Ocean Acidification. The Panel recommended 42 actions in a 2012 report entitled "Ocean Acidification: From Knowledge to Action." A key early action recommended by the Panel was to develop phytoremediation techniques as a potential strategy for mitigating effects of acidification in local waterways. As a concept, phytoremediation is an approach to environmental remediation that uses plants or algae to take up and remove potentially harmful compounds from the environment to improve surrounding conditions. It is widely applied on land for a variety of purposes, including the reduction of carbon dioxide accumulation. For example, large-scale tree planting removes carbon dioxide from the atmosphere. In marine waters, seaweed cultivation could potentially provide a similar strategy for removing carbon dioxide from seawater to improve local conditions by offsetting the effects from ocean acidification.

Serendipitously, soon after the Panel's recommendations were finalized, the Paul G. Allen Family Foundation issued a research competition, the *Ocean Challenge*, calling on scientists from around the world to propose adaptation and mitigation strategies to address acidification. Seizing on this opportunity, a team from the Blue Ribbon Panel submitted a concept proposal and succeeded in securing support through the *Ocean Challenge*. Core members of the project team included Puget Sound Restoration Fund (PSRF), Hood Canal Mariculture (HCM), a Washington State based commercial shellfish farm, the U.S. National Oceanic and Atmospheric Administration (Pacific Marine Environmental Laboratory and Manchester Research Station), University of Washington Applied Physics Lab, Washington Sea Grant, System Science Applications, Washington Department of Natural Resources, and other advisory partners. During the team's negotiations with the Paul G. Allen Family Foundation on the final project, the U.S. Navy directed additional funding towards the project.

Thus began an investigation into whether seaweed cultivation could draw down CO₂ within the kelp farm and improve conditions for calcifying species. The field study was conducted at a five-acre seaweed and shellfish farm operated by HCM, located off Hood Head, just north of the Hood Canal Bridge in Jefferson County, Washington. After acquiring the necessary permits, propagating kelp seed, and outplanting sugar kelp (*Saccharina latissima*), the team measured the effect of kelp on several metrics of seawater chemistry and on a small suite of calcifying organisms within the kelp farm. Additionally, the team developed a computer model that simulates environmental variables and kelp growth, and then integrates the sampling data into an interface that graphically depicts the effect of kelp cultivation on seawater chemistry.

Combined funding from the Paul G. Allen Family Foundation and the U.S. Navy enabled two years of field investigation at the Hood Head demonstration site. Overall, the project was conducted 2015–2019 to test key early actions identified by the Washington State Blue Ribbon Panel on Ocean Acidification.

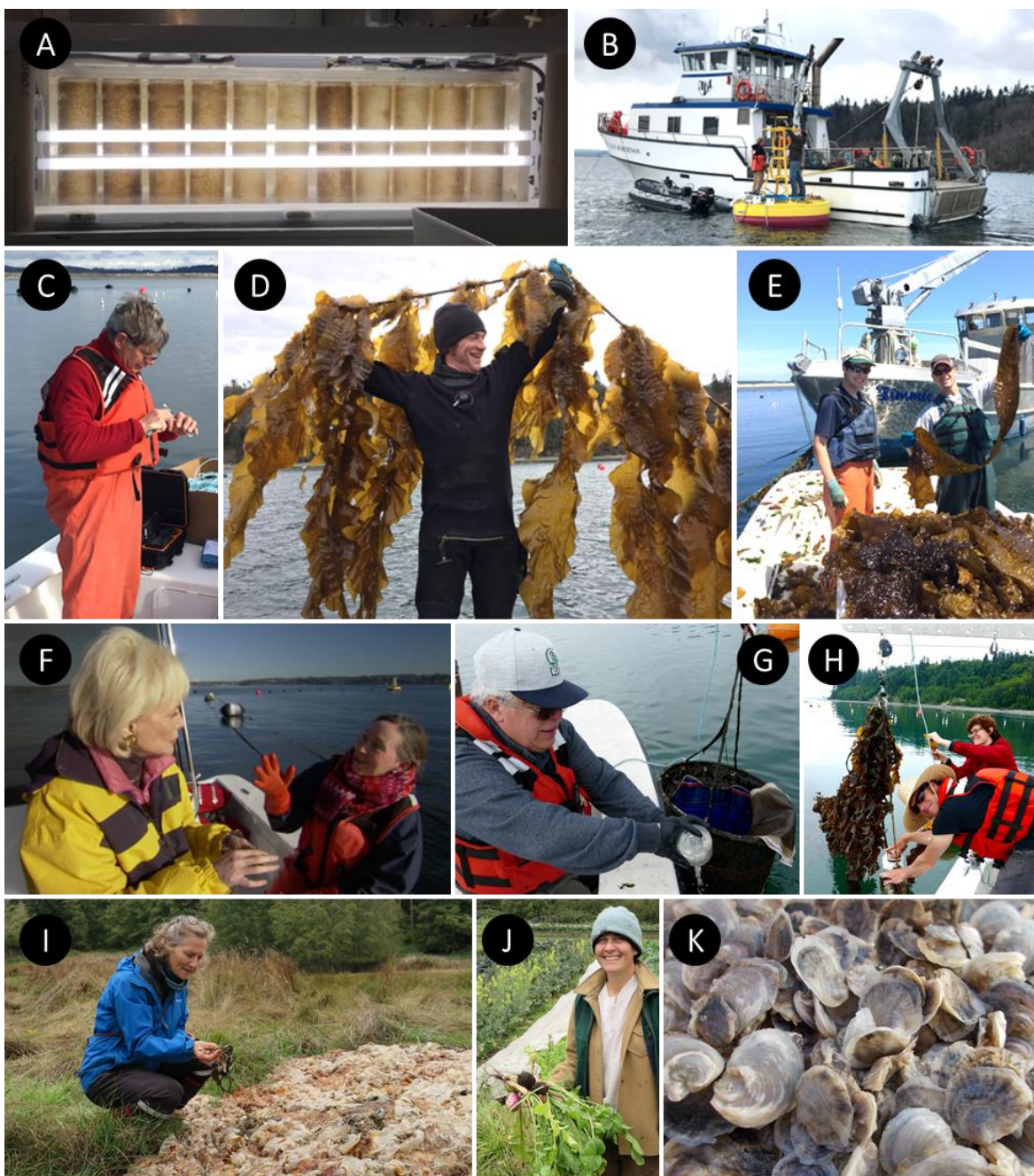


Figure ES1. Project Chronology in Photos. A. Seeded line cultured in kelp lab Dec '16; B. Scientific buoy installation Jan '17; C. Joth Davis preparing for sampling Feb '17; D. Brian Allen lifting seeded line to show abundant growth Mar '17; E. Ryan Cox and Josh Bouma harvesting kelp Aug '17; F. Lesley Stahl with CBS 60 Minutes interviewing Betsy Peabody Dec '17; G. Richard Feeley collecting water samples; H. Brian Allen and Nina Bednarsek collecting bioassays Jun '18; I. Meg Chadsey inspecting SkyRoot Farm's kelp pile (Oct '17), 4 months after delivery to the Whidbey Island farm; J. SkyRoot Farm owner Eli Wheat incorporated seaweed grown at Hood Head demonstration site into his pasture (pictured Oct '17); K. Olympia oysters, one of the species used in bioassays at Hood Head.

PROJECT OUTCOMES & KEY FINDINGS

The establishment of a kelp farm in Puget Sound enabled project scientists to measure, evaluate, and model the physical, chemical, and biological effects of cultivated kelp in a natural environment on a local scale. Project highlights are shown in Figure ES-1. The following is a summary of project outcomes and key findings.

PROJECT OUTCOMES

1. Permitted and installed a commercial-scale kelp farm in Hood Canal, Puget Sound.
2. Established a kelp propagation facility to produce sporophytes on twine for both sugar and bull kelp (*Nereocystis luetkeana*) for outplant at the Hood Head investigation site and for use in bull kelp enhancement trials.
3. Cultivated over 20 metric tons (live weight) of sugar kelp in 2017 and 2018.
4. Monitored standing biomass of sugar kelp over two growing seasons.
5. Conducted seasonal estimates of net production (as amount of carbon fixed per day in tissues) and estimated potential removal of carbon and nitrogen in standing biomass at harvest.
6. Transported sugar kelp grown at Hood Head to Whidbey Island and Quilcene organic farms with the intent of enriching soil in 2017 and 2018.
7. Assessed seawater chemistry conditions at Hood Head in 2017 and 2018 with seasonally-deployed instruments and small boat surveys.
8. Conducted bioassay experiments to evaluate both growth and shell dissolution of Pacific and Olympia oysters, mussels, pteropods, and other pelagic gastropods using mesocosms deployed inside, outside, and at the edge of the kelp farm.
9. Developed a new model to assess the effect of kelp on seawater chemistry that integrates kelp production metrics, seawater chemistry, and comprehensive water property observations to generate fine-scale, 3-dimensional simulations over time.
10. Initiated development of a companion model, called “Puget Sound SeaweedSiteEvaluator,” to assess the potential for candidate kelp farm sites to exert a positive effect on seawater chemistry locally.
11. Engaged the public through high-visibility media outlets and a suite of other outreach activities, generating widespread interest in kelp farming, the development of locally grown seaweed products, and the potential for cultivation of seaweed for restoration purposes. Engagement activities helped leverage well over \$500K in new funding to guide the development of seaweed farms and markets in Washington.
12. Conducted extensive laboratory experiments in 2019 to further assess biological effects in Pacific and Olympia oysters and the biological responses observed in the field.

KEY FINDINGS

Key Finding 1. Farmed kelp offers some potential for removing carbon and nitrogen from seawater at harvest.

The Hood Head investigation demonstrated the capacity to grow two species of kelp successfully in Puget Sound, and to produce a variety of kelp products of interest to local markets. Hood Head is an excellent

site for cultivating sugar and bull kelp, as evidenced by successful kelp cultivation in 2017 and 2018, and represents, at one hectare, the first commercial-scale demonstration of the viability of open-water kelp farming in Washington State. In 2017, 6,364 kilograms (kg) of sugar kelp (wet weight) was harvested and delivered to an organic farm on Whidbey Island, which resulted in the reconveyance of 130 kg of carbon (representing 20.36% of kelp biomass dry weight) and 18 kg of nitrogen (representing 2.85% of kelp biomass dry weight) from sea to land. Had we harvested kelp at peak biomass* in 2017, with 19,417 kg sugar kelp produced, we would have removed approximately 395 kg of carbon and 55 kg of nitrogen. In 2018, estimates for carbon and nitrogen contained in kelp blades grown at Hood Head averaged 21.54% for carbon and 1.99% for nitrogen. If kelp had been removed in 2018 at peak biomass, over 22,000 kg would have been removed from this small farm in Hood Canal, representing 474 kg of carbon and 44 kg of nitrogen. We note that this removal of carbon at peak biomass would be equivalent to the CO₂ emitted by 31–37% of **one** typical passenger vehicle in a year (per EPA web site). Similarly, the amount of nitrogen removed from the marine system at peak biomass would be equivalent to ten 43-lb bags of typical lawn fertilizer. Estimates for carbon removed from Puget Sound only reflect net production, that is, they do not reflect the significant amounts of carbon fixed by kelp and subsequently released back into the water during respiration, the dissolved organic material leaked from fronds, and eroded kelp blades. Nor do they reflect the amount of carbon used to produce the kelp. *Note: Kelp was not harvested at peak biomass in 2017 and 2018 in order to maintain kelp biomass at the project site throughout the monthly sampling cruises April-June.

Key Finding 2. The effect of kelp growth on seawater chemistry was not detected by state-of-the-art sensors and analyses used for assessment.

Differences in seawater chemistry inside compared to outside the kelp farm were below the range of detection by the best available oceanographic instruments and integrated biogeochemical analyses. We attribute this result, in part, to high average current velocities at the Hood Head site that resulted in low average residence time of seawater within the kelp farm. The kelp signal was also likely overwhelmed by the larger signal from springtime phytoplankton blooms in north Hood Canal during the same timeframe that kelp was growing.

Key Finding 3. Kelp may help reduce cumulative adverse effects on calcifying organisms growing within the kelp farm.

Results from a small field study indicated improved conditions for various calcifying organisms (including Pacific and Olympia oysters, bay mussels, and pteropods) that were deployed in mesocosms inside and outside the kelp farm. Inside the kelp farm, we found reduced shell dissolution in all of the examined species. Two oyster species (Pacific and Olympia oysters) showed faster growth inside the kelp farm. It is important to note that the improved benefits are likely due to multiple factors; i.e. more favorable carbonate chemistry conditions, food availability, and energy trade-offs.

We investigated possible drivers of the field results with subsequent laboratory experiments with juvenile Pacific and Olympia oysters. Our laboratory results demonstrated that both oyster species can grow faster and have significantly less dissolution under experimental conditions of higher pH mean and frequency of variability. The amplitude of pH variation in the treatment was 0.2, equating to around 0.7 aragonite saturation state. These results are consistent with the findings of previous investigations. The difference between the laboratory treatments was much greater than observed or predicted effects of the kelp farm. The laboratory results indicated that benefits to oysters are observed after two to four weeks of exposure in the experimental conditions, indicating the beneficial effect of cumulative exposure over time.

Our field results suggest that association with kelp may locally benefit shellfish and other calcifiers, while our laboratory results confirm that Pacific and Olympia oysters benefit from improved pH conditions.

Key Finding 4. Model simulations of the Hood Head kelp farm indicated slightly reduced concentrations of dissolved inorganic carbon.

A key component of this project was the creation of a kelp model to explore phytoremediation effects under varied carbonate chemistry and nutrient (nitrogen) conditions. Field data collected during the two-year field investigation (flow conditions, temperature, salinity, stratification, chemistry, biology, kelp production) were used to drive model calculations. In simulations of farm dynamics during the spring and summer of 2017 and 2018, the largest decreases in dissolved inorganic carbon (DIC) and increases in aragonite saturation were found in the middle of the farm during periods of weak currents.

Although changes to seawater were too small to be measured *in situ*, model simulations showed a very small increase in aragonite saturation (maximum increase was 0.025). Laboratory studies have not demonstrated that changes at this scale have biological effects.

Key Finding 5. The simulated effect of kelp farms on local acidification conditions depends on current velocity, kelp density, and farm size.

An important finding of this investigation was determining more precisely the conditions under which seaweed farming *could* significantly affect seawater chemistry locally. *The Hood Head seaweed farm did not measurably change the seawater chemistry at the site.* However, modeling results suggest that under the right conditions, including current speed, nutrient availability, kelp density, and farm size, seaweed farms could measurably affect seawater chemistry locally. As we populate our toolkit for adapting to or mitigating acidified conditions, it is critical to understand the limits, potential, and correct application of each tool. Our experience also underscores that assessment and modeling are important in designing future kelp farming operations, if one of the intended purposes is nutrient and carbon uptake in the environment.

Key Finding 6. There may be benefits to growing kelp in Puget Sound.

Based on our investigation at Hood Head, we demonstrated that seaweeds can be cultured in Puget Sound at a commercial scale, and that there is strong interest among growers and others for producing food-grade kelp. There is also growing interest among organic farmers in late season kelp biomass for soil enrichment. While limited, biological assessments suggest that growing seaweed in proximity to shellfish may make a positive difference for calcifiers, including oysters. To be clear, seaweed farming will not solve basin-wide acidification problems. Additional research needs to be conducted to determine whether seaweed farming in Puget Sound could improve local conditions at shellfish farms and provide an adaptation strategy that would assist in growing shellfish under increasingly acidifying conditions. (See Future Research section.)

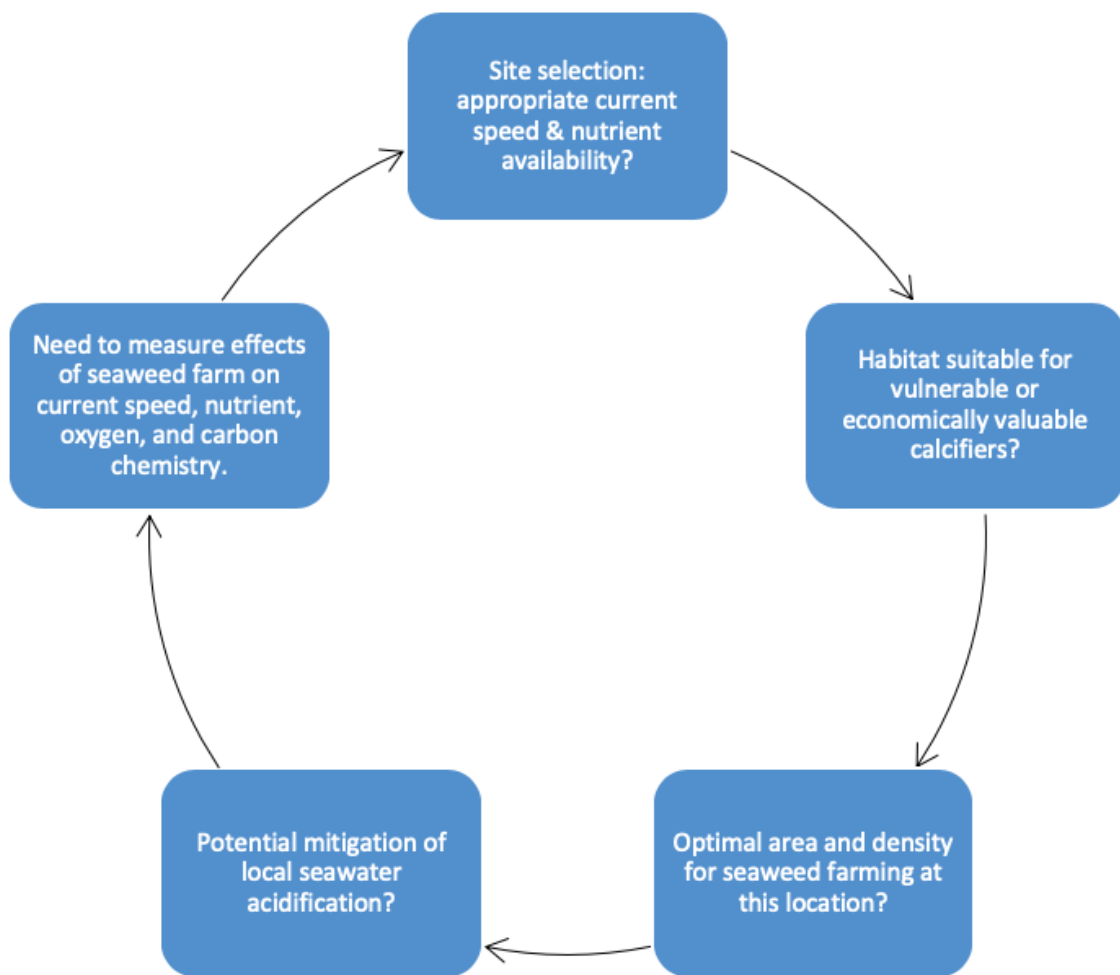
Key Finding 7. Model simulations suggest that kelp farms could be engineered and sited to achieve larger effects on local acidification conditions.

The model proved to be the best vehicle for defining the conditions under which seaweed cultivation could exert a detectable effect on seawater chemistry. In the model, inputs included the seeding density of the kelp, water temperature, solar irradiance, current velocity, ambient nutrient concentrations, and carbonate chemistry variables. The model simulation calculated growth, photosynthetic and respiration rates of the kelp, and the impacts of kelp growth and metabolism on nutrient, oxygen, and DIC

concentrations in seawater flowing through the farm. Modeling results indicate that the Hood Head site – an area of relatively fast-flowing currents with average speed of ~10-15 centimeters/second (cm/sec) at a depth of 3 meters – is a suboptimal location for siting kelp farms if a major objective is to locally reduce dissolved inorganic carbon and counter acidification. However, model simulations indicated that sites with lower current speeds, higher kelp density, and a larger growing area may have a greater local effect on seawater chemistry. In model simulations, the sweet spot that yielded the largest kelp effect occurred when flow rates were 10% of ambient flow observed at the Hood Head site. However, these optimal flow conditions may not exist in Puget Sound, and other complexities (e.g., respiration of detritus, self-shading, flow blocking) require further investigation. The sweet spot will also depend upon having sufficient light intensity and nutrient availability, which are both high at Hood Head. Sensitivity analyses with the model clearly showed that much larger decreases in DIC occurred in simulations where farm size or kelp density were significantly increased. For example, the maximum drawdown of DIC increased from approximately 1 $\mu\text{mol/kg}$ to 35 $\mu\text{mol/kg}$ when kelp densities increased tenfold. For context, the area at the Hood Head farm devoted to kelp cultivation was about 2.5 acres (1 hectare), which was composed of eighteen 500 foot growlines, with ten feet of separation between adjacent lines. The density of kelp grown at Hood Head in 2017 and 2018 was relatively low compared to commercial densities elsewhere in the world, especially in Asia. Therefore, increasing densities at kelp farms in Puget Sound should be feasible.

Key Finding 8. Outreach and publicity associated with this project stimulated new interest in kelp farming in Washington State.

The Hood Head investigation garnered significant publicity and attention. The coupling of multiple project elements – including kelp cultivation, chemical and biological assessment, and modeling – created a unique platform for building interest in actions that can potentially deliver multiple benefits. Seaweed farming workshops hosted by Washington Sea Grant and other partners in 2019 and 2020 attest to this growing interest.



Conceptual diagram of a decision tree for determining whether seaweed farming may have beneficial effects on seawater chemistry for calcifiers at a local scale.

FUTURE RESEARCH

Future Research 1. Adaptation and mitigation strategies associated with moving carbon from sea to land must consider a full carbon analysis.

In order to ensure that a mitigation or adaptation strategy has the intended net effect, all aspects of the carbon cycle manipulation must be considered, including the added emissions required to implement the effort (which were *not* taken into account for this project). Due to the complexity of such a holistic project, we encourage the research community to conduct studies that fully assess carbon cycle implications of, for instance, amending terrestrial soils with seaweeds. Monitoring the long-term fate of kelp-borne carbon and other nutrients in organic soils is an important aspect of a more comprehensive evaluation to assess whether net sequestration has occurred or decomposition of organic material has released carbon and nutrients to the atmosphere and water, respectively. In this example, a thorough accounting of this strategy would weigh the external carbon costs incurred through the harvest, delivery,

and utilization of kelp against the avoided costs associated with conventional agricultural fertilizers, soil management, and water use, all of which require substantial resource inputs. Unless sequestered, respiration and breakdown of the organic material will release carbon dioxide to the atmosphere.

Development of best practices for carbon cycle manipulations intended for adaptation and mitigation strategies is critically needed to ensure implementation will have the desired net effects on carbon (and nutrients). It is clear that the most effective way to address ocean acidification is through rapid decarbonization of society. Thus, we need to reduce CO₂ emissions as quickly as possible, while simultaneously exploring methods for protecting, restoring, or expanding ecosystems that may store large amounts of carbon, and pursuing other approaches that can help remove CO₂ from the atmosphere and seawater.

Future Research 2. Develop co-culture system designs for seaweed and shellfish to optimize culture conditions.

The work supported by this investigation did not assess or quantify the potential importance of cultivating seaweed and shellfish in close physical proximity. Though bioassays were deployed within the kelp farm to assess biological effects, shellfish were not actually cultivated simultaneously with seaweed at the Hood Head kelp farm. Future research should therefore assess the specific biogeochemical conditions in seawater associated with cultivating seaweeds and shellfish together in order to investigate potential beneficial effects.⁴ Because acidification problems are expected to worsen in the coming decades, it is important for seaweed and shellfish farmers to continue to work with researchers to design and assess co-culture systems. Understanding how to co-culture seaweed and shellfish in very close proximity could help the shellfish industry adapt to changing ocean conditions, similar to the way shellfish hatcheries have adapted to acidification by buffering incoming seawater to increase aragonite saturation and the viability of larval oysters.

SEAWEED FARMING AS A POTENTIAL TOOL TO AID IN GROWING MARINE FOODS UNDER CHANGING OCEAN CONDITIONS

Dissolved inorganic carbon (DIC) in the global ocean is increasing at an average rate of 1 μmol per kg seawater per year. Against this backdrop, the Hood Canal kelp farm may have reduced DIC by as much as 1 μmol/kg seawater within the center of the farm during the high growth period. This effect would fall below the limits of detection for laboratory and field methods, but would also counteract a small amount of anthropogenic acidification. Within the farm, preliminary results suggest that oysters and other calcifying species deployed in mesocosms showed less dissolution, and two oyster species also showed increased growth. This suggests that kelp may benefit CO₂-sensitive organisms and underscores the need for more research on the potential of co-culture. It should be added that no amount of kelp grown in Puget Sound will mitigate anthropogenic CO₂ inputs.

For kelp cultivation to potentially improve carbonate conditions for shellfish locally, farms would need to be designed, sited, and sized carefully to realize specific benefits. The model suggests that kelp farms could potentially have a larger effect under different conditions than those observed at Hood Head. In modeling scenarios, reducing current speed by 90% roughly quadruples the decrease of DIC. Increasing the farm size by ~600% or doubling kelp density roughly doubles the effect on DIC. Again, an important caveat here is that these model predictions do not include nonlinear relationships or thresholds such as flow disturbance/blocking by the kelp, nutrient limitation, and shelf-shading. **It is also important to note that even in these scenarios, the maximum predicted kelp farm effects on DIC are small compared to observed natural variation on daily and monthly time scales.** In sum, questions remain about how best to

deploy farming as a tool to combat the effects of acidification and whether the magnitude of farm effects on carbonate chemistry matters for calcifying organisms.

In places where shellfish are already affected by acidification, or where high seawater CO₂ is already occurring or predicted, seaweed farming could be further evaluated as a specific strategy for co-cultivating seaweed and shellfish. Further, if kelp farms can be sited to achieve multiple benefits, the production of marketable seaweed products can help fund these co-culture operations and provide a mechanism for removing some carbon and nitrogen from the marine system at harvest. As an added note, would-be seaweed farmers will need to carefully assess water quality conditions at proposed sites. Ultimately, it may be that seaweed is grown for different reasons in different places.

While assessing various adaptation and mitigation strategies, there are other ocean challenges that also need to be considered. In the years since the Blue Ribbon Panel Report was published, scientists have developed a better understanding of the threat posed by multiple stressors. The process of CO₂ absorption from the atmosphere and the resulting acidification is not the sole factor affecting ocean health. Warming seawater temperatures, hypoxia, harmful algal blooms, emerging diseases, and other changes have created compounding, increasingly stressful conditions for marine organisms beyond ocean acidification alone. This both heightens and complicates the search for remediative actions. In 2012, when the Blue Ribbon Panel identified phytoremediation strategies as a key early action, seaweeds were thought to be potential winners in the CO₂-rich oceans predicted for our future. After all, seaweeds absorb CO₂ from the surrounding seawater and convert it into biomass. Unfortunately, from our vantage point in 2019, we have since witnessed a 90% decline of kelp beds off the Northern California coast due in part to a marine heatwave that reduced kelp populations. We know now that kelps are vulnerable to warming seawater temperatures. It is also broadly understood that increasing atmospheric CO₂ concentrations are contributing to rapid warming of the ocean as well as the atmosphere.⁵ In consideration of all of these factors, seaweed-based phytoremediation strategies will need to be carefully assessed and properly sited when considering acidification. **However, kelp farms will NOT be able to effectively combat the triple threat of acidification, warming, and hypoxia.**

Moving forward, as coastal communities and governments continue to evaluate potential actions to remediate acidification and combat the effects of multiple stressors, we need to focus on actions that can make a difference for the organisms that live and grow in the marine environment. Evidence shows that some species are already negatively affected under increasingly corrosive seawater conditions. The scale and extent of the problem is not yet known, since biological monitoring in the field has been limited. Additionally, corrosivity will increase, heightening the impetus to act now to investigate potential mitigation actions. For shellfish production, this likely means that growing oysters and other shellfish amid changing ocean conditions is going to be increasingly challenging as impacts from acidification worsen, particularly as the shell-building process itself pushes the system toward higher carbon dioxide levels in the immediate environment of the calcifying shellfish.

While kelp cultivation does not pose a fix for acidification or the acceleration of its effects via carbon and nutrient pollution from watersheds, our findings show that kelp farming may produce benefits in the marine environment within the farm. Additionally, kelp farming can help showcase Puget Sound as a living system that produces marine products, which could help motivate and sustain clean water efforts moving forward. We have shown in our study that under the right conditions kelp farming may offer promise for co-culturing sensitive marine organisms. Future research can help refine the uses of this tool.

Finally, while Washington State is particularly susceptible to acidification impacts, due to a unique combination of oceanographic and climate factors, coupled with high freshwater inputs from rain and

snowmelt, we are also equipped with a strong social and cultural legacy in which marine resources are highly valued. Our region is also a known incubator for innovative public/private partnerships that advance cutting-edge, forward-thinking solutions to large-scale collective challenges. Ocean acidification is one of the major challenges of our day, demanding urgent and collective solutions. It is a testament to both the Paul G. Allen Family Foundation and the U.S. Navy that they invested generously in scoping out early-stage potential in-water solutions.

FOOTNOTES

- 1 Bednaršek, N., R.A. Feely, M.W. Beck, S.R. Alin, S.A. Siedlecki, P. Calosi, E.L. Norton, C. Saenger, J. Štrus, D. Greeley, N.P. Nezlin, and J.I. Spicer (2020): Exoskeleton dissolution with mechanoreceptor damage in larval Dungeness crab related to severity of present-day ocean acidification vertical gradients. *Sci. Total Environ.*, doi: 10.1016/j.scitotenv.2020.136610.

Bednaršek, N., R.A. Feely, N. Tolimieri, A.J. Hermann, S.A. Siedlecki, G.G. Waldbusser, P. McElhany, S.R. Alin, T. Klinger, B. Moore-Maley, and H.O. Pörtner (2017): Exposure history determines pteropod vulnerability to ocean acidification along the US West Coast. *Sci. Rep.*, 7, 4526, doi: 10.1038/s41598-017-03934-z.

Osborne, E.B., R.C. Thunell, N. Gruber, R.A. Feely, and C.R. Benitez-Nelson (2019): Decadal variability in twentieth-century ocean acidification in the California Current Ecosystem. *Nature Geosci.*, doi: 10.1038/s41561-019-0499-z.
- 2 Barton, A., B. Hales, G. Waldbusser, C. Langdon, and R.A. Feely (2012): The Pacific oyster, *Crassostrea gigas*, shows negative correlation to naturally elevated carbon dioxide levels: Implications for near-term ocean acidification impacts. *Limnol. Oceanogr.*, 57, 698–710, doi: 10.4319/lo.2012.57.3.0698.

Barton, A., G.G. Waldbusser, R.A. Feely, S.B. Weisberg, J.A. Newton, B. Hales, S. Cudd, B. Eudeline, C.J. Langdon, I. Jefferds, T. King, A. Suhrbier, and K. McLaughlin (2015): Impacts of coastal acidification on the Pacific Northwest shellfish industry and adaptation strategies implemented in response. *Oceanography*, 28(2), 146–159, doi: 10.5670/oceanog.2015.38.

McLaskey, A. K., Keister, J. E., McElhany, P., Olson, M. B., Busch, D. S., Maher, M., & Winans, A. K. (2016). Development of *Euphausia pacifica* (krill) larvae is impaired under pCO₂ levels currently observed in the Northeast Pacific. *Marine Ecology Progress Series*, 555, 65-78. doi: 10.3354/meps11839.

Miller, J. J., Maher, M., Bohaboy, E., Friedman, C. S., & McElhany, P. (2016). Exposure to low pH reduces survival and delays development in early life stages of Dungeness crab (*Cancer magister*). *Marine Biology*, 163(5), 118. doi: 10.1007/s00227-016-2883-1.

Trigg, S. A., McElhany, P., Maher, M., Perez, D., Busch, D. S., & Nichols, K. M. (2019). Uncovering mechanisms of global ocean change effects on the Dungeness crab (*Cancer magister*) through metabolomics analysis. *Scientific Reports*, 9(1), 10717. doi: 10.1038/s41598-019-46947-6.

Waldbusser, G. G., Hales, B., Langdon, C. J., Haley, B. A., Schrader, P., Brunner, E. L., Hutchinson, G. (2015). Ocean acidification has multiple modes of action on bivalve larvae. *PLoS ONE*, 10(6), e0128376. doi: 10.1371/journal.pone.0128376.

Williams, C. R., Dittman, A. H., McElhany, P., Busch, D. S., Maher, M. T., Bammler, T. K., Gallagher, E. P. (2019). Elevated CO₂ impairs olfactory-mediated neural and behavioral responses and gene expression in ocean-phase coho salmon (*Oncorhynchus kisutch*). *Global Change Biology*, 25(3), 963-977. doi: 10.1111/gcb.

- 3 Office of the Governor: Final Policy Brief Changing Ocean Conditions. September 2019.
www.governor.wa.gov.
 - 4 Fernández, P.A., P.P. Leal and Henríquez, L.A. (2019). Co-culture in marine farms: macroalgae can act as chemical refuge for shell-forming molluscs under an ocean acidification scenario, *Phycologia*, 58:5, 542-551. doi: 10.1080/00318884.2019.1628576
 - 5 Durack, P.J., P.J. Gleckler, S.G. Purkey, G.C. Johnson, and J.M. Lyman. (2018). Ocean warming: From the surface to the deep in observations and models. *Oceanography*, 31(2), 41–51, doi: 10.5670/oceanog.2018.227. Available online: <https://tos.org/oceanography/article/ocean-warming-from-the-surface-to-the-deep-in-observations-and-models>
- Jackson, J.M., G.C. Johnson, H.V. Dosser, and T. Ross (2018): Warming from recent marine heat wave lingers deep in British Columbia fjord. *Geophys. Res. Lett.*, 45(18), 9757–9764, doi: 10.1029/2018GL078971. Available online: <https://agupubs.onlinelibrary.wiley.com/doi/abs/10.1029/2018GL078971>

PROJECT REPORT

Following is a detailed summary of all project components funded by a \$1.5M grant from the Paul G. Allen Family Foundation, commencing May 22, 2015 and continuing through December 15, 2019.

The additional \$1M in funding received from the U.S. Navy supported kelp cultivation, scientific assessment, and modeling activities as well as a 3-year lab study being conducted at NOAA's Manchester Research Station 2018-2021 that further examines the effect of kelp growth on carbonate chemistry. The ocean acidification (OA) kelp lab study, which is not included in this report, is designed to augment full-scale field investigations conducted in 2017 and 2018.

1. Site Selection

Authors: Joth Davis, Betsy Peabody

The marine waters of Hood Canal just south of Hood Head in Jefferson County, Washington (Figure 1A and B) were selected as the project site based on two main factors. First, Dr. Joth Davis, one of the Co-PIs on this project, co-founded a sea farm at Hood Head operating on a fully permitted 5-acre DNR lease site,

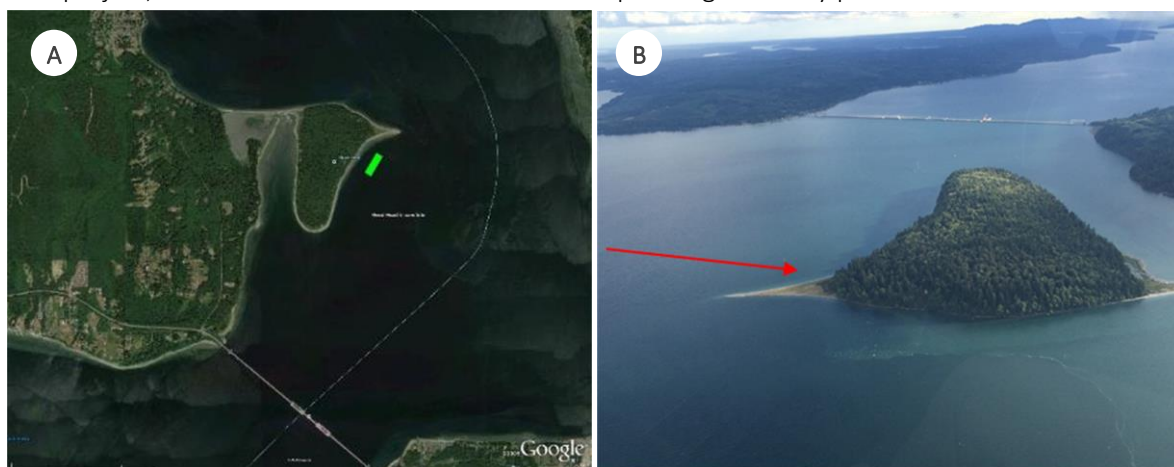


Figure 1. A - Google image showing 5-acre DNR lease (green rectangle) depicted near Hood Head in North Hood Canal, WA. Hood Canal Bridge is in foreground; B - Hood Canal (Hood Head) seaweed cultivation site looking south. DNR lease site is depicted by arrow.

which had been used to support shellfish aquaculture and research in the past. Thus the site was already permitted for shellfish production, which provided some degree of confidence that the project team could successfully obtain permits for seaweed cultivation as well. Second, the lease site is well mixed with ample nitrogen and other nutrients to support commercial-scale seaweed production. This feature was readily demonstrated at the site, where native sugar kelp (*Saccharina latissima*) grows abundantly via natural recruitment on various buoy lines already in place on the farm (Figure 2).

To further examine Hood Head as a potential investigation site, the project team conducted preliminary assessments of the site in summer 2015. Comprehensive drogue studies were conducted on July 17th and August 21st that enabled a good assessment of primary current directional vectors and tidal velocities through the site during different tidal states. This information was critical to obtain and helped inform the NOAA Pacific Marine Environmental Laboratory (PMEL) and University of Washington Applied Physics Lab (UW-APL) assessment team and modeling group with data necessary to help identify the positions to deploy instrumentation on site in the coming months.

Briefly, a GPS was used from a boat to track drogue buoys after release as they traversed the surface

waters intended for seaweed cultivation within the footprint of the study site. Multiple releases were accomplished over a series of incoming and outgoing tides that enabled a good assessment of tidal current direction and velocity as a function of both tidal cycle and amplitude. Results of the drogue studies, including calculations of surface current direction and velocity at different stages of both incoming and outgoing tides over multiple tidal cycles, are detailed in Appendix A.

The results indicated that for much of the duration of outgoing (northerly running) tides, tidal currents *are approximately parallel to the long axis of the cultivation site*. During incoming tides, currents flowing through the cultivation site appear more variable, with tidal flows running in both northerly and southerly directions at different stages of the tide due to the presence of a gyre that becomes established in this part of Hood Canal.

During the time that the gyre impacts seawater on incoming tides, tidal currents (direction and velocity) are variable as they pass through the cultivation site. In summary, data buoys set just upstream and downstream of the 1- hectare seaweed array would enable data to be taken during most outgoing (northerly running) tides and during parts of incoming tides when gyre effects were minimized. In either case, it would be necessary to have reliable and continuous measurements of current direction and velocity within the footprint of the cultivation array to interpret upstream and downstream data taken by instrumentation on the two data buoys planned for deployment.

On February 17, 2016, PSRF met with the assessment and modeling teams to review the Preliminary Assessment Report. Participants from the Assessment Team included Dr. Richard Feely, Dr. Jan Newton, Dr. Simone Alin, Dr. John Mickett and Dr. Nina Bednarsek; Modeling Team participants included Jack Rensel, Dr. Dale Kiefer and Zach Siegrist. Betsy Peabody and Joth Davis (PSRF) moderated the meeting. Note that Jack Rensel (System Science Applications) conducted the preliminary site assessment and Dale Kiefer (System Science Applications), an expert in the field of dynamic flow modeling associated with aquaculture projects and other marine operations, led all other modeling tasks for the project.

2. Permitting

Authors: Joth Davis, Betsy Peabody

A precondition of the funding was successfully obtaining regulatory authorization for developing a combined shellfish and seaweed farm on the 5-acre lease site at Hood Head. PSRF with Hood Canal Mariculture (HCM) obtained the necessary permits. In addition, permits were obtained for the temporary installation of two moored buoys holding instrument arrays. These buoys were positioned just south and north of the kelp cultivation area and within the footprint of the DNR lease. Permits included:

- USACE Individual Permit (NWS-2008-502); Date signed: March 1, 2016
- NMFS concurrence that the proposed action is not likely to adversely affect the subject listed species or their designated critical habitats (NMFS 2015_12-9_Final_HoodCanal_Shellfish_WCR-2015-3713); Date signed: December 9, 2015.



Figure 2. Joth Davis with wild sugar kelp growing on buoy lines at the Hood Head cultivation site in April 2016.

- USFWS concurrence with the USACE's determination that the proposed action "may affect, but is not likely to adversely affect" federally listed species (USFWS 01EWF00-2016-I-0147) with a conservation recommendation to report any fish, birds, or mammals found entangled in nets or shellfish gear; Date signed: January 15, 2016
- DNR 20-B12535 - updated lease for HCM's 5-acre site; Date signed: March 4, 2016
- Ecology-Coastal Zone Consistency for Corps Reference No. NWS-2008-502; Date signed: January 5, 2016
- Jefferson County cam15-001 - determination that no shoreline permit is required for the seaweed farm infrastructure since the project falls under the definition of "existing aquaculture."; Date signed: December 1, 2015
- Jefferson County, SDP16-00020 CUP Permit - Conditional Use permit for installing two oceanographic buoys to support Ocean Acidification Research within a Washington Department of Natural Resources (WDNR) Aquatic Lands Oyster Aquaculture Lease Agreement Area, located just east of Hoods Head; Date signed: August 25, 2016

The site developed for this investigation was the first sea farm permitted for experimental seaweed aquaculture in Washington State since the 1980s. While seaweed farms have multiplied in Alaska and New England, due perhaps to the potential multiple benefits that can be gained from seaweed farming, permitting for mariculture activities in Region 10 of the US Army Corps of Engineers (USACE) remains complicated. Mariculture activities (aquaculture for other than shellfish) require an Individual Permit (IP). As a new permit, this automatically triggers public notice requirements, since there is currently no programmatic or streamlined permit specifically designed for seaweed cultivation. This may create a significant barrier to entry for operators who wish either to add seaweed to an existing shellfish operation, or to create a new mariculture operation that includes multiple species, including seaweeds. In the case of an existing shellfish operation operating under a Nationwide Permit 48 (NWP-48; issued by the USACE specifically for shellfish aquaculture), the grower will need to overlay an IP authorizing seaweed on the same footprint having a pre-existing NWP-48. In the case of HCM, the IP authorized both activities, though later analysis suggested this approach was unwarranted as the original NWP had remained in effect. Application for an IP for a new mariculture activity (e.g., seaweed culture), however, does have the potential to expose an existing operation to new public comment.

Because issuance of an IP for combined seaweed and shellfish culture would be conducted on a site within the Usual and Accustomed Fishing Areas (U&AFA) used by Washington State Treaty Tribes, as affirmed by the Boldt (1974) and Rafeedie (1995) court decisions, it was important for PSRF and HCM to reach out to the affected Tribes to communicate about the proposed plans. This is the most important first step all prospective seaweed farmers should take before the Joint Aquatic Resources Permit Application (JARPA) is filed with the appropriate State and Federal agencies. In the case of this permit application, PSRF made extensive efforts to contact the four affected Tribes that used the Hood Head site as a U&AFA - the Port Gamble S'Klallam Tribe, Suquamish Tribe, Jamestown S'Klallam Tribe and Skokomish Tribe to apprise them of the project before submitting the USACE application on behalf of HCM for a new permit to cultivate kelp together with shellfish at the Hood Head site.

Through email exchanges, phone conversations, and face-to-face meetings with various tribes, we were able to describe the project, answer questions, allay concerns, and build enthusiasm for the project. Both the Suquamish Tribe and the Port Gamble S'Klallam Tribe expressed support. The Suquamish Tribe agreed to inform their fishers of the structure and location to avoid tangling gill nets. They also agreed not to contest the application, since the Hood Head farm was already permitted as an existing shellfish aquaculture site, operating with an NWP even though the waters off Hood Head are used as an important

salmon fishing location for the Tribe. The Port Gamble S’Klallam expressed support for the project and offered to assist with monitoring the habitat value of the kelp array. Additional tribal notifications were sent to the Skokomish Tribe and the Jamestown S’Klallam Tribe in the form of a cover letter describing the project and a copy of the application.

During the Army Corps’ 30-day public notice period, which closed November 12, 2015, the following Tribes submitted comments indicating that they had no objections: Suquamish, Port Gamble S’Klallam, Nisqually, and Squaxin Island Tribes. The Skokomish Tribe was among three groups that had questions, concerns, and/or objections. As a matter of policy, the Skokomish Tribe automatically objects to all new construction projects in Hood Canal, to go on record as a concerned party and ensure that the project applicant meets with the Tribe, and that treaty rights are not impacted by the proposed activity. Once the Skokomish Tribe understood that no new construction would occur outside of a previously permitted area, long associated with shellfish aquaculture, and importantly that shellfish aquaculture would continue at the site as a permitted activity regardless of whether the Army Corps issued a new permit to include seaweed cultivation, they had no further concerns. The Skokomish Tribe contacted the Corps in February 2016 to formally withdraw their objection. This enabled the Corps to issue the final permit March 1, 2016.

To address questions and concerns raised by two non-governmental organizations (NGOs) - the Hood Canal Environmental Council and the West Sound Conservation Council - PSRF met with the boards of these organizations in Fall 2015 to further describe the project and to establish ongoing communication channels.

As mentioned above, the project was inaccurately described by the Army Corps in their public notice, thus miscommunicating the nature of the project as “new construction.” This created additional permitting hurdles and fanned local, anti-aquaculture flames. However, the public notice also precipitated some good discussions with Tribes and community groups and gave us a chance to describe the purpose of the investigation in greater detail, elevate the project’s visibility, and elicit interest from entities that might not otherwise have been engaged.

3. Kelp Seed Propagation

Authors: Betsy Peabody, Joth Davis

In Fall 2015, a seaweed propagation facility was completed and housed (Figure 3) at the Kenneth K. Chew Center for Research and Restoration at NOAA’s Manchester Research Station in Manchester, Washington. The facility, which produced seeded lines of sugar kelp sporophytes for outplant at the Hood Head site to support the 2017 and 2018 field investigation, was composed of a 20’ long insulated, stainless steel-lined container equipped with a refrigeration unit. The interior of the facility was refitted as a small laboratory supplied with running seawater, filtration and UV sterilization equipment and tanks to store chilled and treated seawater. The heart of the facility was comprised of five specialized polycarbonate tanks supplied with fluorescent lighting designed to incubate spools of twine seeded with newly settled sporophytes under essentially sterile conditions.

Each of the five tanks accommodated 10 spools of seeded twine (250’) with sufficient capacity to supply the cultivation site with the necessary amount of plants for



Figure 3. Interior of seaweed cultivation facility.

full-blown cultivation. The cultivation facility was fully tested for its capacity to produce seeded twine in late 2015 and early 2016 and was used to support full-blown seed on twine production in Fall 2016, Fall 2017 and Winter 2018. In 2019, the refrigerated container used to support this project was decommissioned and replaced with a larger kelp lab facility established at NOAA's Manchester Research Station. The new kelp lab facility will hopefully assist in supporting sugar kelp production for new seaweed farms as well as bull kelp propagation for restoration.

4. Kelp Farm Development

Authors: Joth Davis, Betsy Peabody

In 2016, a 1-hectare (2.5-acre) culture system was designed and installed at Hood Head within the 5-acre DNR lease. As part of the design process, engineering studies were conducted to guide decisions regarding the upgrading of existing moorings at the HCM site on Hood Canal. Based on current velocity and direction data and anticipated loading due to seaweeds growing on culture lines, HCM embarked on a major mooring upgrade and construction of the seaweed cultivation lattice beginning in September 2016. The following upgrades to the culture system were accomplished.

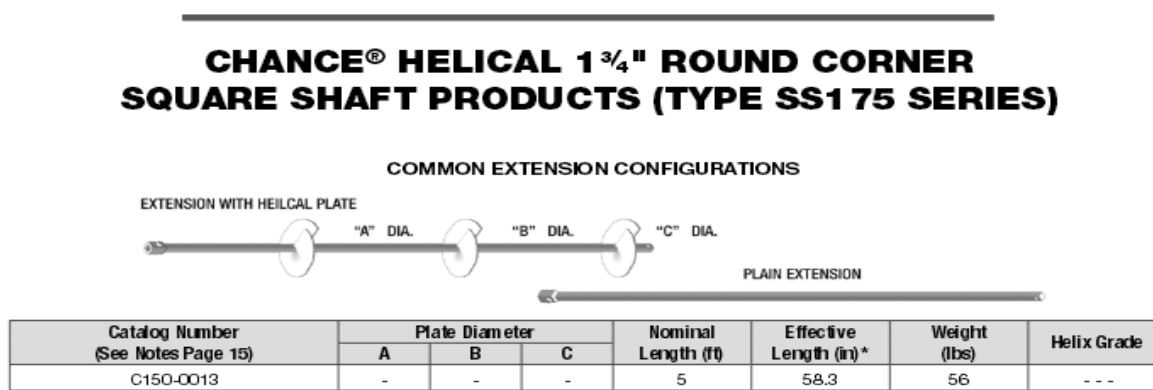


Figure 4. Description of Helix™ anchors used for Hood Head mooring upgrades

Helix™ anchors (using both Helix™ SS125 and SS175's) were upgraded in September and early October 2016 to include an added 5' termination section to existing SS125 anchors (shaft diameter 1.25") and/or replacement with a larger diameter Helix mooring (1.75" shaft diameter) (Figure 4). All Helix™ anchors were embedded in the substrate to a depth of approximately 10' using a 5' plain extension (see diagram below for SS175 Helix™ mooring). There are three sets of Helix™ anchors - each set consists of up to 12 anchors spaced at 20' intervals across the south, middle and north perimeters of the 5-acre lease. Holding power is reported to be significant but specific holding in force units is difficult to estimate because it varies with substrate, scope, current, loads and other factors.

Each mooring supporting the seaweed lattice consists of a Helix™ anchor connected to a 20' long section of 3/4" long-link galvanized chain connected to a section of 1.5" diameter 8-braid line (Blue Poly Steel™; BPS), using at both connection points heavy-duty gusseted thimbles and 1.25" galvanized shackles. Shackles were all seized with wire or cable ties. The length of BPS is different at most connections to reflect the desire to maintain a 2:1 scope at each anchoring point, at the terminus of the BPS line. Each anchor at the terminal end of the 8-braid line has a tether section consisting of 1" diameter 3-strand Poly-Dacron of variable length to enable a properly configured connection to the kelp lattice itself (Figure 5). Connections to the BPS were made with galvanized thimbles and 1.25" shackles. The tethers terminate on the perimeter line of the kelp lattice at galvanized (3/4") rings (lines were tied into the lattice and supplied chafing gear to enable adjustment of the tension of the overall system). The lattice is therefore

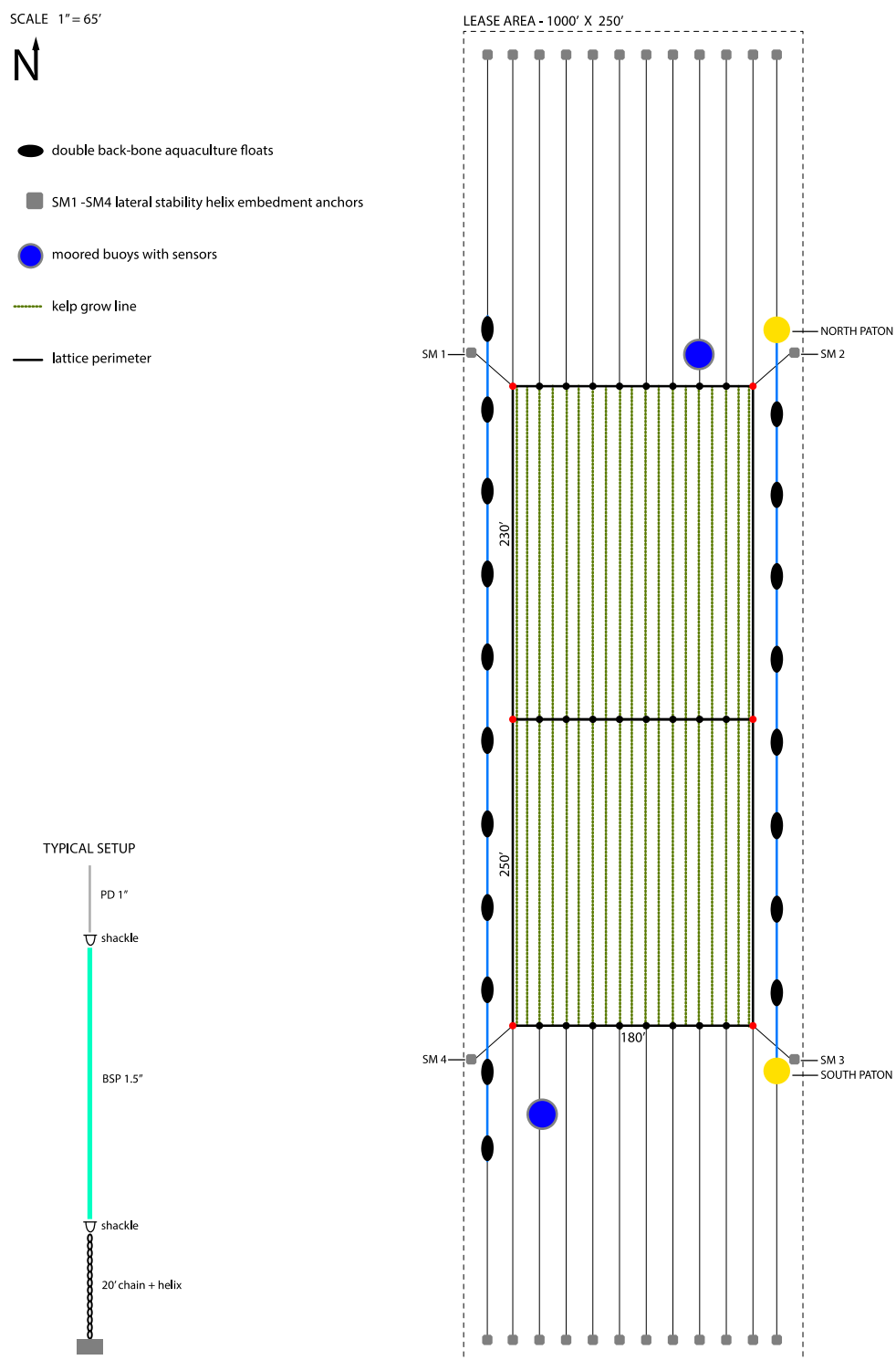


Figure 5. Overhead view of cultivation site (to scale). Position of UW-APL sensor buoys are depicted by black circles on SW and NE sides of seaweed lattice (inner rectangle). Note that only 10 cultivation lines are depicted – an additional 9 grow lines are positioned between the moorings and within the overall seaweed lattice for a total of 19 grow lines. On the perimeter are 2 shellfish grow lines, depicted by black oblong buoys. The typical mooring setup (Helix™ anchor, chain and mooring lines to surface buoys) is also described.

supported by thirty-four separate mooring lines - ten to the north and south of the lattice, respectively and ten in the middle, plus an additional 4 (10' SS175 Helix™) moorings, which serve as additional stabilization points for the kelp lattice (labeled in Figure 5 as SM1-SM4). The lateral moorings were placed to supply additional tension at all tidal elevations. All moorings were supplied with tensioning lines that varied in length according to depth to assure that the lattice was supported evenly. The westernmost positions are the shallowest, with depth increasing in an easterly direction. The seaweed lattice itself consists of a pair of 3-strand BSP rope rectangles (250' x 180' on the south end and 250' x 180' on the north end) shackled together and moored on the midline set of 12 anchors (Helix™ moorings with 10' 3/4" long link chain and 8-braid BSP line to the surface). The perimeter lines themselves consist of 1.12" diameter 3-strand BSP line with connections at the corners consisting of galvanized gusseted thimbles and 1.5" shackles on all connections (see Figure 5 for clarification of setup). Spaced at 10' intervals within the lattice area are 19 cultivation lines, each line consisting of 7/16" diameter Poly-Dacron line. The lattice itself is suspended by Polyform™ buoys, positioned above each mooring connection (30 buoys total) (Figure 5). The weight of the termination tackle maintains the system at the approximate prescribed depth of 3m though individual stabilizing droppers (consisting of a 3m long section of PVC pipe supported at the surface by a Spongex™ buoy and a 10 lb. weight below the grow line) were added at approximate 100' intervals along each of the grow lines to maintain the lines at the prescribed depth. The culture system was completed on December 9th, 2016 and seeded twine with attached sporophytes deployed a few days later. Figure 6 provides a rendering of the system from an underwater perspective.

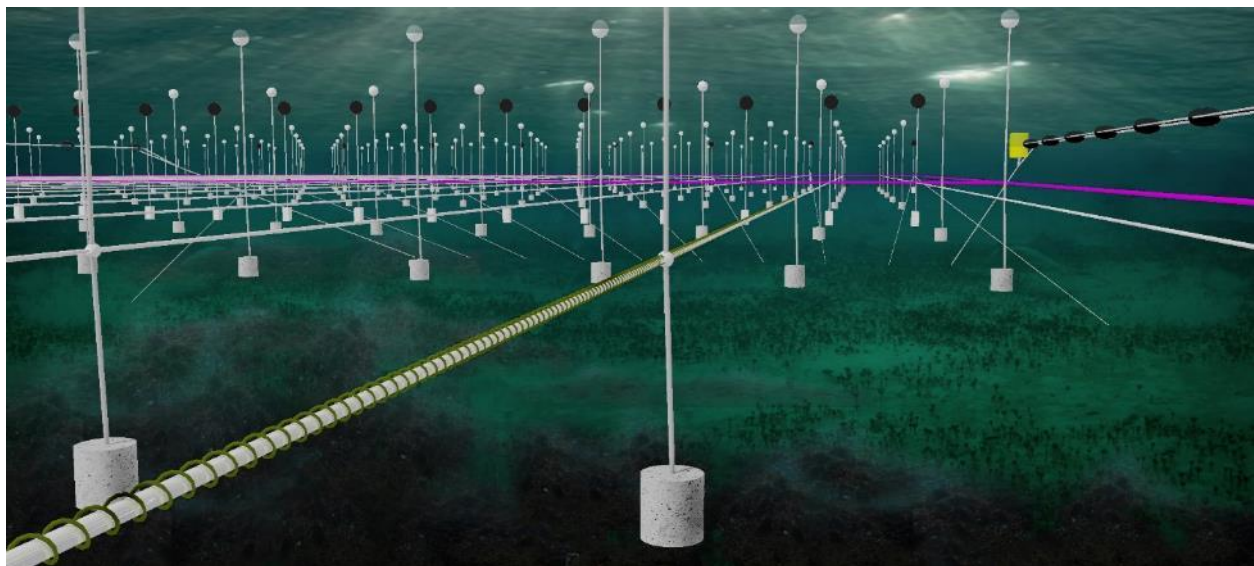


Figure 6. A rendering of the underwater seaweed lattice showing mooring infrastructure with seeded sporophytes wound onto grow line. Rendering credit – Hannah Garfield

As discussed at length with the Assessment and Modeling Teams, the best position to moor the two UW-APL sensor buoys was deemed as close to the kelp field as possible, both “upstream” and “downstream” of the predominant northeast trending tidal current flow on outgoing tides. It was unfortunately not possible to position a mooring buoy in the middle of the kelp field, since installation and subsequent removal would have compromised the integrity of the moorings and the floating aquaculture system, but it was thought that upstream/downstream measurements could give us the information we needed. The plan, therefore, was to deploy the pair of sensor buoys within the DNR lease footprint in late January

2017, just outside the seaweed lattice itself, on the southwest and northeast corners of the system, respectively (see Figure 5 for sensor buoy position relative to the seaweed lattice). The south buoy was placed adjacent to Stabilization Mooring 4 and potentially tie into existing moorings on the SW corner of the mooring system using several attachment points coming off the Helix™ moorings installed to the south. The north sensor buoy was located just to the west and adjacent to the north PATON, made fast to stabilization buoy SM2 and several Helix connections on both the north row and middle row of moorings. Note that depths at the SW corner of the site are ~11m at MLLW while depths at the NE corner are ~18m at MLLW. Sensor buoy mooring lines would need to be maintained clear of the kelp lattice, using chain or weights.

5. Kelp Cultivation

Authors: Joth Davis, Betsy Peabody

To support full-scale cultivation and scientific assessment at the Hood Head site in 2017 and 2018, the kelp team produced and outplanted 8,170 feet of line seeded with sugar kelp in December 2016 and 10,000 feet of seeded line in February 2018. In 2016, the seeded line was wound onto 19 cultivation lines while in 2018, the seeded line was deployed onto 17 cultivation lines. Over the course of the growing season during the two years of field investigation, the Hood Head demonstration farm produced about 20 metric tons of sugar kelp in 2017 and about 22 metric tons (live weight) in 2018.

As described earlier, the seeded line that was cultivated at the Hood Head site was produced by PSRF at the kelp propagation lab established at NOAA's Manchester Research Station. Spools containing the kelp sporophytes on twine were held at the approximate temperature of their production tanks (~10°C) during transport to the Hood Head site and subsequent deployment. Because outside temperatures were rather cool (3-5°C) each year during the deployment phase, sporophytes on spools were maintained in seawater baths during transport and just up to deployment. Transport between the cultivation lab and the boat launch in Port Gamble was accomplished by placing individual spools into a specially constructed framework that held up to 40 spools independently while submerged in 10°C seawater in a standard 450L plastic fish tote (Figure 7). Transport of the spools from truck to boat was accomplished by moving the frame holding the spools from the truck to the boat and into a second tote filled with ambient seawater for transport to the cultivation site (2 nm away) (Figure 8). On site, the process of de-spooling the seeded twine proceeded without delay. The grow line was first detached from the lattice perimeter line. The unattached grow line was slipped through the PVC pipe containing the wound twine with attached sporophytes and the grow line reattached to the lattice. With the boat slowly moving down the length of the grow line, the twine on



Figure 7. Spools in specially constructed framework



Figure 8. Transport of seeded spools was accomplished in totes containing seawater at ambient temperature.

the spool slowly unwound in spiral twists down the length of the grow line. At the end of the grow line, the twine was tied off to the line and the spool removed. This process was repeated for each of the 38 (19 x 2) grow lines. During this critical phase of the process, care was taken to ensure that the twine was tightly wrapped and in contact with the grow line as it unwound. Substantial video footage of this activity was taken on December 6, 2016 by the Vulcan Philanthropy film crew, to contribute to the video found here: <https://youtu.be/T7fMSRFPna4>

5.1 Summary of kelp production in 2017 and 2018

To support the assessment team's schedule (April – June) for continuous monitoring and field sampling over two seasons of sugar kelp production, it was necessary to maintain the grow lines of sugar kelp well beyond the normal time frame for commercial cultivation. As a result, there was a period associated with peak kelp production at the Hood Head farm in June of 2017 and 2018, followed by rapid degradation of material in the weeks following. Peak production of sugar kelp grown on 19 cultivation lines in 2017 was estimated at 19,417 kilograms (kg; live weight). In 2018, total production grown on 17 cultivation lines was estimated at 15,500 kg. An additional amount of sugar kelp (estimated 6,869 kg) was harvested from the kelp farm in 2018 for a total production estimate for the 1 hectare site of 22,370 kg (live weight).

5.2 Sampling protocol for carbon and nitrogen content

Carbon and nitrogen content in sugar kelp grown at Hood Head was measured in 2017 and 2018 during the field investigation. To determine whether sugar kelp sporophytes contained varying quantities of carbon and nitrogen over a growing season, carbon, hydrogen and nitrogen (CHN) content in individual kelp fronds was estimated twice in 2017 (4/3, 4/25) and monthly April – June in 2018. Variability in carbon and nitrogen content was also sampled within individual kelp blades in 2017.

The following sampling protocol was used for determining carbon and nitrogen content in kelp fronds. Kelp blades were sampled following the routine collection of plants from the Hood Head kelp farm (Figure 9). Blades with stipes attached were returned to the PSRF laboratory in clean plastic baggies where sections of the blade (12mm x frond width) were removed at five positions, corresponding to approximately co-equal sections along the length of the frond (Figure 10). For each strip, a live tissue weight was recorded and the strip subsequently dried (70°C for 48 hours), weighed and pulverized to



Figure 9. Sampling sugar kelp, 2017.

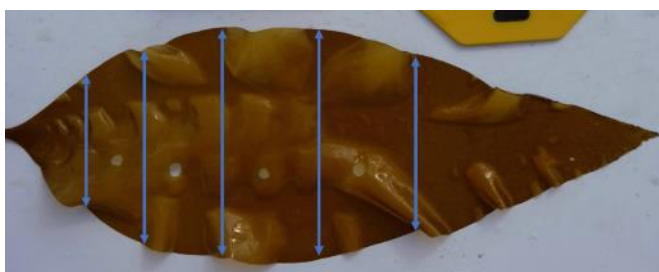


Figure 10. Positions for excision of strips (on a sugar kelp sporophyte for estimates of carbon and nitrogen content.

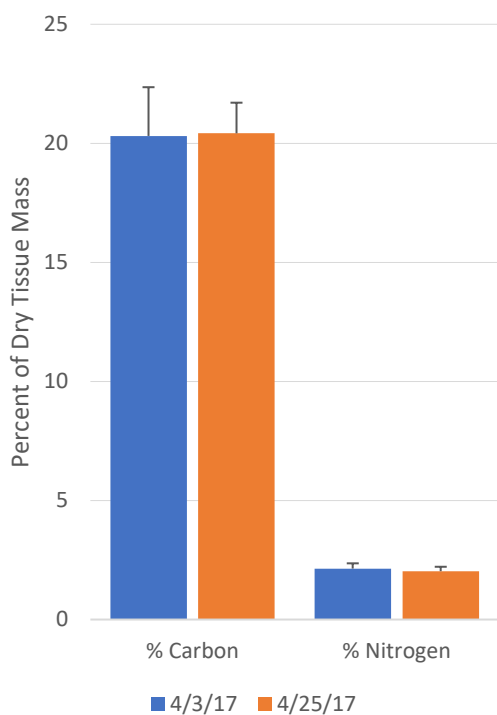


Figure 11. Elemental carbon and nitrogen content of sugar kelp measured as a percent of dry tissue mass in 2017 (mean +/- standard deviation). No significant differences were observed between sampling dates or in different parts of the sporophyte.

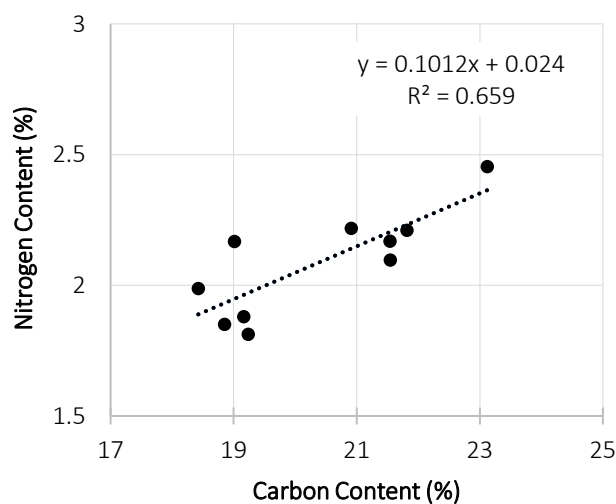


Figure 12. Carbon and nitrogen content in sugar kelp fronds are highly correlated in 2017 sampling with higher carbon content in samples corresponding to higher nitrogen content.

a fine powder. Because the analysis relies on the measurement of elemental nitrogen and carbon in very small amounts of dry material (i.e., a few milligrams) it was important to prevent contamination of samples during handling and to ensure that samples were prepared so to ensure a homogenous sample. To avoid contamination, dried samples were placed into snap-cap plastic vials and stored in a desiccator at the PSRF laboratory to await CHN analysis.

CHN sampling was accomplished using a Leeman Labs Model CEC440 Elemental Analyzer at the UW School of Oceanography Marine Chemistry Laboratory. This approach uses the unique elemental signature of carbon, hydrogen and nitrogen to assess the percentage of each element in a sample using gas chromatography. Specifically, a sample of pulverized kelp frond was combusted in an excess of oxygen and various traps used to collect the combustion products, including carbon dioxide, water, and nitric oxide. The masses of these combustion products were then used to calculate the elemental carbon, hydrogen and nitrogen content in the dry sample.

Results of elemental analysis for the limited sampling in 2017 indicated no statistically significant differences in carbon and nitrogen content, as a percentage of dry tissue mass, in kelp fronds with respect to either date or position within the blade (Figure 11). Overall, mean carbon and nitrogen content for kelp blades sampled in April 2017 was 20.4% and 2.09%, respectively for the ten samples assessed (Figure 11). Though no pattern was observed for carbon and nitrogen content by blade position, carbon and nitrogen content were highly correlated within individual samples; samples having high carbon were also characterized by high nitrogen content (Figure 12).

In 2018, sampling for carbon and nitrogen focused on the measurement of temporal variability in carbon and nitrogen content as a component of dry tissue mass of kelp blades. Sampling protocols used were similar to 2017 except sporophytes were collected in mid-April, mid-May and mid-June and replicate samples prepared for CHN analyses. Results indicate a difference in carbon content over the course of the growing season in 2018, with plants sampled

in June having a significantly higher carbon content than observed in April (*ANOVA*; $F=8.07$; $p<.05$). No seasonal differences in nitrogen content were observed in 2018, however, with plants having a mean nitrogen content of 1.97% as a percent of dry weight. Summary statistics for carbon and nitrogen content in kelp sporophytes sampled in 2017 and 2018 are tabulated in Table 1 and shown in Figure 13.

Date	Carbon (%)	SD	Nitrogen %	SD
4/3/17	20.31	2.05	2.14	0.22
4/25/17	18.83	1.28	1.93	0.11
4/19/18	18.22	2.21	2.45	0.37
5/17/18	21.82	4.04	4.04	0.67
6/14/18	24.59	1.27	1.27	1.11

5.3 Summary of net production of sugar kelp in 2017 and 2018

Table 1. Summary values for percent carbon and nitrogen in kelp sporophytes observed in 2017 and 2018 (Mean and Std. Dev.).

Bimonthly sampling for kelp standing

biomass was initiated beginning late spring for both sampling years and continued through the end of June. Sampling was conducted by a combined team that included PSRF and HCM personnel. Though efforts were made to conduct sampling at weekly intervals between late March and late June during both years of the project, sampling was conducted using a small boat. As a result, weather conditions often dictated specific sampling dates for both years.

For all sampling, the specific location for sampling individual plants was determined by first locating a randomly selected point within a 3-meter distance along a designated grow line, either north or south of one of the four dropper lines associated with each grow line (N=19 lines in 2017, N=17 lines in 2018). The droppers (stabilization buoys maintaining the grow line at the specified depth of 3m) were located at approximately 25m intervals along the length of each grow line.

Sampling protocols included the following steps. The kelp grow line was hoisted to the surface at the specified dropper location and a 3m section of line, either north or south of the dropper, draped over the side of the boat alongside a 3 meter ruler (0.1 meter increments). A GPS location was recorded for each sample site. For each of the grow lines, a randomly selected point along the grow line was selected and all plants within a 0.25 meter section removed, placed into a plastic bag and stored in a shipboard cooler. Samples were returned to the PSRF laboratory for biomass estimates. Laboratory processing included the following steps. First, the sporophytes for each sample location were removed from the storage bag and counted, patted dry with paper toweling and blade length measured to the nearest millimeter (mm) at two points: 1) from the stipe (base of the highest haptera) to the

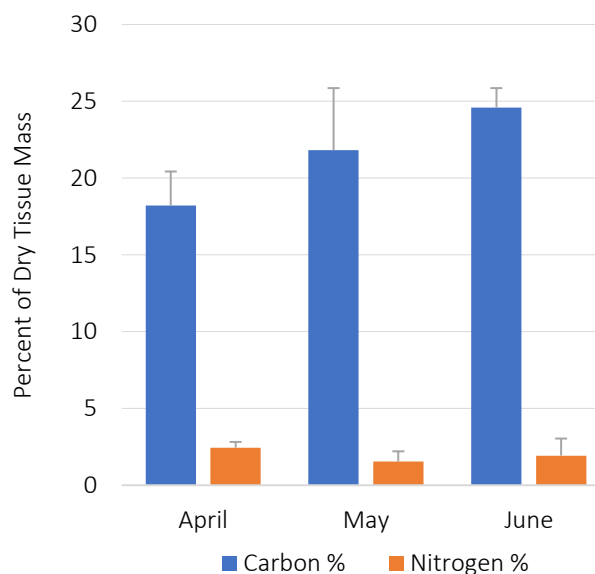


Figure 13. In 2018 sampling, carbon and nitrogen content varied seasonally with significantly higher carbon content in sporophytes observed in June compared to April ((mean +/- standard deviation). Nitrogen content did not significantly vary seasonally.

base of the blade and; 2) from the base of the blade to the blade end. These data enabled estimates to be made of standing biomass, population estimates and total plant density for discrete locations on the project footprint. These values were then extrapolated to generate estimates of total abundance, plant density and total biomass for the seaweed farm overall.

5.4 Novel sampling method for measuring net primary production in sugar kelp

We developed a modified approach to the measure of net production in sugar kelp using image analysis sampled from photographs taken in the field. Sampling depended on making repeated measurements and photos of selected plants that were sampled initially (day 0) and then again either 7 and/or 14-days later to estimate the increase in blade biomass as a result of tissue growth. The method also enabled a measure of blade loss (mainly at the distal ends of blades) due to erosion. Changes in blade area then can be assigned to either net production (blade accretion) or loss due to erosion.

The specific protocol included the following steps. First, individual sporophytes were selected using the protocol described above. Kelp plants were removed by carefully peeling away the haptera holding the sporophyte to the grow line. The point of plant removal was marked with a numbered plastic tag. Individual plants were placed onto a white board aboard the boat and total length of the blade measured

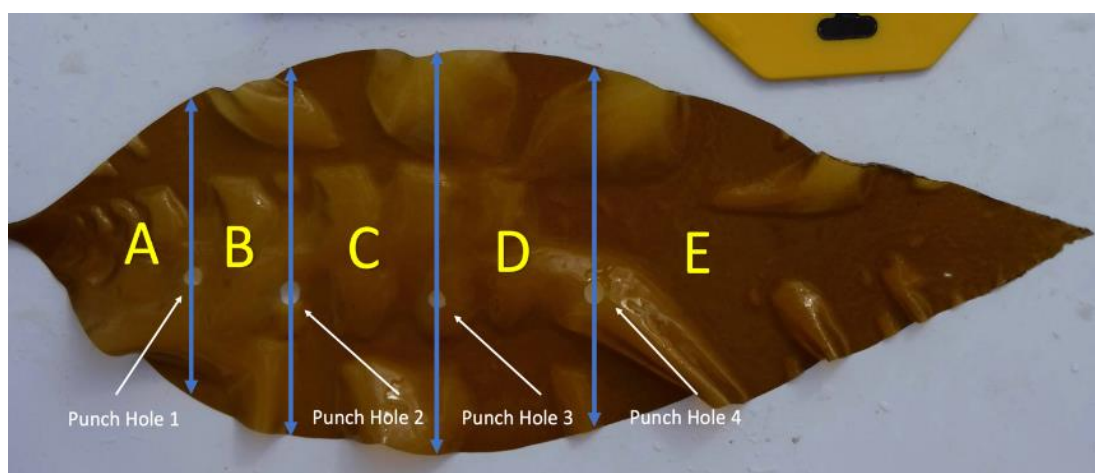


Figure 14. Sugar kelp sporophyte showing the typical position of punched holes made in the field. The arrows demarcate the margins of the five sections in this blade measured for total area using Image J.

(1mm precision). Second, four holes (3mm or 4mm in diameter) were punched into the blade using a cork borer, in a line along the mid-section of the blade (Figure 14), dividing the blade into 5 quadrants. Distances between the punched holes were dependent on initial blade length. Next, the distance from the base of the blade to the mid-point for each of the four holes was measured and recorded (1mm precision). The blade was then photographed, with an associated tag and ruler included in each photo, to preserve scaling for later image analysis. The plant was then “tagged” for later use by attaching a small cable tie around the stipe. Finally, the plant was reattached to the grow line at the cow tag position using a cable tie.

Plants designated for net production and erosion rate estimates were re-sampled either 7 and 14 days later and the same set of measurements and photographs recorded.

Photographs were subsequently uploaded from the field camera to a computer and total blade area for each blade “quadrant” (blade area between the base and first hole, first hole to second hole, etc.) estimated from individual photos using the image analysis program, *Image J*. For each photo, the area devoted to each section of the blade was calculated, using a pre-positioned square of known area in the field of each photo to calibrate the measurements. Sub-divided blade segments are labeled A-E (Figure 14). This process was repeated for photographs of blade area taken in the field for the same plants 7 and 14 days later, following initial measurements. This enabled precise measurements to be made for increase in blade area due to tissue accretion and blade loss due to erosion. As expected, the region of the blade having blade loss was generally observed between punched hole #4 and the blade tip (quadrant 5).

Following either a second or third sampling (generally 7 days apart), kelp plants were returned to the PSRF laboratory and processed for wet and dry weight and tissue analysis. Wet weights for whole plants were obtained following the protocol outlined above for biomass estimates. Dry weight estimates for each plant were obtained by removing a lateral strip of blade with a known area from each of the blade quadrants. These samples were placed into pre-weighed aluminum boats and weighed prior to drying at 60°C for 48 hours. Dry weights (0.1 gram precision) were recorded for replicate blade sections and data extrapolated to the entire blade to provide an estimate of total dry mass of blades on a per square cm basis.



Figure 15. Encrusting bryozoan, *Membranipora membranacea*, on kelp blades.

For individual blades, the sum across all quadrants for accreted blade area divided by the number of days between successive measurements, represented a measure of net production (mg per day) for individual kelp plants. Blade area loss via erosion was similarly tabulated for individual blades. Finally, subsamples of dried blades were retained for later assessment of total carbon and nitrogen content to enable estimates of carbon and nitrogen gain/loss per day over the growing season for kelp tissues.

5.5 Results of sugar kelp net production in 2017

Rapid increase in overall biomass of sugar kelp was observed between January and early June with some blades exceeding 5 meters in length by June 2017. Net production estimates for kelp sporophytes sampled over an approximate 2-month period (April 3, 2017-June 6, 2017) was high during early sampling followed by reduced blade accretion later in the spring. This reduction in growth was also accompanied

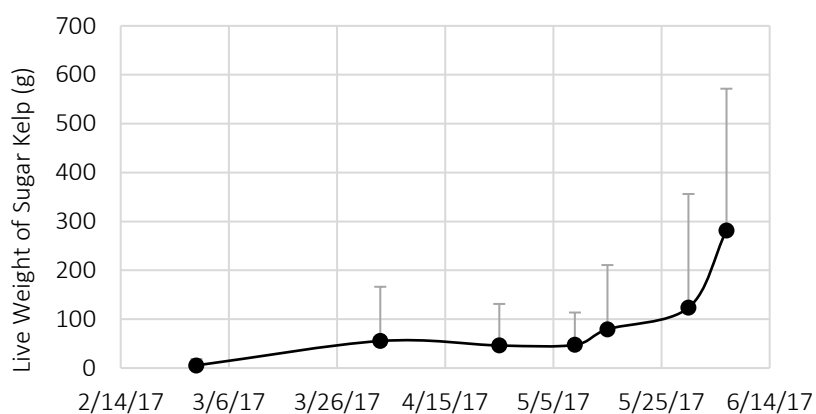


Figure 16. Mean biomass of replicate sugar kelp plants sampled on 19 cultivation lines in February and early June 2017 (mean and standard deviation).

by increased blade loss due to erosion. Sporophytes were also overgrown by encrusting invertebrates including the bryozoan, *Membranipora membranacea*, covering up to 80% of kelp blades by late May and June (Figure 15). Degradation of plants, mainly at the distal end of the blades, was observed beginning in late April. By early June, plants began to exhibit reduced growth and increased blade loss, due to erosion, mainly at the distal ends of blades.

5.6 Sampling and Estimates for Kelp Biomass in 2017

Individual kelp plants sampled on 19 grow lines in 2017 exhibited significant growth between early April 2017 and early June, with estimates of standing biomass peaking in late June (Figures 16 and 17). Peak biomass of sugar kelp in early June was estimated at approximately 19,417 kg live weight. This estimate was based on measurements of plant density, summed over all 19 grow lines, and biomass estimates made on individual plants over the course of field sampling.



Figure 17. Seeded kelp line, March 2017

5.7 Estimates of net production in 2017

In 2017, sampling for net production of kelp plants was accomplished for plants on 4-25-17, 5-2-17, 5-15-17, 5-17-17, 5-30-17 and 6-6-17. Data collection followed the protocols described above. Based on an analysis of blade surface area, net production rates of sugar kelp increased significantly between late February through April, decreased in the first half of May before increasing again after May 15th (Figure 18). Note that only accretion of blade tissue was directly measured. A significant amount of fixed carbon is lost through the leakage of dissolved organic material (DOM) from kelp blades. These organics, including carbon, are difficult to measure and were not directly assessed in this field study. Instead, an estimate for DOM production from the literature was used to calculate total exudite production, which was then factored into estimates. Note the significant decrease in net production measurements for kelp during the first half of May. This decrease may be attributed to a period of significant shading of the kelp by suspended plankton as this period corresponded to measurements of high phytoplankton production (Figure 18).

A simple calculation suggests that if PSRF had harvested all the sugar kelp at peak biomass (2,264 kg dry mass @ 11.7% of the 19,417 kg wet mass) during the first week of June 2017, then approximately 443 kg of carbon and 53 kg of nitrogen would have been removed from the water column. By early July, when kelp was harvested at the end of the sampling program, decreases in kelp biomass had occurred due mainly to the growth of epibiont fouling, which resulted in an increased rate of erosion and blade loss. As such, at the time of harvest for SkyRoot Farm in July, only 6,372 kg wet weight (743 kg dry weight) was available for harvest. At that time, kelp material consisted mainly of degraded blades and holdfasts, though a significant amount of wild kelp growing on the cultivation lines was also harvested and included in this estimate. If carbon and nitrogen content was similar to that in kelp blades sampled in April 2017 then about 145 kg carbon and 15 kg nitrogen would be the values for estimated removal of carbon and nitrogen at the time of harvest.

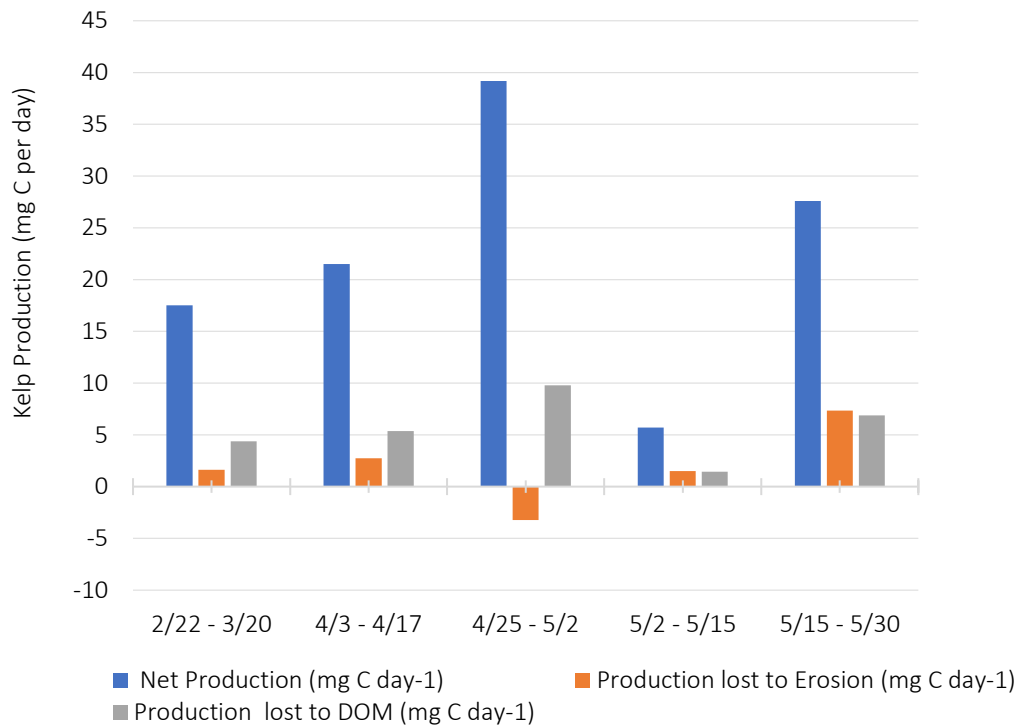


Figure 18. Estimates for different components of production in sugar kelp in 2018 (mg C per day). Estimates for net production (rate of increase in blade tissue) and carbon loss to the water column due to erosion of blades are based on field measurements. Estimates carbon loss of dissolved organic material leaked from sporophytes was estimated as 25% of the total sporophyte biomass. Carbon loss due to respiration was not measured.

5.8 Sampling and Estimates for Kelp Biomass (2018)

Sample collection for sugar kelp biomass and net production at the Hood Head cultivation site was initiated on April 12, 2018 and completed for the second project year by July 3, 2018, with ten complete data sets collected during that time frame. Similar to 2017, during each site visit an average of five plants were sampled using the methodology described above. Briefly, individual sampling points were selected from the overall kelp array by randomly generating a cultivation line number (1-17), a position north or south of the midline, and a distance from a dropper buoy. From that position, plants were sampled from 1.00 to 10.00 meters in 0.25-meter increments from the randomly selected position on the kelp grow line. Results for net kelp production indicated that like 2017, kelp growth progressed rapidly during the spring and early part of the summer (Figure 19). Note the decline in total biomass in mid-June 2018, again a period that corresponded with high phytoplankton production at Hood Head. However, herbivory of kelp blades near the stipe of the plants, associated with a small herbivorous gastropod, *Lacuna vincta*, was also observed during this time frame. Interestingly, kelp production resumed until the end of the sampling period in early July. Estimates of standing kelp biomass, based in this case on measurements of blade area, indicate that peak standing biomass occurred in late June 2018.

5.9 Assessing standing biomass of wild kelp on kelp farm lattice

There is a significant infrastructural component associated with the Hood Head kelp farm that was colonized by wild kelp plants in both 2017 and 2018. The grow out lattice consists of mooring lines, structural lines and buoys on the perimeter of the one-hectare farm that support the 34 grow lines. In

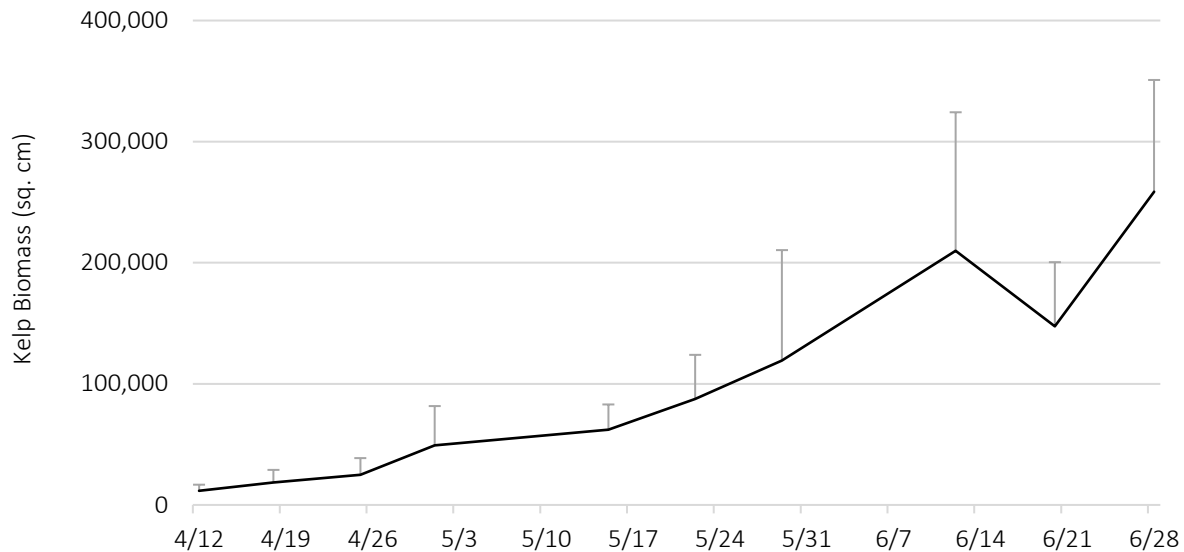


Figure 19. Standing kelp biomass on cultivation lines (mean plus standard deviation) based on sampling of random plants over the sampling period, April 12 - June 28, 2018 inclusive.

2018, an assessment was made to approximate the biomass of wild kelp associated with the infrastructure itself, with and independent of the seeded grow lines.

Cultivation lines seeded in 2018

- 250' sections on South half of the farm x 17 cultivation lines = 4,250 ft
- 230' sections on North half of the farm x 17 cultivation lines = 3,910 ft
- Total = 8,160 ft of seeded line

Locations with natural settlement of sugar kelp on lattice and associated moorings

- Mooring lines: 400 ft. (10 at North & South ends, 20 total; kelp removed down to 20 ft.)
- Longitudinal lines: 1000 ft.
- Lateral lines: 180' x 3 = 540 ft.
- Vertical black buoy lines: 24 x 10' = 240 ft.
- Double back lines: 500' x 4 = 2000 ft.
- Total = 4,180 ft.

At peak production, a total of 15,500 kg (live weight) of sugar kelp was contained on 17 cultivation lines with an additional 6,869 kg (live weight) contained on the kelp lattice and mooring components associated with the cultivation infrastructure at Hood Head. Together, the total biomass of sugar kelp contained on the farm was therefore approximately 22,370 kg (live weight). Average production per lineal meter of cultivation lines in 2018 was about 5.6 kg per lineal meter (3.7 lb. per lineal foot) of grow line.

5.10 Estimates for Net and Total Production in Sugar Kelp in 2018

Like 2017, an analytical approach based on making discreet measurements of changes in kelp blade biomass over the cultivation season was used to assess net production of kelp grown on cultivation lines. Data taken in 2018 demonstrated pronounced seasonal changes in net production (blade accretion) during the same time frame as observed in 2017. Similarly, blade area loss due to erosion occurred between early April and late June; accretion of tissue in blades dominated in the early spring before tissue

loss as blade erosion became evident, beginning in early May and continuing through the end of sampling in late June. Note that a period of low net production associated with blade growth was observed for the period May 29-June 12, again corresponding to a period of peak primary production of phytoplankton in

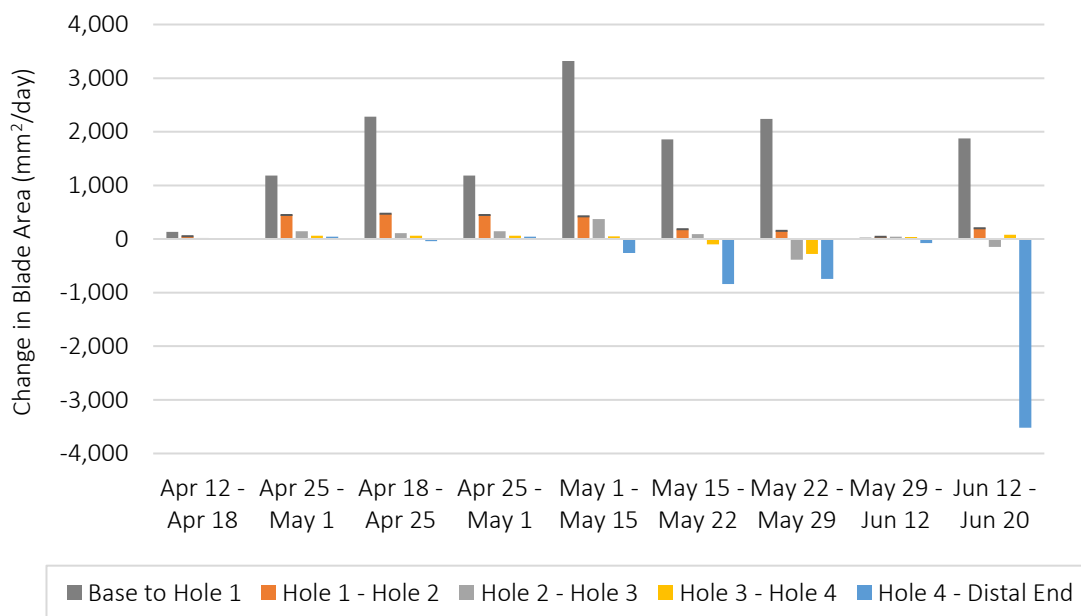


Figure 20. Mean kelp tissue production and erosion. Estimates of daily net production (sq. mm tissue produced) in individual kelp blades sampled over the 2018 cultivation period peaked in late April. Blade loss as erosion dominated in June as sporophytes deteriorated.

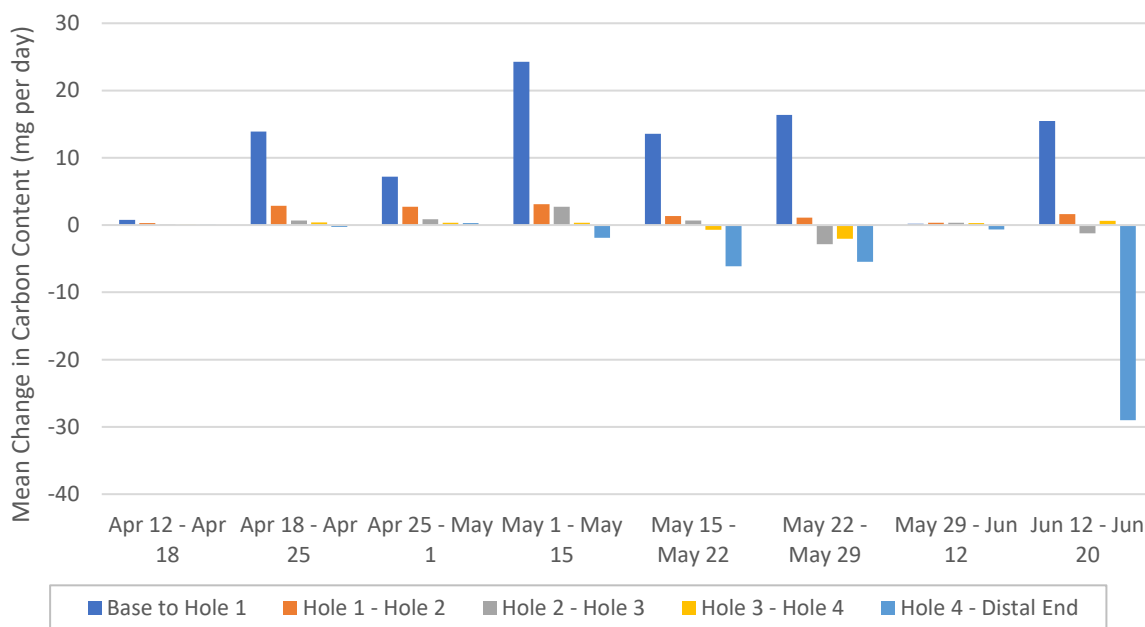


Figure 21. Carbon content ($\text{mg C} \cdot \text{day}^{-1}$) as a percent of dry tissue mass within individual blades sampled in 2018, including the net of total production contained in tissues for individual blades sampled in 2018.

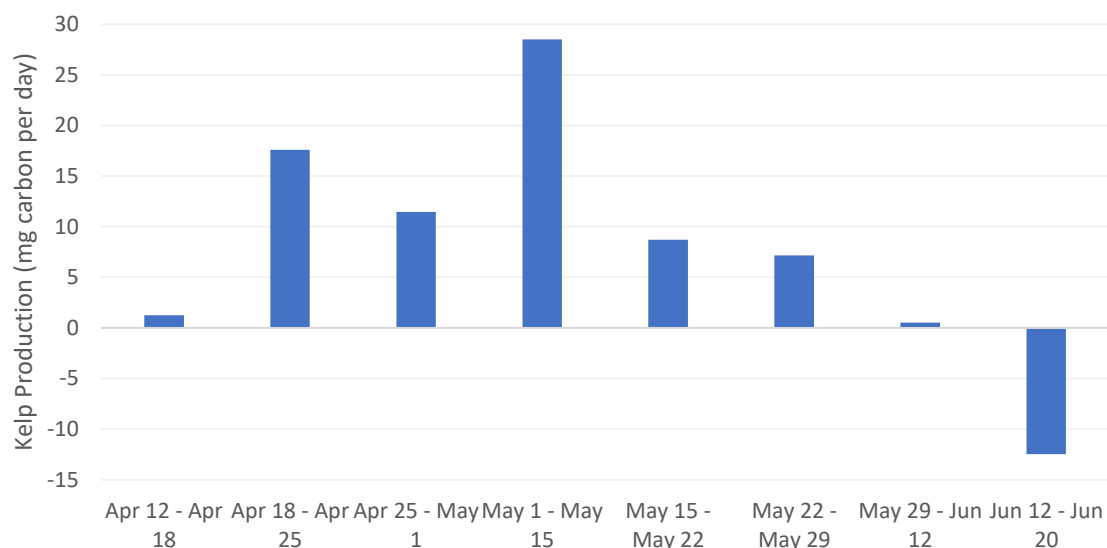


Figure 22. Net production and loss via erosion in individual kelp blades measured in 2018. (mg carbon per day⁻¹).

north Hood Canal, suggesting that kelp plants were likely shaded from natural light, and limited their growth during this time frame (Figure 20). Estimates of kelp production (mg carbon day⁻¹) for individual sampled blades over the course of the growing season demonstrated significant variation in carbon content by position within the blade (Figure 21). Carbon content contained in sporophytes compared to carbon lost via tissue erosion in individual sporophytes sampled in 2018 and demonstrated a peak in early May followed by a decrease as blades eroded and released the carbon back to the sea (Figure 22).

Like 2017, estimates of carbon and nitrogen content in kelp biomass were made in 2018 based on sampling carbon and nitrogen in individual plants in April, May and June 2018 (see results detailed above). Applying these seasonal values for carbon and nitrogen to estimates for dry kelp biomass, carbon and nitrogen content peaked in late May in North Hood Canal. Had all the kelp been harvested at that time, this would have resulted in the removal of about 306 kg carbon and 57 kg nitrogen, respectively from the cultivation lines (Table 2).

Date	Biomass Cultivation Lines (kg)	Dry Mass (kg)	Carbon Content (kg)	Nitrogen Content (kg)
4/12	631	63	11	1
4/19	2,140	214	39	5
4/25	3,980	398	73	10
5/1	8,107	811	177	33
5/16	9,088	909	56	37
5/22	8,523	852	186	34
5/29	14,100	1,410	306	57
6/12	7,377	738	181	9
6/20	4,856	486	119	6
6/28	1,495	149	37	1

Table 2. Estimates of mean standing biomass and carbon and nitrogen contained in sugar kelp sporophytes on the Hood Head farm in 2018 exclusive of the natural set of sugar kelp on farm lattice.

6. Kelp Harvest

Authors: Joth Davis, Betsy Peabody, Meg Chadsey

6.1 Food grade harvest activities

During the 2017 and 2018 field investigations, small quantities of sugar kelp grown at the Hood Head investigation site were harvested to support research and nascent marketing efforts to build interest and lay the groundwork for locally grown sea vegetables. Activities included:

- July 22, 2017, PSRF assisted with a seaweed cooking demonstration at Tom Douglas's Hot Stove Society in Seattle.
- May 23, 2018, 4 kg raw wet weight food-grade material was harvested and delivered to 21 Acres, an incubator kitchen located in Woodinville that provides facilities for food products that are being processed for market. The kelp was prepped and dried in 21 Acres' commercial dehydrator by PSRF, Washington Sea Grant and culinary partners Sustainable Collaborative, with a yield of 3 kg wet weight (0.3 kg dry weight).
- June 13, 2018, 136 kg of kelp was harvested and delivered to Ron Johnson at NOAA for processing experiments. This included 68 kg of seeded kelp from the cultivation lines, and 68 kg of naturally recruited kelp attached to the surrounding culture frame. Material from the cultivation lines was experimentally processed into a fish feed additive for sablefish aquaculture to determine how it may improve fish health. The natural set non-fouled kelp was placed in a bio-digester for extraction of ethanol for biofuel. The protein byproduct will be used for a different application, possibly involving fodder for chickens.
- June 13, 2018, 8 kg raw weight food-grade kelp (including both seeded and natural set kelp material) was harvested and delivered to 21 Acres for dehydration (Figure 23). The processed yield was 6 kg wet weight (0.6 kg dry weight).
- The dried material described above was used for 1) a kelp tasting kit developed by Washington Sea Grant and the UW Communications graduate students for showcasing locally-grown kelp to restaurants and culinary institutions; 2) culinary experiments with value-added kelp products by Sustainable Collective, an offshoot of 21 Acres; 3) a (favorable!) assessment of the local dried kelp material by a Japanese kelp buyer; and 4) local kelp preparations served to an international society of female culinary professionals, Les Dames D'Escoffier, at their 2018 conference in Seattle.



Figure 23. Sugar kelp being washed and prepared for further processing.

6.2 Late-season kelp harvest to remove biomass (and carbon and nitrogen)

In 2017, harvest of the remaining kelp from the Hood Head cultivation site occurred July 12-14 (Figure 24). The harvest operation involved multiple players and depended on precision timing with respect to the delivery of degrading kelp to SkyRoot Organic Farm on Whidbey Island. Dr. Eli Wheat, UW College of the Environment agroecology expert, owns an organic farm on Whidbey Island near Clinton. After learning about the project from Meg Chadsey at Washington Sea Grant, Dr. Wheat enthusiastically agreed to take as much kelp as we could harvest from the cultivation site once sampling and assessment

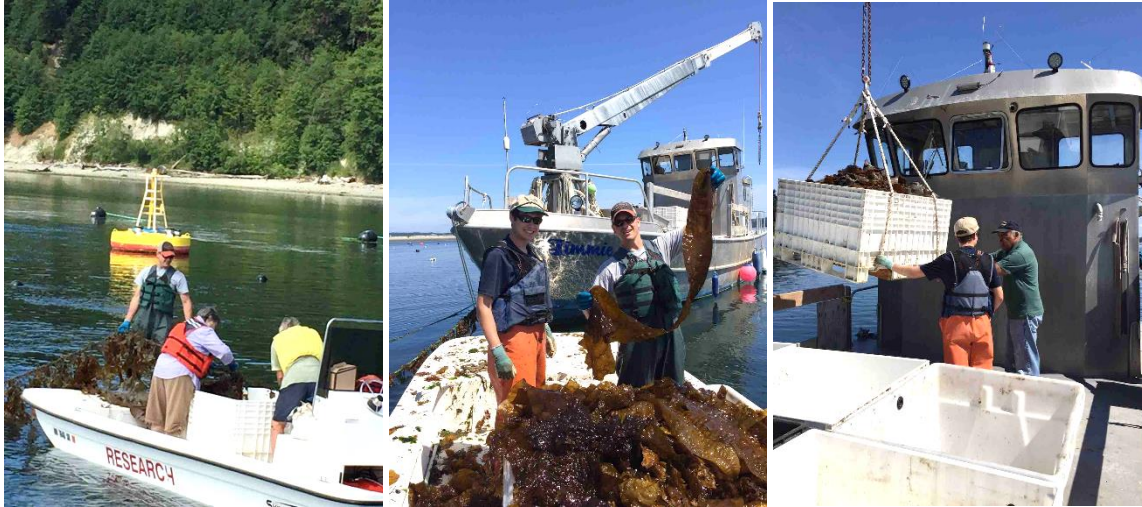


Figure 24: Sugar kelp harvest at Hood Head July 2017 and preparation for transport to SkyRoot Farm on Whidbey Island.

activities were concluded in late June 2017. Dr Wheat planned to involve UW students in soil enrichment trials to optimize the integration of kelp carbon and nutrients into the soil without tilling it (since tilling disturbs soil ecology and depletes stored organic carbon).

Coordination of the kelp harvest was managed by HCM and PSRF and involved contracting with a local barge operator to assist in the transport of harvested kelp from the Hood Head farm to the Mutiny Bay boat launch 11 miles away on the shore of Whidbey Island where it would be loaded into a dump truck and transported to SkyRoot Farm. On July 12 and 13, PSRF harvested all remaining, late-season kelp from the Hood Head cultivation site with the help of volunteers. The harvest method consisted of cutting and loading kelp blades and holdfasts into fish totes and delivering loaded totes to a barge tied up alongside the perimeter of the Hood Head farm.

Totes were offloaded from the harvest boats using a crane. A total of 10 fish totes were loaded on each of the two days and subsequently transported by barge to Whidbey Island (Mutiny Bay Boat Launch) and offloaded at the peak of the high tide the following morning into a dump truck positioned at the end of the boat launch. Over the two-day period, an estimated 6.35 metric tons live weight of kelp was harvested and delivered. This represented roughly 32 percent of the peak biomass growing at Hood Head in June 2017 (19.4 metric tons live weight). As mentioned earlier in this



Figure 25. Offloading kelp from boat to dump truck at Salisbury Point boat ramp July 20, 2018



Figure 26. Photo of degraded natural set kelp covering infrastructure lines that was removed by Research Support Services (RSS) on July 16, 2018.

report, degradation of kelp material occurred between early June and early July. This information was very useful in developing the 2018 cultivation and harvest plan. If the goals were to 1) optimize carbon and nitrogen removal; and 2) optimize the quantity of kelp material harvested, the 2018 kelp crop would need to be harvested in June at the latest. It was important that lines and the culture system) be completed prior to the third and final UW-APL/PMEL sampling cruise on July 23, 2018. The third cruise was intended to capture “non-kelp” seawater conditions post-harvest, so an expanded effort was mounted in 2018 to remove as much kelp from the site as possible. To accomplish this objective, a subcontractor engaged by the PSRF during July 16-18 removed an estimated total of 6,869 kg live weight of natural set kelp from the infrastructure lines around the perimeter of the kelp cultivation area (Figures 25 and 26). During July 19 and 20, PSRF and HCM harvested approximately 4,545 kg of the remaining late-season kelp from the Hood Head cultivation lines (Figure 27) for delivery to a no-till vegetable farming operation in Quilcene for composting.



Figure 27. Max Calloway and Tara Nikomborirak with PSRF harvesting end-of-season kelp July 19, 2018

7. Chemical assessment of seaweed cultivation array

Authors: Simone Alin, Dick Feely, Jan Newton, John Mickett, Micah Horwith

7.1 Buoy and sensor deployment and performance

On January 25th, 2017 two moorings were deployed within 20 feet north and south of the kelp array with upward-pointing, bottom-mounted current meters adjacent to each surface buoy (Figure 28). All sensors subsequently described were deployed from then until the conclusion of field season 1 (June 26, 2017). The current meters were set to record velocity over the water column every six minutes. Both buoys were equipped with pCO₂ systems and peripheral instruments to measure concentrations of CO₂ in the water and air as well as near-surface pH, temperature, salinity, density, DO, and for one of the moorings, chlorophyll concentration and turbidity (the latter two were not funded by this project). Both moorings were also instrumented with state-of-the-art SeaBird SeapHOx sensors at 3 m depth, measuring pH, DO, temperature, salinity, and density every 10 minutes. Finally, both moorings also had a current meter located just above the SeapHOx sensor at 2.5 m depth, measuring water velocity at this depth every 14 seconds.



Figure 28. Photo of kelp array and monitoring moorings looking northeast.

During field season 1, both SAMI pH systems deployed by PMEL had to be replaced due to faulty components (on one, a battery; on the other, a pump). Thus, on May 1st, pH sensors at both the northern and southern kelp sites were swapped out. We note that there was no budget for the added person-time and effort required to make this happen, due to the very tight nature of funding for this project. We further note that the PMEL Carbon Group purchased SAMI pH systems rather than the SeaFET systems originally in the PAFF budget, due to their better usability and performance in the field over the period of time between when this work was first proposed and the inception of this field effort. SAMI pH systems cost several thousand dollars more than the SeaFET systems (again, a funding shortfall).

Instruments deployed in field season two, which spanned from January 24 to July 25, 2018, mirrored that in season one with the exception of a significant upgrade to the SeaBird SeapHOx sensors. Again, a fluorometer was donated to the project and deployed on the North Buoy. Over the previous year Seabird worked to upgrade the SeapHOx instrument, changing both firmware and hardware. This improved the reliability, accuracy and sample frequency. This upgrade resulted in an overall improvement of pH measurements in season two (from 35% to 69% coverage just for the SeapHOx instruments), improving frequency from one sample in ten minutes to one sample in two, and reducing pH uncertainty from about 0.05 to 0.02. Accounting for duplicate pH measurements from the SAMI on each mooring, we had nearly 100% pH coverage in season two. For pCO₂ measurements, however, coverage decreased in the second field season with the system on the North Buoy not producing any usable results. We significantly benefited from the dedicated assistance of Seabird engineers and scientists in year two, who worked closely with us to prepare and deploy the two SeapHOx instruments. These units were serial numbers one and two—a testament to the fact that we were truly using the best-available technology to measure pH in the ocean over long durations.

In addition to the deployments described above, in April 2018, PSRF deployed four custom built durafet-based sensors to monitor temperature and pH in and outside of the kelp array, further described in section 7.10.

7.2 Results from the 2017 and 2018 moored observations

Current meter records indicate that the residence time—or duration that an average parcel of water spends within the patch is short—less than 30 minutes. Because of this there is little time for the kelp to act on any single parcel of water, resulting in a very small change of carbon chemistry due to kelp photosynthesis over this time. We found, unfortunately, that these changes could not be separated from other variability using state-of-the-art sensors and rigorous and careful analysis of the measurements. Even though we determined pH resolution in 2018 to be approximately 0.02 pH, or roughly half of SeaBird published values, we were unable to separate the kelp signal from other variability. Modeling results suggest for a best-case scenario (strong sunlight and weak currents) kelp would increase pH by roughly five times less than this resolution (0.004) over the residence time. In addition, changes in the upstream and downstream direction of the currents over the deployment suggest that as the kelp grew, it acted to block the downstream flow (Figure 29). Thus, in addition

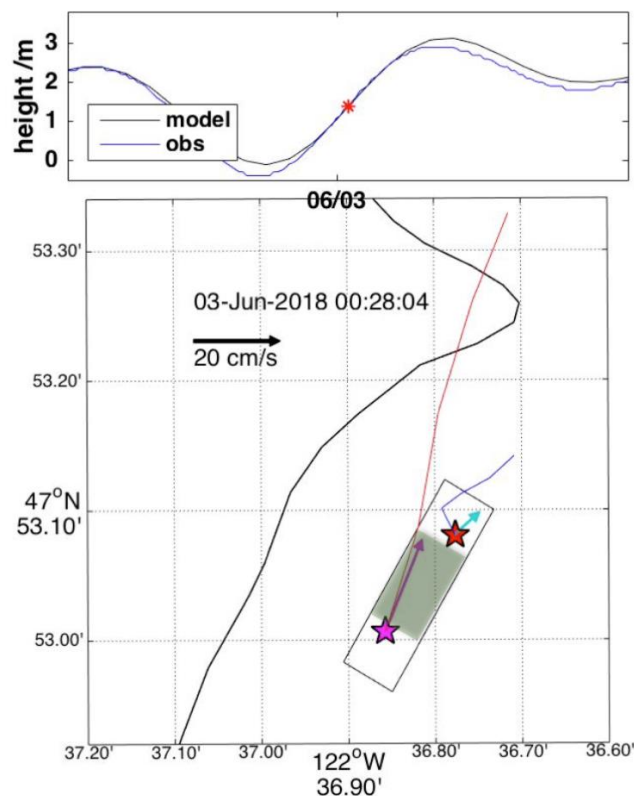


Figure 29. Lower panel: current vectors and paths indicate that in June 2018, kelp likely modified the flow downstream of the kelp array. The length of the red and blue lines, which are progressive vectors of flow, indicate the distance water would travel in 10 minutes. The vectors show speed and direction at the respective mooring locations. Top panel: comparison of observed water depth (blue) to the Puget Sound Tidal Model (black) (Lavelle et al. 1988, A multiple connected channel model of tides and tidal currents in Puget Sound, Washington, NOAA Tech. Memo. ERL PMEL-84, 108 pp.).

to short residence times, the kelp may have resulted in both lateral and vertical mixing of any carbon chemistry change that it brought about.

In the 2018 growing season (May 1 to July 15), average flow speed and standard deviations were 10 ± 8 cm/s at the North Buoy and 16 ± 11 cm/s at the South Buoy. Thus, on average, if the water moved through the entire length of the patch (150 m), it would remain in the patch for about 15–25 minutes. If we could detect a pH change due to kelp photosynthesis, we would expect the measured pH at the downstream edge of the kelp array to be higher than the upstream pH (due to uptake of CO_2), and this difference to be greatest during daylight hours when photosynthesis is at a maximum and flow is weak and oriented along the axis of the long-edge of the kelp array (maximizing residence time in the patch). Despite focusing our analysis on the times when we would expect the greatest signal, however, we found no correlation between this north-south pH difference and patch residence time, indicating that pH variability between the two buoy locations was more strongly influenced by factors other than kelp photosynthesis, or that variability at these small differences was largely instrument noise (beyond resolution).

Chlorophyll and pH are strongly correlated (Figure 30)—particularly earlier in the 2018 deployment, indicating that most pH changes are associated with phytoplankton photosynthesis and respiration and, thus, complicating the goal to parse out the kelp signal from the larger phytoplankton signal.

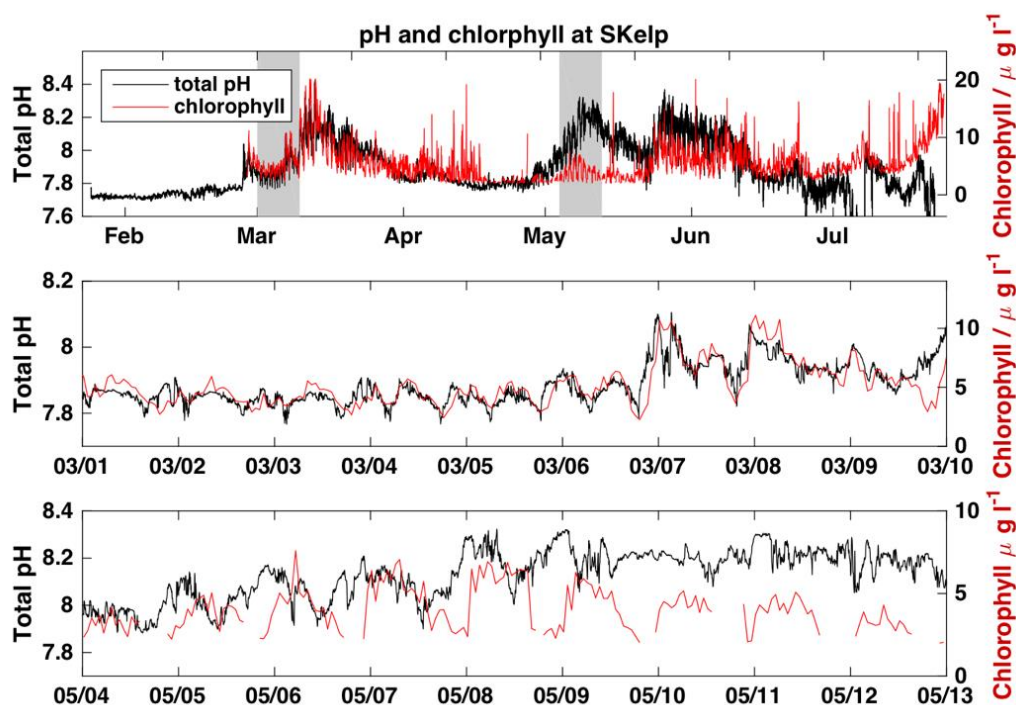


Figure 30. Plot comparing pH and chlorophyll as estimated from the fluorometers at the mooring locations in 2018.

Much of the time currents and pH changes are also strongly correlated (Figure 31), indicating that most of the observed short timescale (<day) variability of carbonate chemistry variables is due to gradients of properties being advected past the moorings, as opposed to a “local” change taking place at the mooring site. Most of the current variability is due to the tides. As the correlation follows the tidal cycle, these

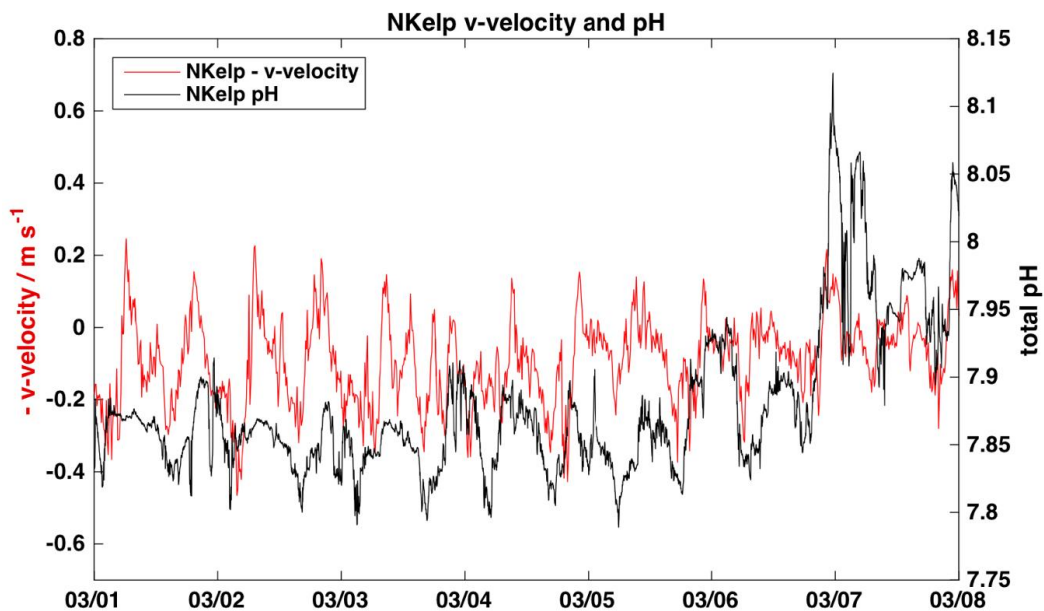


Figure 31. Along-channel currents (red) and pH (black) at the North Kelp buoy in March of 2018, showing the strong correlation of currents and pH variability

lateral gradients have dominant scales as large or larger than the tidal excursion, or several kilometers or more. This is much larger than the scale of the kelp patch (500 ft) so is unrelated to the presence of the kelp.

Comparison of different pH sensors and bottle observations indicated that pH uncertainty is approximately 0.02 pH. This uncertainty was significantly reduced by carrying out post-deployment calibrations and corrections (Figure 32). Despite this increased confidence in these measurements and the relatively low uncertainty (roughly half of SBE published accuracy of ± 0.05), this value remains roughly five times greater than maximum estimated pH changes due to photosynthetic carbon uptake/growth by the kelp.

7.3 Specific Key Performance Indicator for Moored Observations: Percent data return during mooring operational time

To review, UW-APL/PMEL Carbon Group had four pH sensors deployed for both the spring/summer 2017 and 2018 deployments, with two on each mooring—one at 1 m depth (SAMI) and one at 3 m depth (SeapHOx). Due to the close proximity of the two sensors on each mooring, these measurements can be largely thought of as measuring the same water. For 2017 the North Buoy the 1-m depth SAMI pH sensor had 100% data return for the duration of the deployment. At South Buoy, the SAMI was reporting erroneous data from March 28 to April 28, so we had good data 80% of the time. At the North Buoy the SeapHOx operated 70% of the time, and at the South Buoy, the SeapHOx largely failed—recording data for only three days of the 152-day deployment. In 2018 this picture improved, and considering redundancy, there was 100% pH coverage. In 2018, however, the pCO₂ system on the North Buoy failed leading to only measurements on the South Buoy (50% coverage).

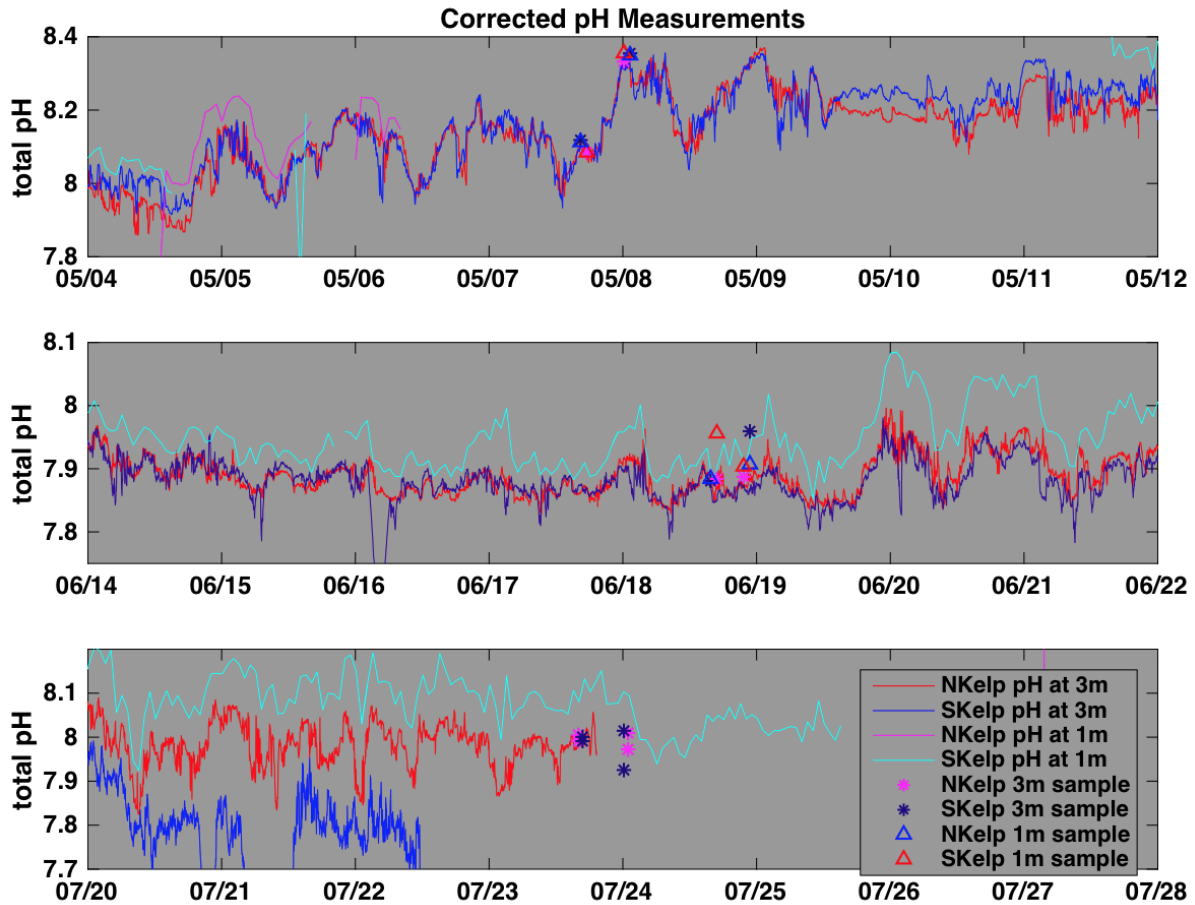


Figure 32. Comparison of pH measurements at the two moorings over select periods of the 2018 deployment. Symbols indicate bottle samples, while lines indicated mooring sensors (SAMI at 1 meter, SeapHOx at 3 meters). Note the difference of as much as 0.1 pH between sensors by the end of the deployment. SKelp SeapHOx pH (blue line) were flagged bad in late July (bottom plot).

2017:

- Velocity sensors: 70%
- pH sensors: 63% (however, we had 100% pH coverage at the North Buoy and 80% coverage at the South Buoy, because we deployed duplicate pH sensors for redundancy)
- pCO₂ systems: North Buoy: 100%, South Buoy: 77% (average = 88.5%)
- Salinity, Temperature, Oxygen, Depth: all 100%

2018:

- Velocity sensors: 100% (although data quality for one of the bottom landers was poor)
- pH sensors: ~60% average over all sensors (although we had close to 100% pH coverage at each buoy for the 2018 deployment considering that at least one of the two sensors was working at any one time)
- pCO₂ systems: North Buoy: 0%, South Buoy: 100% (average = 50%)
- Salinity, Temperature, Oxygen, Depth: all 100%

7.4 Notes on sensor performance

SeapHOx sensors in general performed better than the SAMI sensors, although they had their share of problems, including a malfunction of the CTD on one of them. Due to redundancy of data collected on the mooring, we were still able to calculate pH from this sensor, however. SBE SeapHOxes had 62% and 76% data coverage respectively, for an average of 69%. SAMIs had 60% and 28% data coverage, or an average of only 44% coverage. For the pCO₂ sensors, performance was also only fair, with the system on North Kelp not providing any usable pCO₂ data for 2018, but South Kelp working for the full deployment. We do note, however, that the environment in which they were deployed experiences extreme biofouling, contributing the higher-than-usual incidence of sensor and CO₂ system failures.

7.5 CO₂ system parameters calculated from moored surface (1 m) measurements

After final quality control on all 1-m depth observations of pCO₂ and pH (SAMI), we noted numerous gaps in the pH and pCO₂ records due to instrument failures. Fortunately, at least one of the sensors at each mooring site was usually operational during most of the rapid growth periods for kelp. Notable exceptions were during mid-April to mid-May 2017 at South buoy and prior to mid-March as well as part of May 2018 at North buoy (Figure 33), when gaps in both sensor records prevented calculation of other carbonate system parameters.

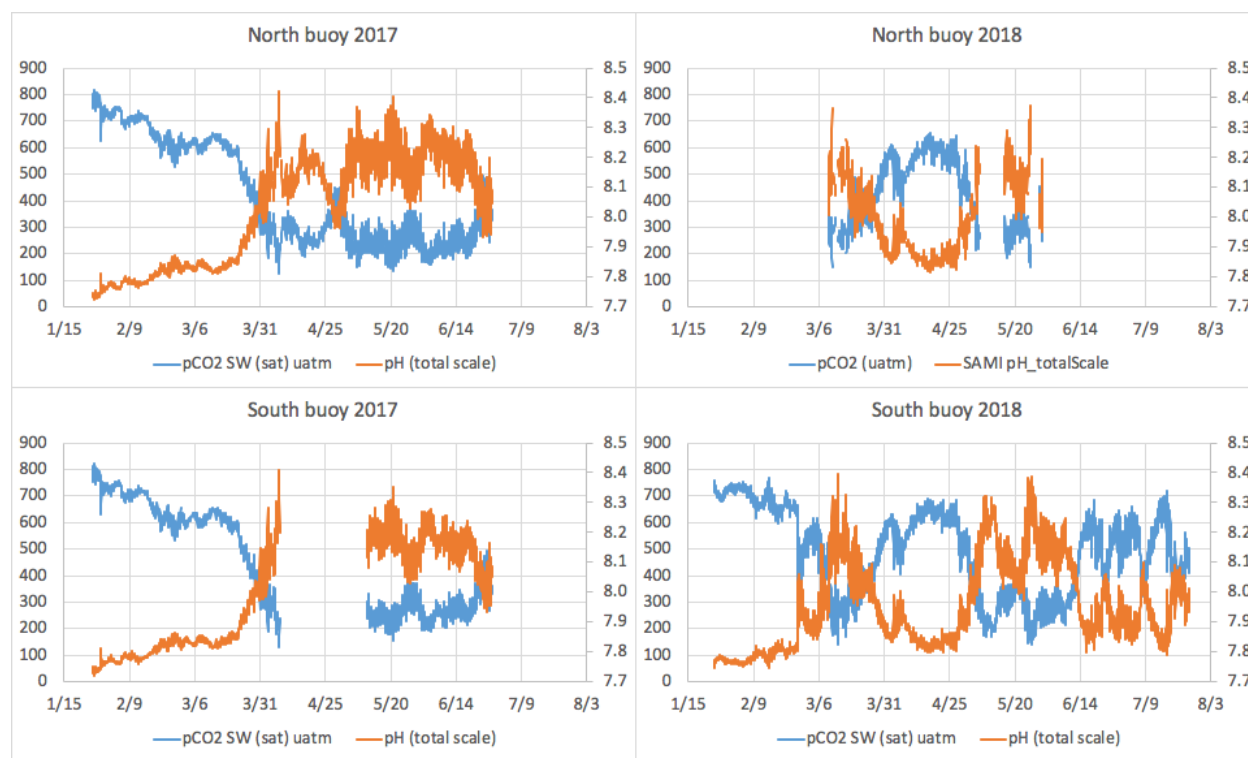


Figure 33 Finalized time-series of pCO₂ (µatm, left axes) and pH (total scale, right axes) measured at North (top) and South (bottom) buoys in 2017 (left) and 2018 (right). All are plotted on the same scale to facilitate comparison across sites and years.

For all other intervals, we used either pCO₂ (preferentially) or pH (when pCO₂ was deemed of lower quality), along with estimated total alkalinity (TA), based on a published empirical relationship between TA and salinity (Fassbender et al. 2016, Estimating Total Alkalinity in the Washington State Coastal Zone:

Complexities and Surprising Utility for Ocean Acidification Research, *Estuaries and Coasts*, DOI 10.1007/s12237-016-0168-z), to calculate all other carbonate system parameters (pH or pCO_2 [if one parameter was missing], dissolved inorganic carbon [DIC] concentration, aragonite and calcite saturation states (Ω_{arag} and Ω_{calc}), and Revelle factor [RF; a measure of buffering capacity]) using CO2SYS. Published work using the same pCO_2 and pH sensors, in combination with TA estimated using a salinity proxy, shows that the effect on the resulting uncertainty of calculated aragonite saturation state is half as high using the pCO_2 -TA pair ($\pm 5\%$) than it is using the pCO_2 - pH pair ($\pm 10\%$), even though the pH is directly measured rather than estimated by proxy (Sutton et al. 2016, Using present-day observations to detect when anthropogenic change forces surface ocean carbonate chemistry outside pre-industrial bounds, *Biogeosciences*, DOI 10.5194/bg-13-5065-2016). Thus, for all good finalized pCO_2 data, we used the pCO_2 -TA pair for CO2SYS calculations, which gives approximate resulting uncertainties on calculated Ω_{arag} of ± 0.05 at $\Omega_{arag} = 1$, ± 0.10 at $\Omega_{arag} = 2$, and ± 0.15 at $\Omega_{arag} = 3$. Errors on calculations done using pH as an input parameter would thus be twice as high (± 0.1 at $\Omega_{arag} = 1$, ± 0.2 at $\Omega_{arag} = 2$, and ± 0.3 at $\Omega_{arag} = 3$). Measurement uncertainties for pCO_2 and SAMI- pH (total scale) are $\pm 2 \mu atm$ and ± 0.018 , respectively (Sutton et al. 2016).

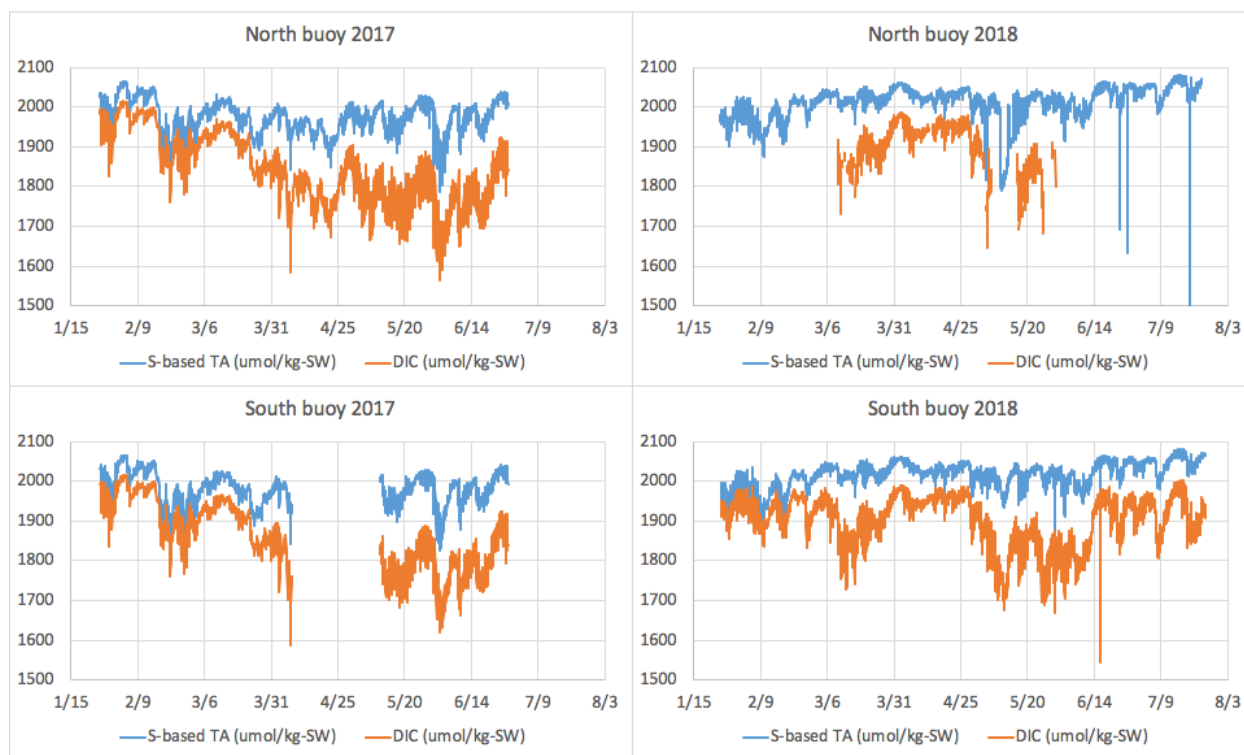


Figure 34. Estimated TA time-series (blue) and calculated DIC values (orange) for North (top) and South (bottom) buoys in 2017 (left) and 2018 (right). All are plotted on the same scale to facilitate comparison across sites and years.

Plots of calculated DIC and estimated TA (by S proxy) show that at both sites and both years, there was a progression toward a greater disparity between DIC and TA values (with DIC values always lower than TA values) as the growing season progressed, which we interpret as reflecting phytoplankton primary production (Figure 34).

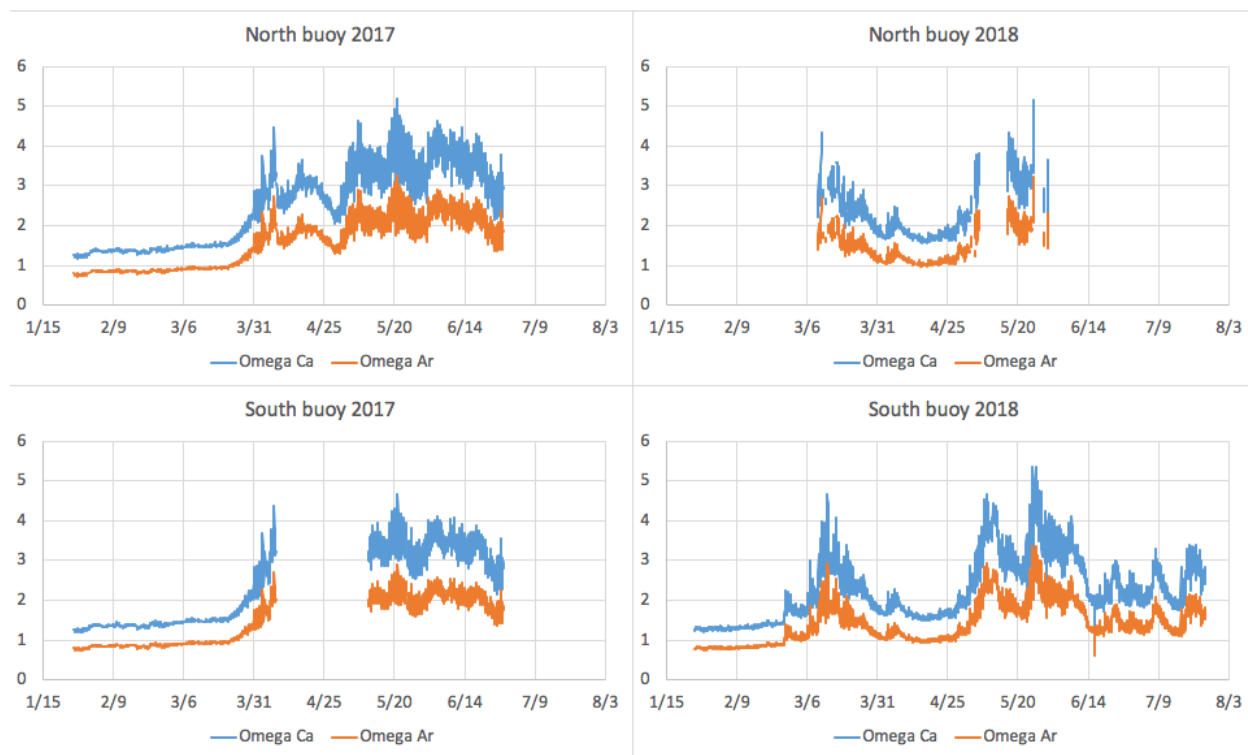


Figure 35. Calculated calcite (blue) and aragonite (orange) saturation time-series for North (top) and South (bottom) buoys in 2017 (left) and 2018 (right). All are plotted on the same scale to facilitate comparison across sites and years.

The calculated aragonite saturation time-series show that both sites had undersaturated conditions at the surface during winter and early spring in both years, and both sites had aragonite values hovering around 1 (saturation threshold) during April 2018 (Figure 35). While calcite saturation values were always supersaturated, values approached the saturation threshold for calcite (<1.5) during winter as well.

7.6 Sampling cruises and methods

We conducted 3 cruises per field season during the project, to sample seawater within and outside of the kelp plot. The 2017 field season cruise dates were March 9, May 25, and June 26. During the 2018 field season, cruise dates were shifted later to better capture the growing season and were conducted May 7, June 18, and July 23. During all but the March 2017 cruise, two passes were made through sampling stations, or a subset thereof (Figure 36). We attempted to sample during slack tides and on days with weaker tidal cycles to ensure maximum residence time within the kelp patch, on all cruises, however, vigorous circulation was unavoidable even during the weakest parts of the tidal cycle (Figure 37).

7.7 Carbon, nutrient, and other cruise measurements

On each pass through the kelp patch, CTD casts were done at 7–10 stations, with sensors mounted on the CTD

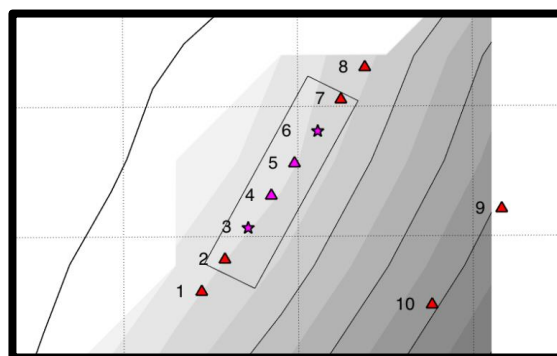


Figure 36. We originally selected ten sampling stations, eight of them falling along a transect representing the dominant flow direction (1–8 on the map) observed during the preliminary circulation study, and two of them outside the patch in a direction that should be unaffected by kelp patch biogeochemical influences (9–10).

frame measuring temperature, salinity, depth, and oxygen concentration from the surface to near-bottom waters. In addition, Niskin bottles collected seawater for subsequent analyses of biogeochemistry at depths of approximately 1–2, 3–4, and 10–20 meters. Measurements included DIC, oxygen, and nutrient concentrations (phosphate, silicate, nitrate, nitrite, and ammonium) and total alkalinity (TA) titrations (Figure 38). Maximum kelp densities were noted at ~3 m depth, so if kelp uptake of DIC and

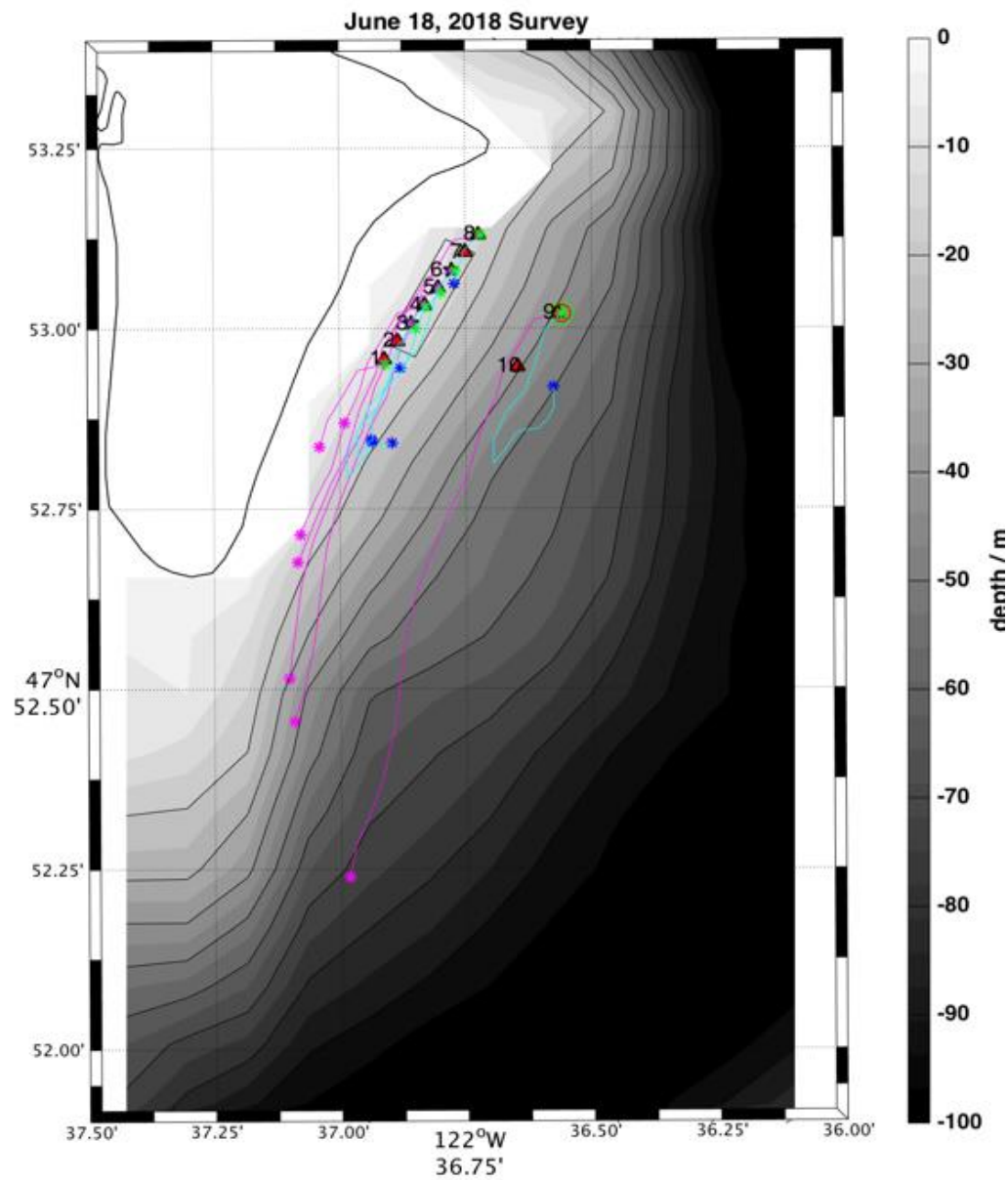


Figure 37. Estimate of the role of currents on CTD/bottle sampling during the June 2018 survey, accounting for water movement over the survey duration. Green stars show the actual survey stations. Magenta stars are estimated starting points for water parcels during the first of two surveys, referenced in time to the start of the survey, with their theoretical paths shown as magenta lines. The second survey of the day is shown in cyan and blue. Starting and ending stations for each of the two surveys are circled in green and red respectively (station 9 in this case for both surveys). Assuming spatially-uniform currents, most of the water sampled in the kelp patch during the first and second surveys started out south of the patch when sampling started at station 9.

production of dissolved oxygen (DO) were affecting carbon and oxygen dynamics in and around the kelp patch, we would expect to see the lowest DIC (highest DO) in the middle of the kelp patch and at the middle depths (3–4 m).

Water samples from cruises were analyzed within a few months after each season's cruises, using standard methods accepted within the chemical oceanography community (oxygen by Winkler analysis, nutrients using WOCE methods, DIC and TA as described in Dickson et al. 2007, *Guide to Best Practices for Ocean CO₂ Measurements*, PICES Special Publication No. 8). Results were plotted up by depth and according to position in the sampling transect to look for spatial patterns that may be associated with kelp drawdown of DIC.

After CTD, DIC, TA, and nutrient data were finalized, we calculated all additional carbonate system parameters, including pH (a measure of acidity), partial pressures of carbon dioxide (pCO₂), saturation states of aragonite (Ω_{arag}) and calcite (Ω_{calc}), and RF (lower numbers indicating better buffered seawater than higher numbers) using CO₂SYS and community-recommended dissociation constants for carbonic acid and other chemical species.

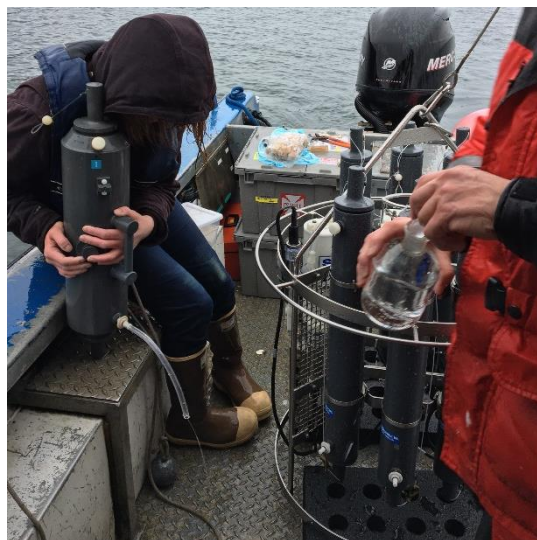


Figure 38. Sampling on one of the kelp patch cruises. The round metal structure is the frame holding the CTD (conductivity-temperature-depth) sensors and the small, gray Niskin bottles. A 500-mL glass sample bottle, used for collecting DIC+TA samples, appears in the foreground.

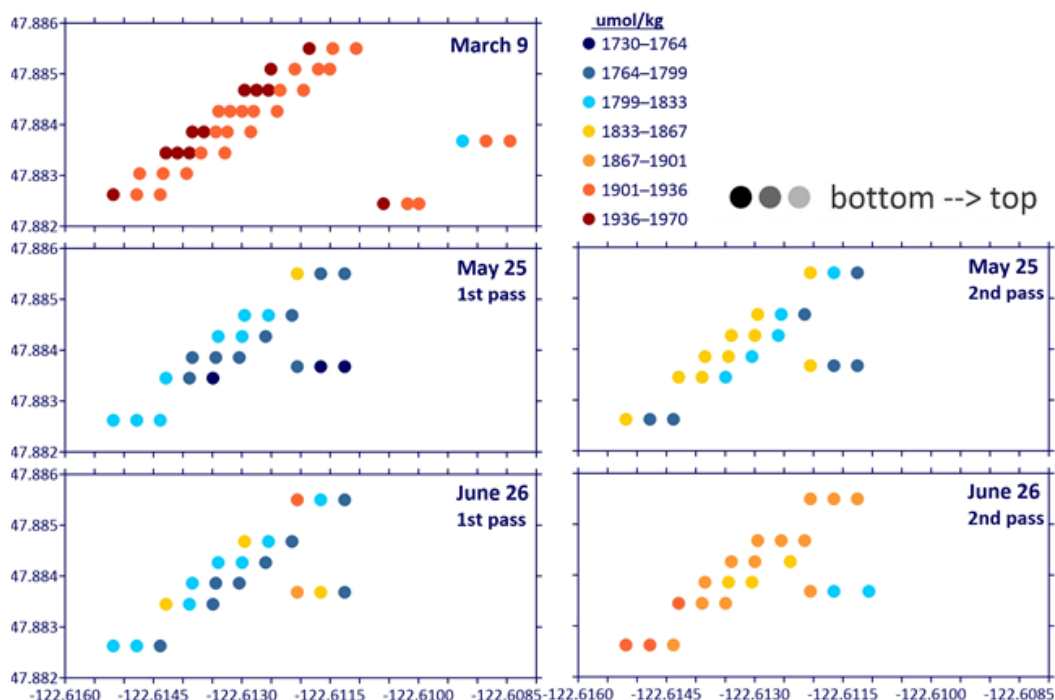


Figure 39. DIC concentrations ($\mu\text{mol/kg}$) from all stations and all cruises during the 2017 field season. We see no spatial or depth pattern that appears consistent with kelp uptake of CO₂ (a component of DIC) during any of the cruises. While there is lower DIC at the surface during the 2nd pass through the kelp array on May 25, we note that the lowest DIC values are at the edges or outside the patch, which is the opposite of what we would expect if kelp uptake was drawing down CO₂ within the patch. Highest DIC values were seen during the March cruise.

After an initial post-field season meeting each year, where preliminary results and interpretations were discussed, all cruise results were finalized, and final data were provided to the modeling and biological teams.

7.8 Cruise results summary: Measured variables

During both field seasons, we observed spatial and depth patterns that did not reveal substantial uptake of DIC or release of DO by kelp production (Figures 39–41, DO data were only available for 2017).

We note that the bins in the color scales for Figures 39–41 are somewhat broad, such that a DIC uptake signal could potentially be missed where the color scale is too coarse to reveal drawdown. However, we note that model-generated estimates of kelp drawdown of DIC ($\leq 1.5 \mu\text{mol/kg}$) suggest signals that would fall within the error on the DIC measurements ($\pm 2 \mu\text{mol/kg}$ or better, which represents $\sim 0.1\%$ uncertainty).

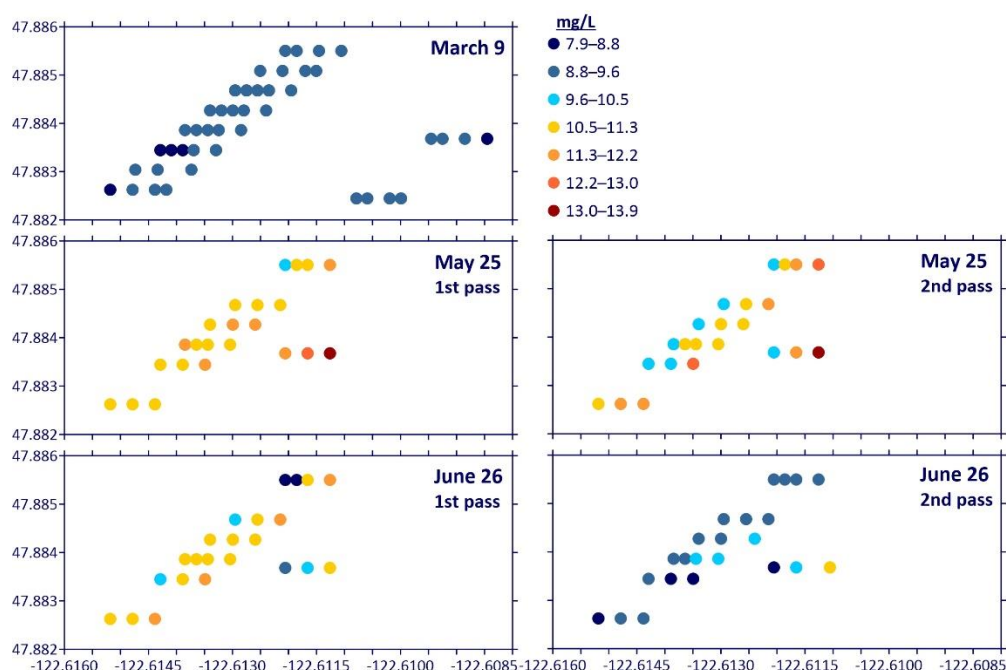


Figure 40. Oxygen concentrations (mg/L) from all stations and all cruises during the 2017 field season. Again, we see no sign of spatial or depth differences in oxygen reflecting the expected patterns of oxygen within and around the kelp patch if kelp production of DO were significant. In contrast, again, we see on more than one occasion that the surface sample at the station outside the patch (the dots to the right of the transect line) have the highest DO values during a given cruise. Lowest DO values were observed during the March cruise.

We also note that the time between adjacent CTD casts (19.5 ± 6.4 minutes) is roughly as long as the residence time of seawater in the patch, such that we could never truly capture the spatial pattern in the kelp patch vicinity, as the time taken to complete a pass through the stations would be at least five times the residence time of water in the patch (i.e., $7\text{--}10$ stations $\times \sim 20$ min/station = $140\text{--}200$ min/survey vs. 30 min residence time). Thus, a mass of water would long since have left the patch between the time we started the sampling pattern and the time we occupied the mid-patch station.

7.9 Calculated parameters of relevance for biology

Saturation states for the calcium carbonate mineral form aragonite (Ω_{arag}) are of particular relevance to

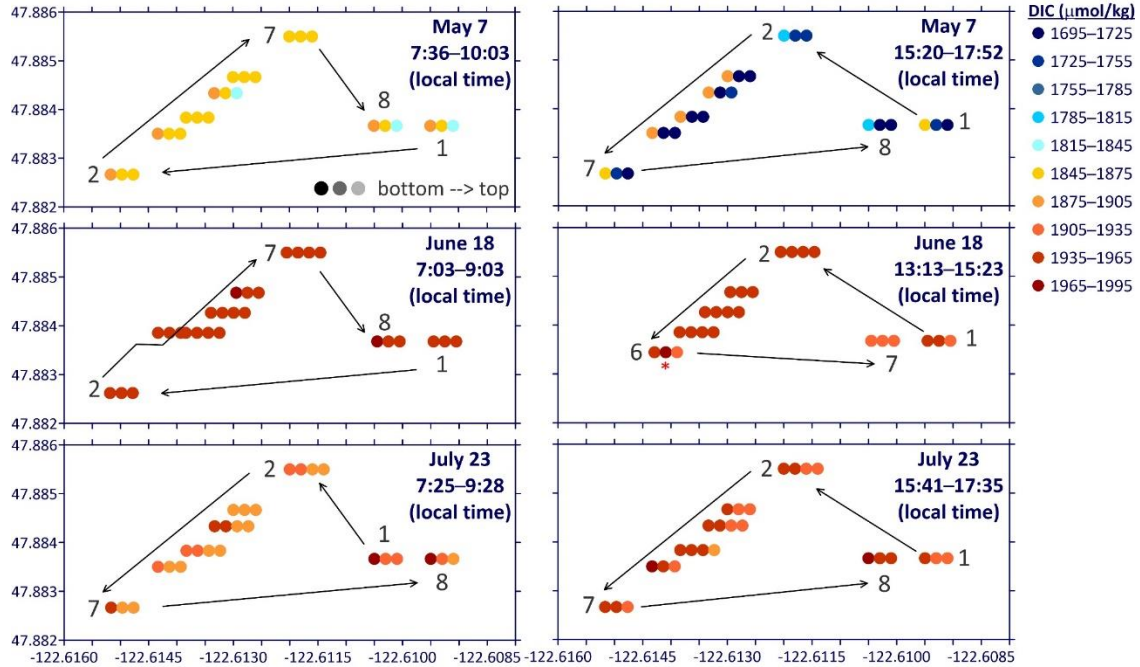


Figure 41. DIC concentrations ($\mu\text{mol/kg}$) from all stations and all cruises during the 2018 field season. Spatial and depth patterns are similar to 2017 in terms of not showing any conclusive spatial pattern reflecting kelp uptake near the surface in mid-patch on any of the six passes through the patch. During the afternoon pass through the patch on May 7, the two surface samples at all locations suggest that a local phytoplankton bloom may have drawn down CO_2 throughout the sampling area. This sampling event also corresponded with the largest freshening event seen during either field season's cruises (salinities near 28, not shown).

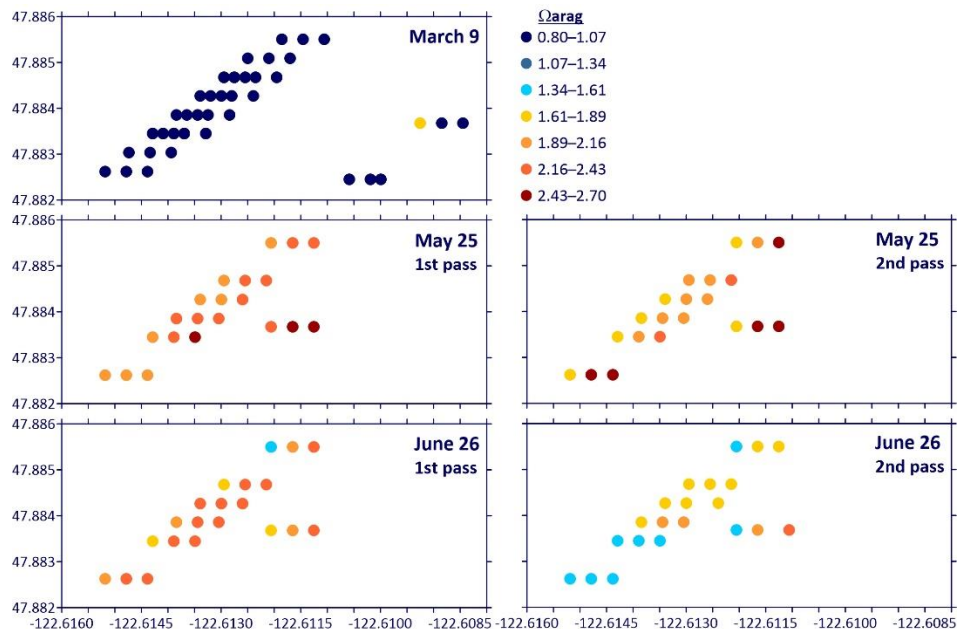


Figure 42. Aragonite saturation states (Ω_{arag}) from all stations and all cruises during 2017. We note that the only cruise during either year that showed any undersaturated conditions was the March 2017 cruise.

shellfish calcification and dissolution. Here we show Ω_{arag} values for all cruises in both years (Figures 42

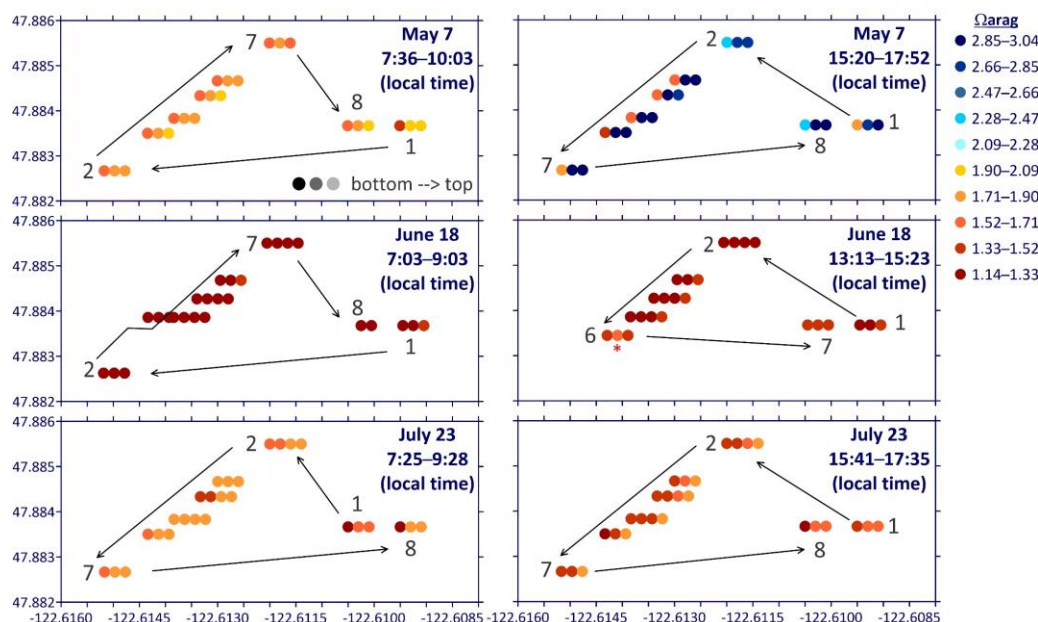


Figure 43. Aragonite saturation states (Ω_{arag}) from all stations and all cruises during 2018. (Note the opposite direction of color scales between previous figure and this one.)

and 43). Values above 1 represent conditions of supersaturation, where calcification should be relatively easy, whereas values under 1 are undersaturated or “corrosive” and dissolution processes may become more prevalent. However, sensitivity to saturation states can vary across species, so their realized dissolution threshold may occur substantially higher than the thermodynamic threshold of 1.

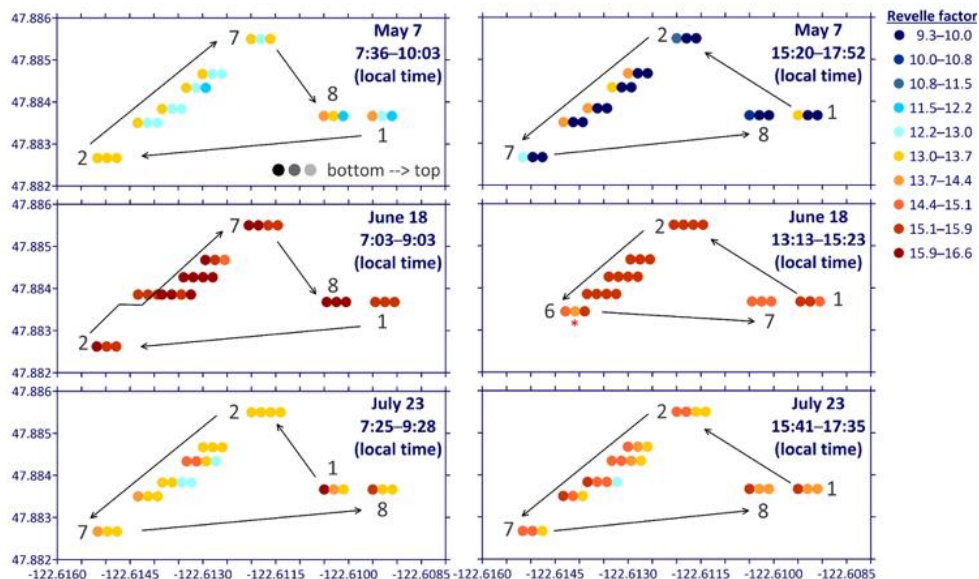


Figure 44. Revelle factor values, all stations, all cruises 2018. Results suggest that pCO_2 changes of 9–17 μatm per 1 $\mu\text{mol/kg}$ increase of DIC would have resulted near the kelp patch experiment due to addition of CO_2 . Alternately, we should have seen a decrease of 9–17 μatm pCO_2 per 1 $\mu\text{mol/kg}$ decrease of DIC due to kelp uptake of DIC.

The overall range of Ω_{arag} values spans roughly two units in each year (0.8–2.70 in 2017, 1.14–3.04 in 2018). Lowest values overall were in March 2017, with secondary minima at some stations and depths in June 2017 and lowest 2018 values occurring during the June 18th cruises. Highest Ω_{arag} values were observed during May cruises in both 2017 and 2018.

Revelle factor is closely related to the seawater buffering capacity, which is what the kelp array was deployed to increase, for the benefit of other organisms. RF is expressed as the rate of change of pCO_2 (in μatm) per unit change in DIC (in $\mu\text{mol/kg}$). So, for example, an RF of 19 indicates that pCO_2 would increase by 19 μatm when DIC increases by 1 $\mu\text{mol/kg}$ due to respiration or anthropogenic CO_2 uptake. Conversely, at low RF (e.g. 8), CO_2 would increase by only 8 μatm per 1 $\mu\text{mol/kg}$ change in DIC. The year 2 cruise data show (Figure 44) that, while there are significant differences among the six cruise passes through the kelp array (likely due to differences in water masses and physical processes), we lack evidence of any major change in buffering capacity due to the presence of the kelp patch.

7.10 Additional deployment of pH and temperature sensors - 2018

Deployment: In April 2018, PSRF deployed four custom built durafet-based sensors to monitor temperature and pH in and outside of the kelp array. All sensors were secured to lines and deployed at depths of approximately 2m. One sensor was deployed at the Hansville Buoy (47.907 N, 122.627 W), which was selected for its presumed independence from the influence of the kelp array. Another sensor was deployed at the southern edge of the kelp array. Two sensors were jointly deployed at the center of the kelp array. In August 2018, PSRF retrieved all sensors, and WDNR downloaded and analyzed data. All sensors collected measurements of temperature and pH at 10-minute intervals, for

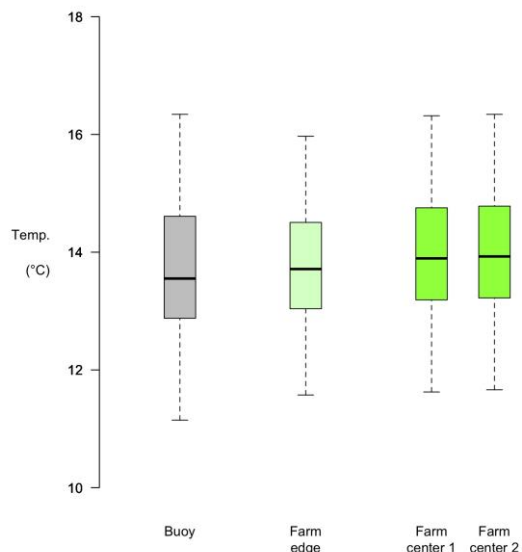


Figure 45. Temperature between 4-26-18 to 8-6-18 (n=14,832).

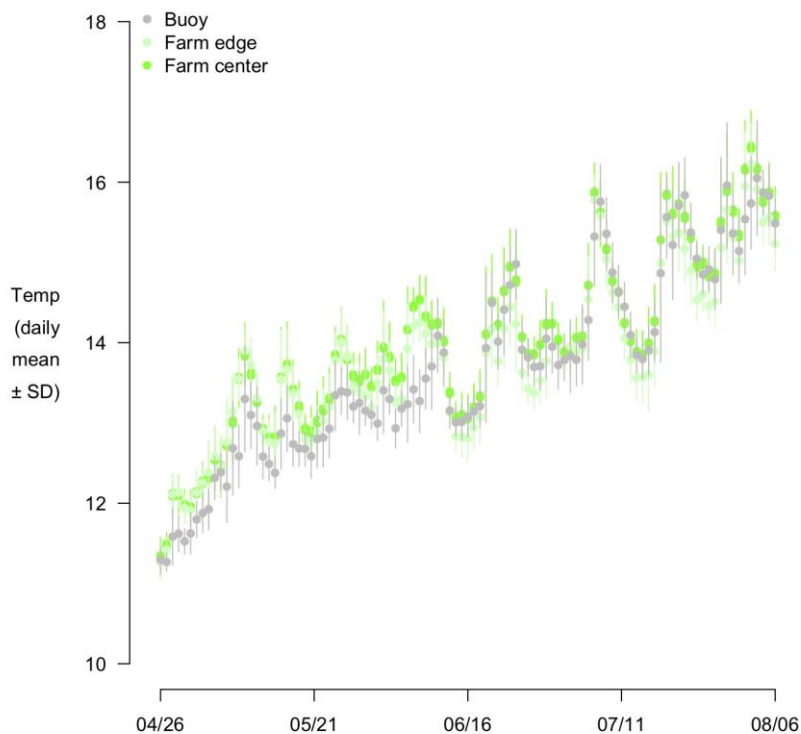


Figure 46. Daily means in temperature from 4-26-18 to 8-6-18.

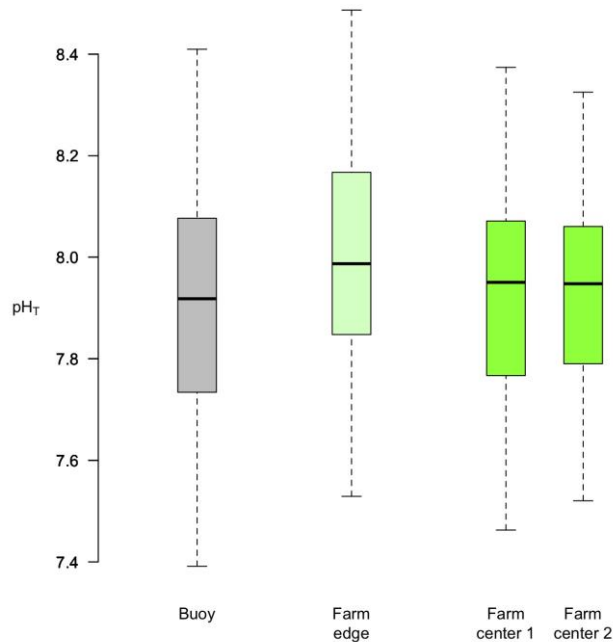


Figure 47. pH_T between 4-26-18 to 8-6-18 (n=14,832).

a total of 14,382 observations across the period of deployment.

Sensor performance: On average, the jointly deployed sensors at the center of the kelp array yielded similar observations of pH (mean difference = 0.0002 pH units) and temperature (mean difference = 0.0321°C), offering grounds for confidence in the reproducibility of measurements. The sensor at the edge of the kelp array appeared to malfunction from 6-30-18 to 7-2-18, registering unrealistic temperature values (<0°C). Immediately thereafter, the sensor registered pH readings that were notably higher than other instruments until roughly 7-22-18. These issues could have been due to a faulty connection between the durafet and the datalogger; similar malfunctions have occurred during other deployments because of physical disturbance. Besides the sensor at the edge of the kelp array, there was no evidence of instrumental failure (e.g., loss of durafet signal) or battery failure (<3V for the durafet and/or <9V for the data logger) in other sensors.

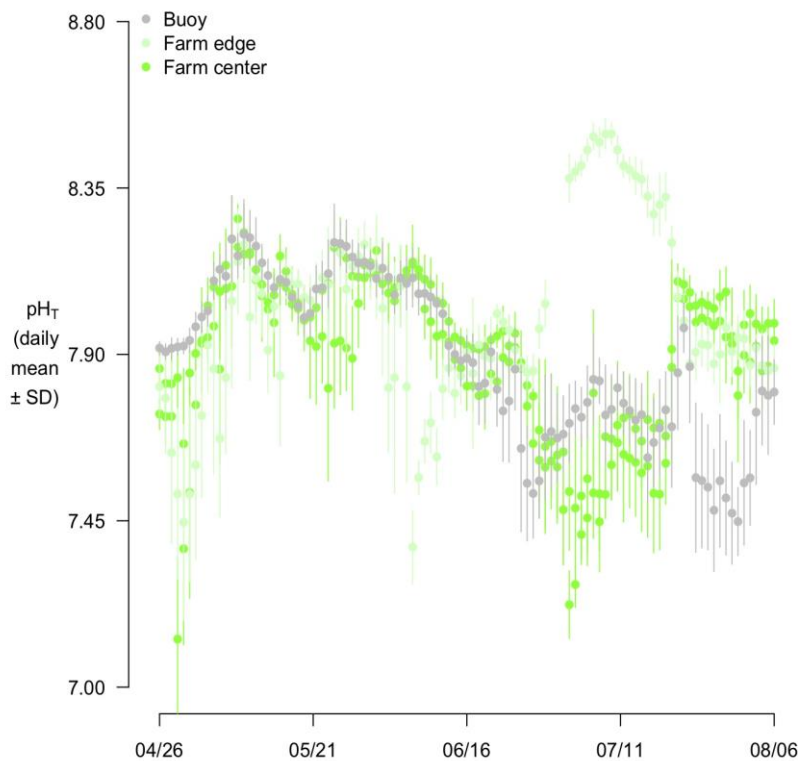


Figure 48. Daily means in pH_T from 4-26-18 to 8-6-18.

Effects of kelp array: Over the period of deployment, the center of the kelp array was slightly warmer ($14.0 \pm 1.2^{\circ}\text{C}$) than the edge of the kelp array ($13.8 \pm 1.1^{\circ}\text{C}$) and the buoy ($13.7 \pm 1.3^{\circ}\text{C}$), though differences were negligible (Figures 45 and 46). On average, pH at the center of the kelp array (7.90 ± 0.22 pH units) was essentially the same as pH at the buoy (7.89 ± 0.23 pH units). pH at the center of the kelp array was lower than pH at the edge of the array (8.00 ± 0.27 pH units); however, excluding data from the period of possible malfunction (6-30 to 7-22-18), pH at the edge of the array (7.91 ± 0.22 pH units) was similar to the center (Figures 47 and 48).

8. Biological assessment of seaweed cultivation array

Authors: Nina Bednarsek, Dick Feely

Biological assessments were performed at the Hood Head investigation site in 2017 and 2018, with subsequent laboratory experiments conducted in 2019.

8.1 Assessments at Hood Head

Beginning in June 2017, 4 mesocosms (3 meter long columnar sailcloth nets) were pre-deployed at Hood Head to facilitate rapid deployment of pteropods following collection with the boat. On June 11th, Drs. Nina Bednarsek and Dick Feely collected ~300 pteropods in deep water during an all-night sampling trip off Whidbey Island aboard a NOAA contract vessel equipped with a davet and BONGO net. Two of the 4 mesocosms pre-deployed at Hood Head were filled with pteropods, one within the kelp array attached to one of the kelp lines, and one outside the kelp array attached to one of the perimeter lines on the southwest side. The pteropods were transferred on June 12th. Approximately two-thirds of the pteropods were recovered on June 19th from the mesocosm positioned within the kelp array. Pteropods from the mesocosm positioned on the outside perimeter line were recovered in July and subsequently analyzed by Dr. Bednarsek.

Two of the original mesocosms were redesigned for the 2018 deployment; mesh was too small to enable effective water circulation, and there were holes near the zippers at both ends that needed to be covered to prevent escapement. In addition, we built 4 new, more structurally sound mesocosms. On June 9th, 2018, we deployed the 2 old and 4 new mesocosms; 4 within the kelp farm and 2 around the ORCA mooring site. The night before the deployment, we conducted overnight pelagic gastropod sampling in the northern part of the main basin of Puget Sound. Timing of sampling was chosen to catch pteropods and gastropods (combined as ‘pelagic calcifiers’) as they were vertically migrating towards the surface during the nighttime. We collected 240 *Limacina helicina* individuals, the most common and important pteropod species in the Puget Sound. We also collected numerous pelagic gastropods that were deployed in the mesocosms together with pteropods. On June 10th, the day of pteropod deployment at Hood Head, only intact organisms were distributed between 6 mesocosms, with 60 individuals in the control mesocosms, and the remaining 40 between four mesocosms in the kelp array. Although not enumerated, we also deployed pelagic gastropods in the same mesocosms with pteropods.

While the kelp mesocosms were deployed with the use of weights, diver assistance was needed with the deployment and recovery of the newly designed mesocosms. Control samples of pteropods and gastropods (n=10) were preserved in 100% ethanol and brought to the lab for scanning electron microscopy (SEM) analysis to investigate if any shell dissolution had already occurred in the field, and to establish baseline dissolution levels prior to mesocosm exposure. In addition to the mesocosms, we deployed meshed boxes with individual Pacific oyster (*Crassostrea gigas*; sample size N =515) and Olympia (*Ostrea lurida*; sample size N= 379) oysters, and blue mussels (*Mytilus trossulus*; sample size N=244) for six weeks, starting mid-day with the overall exposure of 6 weeks. The oysters and mussels were deployed in mid-May period, approximately 4 weeks prior to pteropod deployment.

Pteropods and other pelagic gastropods that were captured in the BONGO net remained in the mesocosms for 2.5 weeks, with the termination of the exposure experiments occurring on June 29th. During this time, pteropods were exposed to a variety of carbonate chemistry conditions, including phytoplankton blooms, diel variability in carbonate conditions, and other conditions potentially impacting level of shell dissolution in the mesocosms. Two of the newly constructed mesocosms were lost before the pteropod retrieval. Water samples were collected at these sampling locations for corresponding DIC/T-alk analyses. Instead of mature organisms that were planted in the mesocosms, we retrieved much

smaller individuals, indicative of the spawning activities in the mesocosms and subsequent mortality of the larger, mature organisms. Smaller (<150 μ m) individuals were preserved in 100% ethanol for subsequent shell examination under SEM. In addition, we retrieved the oysters and mussels, and collected kelp samples that have been exposed in the field for approximately 6 weeks.

We successfully obtained pteropods and gastropods from three mesocosms: two treatment mesocosms from the kelp array at the edge and one at the mid-array. While the pteropod retrieval success was low, we managed to retrieve several gastropods, which were combined together with pteropods (N=26) into the 'pelagic calcifiers' group for the subsequent analyses. Out of 26 organisms, 22 were retrieved at the 'edge', while 5 were retrieved within the kelp ('mid' treatment). These organisms were analyzed against the control samples (n=10) that were not exposed in the field and did not show any shell dissolution.

For pelagic calcifiers, we developed a categorization scheme of dissolution following Bednarsek et al. (2012) and Diaz et al. (2019) protocol. This scheme categorizes the severity of dissolution into three categories and includes the scores of different features as well as the patch severity.

Evaluating shell dissolution in pelagic calcifiers (Figure 49), preliminary statistical comparisons between different sites ('edge' and 'mid') showed significantly different dissolution levels among the control, edge and mid treatment (Kruskal-Wallis

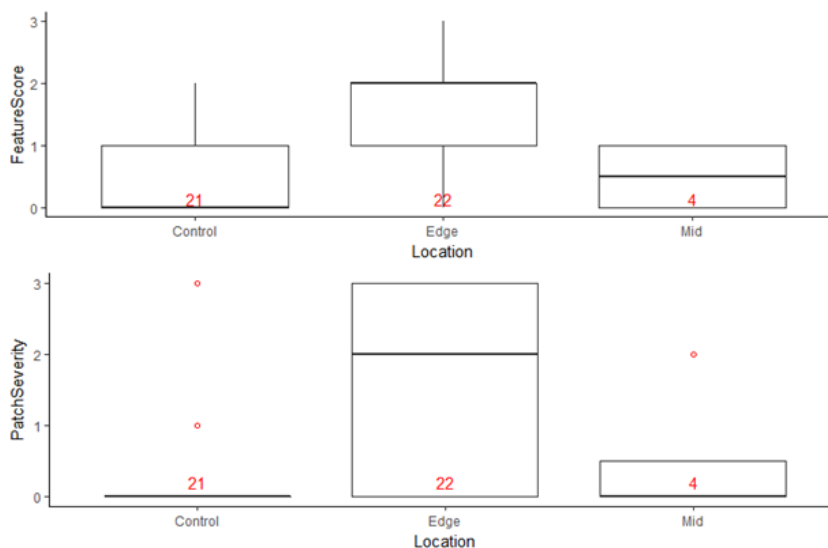


Figure 49. Shell dissolution of pelagic gastropods from the control (pre-exposed), the 'edge' and 'in'. Dissolution Score differed significantly among the control (median of 1), edge (median of 2), and mid (median of 1) treatments (Kruskal-Wallis rank sum test: $H = 6.6273$, $df = 2$, p -value = 0.03638).

rank sum test: $H=6.6273$; $df=2$; $p=0.03638$). Feature Score differed significantly among the control, 'edge', and the 'mid' treatments (Kruskal-Wallis rank sum test: $H = 14.773$, $df = 2$, p -value = 0.0006). Control and edge patch severity was significantly different ($p=0.0006$); however control and mid ($p=0.9236$) and edge and mid ($p=0.0706$) were not significantly different (Dunn multiple comparison test with Benjamini-Hochberg adjusted p -values). Patch severity differed significantly at significance level $p<0.05$ among the three treatments (Kruskal-Wallis rank sum test: $H = 12.868$, $df = 2$, $p = 0.0016$). It has to be noted that the dissolution scores are preliminary results and subsequent analyses are expected.

Similar to the pelagic gastropods, shell dissolution analyses were conducted for Olympia and Pacific oysters, as well as for the bay mussels. Shell dissolution was observed within the upper crystalline layer of the growing edge of the three species, the area of active growth during the exposure in the field. We analyzed 5 organisms from each treatment, 'mid', 'edge' and 'out' treatment, generating some 20-30 images for each shell. The features observed were exposed crystals, crosses and several other features observed during the shell analyses observations, such as the circles, hexagons, folds, all found in the crystalline structure (Figure 50). For the bay mussels, different scoring was used because the growth

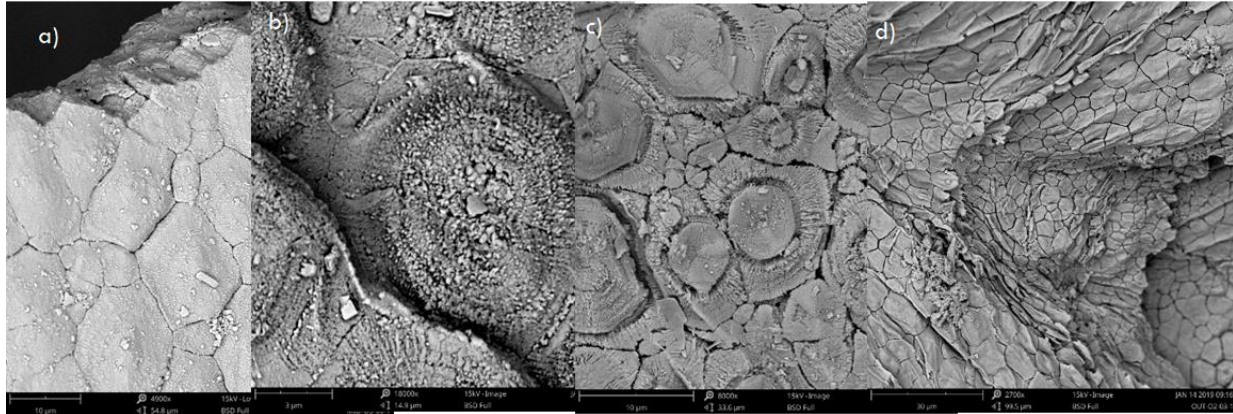


Figure 50. Dissolution scoring features that were evaluated in Olympia (*Ostrea lurida*) and Pacific (*Crassostrea gigas*) oysters. The intact shell (a) can be under various treatments modified into the exposed crystals (b), circles (c), or folds (d).

patterns are different compared to both the oysters. We evaluated the amount of porosity, where porosity score progressively increases with the amount of observed porosity (Figure 51).

Similar to the pelagic gastropods, shell dissolution analyses were conducted for Olympia and Pacific oysters, as well as for the bay mussels. For both of the oyster species, there was significantly more dissolution in the 'out' treatment compared to the mid ($F=9.402$; $p=0.0009$: Figure 52). While for Olympia, the 'edge' and 'mid' was also significantly different, this was not the case for the Pacific oyster, and confirmed statistical increase in porosity in the 'out' compared to the 'mid' treatment ($p<0.05$).

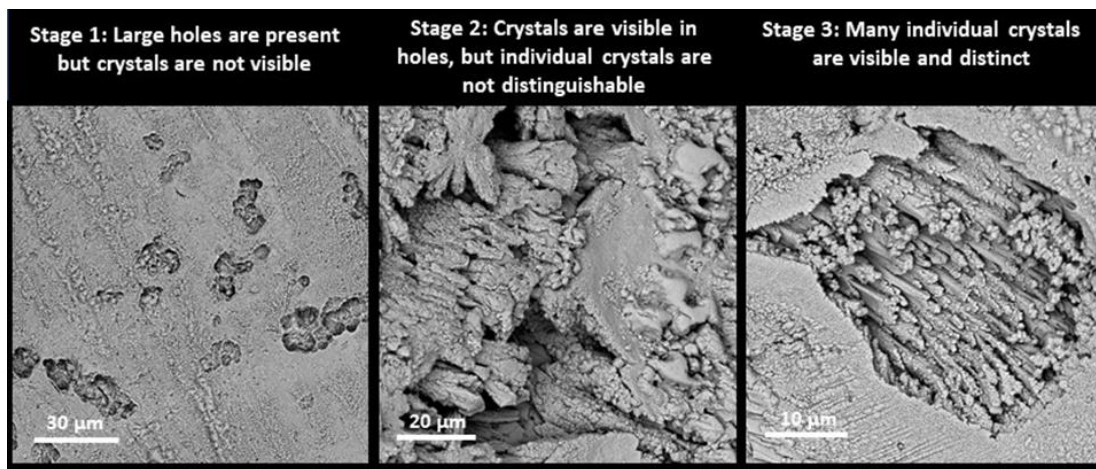


Figure 51. Dissolution scoring for the bay mussels (*Mytilus trossulus*) was based on the porosity that was categorized into three stages (Stage 1-3).

We also measure length and weight of all investigated organisms from both Pacific and Olympia oysters at 'mid', 'edge' and 'out' treatment to be able to assess any potential difference in growth at specific locations. Our results demonstrated significantly faster growth, in both length and weight parameters, in Olympia oyster in the 'mid' treatment, while the growth in the 'out' treatment and 'edge' was slower (Figure 53). As for the Pacific oyster, much more variability was observed in the pre-exposed samples. Nevertheless, the slope of length extension over time demonstrated fastest growth for the 'mid' and 'edge' treatment and slower extension in the 'out' treatment. The same was observed for the weight increase in the 'edge' treatment compared to the 'out', while the shells in the 'mid' treatment were not

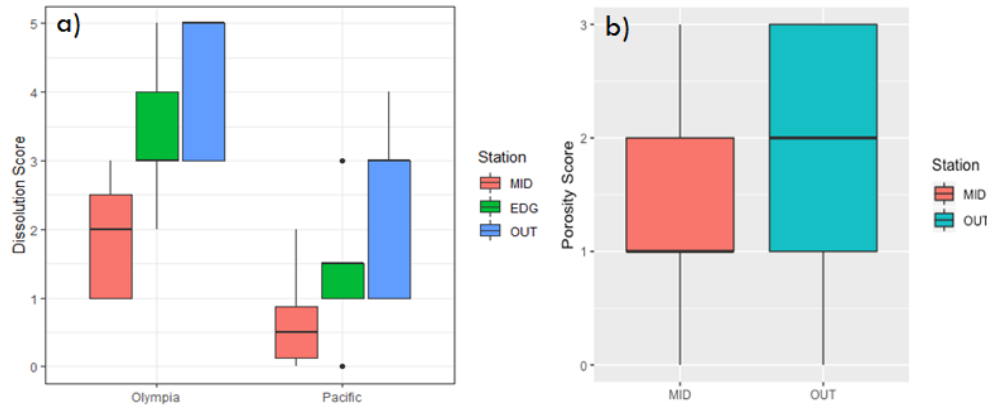


Figure 52. Box plot of dissolution score of Olympia (a) and Pacific oyster, as well as the bay mussel (b) after the exposure at three stations are indicated in colors (Out=red; Edge=blue; Mid=green).

significantly different from the 'out' (Figure 53). Such analyses were not possible for the bay mussels because the pre-exposed organisms were not measured.

The overall results from analyses indicate that the kelp provided improved habitat conditions with respect to OA in which examined pelagic and benthic calcifiers were growing, with faster growth and less dissolution indicating that the overall cumulative exposure improved calcifiers' capacity to calcify and their health. Our preliminary results using the isotopes to investigate trophic transfer suggest that it is predominantly the improved carbonate chemistry conditions that contributes to observed positive biological responses in the oysters, while food availability within the kelp array plays only a minor role.

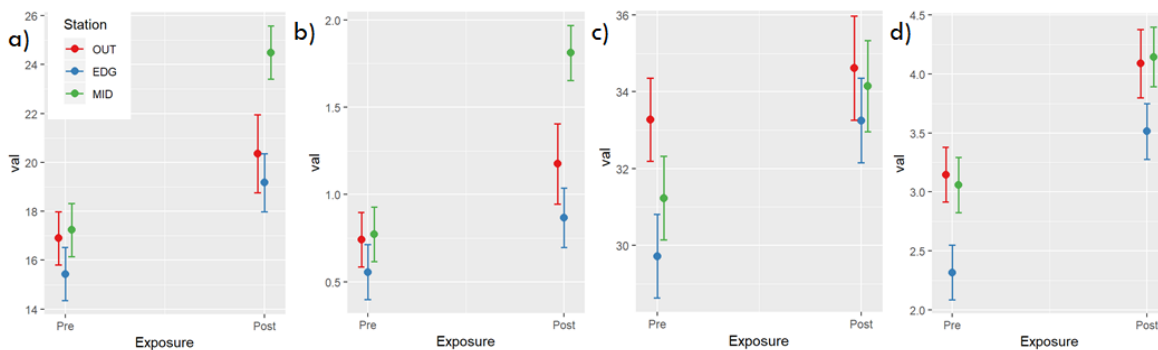


Figure 53. Length and weight increases of the Olympia oyster (a,b) and Pacific oyster (c, d) before the exposure (Pre) and after the exposure in the field (Post). The stations are indicated in colors (Out=red; Edge=blue; Mid=green).

8.2 Assessments in the laboratory

8.2.1 Introduction and methodology

Conducting the fieldwork before the experiments helped us investigate the extent of expected positive effects of kelp array in the field. We observed positive effects (i.e., reduced dissolution and increased growth) on pelagic (pteropods and gastropods) and benthic calcifiers (Olympia and Pacific oysters, bay mussel) observed inside the kelp farm compared to outside. However, because of limited sampling opportunities during the six-week exposure in the field, we formed hypotheses that needed to be mechanistically tested in a laboratory setting. Predominantly, we needed to address the question of what is a minimum duration of exposure to conditions inside the kelp to observe improved biological responses

in calcification and growth. In addition, we needed to understand if only improved carbonate chemistry conditions, and not food availability characteristic for the kelp farm, contributes to increased growth under favorable conditions for calcification.

To do so, we conducted a set of dynamic experiments in the Southern California Coastal Water Research Project's (SCCWRP) state-of-the-art laboratory, mimicking daily dynamic conditions at the kelp farm as closely as possible. Our goal was to determine if the kelp farm can mitigate against OA by generating favorable habitat (conditions) for the calcifying organisms.

The experiments involved the spat life stage of Olympia (*Ostrea lurida*) and Pacific (*Crassostrea gigas*) oysters. 2,000 spat of each species were kept in a variety of experimental treatments for 6 weeks, with biological parameters measured every 2nd week. During the treatments, the oysters were fed the 'Shellfish Diet', which is a mixture of six marine microalgae used in hatcheries for feeding oysters. Conditions for each treatment were stable and consistent in the system from weeks 1 thru 6. To avoid ammonia build-up or low oxygen conditions that could have potentially harmed the oysters or confounded results, we monitored ammonia and oxygen daily in all experimental bottles.

We had five distinct treatments (85 bottles total), and each treatment had 5 replicates, with 20-30 oysters in each replicate. Based on model outputs, we tested two complementary hypotheses: 1) small-scale changes of increased amplitude and diel frequency (with two peaks and two valleys over a 24-hour period) of favorable saturation state conditions can create benefits for the calcifiers, and 2) cumulative exposure over prolonged duration results in cumulative positive effects.

We chose the design, duration and amplitude and the frequency of exposure to align with and validate field data as close as possible. Since we were not able to replicate small scale changes (a maximum increase of 0.025 unit change in aragonite saturation state), we focused on replicating the amplitude and the frequency of the exposure to be reflective of the conditions in the kelp array. As such, control treatment with mean pH=8 and adherent variation simulated the conditions in the kelp array in its earlier growth phases when the daily amplitude was not so distinct (Treatment #1). Later in the season, the amplitude of approximately 0.2 pH units was much more pronounced. To reflect this amplitude, one of the laboratory experimental conditions was designed as pH=8 as a mean value with two peaks and two valleys over a 24 hour period, starting from pH 8.0 with amplitude 0.2 (i.e., pH varied from 7.9-8.2) and frequency of exposure with two peaks and two valleys over a 24-hour period (Treatment #2). The transition between high and low pH states took 3 hours and endpoint conditions were held for 5 hours. Treatment #2 is a focus of the remainder of this report, referred to as the "kelp treatment".

Furthermore, although the mean pH conditions of the Treatment #3 were not entirely reflective of the kelp conditions, the amplitude of the exposure was, hence we use the treatment of mean pH of 7.7 and amplitude of 0.2 pH unit change (e.g., pH varied from 7.5-7.9) to be partially reflecting kelp conditions. Treatment #2 compared to #3 would help discern the effects of lower pH combined with reduced frequency on the oyster biological effects.

For mechanistic underpinning of the observed biological responses, we have also added two additional experiments. As such, Treatment #4 had pH 7.7 and amplitude of 0.5 (i.e., pH varied from 7.2-8.2), which was the maximum amplitude observed in or outside the kelp less frequently and was used to understand the impact of high amplitude variation. Lastly, to be able to discern the effects of mean vs dynamic exposure on the oysters, we added Treatment #5 with static mean pH of 7.7 and no amplitude in exposure added.

Measurement of biological parameters: We collected the same biological parameters as in the field (i.e., increase in length and weight, shell dissolution and growth irregularities) to compare lab and field treatments, and to provide a comprehensive biological assessment of the oysters. Length and weight were measured for each individual, amounting to 8,000 data points. It is important to note that we have labelled each individual oyster to be able to track each individual through time and treatments because this yields much greater statistical power (Figure 54).

To conduct measurements faster, we developed a machine learning algorithm that automatically recognized oyster species, and length of each individual. Shell biomineralization features were identified and semi-quantified using SEM, focusing on features that are positive (i.e., folds, cracks, wrinkles) and negative signs (i.e., exposed crystals, circles, crosses, irregular calcification patterns) of net calcification. Finally, we assessed physiological and energetic status of organisms (i.e. ingestion/feeding, respiration). For ingestion and feeding, we recorded changes in feeding requirements and respiration, measured over 4-hours on 8 oysters of each species and treatment on a biweekly basis. However, since the ingestion measurements require at least 6-7 hours to be conducted, this time interval was incompatible with the exposure in the Treatment #2, and as such, the ingestion measurements were not conducted on the samples from the kelp-like Treatment #2. The results of additional biological responses of transcriptomics are still in processing, and so are the statistical analyses of the growth in various conditions. The latter is largely due to enormous variability in growth between individual oysters.

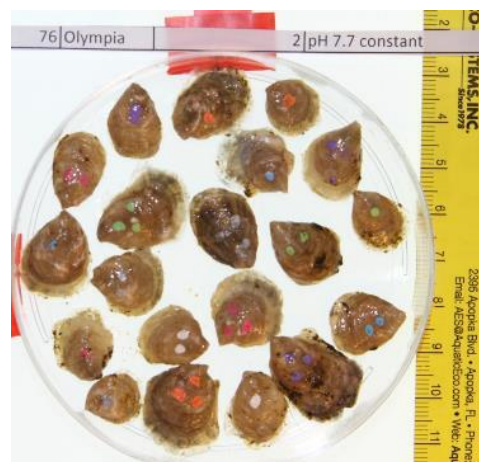


Figure 54. Individually marked Olympia oysters (treatment 2).

8.2.2 Results

Positive changes in calcification in the kelp experimental conditions

Olympia oysters showed an increase in calcification as measured by positive shell features (i.e., folds, cracks, wrinkles) in the kelp treatment (blue, left panel) compared to the dynamic treatment (red, left panel) indicative of outside of the kelp farm. Significant differences in calcification between the two

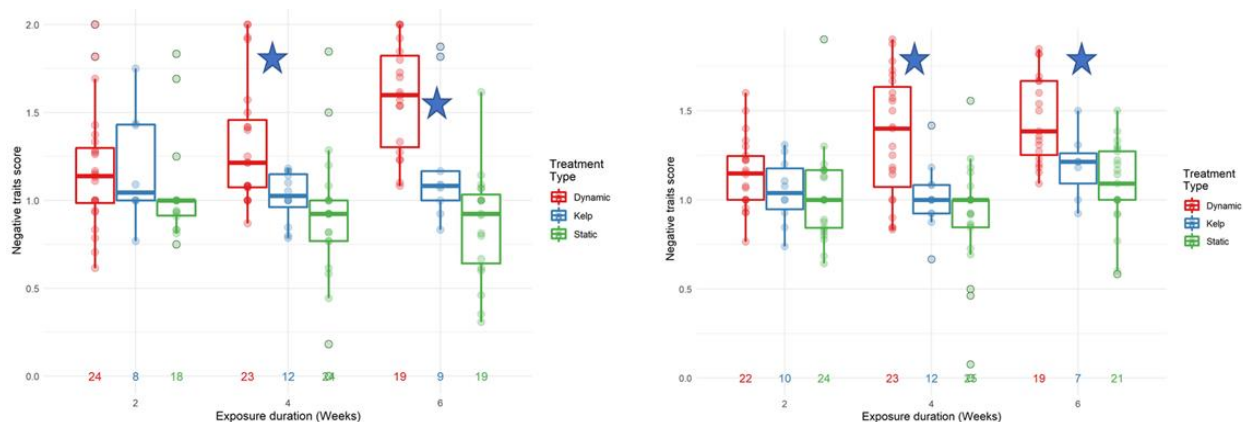


Figure 55. Comparison of dynamic conditions (Treatment # 3) and static conditions (Treatment #1) with the kelp (Treatment #2) for Olympia (a) and Pacific (b) oyster pointing towards reduced negative traits (exposed crystals, irregular growth).

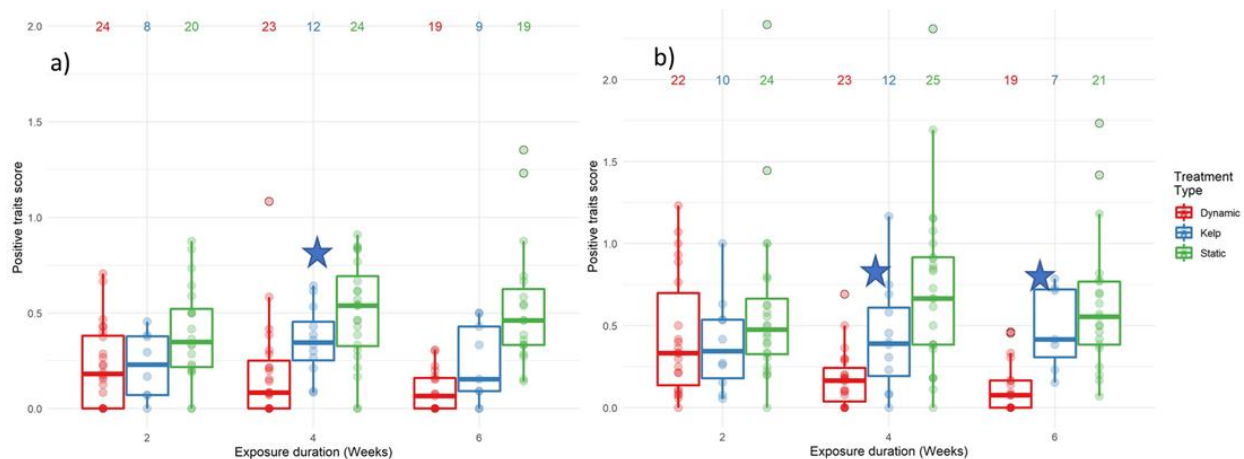


Figure 56. Comparison of dynamic conditions (Treatment #3) and static conditions (Treatment #1) with the kelp (Treatment #2) for Olympia (a) and Pacific (b) oyster towards the biomineralization features (folds, cracks, wrinkles).

treatments were noticeable already in week 4, with significant improvements also demonstrated in week 6. There were no observable positive calcification differences in week 2. The same improved calcification results were observed for Pacific oysters (right panel) after week 4 (Figure 55).

Reduced shell dissolution in the conditions of the kelp farm compared to the dynamic conditions

Olympia oysters showed decreased dissolution (as determined by negative shell traits – e.g., exposed crystals, irregular growth) in the kelp treatment) compared to the dynamic treatment representative of outside of the kelp farm. Significantly less dissolution was noticeable in week 4 and continued in week 6. Reduced dissolution was not observed in week 2. The same reduced shell dissolution results were observed in Pacific oysters after week 4 of exposure in conditions similar to the kelp farm (Figure 56).

Reduced severity of shell dissolution in the conditions of the kelp farm compared to the dynamic conditions

In addition to comparing the extent of dissolution, we also compared the severity of dissolution between the kelp and dynamic (i.e., outside kelp) treatments for the two species. Light dissolution, which is a precursor of dissolution (green, Figure 57)

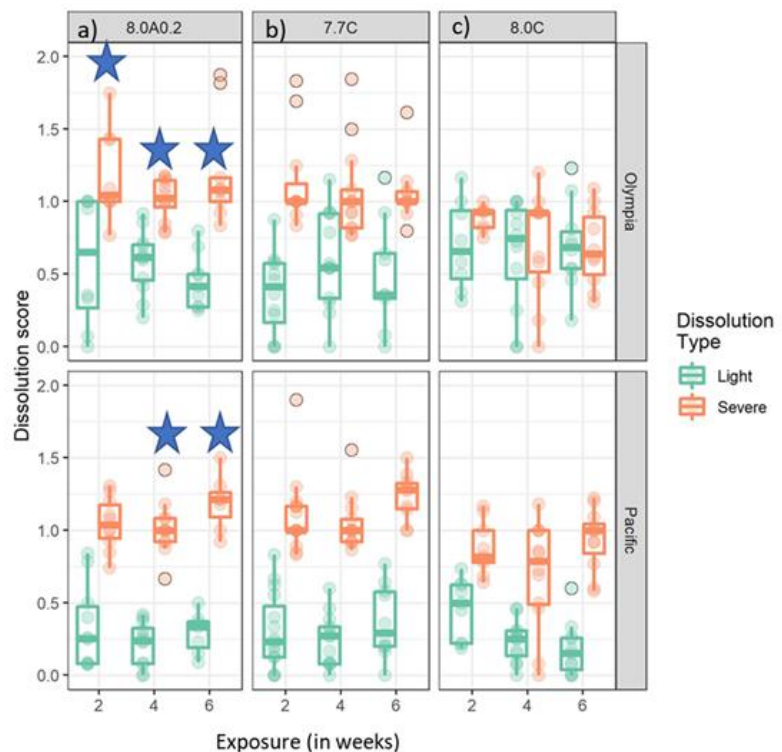


Figure 57. Comparison of the light and severe oyster shell dissolution between Olympia (upper panel) and Pacific (lower panel) oyster for the kelp conditions (Treatment #2), static conditions (Treatment #3) and control (Treatment #1).

decreased over time, while more severe dissolution increased over time but its magnitude varied by treatment (orange, Figure 57). Olympia oysters showed significantly less severe dissolution in the kelp treatment compared to the dynamic treatment in weeks 2 and 4 (top panels, Figure 57). For Pacific oysters, less severe dissolution was observed in weeks 2 and 4 in the kelp compared to the dynamic treatment (bottom panels, Figure 57).

No change in respiration between treatments

Comparing respiration rates of the two oyster species between kelp and dynamic treatments, we did not observe significant differences over time or between treatments for either species. This likely indicates that the energetic status of the oysters was not changed due to the treatment effect.

8.2.3 Conclusions

The experimental conditions that mimicked kelp conditions in the field promoted biomineralization scope, i.e. increased calcification and reduced extent and severity of shell dissolution. The two oyster species showed similar response to the treatments. Conversely, there were no differences in respiration rates. Based on these responses it is likely that improved growth detected in the field is a result of improved calcification and decreased dissolution. It is worth noting that the time mattered as the beneficial effects increased over time. Feeding on kelp seems not to be a primary driver of beneficial responses. Overall, the mechanism behind benefits of the kelp farm are not reflecting instantaneous responses on a diel basis, but rather cumulative conditions over the exposure time.

9. Modeling the effect of seaweed on ocean acidification

Authors: Dale Kiefer, Zach Siegrist

9.1 Description of the Seaweed AquaModel

System Science Applications has developed a robust working model of sugar kelp growth and physiology. We have incorporated this model into our *Hood Head Kelp Farm Model*, a project within the Environmental Analysis Systems (EASy) GIS software known as *Seaweed AquaModel*. Working with data provided to us by collaborators taking field measurements, we have tuned the model to the field conditions during two years at an experimental sugar kelp farm located near Hood Head in Puget Sound, Washington.

9.1.1 Growth and physiology model

9.1.1.1 General Description

The *Saccharina* frond model was developed with the *Mathematica* computer program and is based in part on the model of Broch and Slagstad (2012). Broch and Slagstad's model describes seasonal growth and composition of sugar kelp based on field data recorded by Sjøtun (1993) at a fjord in western Norway. We have adapted much of this model to better reflect environmental conditions and kelp growth patterns recorded in Puget Sound.

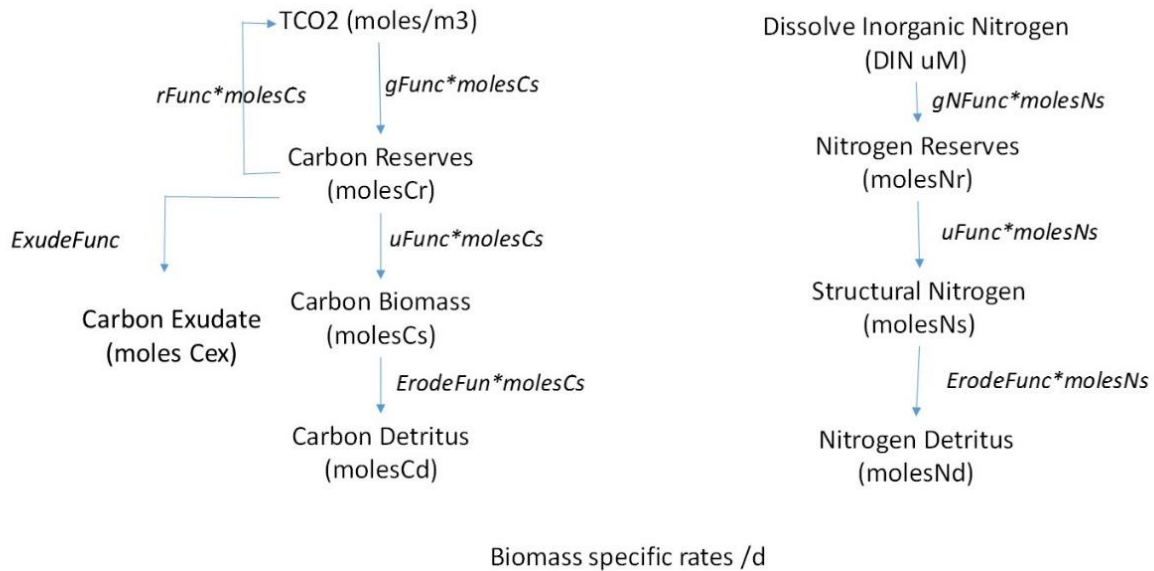


Figure 59: Model system of fluxes for an individual *Saccharina* frond.

Our model is a series of coupled functions shown in Figure 59. These functions simulate the growth and metabolism of an individual kelp frond.

Figure 59 shows the carbon and nitrogen pathways described by the series of functions. As shown, TCO₂ (or total DIC) is photosynthetically assimilated by the frond and transformed into carbon reserves, Cr. In turn, these reserves are transformed into structural carbon, Cs; exuded carbon, Carbon Exudate; or TCO₂ via respiration. The structural carbon can be harvested and may also be lost as detritus via erosion. A similar set of processes are described for nitrogen. The rates of these processes vary with environmental conditions that include water temperature, solar irradiance and daylength, the concentration of TCO₂ and DIN (dissolved inorganic nitrogen), and current velocity. Many of these environmental variables were measured by the Hood Head field teams and have been incorporated into our model.

Figures 60 and 61 show inputs of temperature and instantaneous irradiance for an initial run of the prototype frond

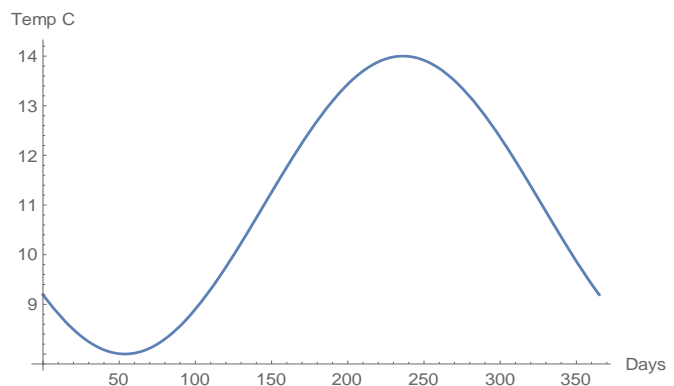


Figure 60. Plot of daily water temperature values used in an initial run of our prototype *Saccharina* frond model.

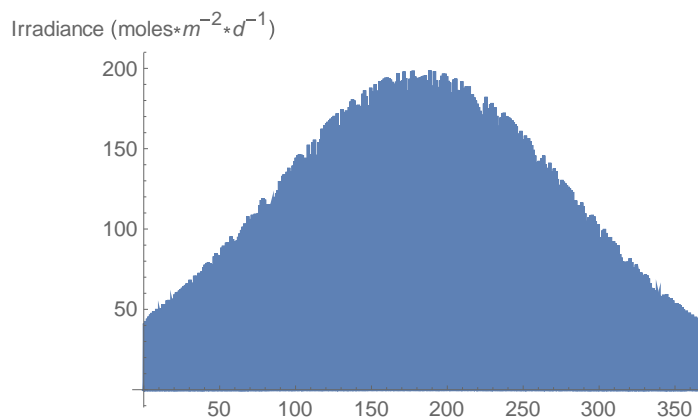


Figure 61. Plot of instantaneous daily irradiance values used in an initial run of our *Saccharina* frond model. Irradiance levels are based on monthly irradiance levels reported in Seattle, WA.

model. The diel cycle in irradiance cannot be seen because of the compressed time scale. In this initial simulation the currents were assumed to be constant at 10 cm/s and the concentrations of dissolved inorganic nitrogen and total inorganic carbon were assumed to be constant at 10 μ M and 2100 μ M, respectively.

Figures 62-65 show the results of our initial frond simulation. Figure 62 shows the simulated rate of increase in the surface area of a frond that was seeded into the Hood Head farm on January 1 with a surface area of 1 dm² and tracked for 1 year. We note that the frond reached its maximum size of about 40 dm² after about 6 months of growth. This maximum size agrees closely with the maximum size of *Saccharina* fronds in the Broch and Slagstad study in Norway (upper left panel of Figure 66). The slow growth during the first 100 days of our simulation is caused by the combined effects of the small initial size of the frond, cold water, and low irradiance. Figure 63 shows the corresponding structural carbon of the frond. Figure 64 shows the daily increase in frond structural carbon. We note that the maximal daily increase occurs near the end of the period of growth during the first 6 months and that the maximal daily increase approaches 0.008 moles carbon per day – corresponding well with the patterns of maximal growth in frond area measured in the Norwegian fjord analyzed by Brock and Slagstad (upper right panel of figure 66). Finally, Figure 65 shows the simulated instantaneous rate of carbon assimilation; this includes photosynthetic uptake during the day and respiratory loss at night. The actual cycle of photosynthesis and respiration cannot be depicted because of the compressed time scale. We note that rates of respiration are much lower than rates of photosynthesis until the fronds approach their maximum size and stop growing.

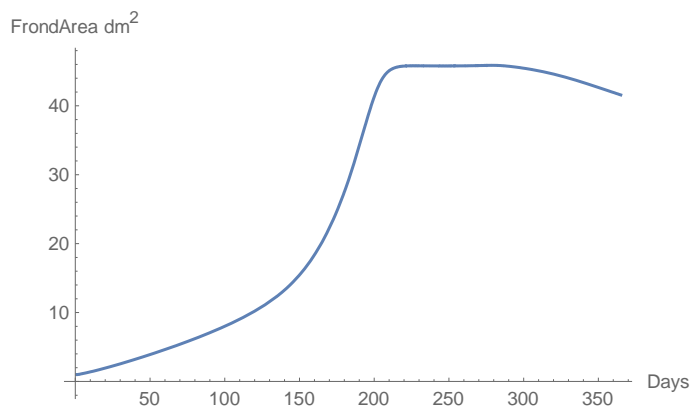


Figure 62: Plot of model-calculated daily frond area (units of square decimeters).

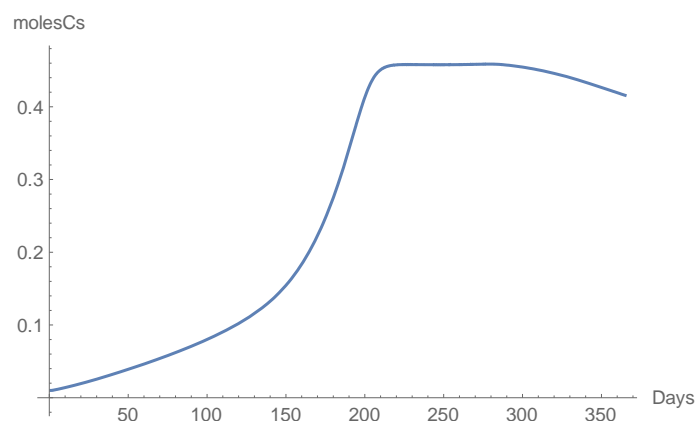


Figure 63: Plot of model-calculated daily frond structural carbon content (units of moles).

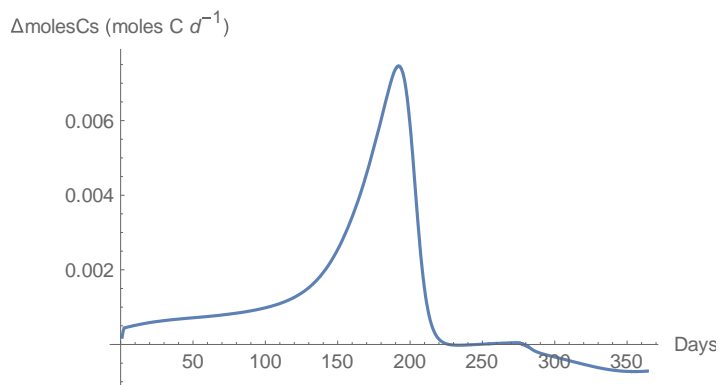


Figure 64: Plot of model calculated daily rate of change in frond structural carbon (units of moles/day).

In Figure 66 the dashed and solid lines are the results of simulations by Broch and Slagstad (2012) of *Saccharina* growth during an annual cycle. The crosses and circles are field measurements by Sjøtun (1993). The lower two panels provide information on seasonal changes in the ratios of carbon reserves (Cr) and nitrogen reserves (Nr) to the structural dry weight of the fronds. Our model provides a similar dynamic of seasonal changes in ratios of reserves to structural biomass.

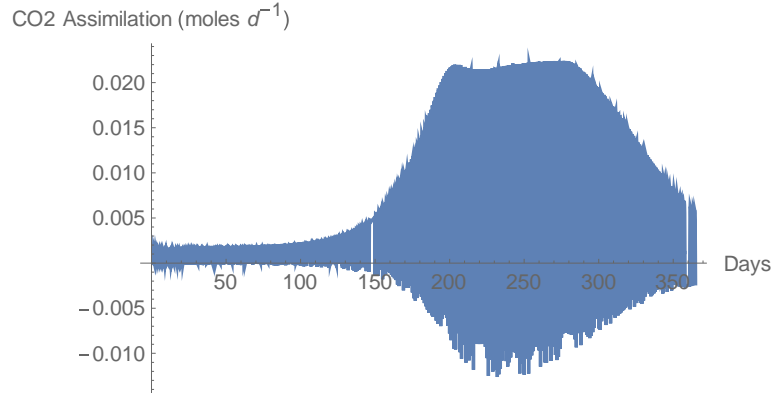


Figure 65: Plot of model output of CO₂ assimilation rates (units of moles/day).

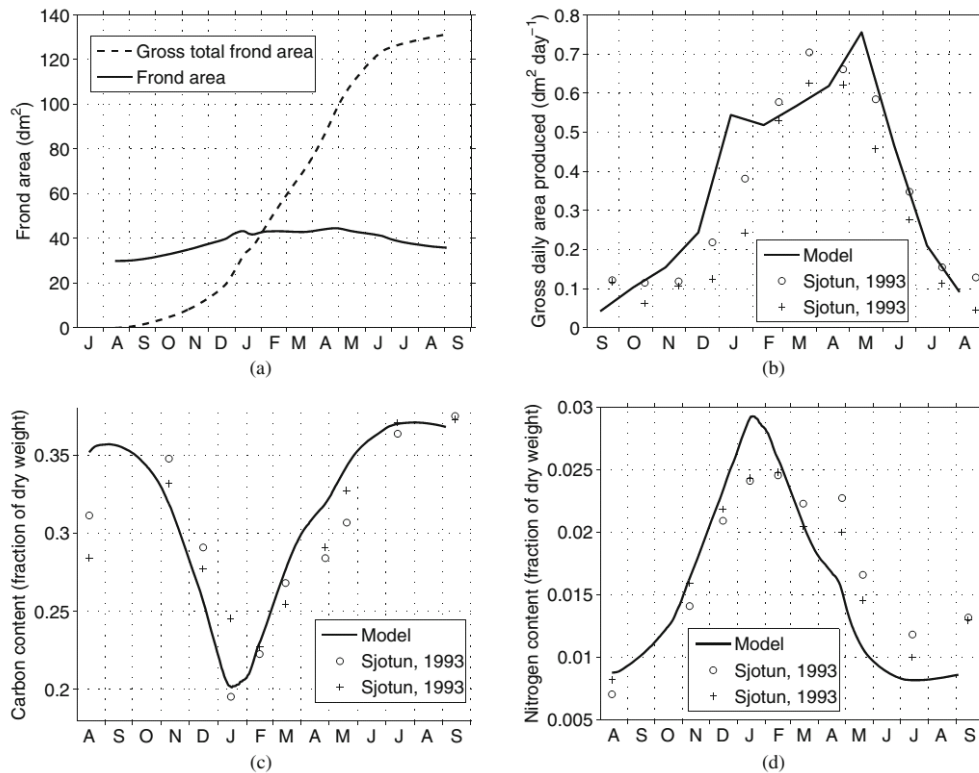


Fig. 3 **a** The *solid line* represents simulated standing frond area and the *dashed line* the simulated gross area produced. **b** Gross daily frond area produced. *Solid line*, averages of the daily area produced for the previous 30 days. *Circles*, daily area produced estimated from Sjøtun (1993) 2-year plants. *Crosses*, daily area produced estimated from Sjøtun (1993) 3-year plants.

c Carbon content expressed as fraction of dry weight. *Solid line*, model results. *Circles*, Sjøtun (1993) proximal/meristematic tissue. *Crosses*, apical frond tissue. **d** Nitrogen content expressed as fraction dry weight. *Solid line*, model results. *Circles* (o), Sjøtun (1993), 2-year plants. *Crosses*, Sjøtun (1993) 3-year plants

Figure 66. Extract of four figures from Broch and Slagstad (2012) in which seasonal growth and composition of sugar kelp was modeled based on field data recorded by Sjøtun (1993) from a fjord in western Norway. Our model is designed to follow similar patterns of growth and production but based on parameters local to the Hood Canal study site.

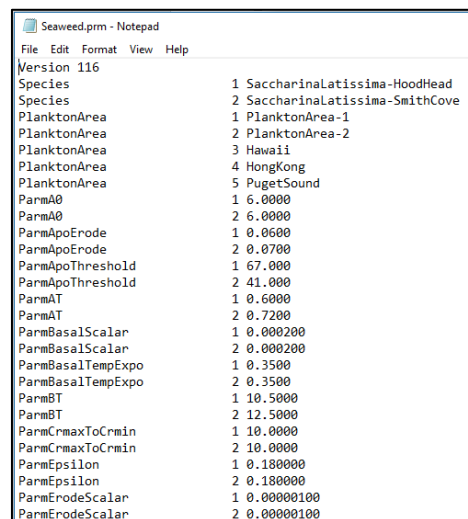
9.1.1.2 Kelp phenotypes

Our model describes multiple phenotypes for a single kelp species. In Year 2 of the experimental farm project, researchers found that the planted “Smith Cove” kelp had significantly different phenotypical growth and development compared to native “Hood Head” kelp. A large quantity of the native kelp ended up on the kelp lines along with the seeded kelp, and so we decided to include both phenotypes into our simulation in order to better model the experimental farm.

The growth and metabolism of both phenotypes are determined by 28 parameters set by the user. These parameters are located in an external text file that is read by EASy (Figure 67). Once the code was implemented, a series of tuning simulations was run in order to generate reasonable species parameters for both the native “Hood Head” and the planted “Smith Cove” phenotypes of sugar kelp.

9.1.1.3 Effects of light intensity within the water column on kelp growth

We added code to the Broch and Slagstad model to improve calculation kelp growth as determined by light intensity. The present kelp physiological model is now affected by both factors. We include functions that determine light intensity at varying depths of the kelp. As kelp are elongated and do not necessarily grow horizontally in the water, our function attempts to determine the amount of light hitting the kelp based on a) the size and length of the kelp; b) the depth of the kelp holdfast; c) the average depth of the kelp, based on the previous two factors; d) the current speed; e) attenuation of light by the turbidity of the water; and e) the amount of self-shading based on the local kelp density and a kelp shade factor that represents the fraction of light that can pass through one layer of kelp. We found that other kelp models do not account for these factors in the same level of detail.



Parameter	Value
Version	116
Species	1 SaccharinaLatissima-HoodHead
Species	2 SaccharinaLatissima-SmithCove
PlanktonArea	1 PlanktonArea-1
PlanktonArea	2 PlanktonArea-2
PlanktonArea	3 Hawaii
PlanktonArea	4 HongKong
PlanktonArea	5 PugetSound
ParmA0	1 6.0000
ParmA0	2 6.0000
ParmApoErode	1 0.0600
ParmApoErode	2 0.0700
ParmApoThreshold	1 67.000
ParmApoThreshold	2 41.000
ParmAT	1 0.6000
ParmAT	2 0.7200
ParmBasalScalar	1 0.000200
ParmBasalScalar	2 0.000200
ParmBasalTempExpo	1 0.3500
ParmBasalTempExpo	2 0.3500
ParmBT	1 10.5000
ParmBT	2 12.5000
ParmCrmxToCrmin	1 10.0000
ParmCrmxToCrmin	2 10.0000
ParmEpsilon	1 0.180000
ParmEpsilon	2 0.180000
ParmErodeScalar	1 0.00000100
ParmErodeScalar	2 0.00000100

Figure 67: Portion of the parameter file that contains parameter values for both “Hood Head” and “Smith Cove” phenotypes of the sugar kelp grown during the Year 2 field experiment.

9.1.1.4 Kelp apoptosis and enhanced erosion effects

One of the drawbacks of our initial model was that it did not account for the significant degradation and erosion experienced by kelp after it reached peak biomass in late spring and early summer (Figure 68, left). We added significant functionality in our model to account for this (Figure 68, right). We decided to model kelp cellular apoptosis, which is controlled by an internal flag that switches on once a specified kelp size is reached. Once the apoptosis ‘flag’ is flipped, erosion rates increase while internal cellular processes (respiration, growth, etc.) cease. This flag for apoptosis, along with other new parameters related to rates of erosion, is one of the many species parameters found in the species parameter file described above and shown in Figure 67.

9.1.2 Hood Head Kelp Farm Model

9.1.2.1 General Description

The series of coupled functions that comprise the *Saccharina* frond model are incorporated into our *Hood Head Kelp Farm Model*. The *Hood Head Kelp Farm Model* is a 3-dimensional simulation of growth and

metabolic activity of farmed sugar kelp, associated flow and transformation of nutrients, oxygen, DIC, and particulate wastes in the waters within and surrounding the farm. While the *Saccharina* frond model deals with the physiology of an individual kelp frond, the *Hood Head Kelp Farm Model* simulates the physiological and ecological dynamics of the entire set of lines of fronds of the farm.

The *Hood Head Kelp Farm Model* (see Figure 59) operates within the Environmental Analysis Systems (EASy) GIS software known as *Seaweed AquaModel*. The EASy GIS contains the software tools to plot and map a variety of outputs, including *Saccharina* frond area, frond carbon and nitrogen content, carbon detritus, as well as environmental parameters such as temperature, salinity, pH, current speed, saturation values for aragonite and calcite, and concentrations of oxygen, dissolved inorganic nitrogen, species of DIC (Figure 69).

The map and plots in Figure 69 are from a single time step (June 17th, 2017) in a 6 ½ month simulation. The false color map shows the distribution of DIC at a depth of 1.5 meter at the Hood Head Farm. The blue and purple plume of decreased DIC flowing downstream from the farm is caused by the photosynthetic assimilation of carbon dioxide by the kelp within the farm. The color code for the concentration of DIC (μM) is shown in the upper right corner, as is the scale of current velocity (cm/s). The simulation control panel, which is used to control model simulation, is in the lower right corner. The plots on the left provide time series information on current velocity at the surface and at depth, growth rates and biomass of farmed kelp. They also provide 1-dimensional vertical profiles and 2-dimensional cross sections of water temperature, DIC, oxygen, and nutrients. The large red rectangle is the model's gridded computational field, and the smaller black rectangle is the boundary of the Hood Head experimental kelp farm. The red line running through the center of the farm defines the transect of the colored, 2-dimensional plots for DIC and ΔDIC . The grey dots in the figure are stations where time series data from the simulation are stored and later examined to compare upstream and downstream water parameters.

Following initial development of the *Saccharina* frond model and incorporation into the *Hood Head Kelp Farm Model*, we continued to develop and tune several algorithms within the model. The model has been updated based on model testing and tuning, additional research, and ongoing communication with the cultivation, production, and environmental monitoring teams. Much of this is described in greater detail below.

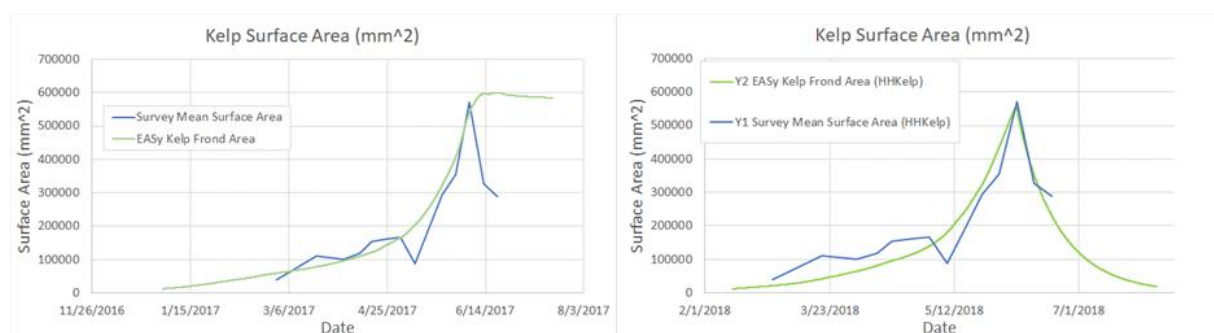


Figure 68. Plots of kelp surface area for Year 1 (left) and Year 2 (right). Blue lines are kelp surface area measured in the field, and green lines are simulated kelp surface area. The Year 1 simulation on left does not account for the significant erosion and degradation experienced after peak biomass as seen in the field data; the Year 2 model on right accounts for this loss and matches well to field results.

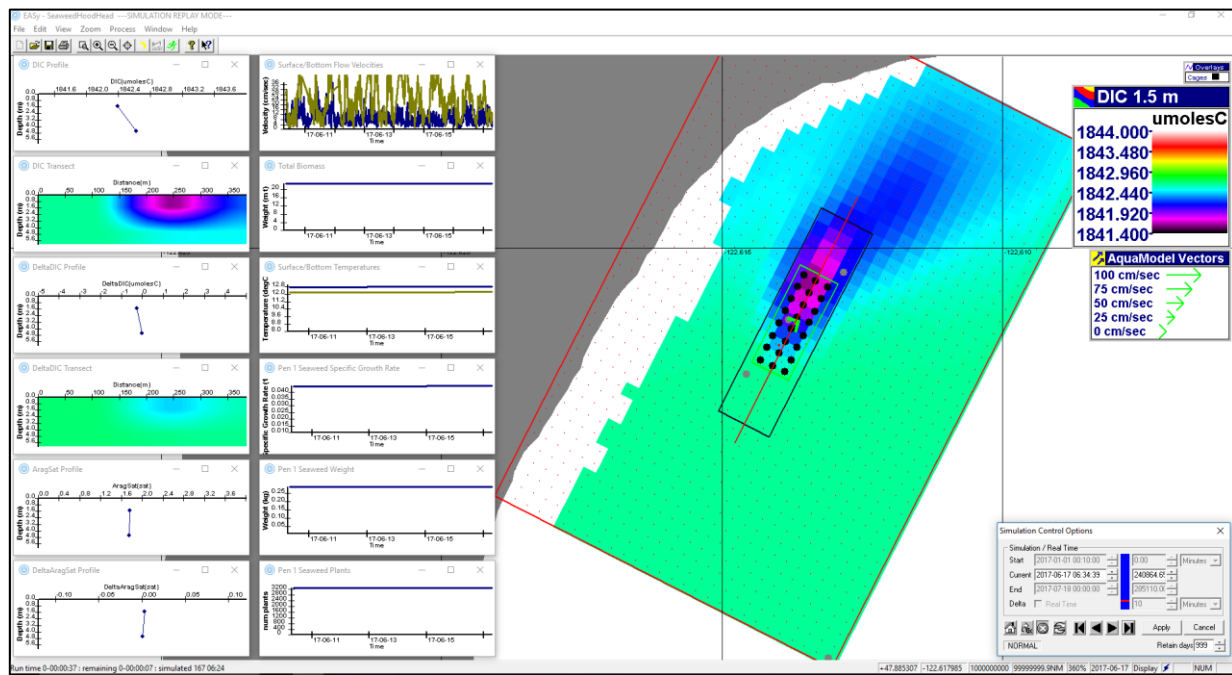


Figure 69. Screenshot of the EASy GIS Hood Head Kelp Farm Model with a variety of user-selected plots on display. Snapshot was taken at one timestep, late into the simulation run. Background color map shows the distribution of DIC at a depth of 1.5 meter at the Hood Head Farm. The blue and purple plume of decreased DIC flowing downstream from the farm is caused by the photosynthetic assimilation of carbon dioxide by the kelp within the farm.

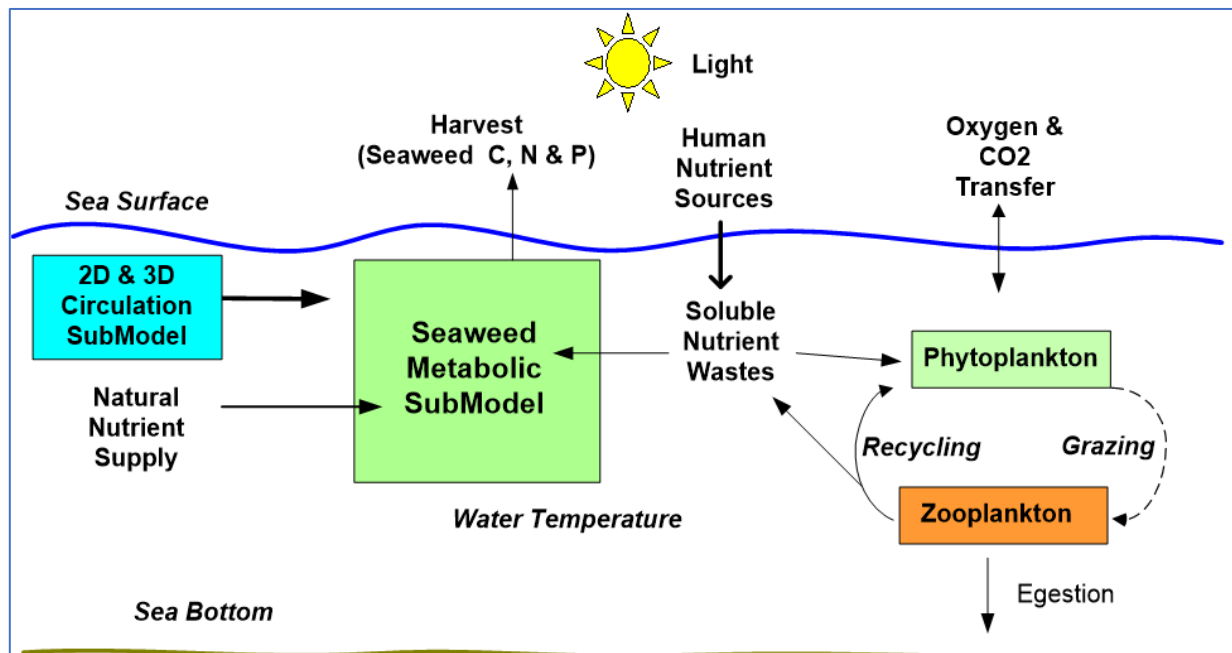


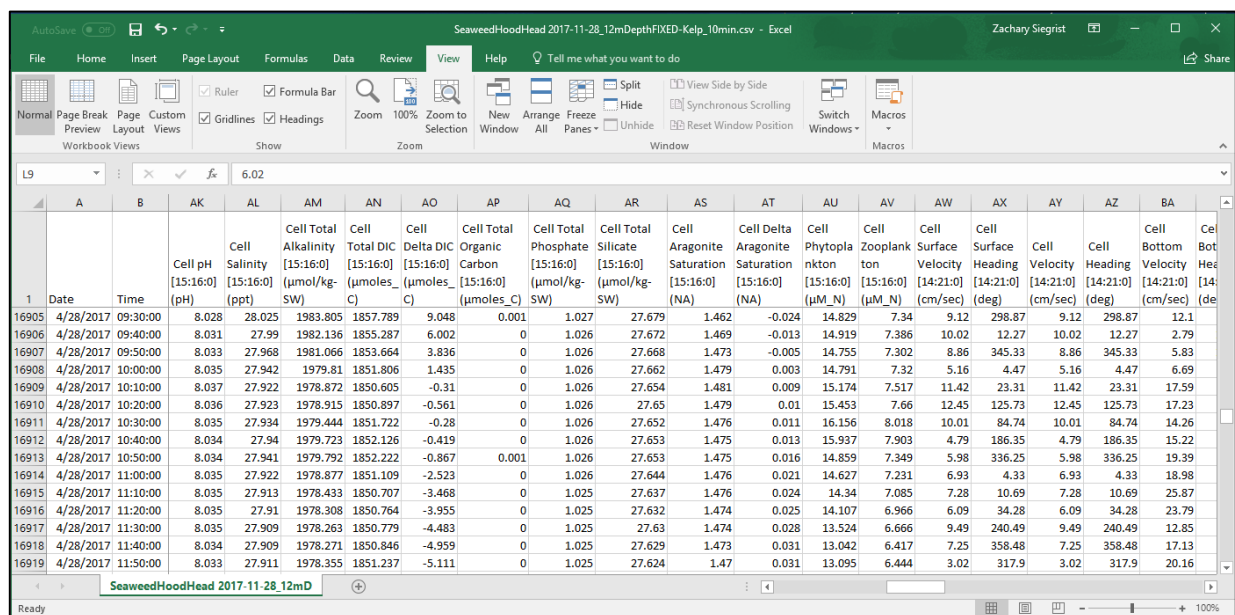
Figure 70. Seaweed AquaModel system consists of submodels for the growth and metabolism kelp within the is kelp farm and the planktonic community. These dynamics are driven by either 2-dimensional or 3-dimensional currents, surface irradiance, dissolved nutrients, oxygen and carbon dioxide gas exchange, and dissolved inorganic nutrients, DIC, dissolved inorganic oxygen, and water temperature.

9.1.2.2 Incorporation of nitrogen-phytoplankton-zooplankton subroutines

We have incorporated a nitrogen-phytoplankton-zooplankton (NPZ) subroutine into the *Hood Head Kelp Farm Model* (Figure 70). Plankton ecologies compete with kelp for light and nutrients; thus, our model should be more accurate with the inclusion of our NPZ subroutines. The NPZ submodel has previously been used successfully in a range of other projects of the EASy GIS software. To date, there has been very limited tuning of the NPZ submodel integration into the *Hood Head Kelp Farm Model* but the submodel can be easily tuned in the future.

9.1.2.3 Data output

In addition to plotting and real-time 3D visualization of the model simulation, EASy also allows for a host of detailed data output to an external .csv file (Figure 71). These data can be from the locations of the sugar kelp lines themselves, as well as from multiple ‘capture cells’ selected by the user and located anywhere within the boundaries of the modeled area. These data can then be processed externally for more in-depth analyses.



	A	B	AK	AL	AM	AN	AO	AP	AQ	AR	AS	AT	AU	AV	AW	AX	AY	AZ	BA	BB
	Date	Time	Cell pH [15:16:0] (pH)	Cell Salinity [15:16:0] (ppt)	Cell Total Alkalinity [15:16:0] (μmol/kg-SW)	Cell Total DIC [15:16:0] (μmoles_C)	Cell Delta DIC [15:16:0] (μmoles_C)	Cell Total Organic Carbon [15:16:0] (μmoles_C)	Cell Total Phosphate [15:16:0] (μmol/kg-SW)	Cell Total Silicate [15:16:0] (μmol/kg-SW)	Cell Aragonite Saturation [15:16:0] (NA)	Cell Delta Aragonite Saturation [15:16:0] (NA)	Cell Phytoplankton [15:16:0] (μM_N)	Cell Zooplankton [15:16:0] (μM_N)	Cell Surface Velocity [14:21:0] (cm/sec)	Cell Surface Heading [14:21:0] (deg)	Cell Velocity [14:21:0] (cm/sec)	Cell Heading [14:21:0] (deg)	Cell Bottom Velocity [14:21:0] (cm/sec)	Cell Bottom Heading [14:21:0] (deg)
16905	4/28/2017	09:30:00	8.028	28.025	1983.805	1857.789	9.048	0.001	1.027	27.679	1.462	-0.024	14.829	7.34	9.12	298.87	9.12	298.87	12.1	
16906	4/28/2017	09:40:00	8.031	27.99	1982.136	1855.287	6.002	0	1.026	27.672	1.469	-0.013	14.919	7.386	10.02	12.27	10.02	12.27	2.79	
16907	4/28/2017	09:50:00	8.033	27.968	1981.066	1853.664	3.836	0	1.026	27.668	1.473	-0.005	14.755	7.302	8.86	345.33	8.86	345.33	5.83	
16908	4/28/2017	10:00:00	8.035	27.942	1979.81	1851.806	1.435	0	1.026	27.662	1.479	0.003	14.791	7.32	5.16	4.47	5.16	4.47	6.69	
16909	4/28/2017	10:10:00	8.037	27.922	1978.872	1850.605	-0.31	0	1.026	27.654	1.481	0.009	15.174	7.517	11.42	23.31	11.42	23.31	17.59	
16910	4/28/2017	10:20:00	8.036	27.923	1978.915	1850.897	-0.561	0	1.026	27.65	1.479	0.01	15.453	7.66	12.45	125.73	12.45	125.73	17.23	
16911	4/28/2017	10:30:00	8.035	27.934	1979.444	1851.722	-0.28	0	1.026	27.652	1.476	0.011	16.156	8.018	10.01	84.74	10.01	84.74	14.26	
16912	4/28/2017	10:40:00	8.034	27.94	1979.723	1852.126	-0.419	0	1.026	27.653	1.475	0.013	15.937	7.903	4.79	186.35	4.79	186.35	15.22	
16913	4/28/2017	10:50:00	8.034	27.941	1979.792	1852.222	-0.867	0.001	1.026	27.653	1.475	0.016	14.859	7.349	5.98	336.25	5.98	336.25	19.39	
16914	4/28/2017	11:00:00	8.035	27.922	1978.877	1851.109	-2.523	0	1.026	27.644	1.476	0.021	14.627	7.231	6.93	4.33	6.93	4.33	18.98	
16915	4/28/2017	11:10:00	8.035	27.913	1978.433	1850.707	-3.468	0	1.025	27.637	1.476	0.024	14.34	7.085	7.28	10.69	7.28	10.69	25.87	
16916	4/28/2017	11:20:00	8.035	27.91	1978.308	1850.764	-3.955	0	1.025	27.632	1.474	0.025	14.107	6.966	6.09	34.28	6.09	34.28	23.79	
16917	4/28/2017	11:30:00	8.035	27.909	1978.263	1850.779	-4.483	0	1.025	27.63	1.474	0.028	13.524	6.666	9.49	240.49	9.49	240.49	12.85	
16918	4/28/2017	11:40:00	8.034	27.909	1978.271	1850.846	-4.959	0	1.025	27.629	1.473	0.031	13.042	6.417	7.25	358.48	7.25	358.48	17.13	
16919	4/28/2017	11:50:00	8.033	27.911	1978.355	1851.237	-5.111	0	1.025	27.624	1.47	0.031	13.095	6.444	3.02	317.9	3.02	317.9	20.16	

Figure 71. Example of simulation data output to a .csv file.

9.1.2.4 Inclusion of the CO2sys water carbon chemistry model

Mid-way through the first year of the Hood Head project and after conversations with the University of Washington water chemistry team, we decided to replace our water chemistry carbon model, developed primarily from Peng et al., 1987, with code extracted from the co2sys.xls calculator developed by Pelletier, Lewis and Wallace (available at https://fortress.wa.gov/ecy/ezshare/eap/ZipFiles/co2sys_ver25b06.zip). This allows us to calculate model aragonite and calcite saturation values, key values in tracking the effects of OA, using the same formulae as the rest of the project team.

The key CO2sys functions were extracted out of the co2sys.xls Excel macros and integrated into EASy's Visual Basic code. The CO2sys user inputs (temperature, pressure, inorganic carbon, etc.) are linked to real-time environmental and water chemistry model values generated by the *Hood Head Kelp Farm Model*. This enables our model to generate real-time aragonite and calcite saturation values for the entire

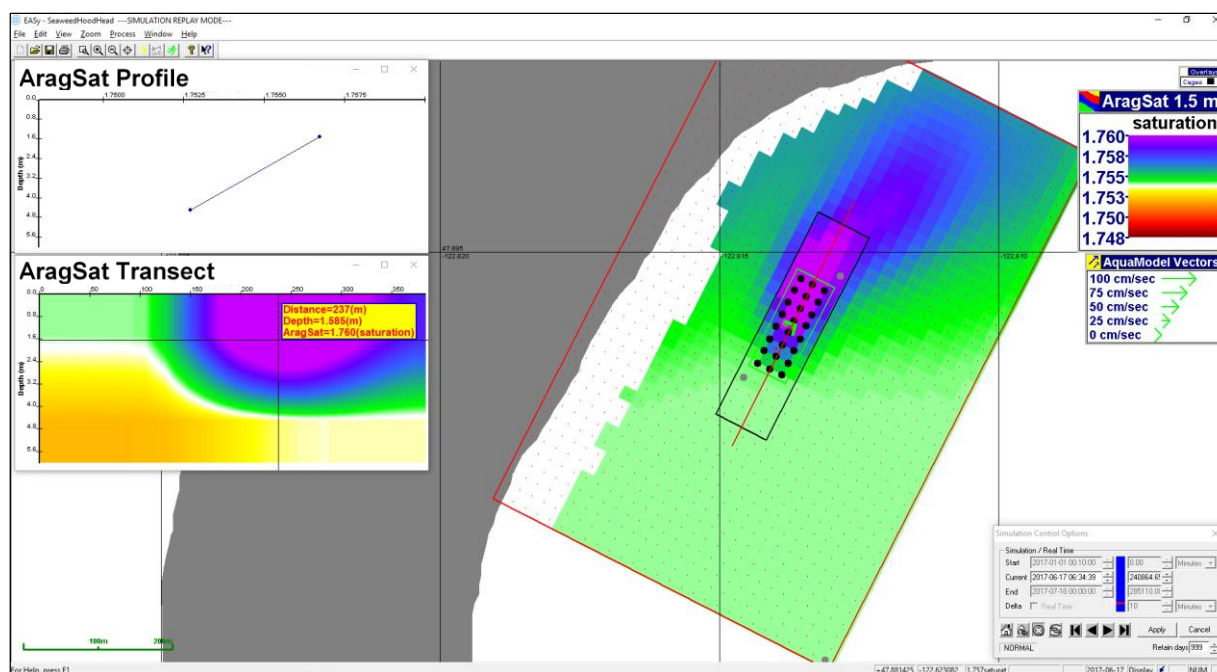


Figure 72. Screenshot of the EASy GIS Hood Head Kelp Farm Model with user-selected plots of aragonite saturation depth profile and transects (at left), background false color imagery of real-time aragonite saturation at 1.5m depth (middle), and project legends and simulation controls (right) on display.

3-D modelling domain, which can be visualized as false-color images as the model runs (Figure 72). Aragonite and calcite saturation values as well as other outputs from the CO2sys code can also be output to an external .csv data file.

In addition to incorporating the CO2sys functions into our code, we have improved the graphical user interface for the CO2sys calculator input. The user can select different initial inputs to the CO2sys calculator system (Figure 73), much like the original Excel-based version.

9.1.2.5 Environmental tuning and ambient file input

We have tuned the *Hood Head Kelp Farm Model* to provide a good fit to the field measurements at the Farm's study site. We have been provided an extensive data records from the project teams, as well as from the Washington Department of Ecology, and have used these data to not only tune the model but also to provide accurate values for inputs to the simulation. Environmental data from moored sensors and water samples from the Hood Head site that have been integrated into our model include current direction and magnitude, temperature, salinity, pCO2, oxygen, chlorophyll, pH, alkalinity, phosphate, silicate and DIC (Figure 74). Before receiving site-specific data in late August 2017, we also used 11-year averaged climatology data (temperature, oxygen, salinity) taken from the nearby Hansville environmental mooring to aid us in our preliminary tuning. In addition, many of these data sets have been used to create ambient input files. These ambient files are read by EASy to provide ambient environmental water quality data for boundary conditions for calculations within the gridded computational array.

As part of model development, we mapped water column depth (bathymetry) using NOAA online nautical charts as well as sonar depth sounding obtained by the PAFF's field team (Figure 75). These data were incorporated into a text file containing coordinates of latitude, longitude and depth that was then

SeaweedHoodHead Options

Mode: Replay 2-D Mode Data Sources: Array Color:

Capture File: \\SeaweedHoodHead\\Capture2D\\dBasalTempExpoDecreased

Operations: Array Species: Output Plankton: Pens Display: Dissolved Conditions: CO2sys

*****CO2sys calculator parameter inputs*****

It is highly recommended that you leave these settings alone unless you are very familiar with the CO2sys calculator!

Constants: Lueker et al 2000

fCO2 or pCO2: pCO2

Input Parameter Case*: Given TC & fCO2/pCO2

Total boron: Uppstrom 1974

KSD4: Dickson

pH scale: total scale

KF: seacarb

*Input Parameter Case inputs and outputs:
 Given TA and TC -> Calculates pH and fCO2/pCO2
 Given TC and pH -> Calculates TA and fCO2/pCO2
 Given TC and fCO2/pCO2 -> Calculates TA and pH

CO2sys calculator source:
 Pelletier, G., E. Lewis, and D. Wallace. 2007. CO2SYS.XLS: A calculator for the CO2 system in seawater for Microsoft Excel/VBA, Wash. State Dept. of Ecology/Brookhaven Nat. Lab., Olympia, WA/Upton, NY, USA, 2007.
<http://www.ecy.wa.gov/programs/eap/models.html>

Code from calculator version co2sys_ver25b06.xlsm

Apply Ok Cancel

Figure 73: EASy graphical user interface of the CO2sys parameter inputs selection.

	A	B	C	D	E	F	G	H	I	J	K	L	M
	Date	pr	xCO2wat er	xCO2air	pH_tot	SSS	SST	chl	turb	DOuM	DOmgI	DOumolp erkg	sgth
1	1/25/2017 23:17	102.09	804.6	441.1		29.09	8.49	0.76	0.47	275.17	8.81	269.1	22.57
2	1/26/2017 0:17	102.12	807.4	442.3	7.694	29.11	8.5	0.69	0.48	275.09	8.8	269.02	22.59
3	1/26/2017 3:17	102.23	772.8	442.5	7.742	27.99	8.41	0.93	0.43	262.56	8.4	256.98	21.72
4	1/26/2017 6:17	102.33	751.3	446.7	7.765	27.12	8.19	1.03	0.46	261.68	8.37	256.29	21.07
5	1/26/2017 9:17	102.42	786.8	446.5	7.777	27.84	8.32	1	0.47	260.84	8.35	255.32	21.61
6	1/26/2017 12:17	102.55	796.8	449.6	7.683	28.75	8.5	0.9	0.44	261.42	8.37	255.72	22.3
7	1/26/2017 15:17	102.72	814.5	445.1	7.691	28.83	8.45	0.62	0.49	263.14	8.42	257.39	22.37
8	1/26/2017 18:17	102.89	814.8	439.4	7.696	28.96	8.46	0.6	0.49	268.37	8.59	262.48	22.47
9	1/26/2017 21:17	102.88	792.5	433.5	7.704	28.46	8.48	0.67	0.44	264.38	8.46	258.67	22.08
10	1/27/2017 0:17	102.98	759.7	433.6	7.789	28.56	8.52	0.73	0.52	265.01	8.48	259.27	22.15
11	1/27/2017 3:17	103.04	733.2	442.2	7.75	27.51	8.42	0.96	0.45	260.69	8.34	255.25	21.34
12	1/27/2017 6:17	103.11	760.4	439.9	7.722	27.17	8.39	1.1	0.44	263.72	8.44	258.28	21.08
13	1/27/2017 9:17	103.1	771.6	438.8	7.69	27.18	8.37	1.01	0.46	265.87	8.51	260.38	21.09
14	1/27/2017 12:17	103.23	789.3	437.3	7.746	28.49	8.51	0.75	0.47	265.39	8.49	259.66	22.09
15	1/27/2017 15:17	103.25	784.5	441.7	7.745	28.83	8.37	0.61	0.47	287.53	9.2	281.24	22.38

Figure 74. Some of the time series data provided by the environmental monitoring team and subsequently incorporated into the Hood Head Kelp Farm Model.

processed in EASy to generate a detailed bathymetric map. This bathymetric background directs current

flow along lines of constant depth.

The wealth of environmental data provided to us was complimented by data from the cultivation and production teams. Time series of wet and dry kelp sample weights, mean kelp blade lengths and blade areas, and kelp sample carbon and nitrogen contents have enabled us to carefully tune our internal sugar kelp physiology model to match closely with the experimental farm data provided to us. In particular, we have tuned our model with respect to internal carbon and nitrogen content as well as kelp surface area and kelp weight.

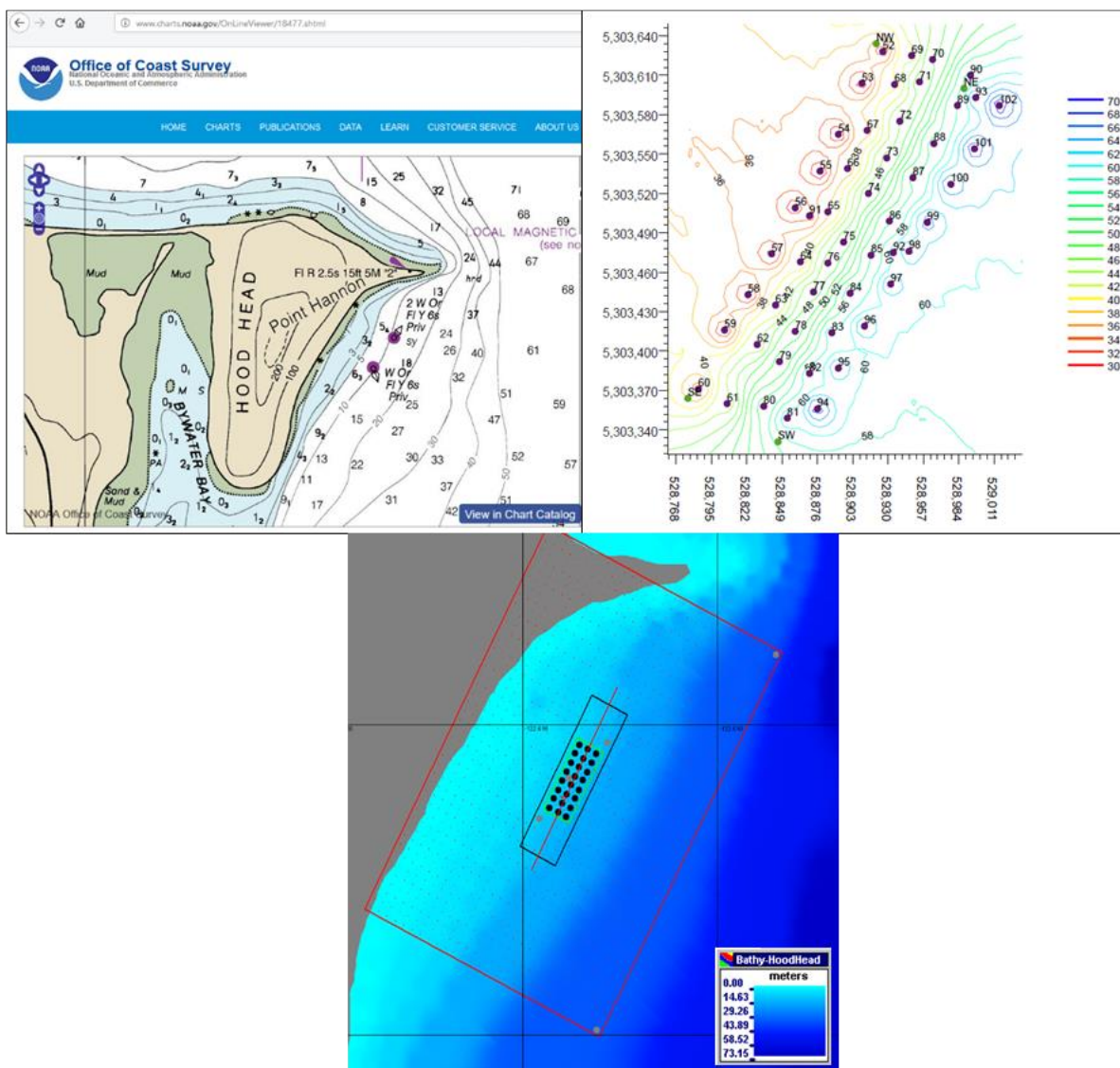


Figure 75. Clockwise from upper-left: NOAA bathymetric chart of the Hood Head study site; PAFF field team sonar data; EASy-generated bathymetry with simulated kelp farm (represented by the light-green rectangle filled with black circles).

9.2 Model Results

9.2.1 2017 Simulations of Farm Impacts

Output from our tuned model matched well with the environmental and kelp growth and physiology data provided to us by the other project teams during Year 1 of the Hood Head project (Figures 76-78).

In the first year of the experiment, our model did not replicate the significant erosion that was observed by the field team after the time of peak growth (as evidenced by the sharp decrease in kelp surface area recorded in late May/early June, Figure 77, blue line). This was addressed in Year 2 and was described in section 9.1.1.4 above.

For our analyses, we set up five output capture cells, designated by the five grey circles (with red labels) seen in Figure 79. Each of the five capture cells is positioned with an [X,Y] coordinate based on the user-designated x,y grid of the simulation. Two capture cells are located at the two far boundary corners of the simulated area; two capture cells are located at the NE and SW corners of the kelp bed, roughly matching the locations of two data equipment moorings; and one capture cell is located directly in the middle of

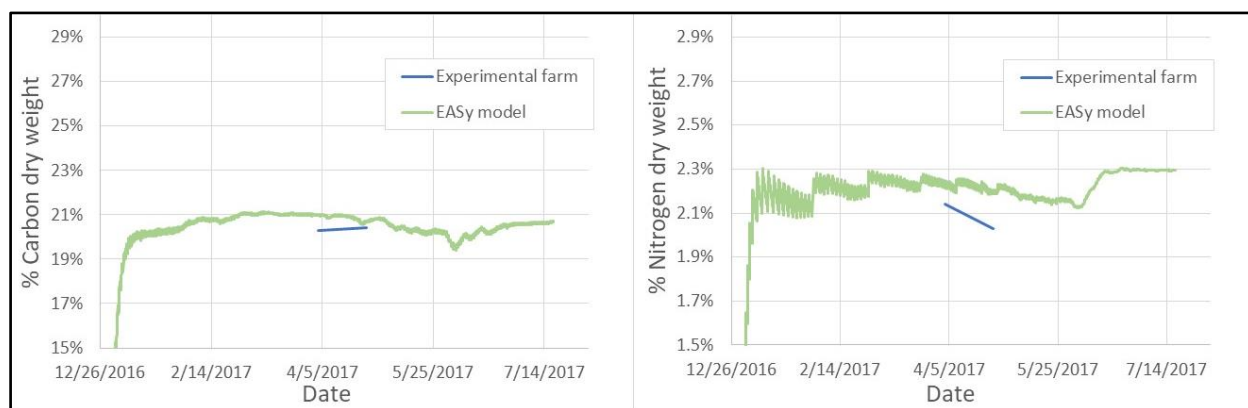


Figure 76. Comparison of time series of percent carbon and % nitrogen dry weight between averaged results of experimental farm kelp sample analysis (blue line) and analyzed output from the Hood Head Kelp Farm Model (green line).

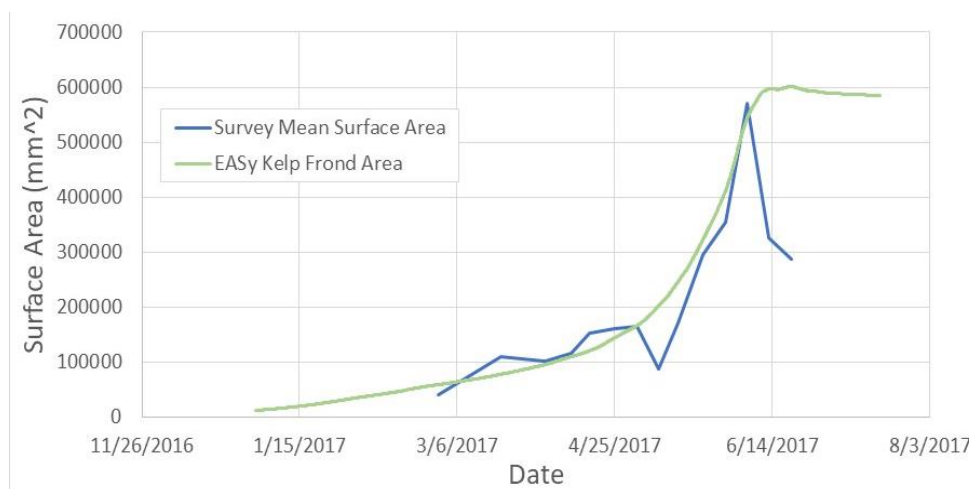


Figure 77. Comparison of time series of kelp surface area (in mm²) between averaged results of experimental farm kelp field measurements (blue line) and output from the Hood Head Kelp Farm Model (green line).

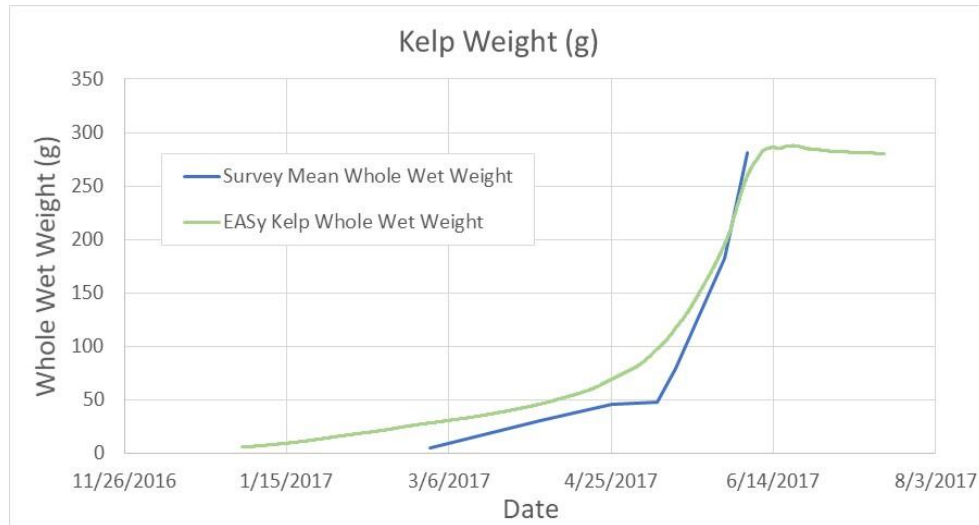


Figure 78. Comparison of time series of kelp wet weight (in grams) between averaged results of experimental farm kelp field measurements (blue line) and output from the Hood Head Kelp Farm Model (green line).

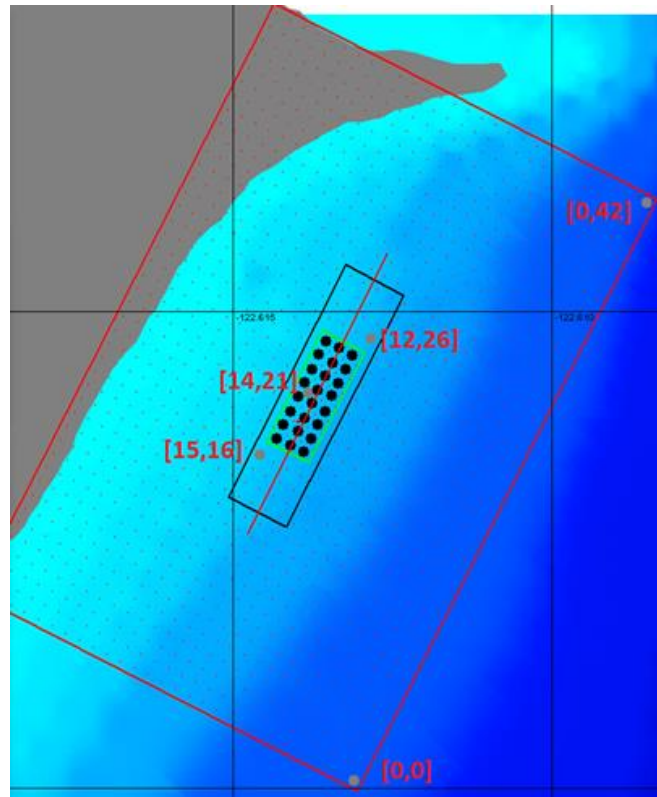


Figure 79. Locations of five capture cells within the simulated Hood Head area. Capture cells are represented as grey circles, with red labels describing the x,y coordinates of each capture cell with respect to the gridded simulated area.

the simulated kelp bed. As a simulation runs, ongoing time series of data recorded at each designated capture cell are output to an external .csv file.

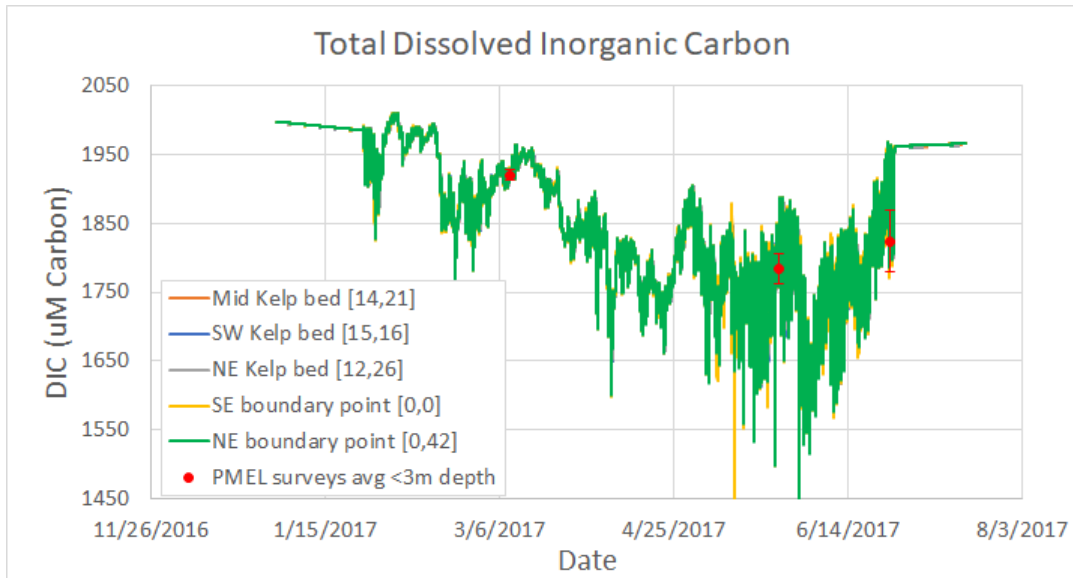


Figure 80. Time series of model output of total DIC. Plotted lines represent data output from the five capture cells, explained above and shown in Figure 79. Red circles and error bars represent average DIC measured at <3m depth taken by the PMEL survey crews.

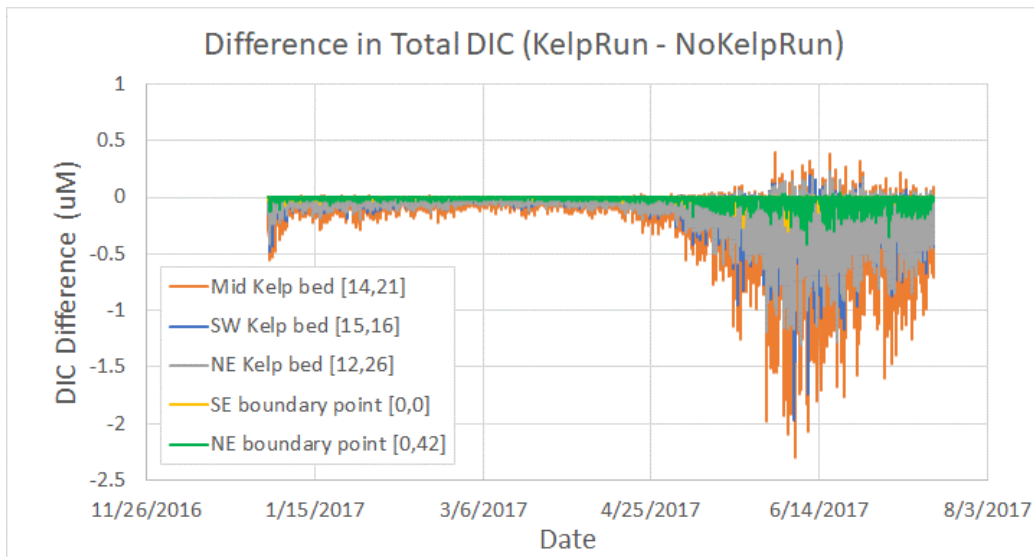


Figure 81. Difference between time series of model output of total DIC of a 'NoKelp' run and a 'Kelp' run. Plotted lines represent difference in data output from the five capture cells.

Figure 80 shows model output of DIC for one simulation run of our Year 1 model. The strong fluctuations of DIC throughout the run are the result of ambient file inputs rather than kelp farm effects.

To tease out direct effects of the kelp farm, we can do two simulation runs: one with kelp, and one without, with all other conditions identical. The output of the two models can then be compared. In fact, when subtracting the output of the 'NoKelp' run from that of the 'Kelp' run, we can see the true effects of the kelp farm on the surrounding water chemistry (Figures 81 and 82).

There is clearly an effect of the kelp farm on both DIC and aragonite saturation. In fact, calculated aragonite saturation is directly dependent on DIC, so it would follow that both have similar changes in

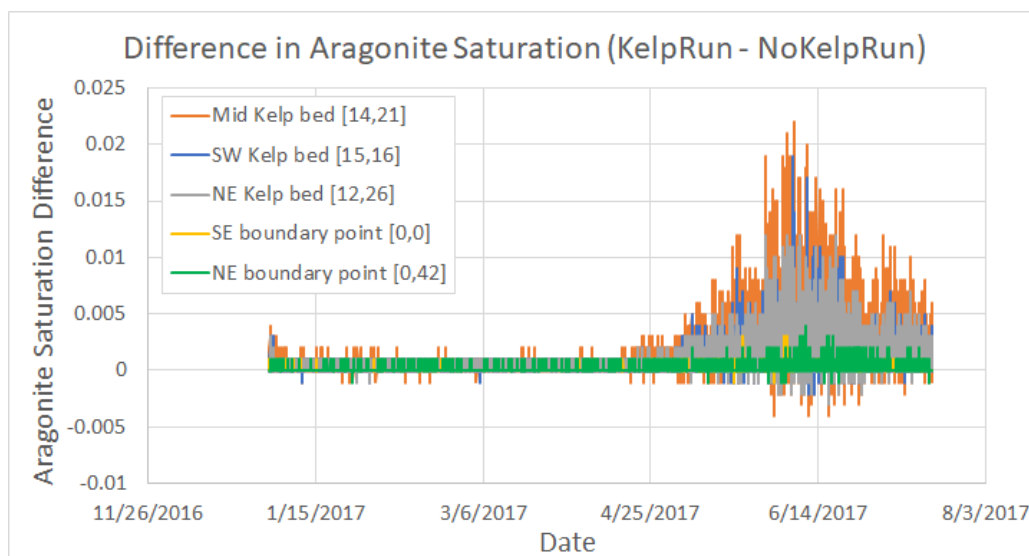


Figure 82. Difference between time series of model output of calculated aragonite saturation of a ‘NoKelp’ run and a ‘Kelp’ run. Plotted lines represent difference in data output from the five capture cells.

magnitude over time. In addition, we see the strongest changes in magnitude at the capture cell in the middle of the kelp bed (coordinates [14,21]), slightly lower changes in magnitude at the two capture cells on the outside corners of the kelp bed ([15,16] and [12,26]), and very low relative change in magnitude at the boundary capture cells ([0,0] and [0,42]).

In addition, the changes are as we would expect: as the kelp grows, it uses and sequesters carbon in the water, resulting in a decrease in measured modeled DIC compared to the ‘NoKelp’ run. Likewise, we see an increase in aragonite saturation.

However, these changes are likely far too small to be measured in the field and are hence difficult to validate. This was an ongoing point of discussion between the project teams, but despite an attempt in Year 2 to generate experimental data with finer resolution, the effects predicted by the model are too small to validate in the field.

9.2.2 2018 Simulations of Farm Impacts

Planted kelp in the Year 2 experiment was obtained from a different location (Smith Cove) compared to planted kelp from Year 1, which came from the Hood Head area. This Year 2 “Smith Cove” kelp had a significantly different phenotype from the Year 1 “Hood Head” kelp: it was much shorter, thicker, and more twisted than its year 1 counterpart. The Year 2 experiment also had a significant amount of native “Hood Head” phenotype kelp that grew on the kelp lines along with the planted “Smith Cove” kelp. Field measurements of biomass, surface area, and blade length were only taken from the planted “Smith Cove” kelp so our simulated Year 2 model had to include both modeled native kelp with growth patterns based on Year 1 results as well as modeled planted kelp based on the Year 2 planted “Smith Cove” kelp.

9.2.2.1 Simulation tuning

After all available Year 2 environmental and physiological data was made available to the modeling team, and all new coding functionality was added to our model, we worked to tune the Year 2 *Hood Head Kelp Farm Model* to Year 2 field results of kelp surface area, weight, and biomass. We were able to tune our model to match these parameters well (Figures 83 and 84). Indeed, Table 3 shows that peak biomass of

both the Year 2 planted “Smith Cove” kelp (based on Year 2 field results) and the Year 2 native “Hood Head” kelp (based on Year 1 field results) match well with peak biomass estimates of the Year 2 field experiment made by the PSRF team.

	FIELD STUDY (US tons)	FIELD STUDY (metric tons)	EASy (metric tons)	Percent Difference
SCKelp	15.41	13.98	14.11	0.91%
HHKelp	7.89	7.16	7.15	-0.15%

Table 3. Comparison of field estimates of peak biomass with EASy Hood Head Kelp Farm Model peak biomass values.

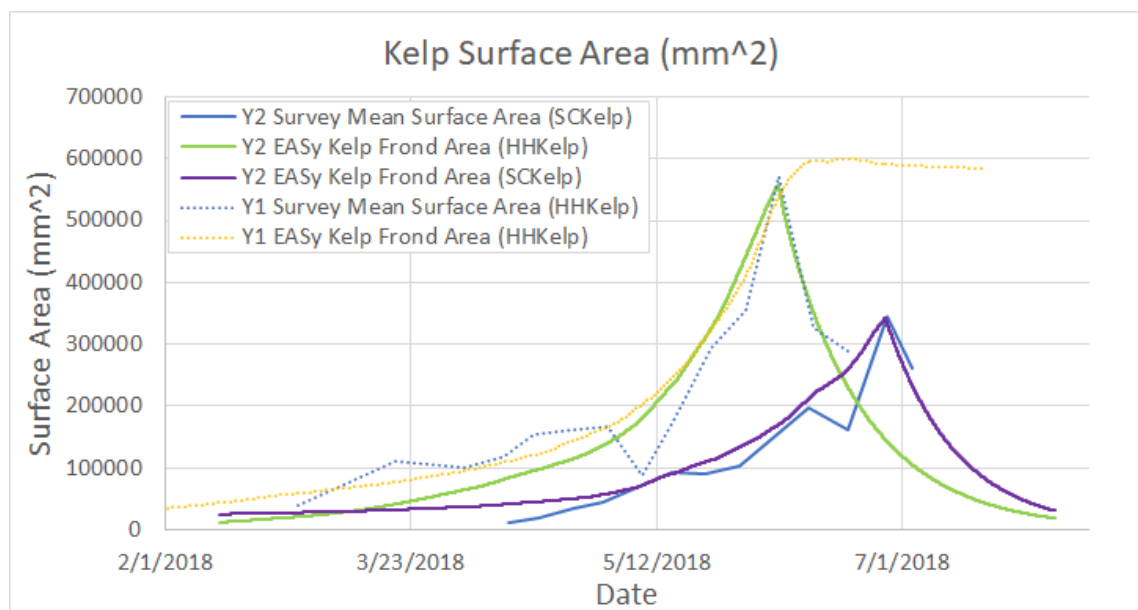


Figure 83. Year 2 field data and simulated model data of kelp surface area over time. Solid blue line represents Year 2 field data of planted “Smith Cove (SC) kelp. Dashed blue line represents Year 1 field data of planted “Hood Head (HH) kelp” transposed into the 2018 Year 2 timeline. Dashed yellow line represents Year 1 simulated EASy HH kelp surface area transposed into the 2018 Year 2 timeline. Solid green line represents Year 2 simulated EASy native HH kelp surface area. Solid purple line represents Year 2 simulated EASy planted SC kelp surface area. Model was tuned so that purple line matched solid blue line, and green line matched dashed blue line.

9.2.2.2 Difference plots

Similar to analyses conducted in Year 1 and discussed in the section above, we teased out direct effects of the kelp farm by doing two simulation runs: one with kelp, and one without, with all other conditions identical. The output of the two models can then be compared. In fact, when subtracting the output of the ‘NoKelp’ run from that of the ‘Kelp’ run, we can see the true effects of the kelp farm on the surrounding water chemistry (Figures 85 and 86).

Similar to results seen in the Year 1 simulation, there is clearly an effect of the kelp farm on DIC, aragonite saturation and calcite saturation. Calculated aragonite and calcite saturation values are directly dependent on DIC, so it would follow that they would have similar changes in magnitude over time. In addition, we see the strongest changes in magnitude at the capture cell in the middle of the kelp bed (coordinates [14,21]), slightly lower changes in magnitude at the two capture cells on the outside corners of the kelp bed ([15,16] and [12,26]), and very low relative change in magnitude at the boundary capture cells ([0,0] and [0,42]).

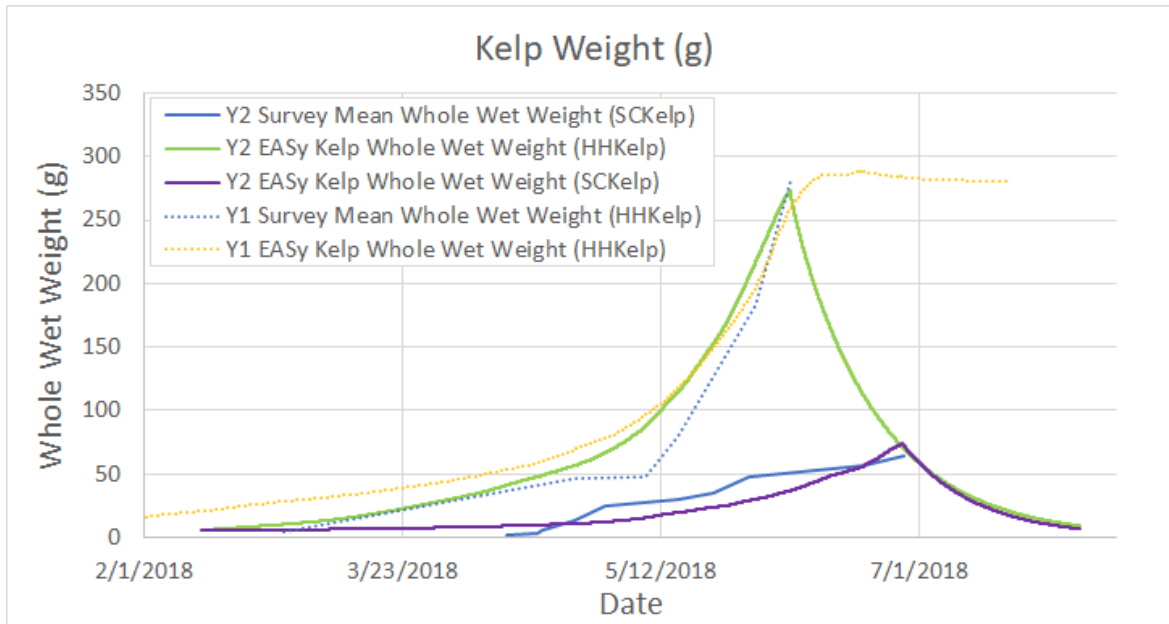


Figure 84. Year 2 field data and simulated model data of kelp weight over time. Solid blue line represents Year 2 field data of planted “Smith Cove (SC) kelp. Dashed blue line represents Year 1 field data of planted “Hood Head (HH) kelp” transposed into the 2018 Year 2 timeline. Dashed yellow line represents Year 1 simulated EASy HH kelp weight transposed into the 2018 Year 2 timeline. Solid green line represents Year 2 simulated EASy native HH kelp weight. Solid purple line represents Year 2 simulated EASy planted SC kelp weight. Model was tuned so that purple line matched solid blue line, and green line matched dashed blue line.

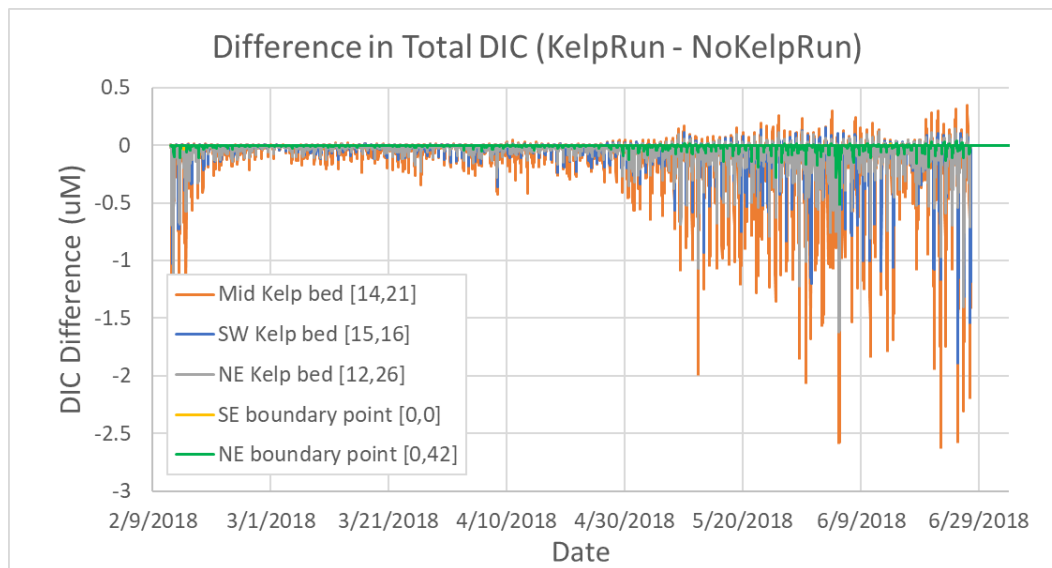


Figure 85. Difference between time series of model output of total DIC of a Year 2 ‘NoKelp’ run and a ‘Kelp’ run. Plotted lines represent difference in data output from five capture cells.

These changes are because as the kelp grows, it uses and sequesters carbon in the water, resulting in a decrease in measured modeled DIC compared to the ‘NoKelp’ run. Likewise, we see an increase in aragonite saturation and calcite saturation compared to the ‘NoKelp’ results.

9.2.2.3 Validation

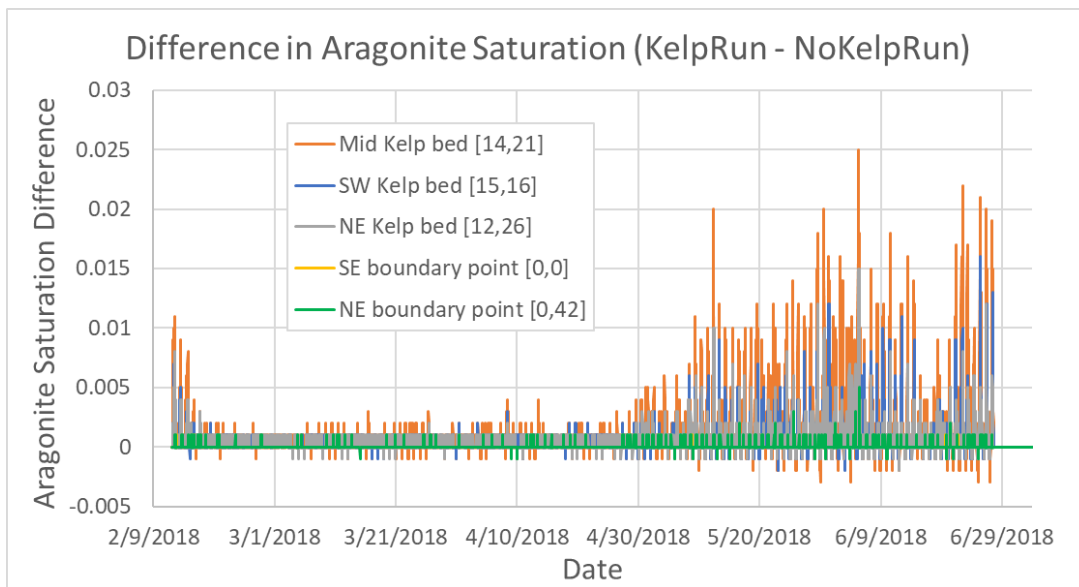


Figure 86. Difference between time series of model output of calculated aragonite saturation of a Year 2 'NoKelp' run and a 'Kelp' run. Plotted lines represent difference in data output from the five capture cells.

Similar to Year 1 results, the changes in water chemistry parameters like aragonite saturation, DIC, pH, etc. are likely far too small to be measured in the field and are hence difficult to validate. Indeed, much of the model is driven by incoming field data – for example, the ambient pH of the water flowing into the model is generated from SeaFET measurements taken from moorings near the experimental farm.

The vast majority of the fluctuations in pH are due to the changes in the ambient waters, rather than internal effects from the modeled farm itself. This is illustrated in Figure 87. Here, we see two plots of modeled pH values taken at different capture cells, along with the real pH values from one of the SeaFET moorings. Although we see large fluctuations in pH over the course of the entire experiment (top plot), when we

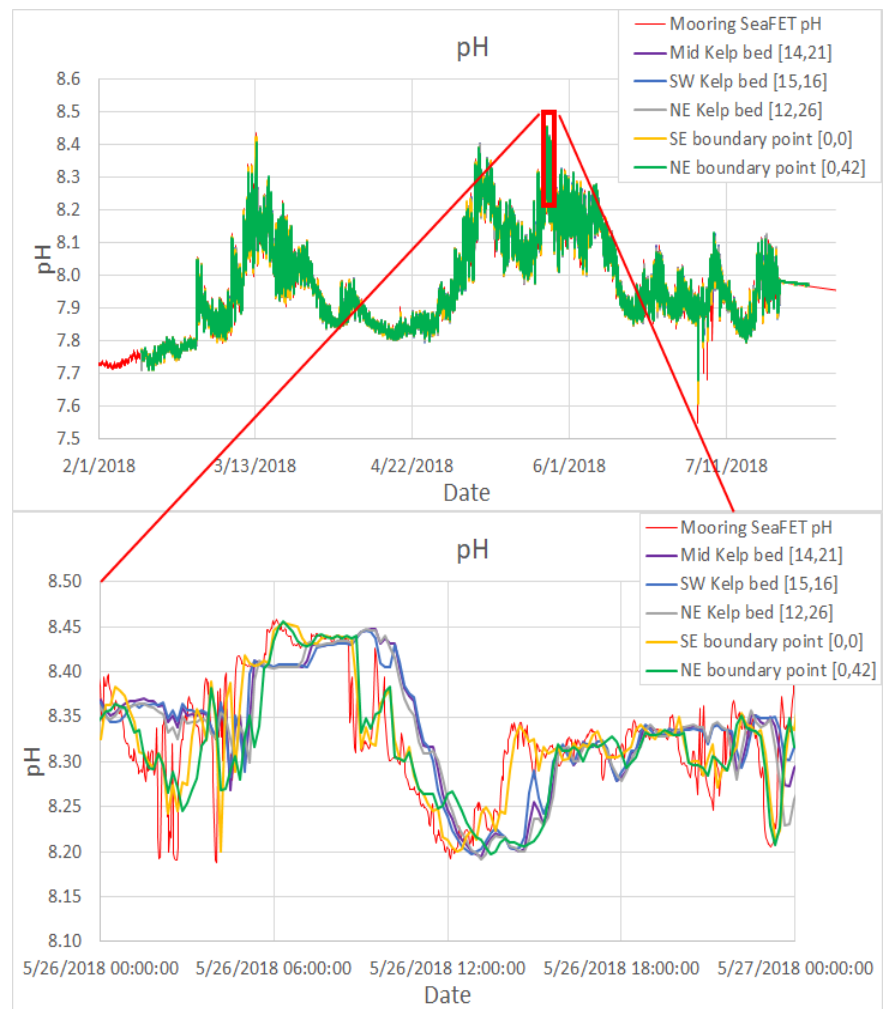


Figure 87. Model pH output at different capture cells; top plot represents the entire Year 2 experiment while the bottom plot shows only one 24-hour period.

zoom into a smaller time period (bottom plot, magnification illustrated with red lines), we can see that most of the simulated pH data closely tracks pH values from the incoming ambient waters (again represented by the Mooring SeaFET pH line). There are small differences between the different capture cell locations but for the most part, these relatively small differences are difficult to measure and validate accurately in the field.

However, to further investigate potential validation of our simulated data, we have still completed some spot comparisons between model output and field survey data (Figure 88). To do this, we first placed digital capture cells into the model at the locations where the field crews surveyed on three cruises during the summer of 2018. The model outputs data to an external .csv file at the designated capture cell locations at every time step of the simulation (here, every 10 minutes). We then extracted the model time series data at the time steps and depths closest to the real-life times and depths at which the survey data were taken. Data used in this analysis were limited to surface depths (between 0-3 meters depth).

Figure 88 shows calcite saturation and DIC model output compared to survey cruise data taken on three different cruises: one on 5/7, one on 6/18 and one on 7/23 and 7/24. Calcite saturation (shown at left) matches up well for the most part. DIC is slightly less similar but still well within reasonable ranges of fluctuation. The most noticeable difference between the model output and the cruise data is in the latter half of the first cruise (top two plots, right-side of each plot). There are distinct differences between



Figure 88. Comparisons of data taken from survey cruises and model output. Left plots show calcite saturation values; right plots show DIC. From top to bottom, plots represent three different cruise times (May 7, June 18 and July 23-24).

model and field data that are not observed in the first half of the first cruise, taken only hours earlier. After studying additional field data taken on the survey cruise, it was determined that a stream of warmer fresher water moved through the survey area at the time of the second sampling, which would account for higher calcite saturation values and lower DIC values. Notably, it was from analyzing the model data that caused us to look closer at the survey data; without the model output we may not have realized that a stream of fresher warmer water had flowed through the survey area at that time.

9.3 Applications of the Model

9.3.1 Varying current speeds

Prior to the completion of the Year 2 field study, we ran a series of experimental simulations while varying the simulated currents. We took the ‘real’ current meter data used in the tuned Year 1 model and

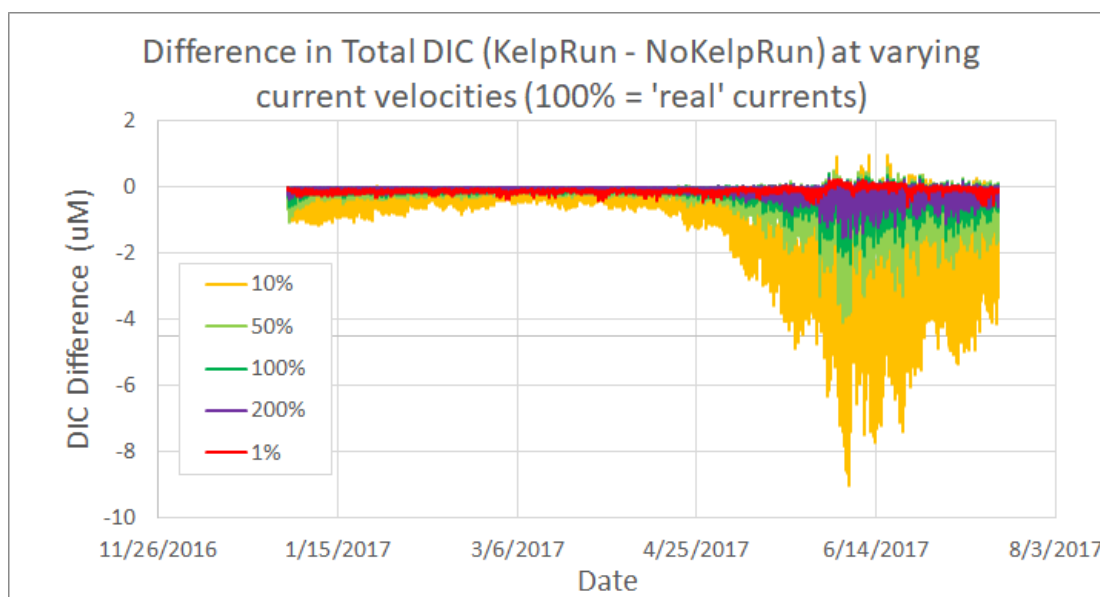


Figure 89. The difference in total DIC at varying current velocities.

modified all current magnitudes by a specified percentage (e.g., 10%, 50%). Results suggested that simulated currents of 10% of the ‘real’ current magnitudes resulted in the greatest uptakes of DIC while not significantly impacting kelp growth (Figure 89).

The results seen in Figure 89 were generated by subtracting the output of a simulation without kelp from a simulation with kelp, with all other variables the same. Data points were taken from a capture cell located in the middle of the simulated kelp farm. The greater the magnitude of the DIC Difference, the stronger the effect from the kelp bed. The strongest effects on DIC were seen in mid June 2017; the ‘real’ current simulation (in dark green) reduced DIC by only ~2 µM while the 10% current simulation (in orange) reduced DIC by up to ~9 DIC.

These results suggest that the Hood Head site – an area of relatively fast-flowing currents (with an average speed of ~0.1 m/sec at 3 meters depth) – may not be the optimal location for siting kelp farms with a goal of reducing DIC and countering OA. Rather, a site with much lower average current speeds (closer to 0.01 m/sec) would likely have a greater effect on reducing DIC. Indeed, a second set of experiments was conducted that ran simulations with fixed current magnitudes (e.g., 0.1 m/s, 0.01 m/s).

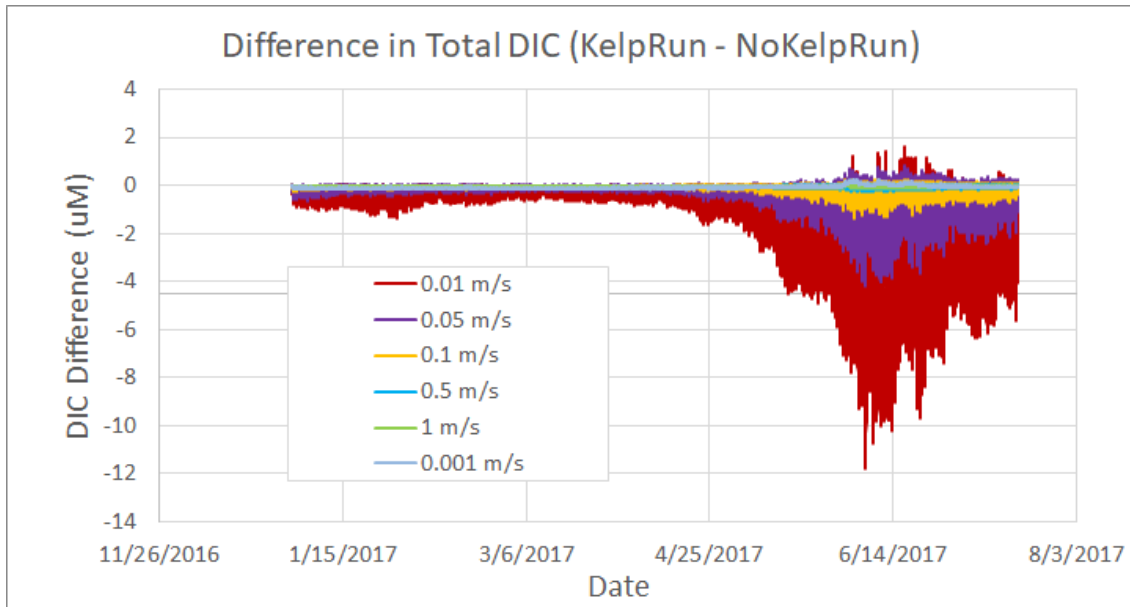


Figure 90. The difference in total DIC at fixed current velocities.

Figure 90 shows the results of these experiments; as predicted, we see the greatest reduction in DIC in the simulation with fixed current magnitudes of 0.01 m/s (shown in dark red in Figure 90).

9.3.2 Varying kelp densities

Several simulations were run in which we varied the densities of the kelp while maintaining the same farm size. Results were as expected: the greater the density of kelp, the stronger effects on the local

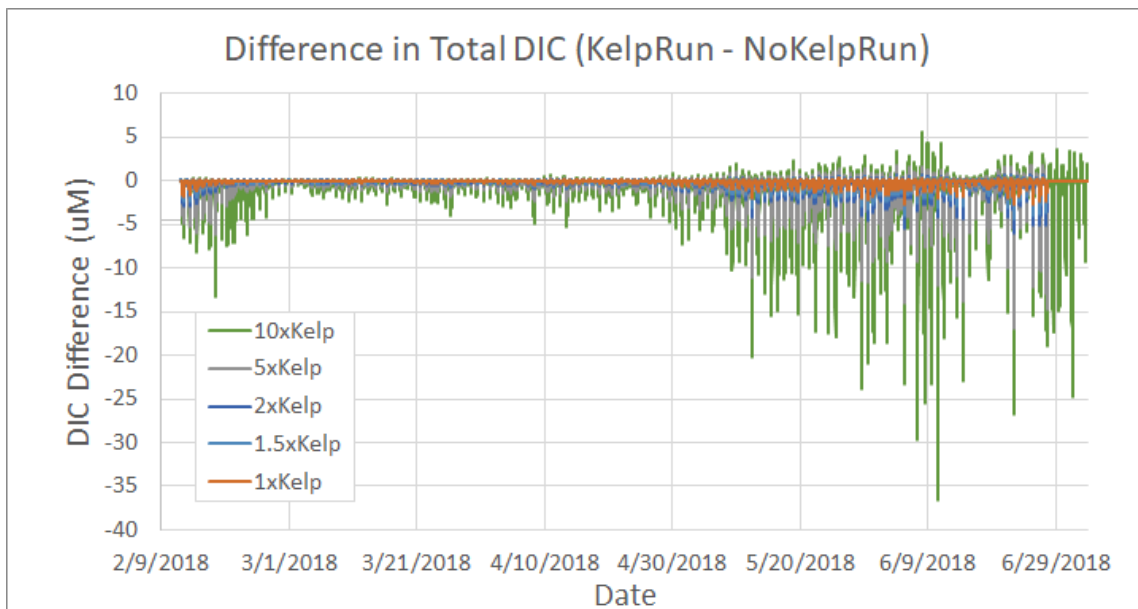


Figure 91. Difference between time series of model output of calculated total DIC of a Year 2 'NoKelp' run and a 'Kelp' run, for simulations of varying densities of kelp. All values taken from capture cell in the middle of the kelp farm. 1xKelp represents the 'real' Year 2 Hood Head kelp farm and other series have multiplied the starting kelp densities by the specified amounts. A 100xKelp simulation was run but is not included in this plot because it overwhelms the other series.

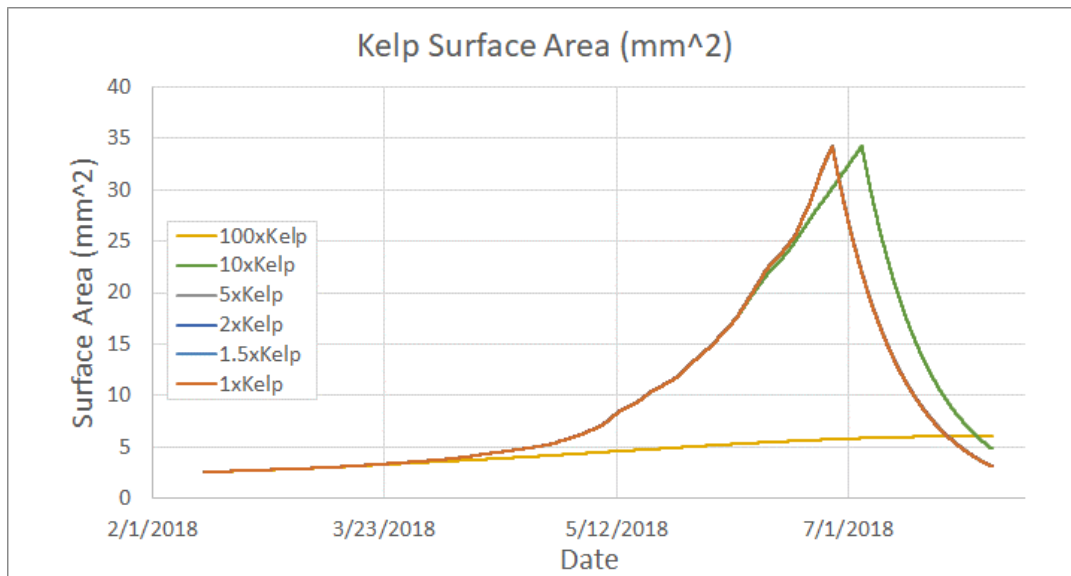


Figure 92. Kelp frond surface area outputs of the varying kelp densities simulations. 1xKelp represents the 'real' Year 2 Hood Head kelp farm and other series have multiplied the starting kelp densities by the specified amounts. Kelp growth rates begin to slow at some point between 5x and 10x densities.

environment (Figure 91). However, kelp growth rates were noticeably slowed once densities became too high (Figure 92) – initial analysis suggests that this is somewhere between 5-10x the density of the actual Hood Head farm site. As densities increase, kelp use up the nutrients available in their local area and are also impacted by increasing levels of self-shading. Other team members have suggested that densities of up to 1.5x those of the Hood Head farm site could be feasible; on the other hand, the model suggests that densities of up to 5x or more could result in similar growth rates and harvest schedules. However, these results have not been investigated and there could be many other factors that might prevent successful farming of higher densities (e.g., dense kelp blocking current flow, increased biofouling, physical space limitations).

9.3.3 Varying farm size

We also ran simulations varying the size of the modeled farm (5 and 10 hectare sizes, compared to the ~0.78 hectare size of the real farm; 10 hectare simulation shown in Figure 93) while maintaining the same density of kelp. As expected, the larger the farm, the greater the effects on the local environment (Figure 94).

Interestingly, increasing the size of the kelp farm seems to have diminishing returns with respect to effects on the local environment. This is evident in Figure 95, which shows kelp biomass on the left, and plots the cumulative difference in total DIC throughout the simulation on the right. The biomass of each simulated farm corresponds roughly to the size of the farm: the 5 ha farm has approximately 6x more biomass than the 0.78 ha original farm, and the 10 ha farm has about twice the biomass of the 5 ha farm (Figure 95, left). But in the cumulative different plot (Figure 95, right) we see that the cumulative effects on local DIC in the center of the 5 ha kelp farm is only about twice as strong as the DIC effects of the 0.78 ha kelp farm. This suggests that perhaps there is some upper threshold of kelp effects on local water chemistry due to current speeds or some other factor and could be investigated further.

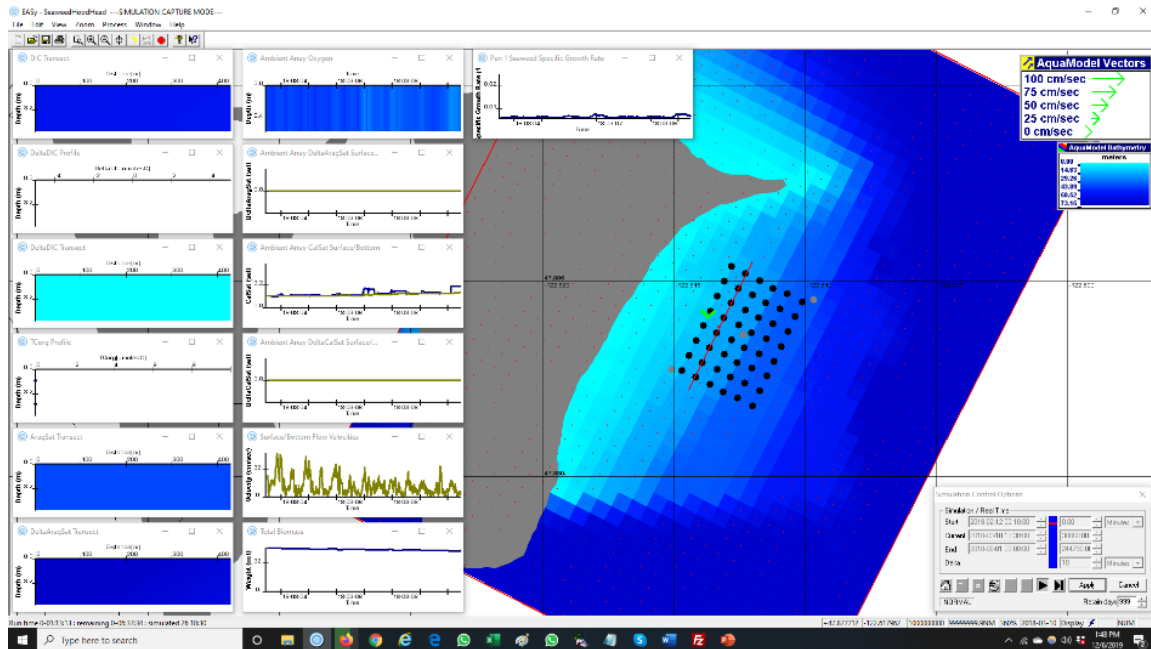


Figure 93. Simulation of a 10-hectare kelp farm near the original Hood Head farm site.

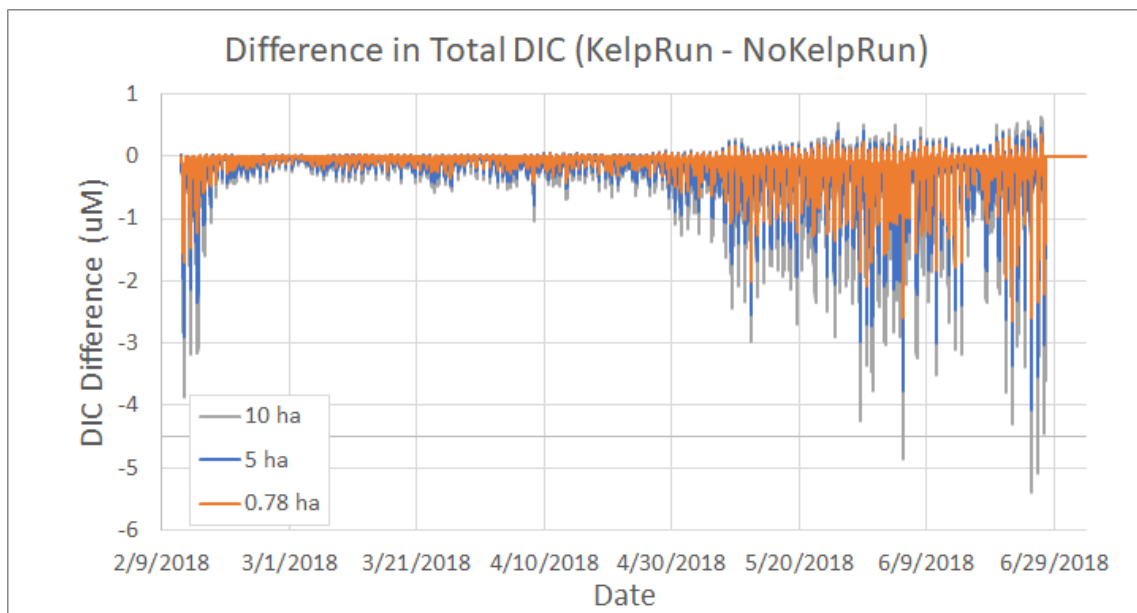


Figure 94. Difference between time series of model output of calculated total DIC of a Year 2 ‘NoKelp’ run and a ‘Kelp’ run, for simulations of varying farm sizes. All values taken from capture cell in the middle of the kelp farm.

9.4 Conclusions

Our model provides a useful tool for analyzing the impact of sugar kelp farms on the inorganic carbon system of waters that surround the farm. The model indicated that there were localized effects on water chemistry due to the kelp farm, but that these effects were too small to be measured by field measurements. We also clearly showed that model parameters of kelp frond surface area, weight, growth

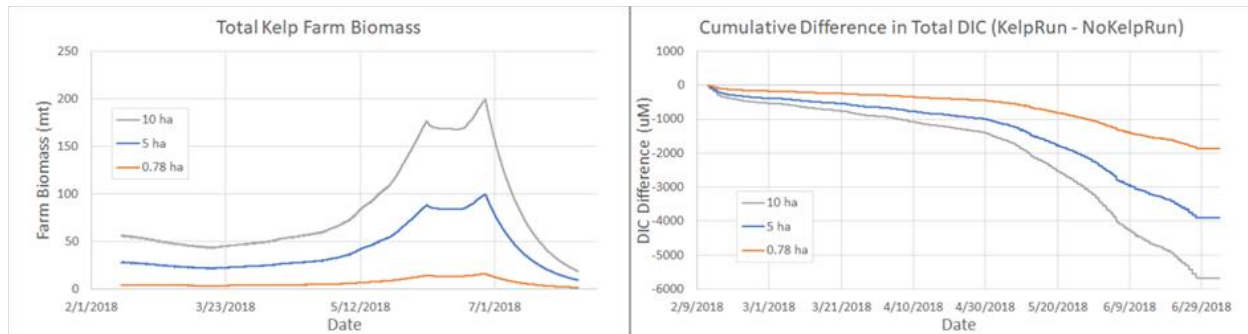


Figure 95. Left: Total kelp farm biomass for three simulated farms of different sizes (0.78, 5 and 10 hectares). Right: The cumulative difference in total DIC through the simulation runs. DIC taken from capture cell located in the center of the kelp farm.

rates, carbon and nitrogen content, and farm biomass were successfully tuned to the Hood Head field studies.

By modifying parameters of the modeled simulation, we found that kelp farms may have a more pronounced effect on local water chemistry if they are in areas of sufficiently slow current velocities (while still maintaining sufficient nutrient concentrations). We also found that increasing kelp densities and increasing the size of the kelp farm itself would both also have greater impacts. Both the model and the *Seaweed Site Evaluator* described below provide powerful tools to optimize remediation of OA with regard to location, size and kelp density within the farm.

10. Seaweed Site Evaluator Model

Authors: Dale Kiefer, Zach Siegrist

The *Seaweed Site Evaluator Model* is an offshoot of the primary *Hood Head Kelp Farm Model* and is currently under development. This project allows users to easily modify the location of a kelp farm and vary the resulting outputs (Figure 96). The 'default' farm is one modeled on the farm tuned in the *Hood Head Kelp Farm Model*. With a few simple clicks of the mouse, a user can create a new kelp farm in any location in the Puget Sound area. All user-designated locations are stored within a menu, and individual farm locations can easily be 'loaded' into the program. Once a farm

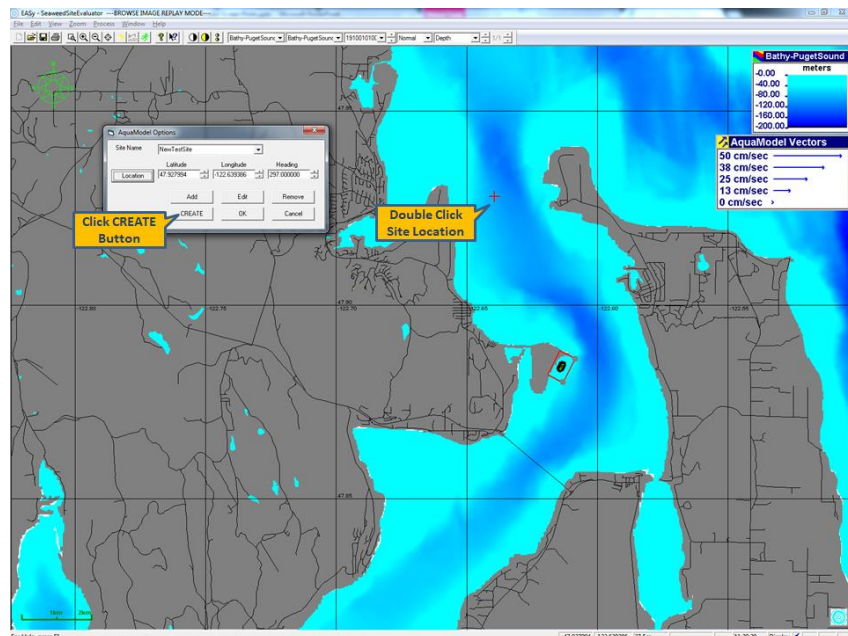


Figure 96. A screenshot of the Seaweed Site Evaluator project, showing the simple process by which a user can move a modeled kelp site around Puget Sound.

location is loaded, the user can then run the model and compare output (including kelp biomass, rates of growth, and effects on carbonate chemistry) between different test sites. In addition, this project may be

expanded in the future to include more accurate environmental data for the Puget Sound region, and/or may also be expanded to other areas outside of Puget Sound.

The utility of the model depends on data inputs for the general area intended for seaweed culture. These data could potentially be available from public data sets (e.g. Puget Sound Regional Synthesis Model (<http://www.prism.washington.edu/story/ORCA+Data+Collection>), Live Ocean: Pacific Northwest Ocean and Estuary Forecasts (<http://faculty.washington.edu/pmacc/LO/LiveOcean.html>), or WDOE Puget Sound and Marine Monitoring dataset (<https://ecology.wa.gov/Research-Data/Monitoring-assessment/Puget-Sound-and-marine-monitoring>)).

11. Engagement Activities, Communication Products, and Publicity

Authors: Meg Chadsey

11.1 Engagement Activities

Throughout the project period, the project team opportunistically created and pursued several engagement activities, which are described below. While not strictly part of the funded project, these activities were driven by broad interest in the project and a barrage of inquiries from the press, local chefs and food professionals, and many others interested in jumping into local seaweed farming. In this way, some of the unfunded portions of the original proposal, involving product and market development, were pursued during the project period.

Meg Chadsey (Washington Sea Grant), served as outreach coordinator for the kelp investigation, and launched the project outreach campaign in April 2017 at Seattle’s Museum of History and Industry’s *Edible City Science Fair* (<http://mohai.org/event/edible-city-science-fair/>) with a display titled *The Power of Kelp*. Visitors learned about OA and the potential of kelp to mitigate its effects while enjoying kelp dishes prepared by Seattle Culinary Academy (<http://culinary.seattlecentral.edu/>) students. Recognizing the double appeal of a delicious new local product that also contributes to a healthy marine ecosystem, Meg made kelp ‘edibles’ a cornerstone of her outreach toolkit (see Communication Products, below). She also supported efforts to build the local kelp market by experimenting with ways to prepare and preserve fresh kelp, and by connecting culinary professionals with locally grown kelp at the 2018 Farmer Fisher Chef Connection, a networking event for commercial food producers and buyers. Hood Canal sugar kelp took center stage at the PSRF benefit *Salishly Delicious*, hosted by the International Women’s Culinary Society Les Dames d’Escoffier (www.ldei.org) at their annual meeting in Seattle on October 11, 2018. Meg Chadsey and Stephen Schreck (PSRF), worked with chefs Bridget Charters and Lisa Nakamura from Tom Douglas’s Hot Stove Society, Asako Sullivan of Sustainable Collective, and Kel Killian of Bainbridge Artisan Resource Network to prepare several kelp-forward dishes for the event, including miso soup with sugar kelp, alder-smoked salmon with bull kelp pickle remoulade, and sugar kelp ice cream. PSRF biologist Brian Allen regaled the audience of over 125 tastemakers from around the globe with stories about the PAFF-funded project and images of the kelp farm.

Meg realized that our project’s partnership with SkyRoot Farm to compost 6,350 kg of Year 1 kelp created an opportunity to frame our project within the larger context of land-sea connections. Although the unexpectedly complex nature of the Year 1 monitoring data precluded much discussion of the first-year outcomes in terms of OA mitigation, a substantial amount of carbon and nitrogen was extracted from the marine environment and returned to the soil, creating a loop where there had previously been a one-way street. The co-benefits of integrating kelp aquaculture with upland farming became another key outreach message, and served as the basis for a December 4, 2017 ‘SOARCE’ webinar titled *Carbon Comes Home—Kelp Aquaculture to Benefit Sea and Soil*, hosted by the NOAA Ocean Acidification Program

(oceanacidification.noaa.gov), which was attended by 137 people from states across the U.S. and from as far away as South Korea.

A second partnership with biofuel expert Dr. Fernando Resende (University of Texas, formerly UW School of Forestry and Environmental Sciences) was also a focal point of outreach efforts. In late 2017, Dr. Resende conducted a successful pilot experiment in which a small amount kelp harvested from the Hood Canal was converted directly to jet fuel components through a novel process based on hydrothermal liquefaction. Unlike most biofuel production technologies which require that starting material be dehydrated prior to conversion, in Dr. Resende's process, the water content of fresh feedstock helps catalyze the conversion process, making it particularly well-suited for kelp. In theory, kelp-based biofuels could reduce carbon emissions from fossil fuel combustion while removing excess carbon from the marine environment. Closing carbon loops became the theme of a second webinar, *Kelping the Sea—Farming Seaweeds for Research and Resources in the Pacific Northwest* (<https://c-can.info/c-can-oar-may-16/>), hosted by the California Current Acidification Network (C-CAN) on May 16, 2018.

11.2 Communication Products

Some examples of communication products spawned by this investigation and related partnerships are:

- ***The Power of Kelp***, a poster developed for the 2017 Edible Science Fair, explains the basis for the Hood Canal investigation (<https://wsg.washington.edu/wordpress/wp-content/uploads/KelpPower.pdf>).
- Meg Chadsey and students in the UW Communications Leadership Program (<https://commlead.uw.edu/>) developed a ***Kelp Tasting Kit*** (<http://oceanlinknw.com/our-work/eat-more-kelp/>) to promote the ecological benefits of kelp and its use as a versatile and nutritious food source. The kit serves to introduce the public and chefs to kelp as a sustainable, healthy, locally-grown food. It includes dried kelp, recipes, an educational brochure, a large standing event banner, and a cooler for easy transport.
- Meg Chadsey partnered with UW Communications Leadership student Fahad Aldaajani and NOAA videographer Paul Hillman to film a short video about the co-benefits of integrating kelp aquaculture with upland farming. This film, also titled ***The Power of Kelp***, highlights the multiple benefits of kelp to our food system as 1) a sustainable and delicious new 'sea food'; 2) an organic alternative to synthetic fertilizers, that can help rebuild soils depleted of carbon and nutrients by industrial agriculture practices; and 3) a 'return ticket' for human-generated carbon and nutrient pollution that is harming our marine environment. It is in the final phases of completion.
- **Washington Sea Grant's Kelp Aquaculture webpage** (<https://wsg.washington.edu/community-outreach/kelp-aquaculture/>) showcases several project-related outreach activities and products. WSG is also developing a suite of web-based communication products for PSRF's project webpage.
- Vulcan, Inc.'s produced a short video highlighting the project - **Kelp Power: Can Seaweed Fight Ocean Acidification?** <https://youtu.be/T7fMSRFPna4>

11.3 Publicity

On the publicity front, audio and video stories about the Hood Head kelp project aired on multiple stations and networks throughout the project period. Following are a few highlights:

- The Seattle Times, July 3, 2016, Studies testing kelp to ease effects of ocean acidification: <https://www.seattletimes.com/seattle-news/studies-testing-kelp-to-ease-effects-of-ocean-acidification/>

- The New York Times, July 4, 2016, Slowing ocean acidification with kelp: https://www.nytimes.com/2016/07/05/science/fighting-ocean-acidification-through-kelp.html?_r=0
- KUOW, January 31, 2018: <http://kuow.org/post/can-kelp-and-seagrass-help-oysters-adapt-major-ocean-change>
- Oregon Public Broadcasting's Oregon Field Guide: January 31, 2018: <https://www.opb.org/news/article/kelp-seagrass-oysters-ocean-change/>; the relevant section that focuses on oysters, eelgrass, and kelp begins 16:24 minutes into the program and ends at 24:30; and February 1, 2018: <https://www.opb.org/television/programs/ofg/segment/eelgrass-oysters-northwest/>
- Marketplace, February 22, 2018: <https://www.marketplace.org/2018/02/22/could-kelp-help-oyster-industry-mitigate-effects-ocean-acidification/>
- The Seattle Times, Pacific NW Magazine, April 19, 2018, Food, innovation and resilience in the face of climate change: <https://www.seattletimes.com/pacific-nw-magazine/food-innovation-and-resilience-in-the-face-of-climate-change/>
- PBS News Hour, July 18, 2018: <https://www.pbs.org/newshour/show/this-aquatic-grass-could-help-shellfish-threatened-by-ocean-acidification>
- CBS 60 Minutes Kelp story, aired April 29, 2018 and again July 15, 2018: <https://www.google.com/amp/s/www.cbsnews.com/amp/news/60-minutes-seaweed-farming-and-its-surprising-benefits/>. Note: to see the video, one needs to be a CBS subscriber.
- Washington Sea Grant's Fall 2018 *SeaStar* Newsletter: <https://wsg.washington.edu/wordpress/wp-content/uploads/SeaStarAutumn18Web.pdf>. An article entitled *Carbon Comes Home* examines how the carbon captured by kelp can deliver environmental benefits.
- Western Washington University's The Planet, December 16, 2018: An interview with co-PI Joth Davis about growing kelp to shelter vulnerable shellfish: <https://theplanetmagazine.net/a-kelping-hand-5128b2a251cf>
- Crosscut, December 4, 2019: <https://crosscut.com/2019/12/could-seaweed-be-washingtons-next-cash-crop>; highlights PAFF team efforts to support the development of seaweed farming in Washington (see Section 12 'Leveraged Projects')

12. Leveraged Projects

Authors: Meg Chadsey

This project has generated intense interest in seaweed farming in our state. Seaweed farming in Washington waters is newly charted territory, with enthusiastic would-be practitioners jostling to enter the industry without adequate understanding of operational and regulatory requirements. Motivated by a desire to see this nascent industry grow in a way that will benefit Washington aquaculture, its coastal communities and our marine waters, Washington Sea Grant in partnership with PSRF and HCM, applied for and received \$99,997 (plus an additional 50% match) in 2019 from the National Sea Grant Program to develop and deliver seaweed farming training for prospective Washington growers over two years. This project leverages (and would not be possible without!) the seaweed farming knowledge, networks and outreach capacity catalyzed by the Paul G. Allen Family Foundation OA/kelp investigation. The program launched on November 20, 2019 with an Introductory Seaweed Farming Workshop (<https://wsg.washington.edu/community-outreach/kelp-aquaculture/seaweed-farming-training/>) attended by over 160 in-person and online participants. A second multi-day intensive training was conducted February 3-5, 2020.

Washington Sea Grant contributed to the development of a second national-level 2019 National Sea Grant proposal and received a \$100,617 (a subaward on a \$1.1 million award to project lead Connecticut Sea Grant; <https://seagrant.uconn.edu/2019/09/19/ctsg-to-lead-partner-on-4-aquaculture-projects-with-2m-award/>) to establish a central clearinghouse hub for science-based practical seaweed aquaculture resources. This hub will inform planning and outreach efforts for federal and state agencies as well as seaweed growers and other stakeholders across the U.S.

Washington Sea Grant also awarded \$9,000 to Dr. Eli Wheat for soil amendment pilot studies, and an additional \$188,498 to Dr. Fernando Resende, HCM and Dr. Eli Wheat to support Resende's kelp-to-biofuel research described in Section 11, and a new UW summer course about the co-benefits of seaweed farming, taught by Dr. Wheat and Meg Chadsey in 2020/2021.

Seaweed farming will likely take root in Puget Sound, if the interest generated by the Hood Canal investigation and the November 2019 and February 2020 seaweed farming workshops is any indication. The three leveraged projects described above are catalyzing a much-needed seaweed farming community of practice in our region and beyond. The project team and others are collaborating to make sure that seaweed farming is done in the best way possible with appropriate guidance and conditions. None of this would have been possible without the support from the Paul G. Allen Family Foundation.

CONCLUSION

Authors: Betsy Peabody, Joth Davis

The establishment of a seaweed farm in Puget Sound enabled project scientists to measure, evaluate, and model the physical, chemical, and biological effects of cultivated seaweed in a natural environment on a local scale. The following is a summary of the project outcomes and key findings also captured in the Executive Summary.

Project outcomes

1. Permitted and installed a commercial-scale kelp farm in Hood Canal, Puget Sound.
2. Established a kelp propagation facility to produce sporophytes on twine for both sugar and bull kelp (*Nereocystis luetkeana*) for outplant at the Hood Head investigation site and for use in bull kelp enhancement trials.
3. Cultivated over 20 metric tons (live weight) of sugar kelp in 2017 and 2018.
4. Monitored standing biomass of sugar kelp over two growing seasons.
5. Conducted seasonal estimates of net production (as amount of carbon fixed per day in tissues) and estimated potential removal of carbon and nitrogen in standing biomass at harvest.
6. Transported sugar kelp grown at Hood Head to Whidbey Island and Quilcene organic farms with the intent of enriching soil in 2017 and 2018.
7. Assessed seawater chemistry conditions at Hood Head in 2017 and 2018 with seasonally-deployed instruments and small boat surveys.
8. Conducted bioassay experiments to evaluate both growth and shell dissolution of Pacific and Olympia oysters, mussels, pteropods, and other pelagic gastropods using mesocosms deployed inside, outside, and at the edge of the kelp farm.

9. Developed a new model to assess the effect of kelp on seawater chemistry that integrates kelp production metrics, seawater chemistry, and comprehensive water property observations to generate fine-scale, 3-dimensional simulations over time.
10. Initiated development of a companion model, called “Puget Sound SeaweedSiteEvaluator,” to assess the potential for candidate kelp farm sites to exert a positive effect on seawater chemistry locally.
11. Engaged the public through high-visibility media outlets and a suite of other outreach activities, generating widespread interest in kelp farming, the development of locally grown seaweed products, and the potential for cultivation of seaweed for restoration purposes. Engagement activities helped leverage well over \$500K in new funding to guide the development of seaweed farms and markets in Washington.
12. Conducted extensive laboratory experiments in 2019 to further assess biological effects in Pacific and Olympia oysters and the biological responses observed in the field.

Key Findings

Key Finding 1. Farmed kelp offers some potential for removing carbon and nitrogen from seawater at harvest.

The Hood Head investigation demonstrated the capacity to grow two species of kelp successfully in Puget Sound, and to produce a variety of kelp products of interest to local markets. Hood Head is an excellent site for cultivating sugar and bull kelp, as evidenced by successful kelp cultivation in 2017 and 2018, and represents, at one hectare, the first commercial-scale demonstration of the viability of open-water kelp farming in Washington State. In 2017, 6,364 kilograms (kg) of sugar kelp (wet weight) was harvested and delivered to an organic farm on Whidbey Island, which resulted in the reconveyance of 130 kg of carbon (representing 20.36% of kelp biomass dry weight) and 18 kg of nitrogen (representing 2.85% of kelp biomass dry weight) from sea to land. Had we harvested kelp at peak biomass* in 2017, with 19,417 kg sugar kelp produced, we would have removed approximately 395 kg of carbon and 55 kg of nitrogen. In 2018, estimates for carbon and nitrogen contained in kelp blades grown at Hood Head averaged 21.54% for carbon and 1.99% for nitrogen. If kelp had been removed in 2018 at peak biomass, over 22,000 kg would have been removed from this small farm in Hood Canal, representing 474 kg of carbon and 44 kg of nitrogen. We note that this removal of carbon at peak biomass would be equivalent to the CO₂ emitted by 31–37% of **one** typical passenger vehicle in a year (per EPA web site). Similarly, the amount of nitrogen removed from the marine system at peak biomass would be equivalent to ten 43-lb bags of typical lawn fertilizer. Estimates for carbon removed from Puget Sound only reflect net production, that is, they do not reflect the significant amounts of carbon fixed by kelp and subsequently released back into the water during respiration, the dissolved organic material leaked from fronds, and eroded kelp blades. Nor do they reflect the amount of carbon used to produce the kelp. *Note: Kelp was not harvested at peak biomass in 2017 and 2018 in order to maintain kelp biomass at the project site throughout the monthly sampling cruises April-June.

Key Finding 2. The effect of kelp growth on seawater chemistry was not detected by state-of-the-art sensors and analyses used for assessment.

Differences in seawater chemistry inside compared to outside the kelp farm were below the range of detection by the best available oceanographic instruments and integrated biogeochemical analyses. We attribute this result, in part, to high average current velocities at the Hood Head site that resulted in low average residence time of seawater within the kelp farm. The kelp signal was also likely overwhelmed by

the larger signal from springtime phytoplankton blooms in north Hood Canal during the same timeframe that kelp was growing.

Key Finding 3. Kelp may help reduce cumulative adverse effects on calcifying organisms growing within the kelp farm.

Results from a small field study indicated improved conditions for various calcifying organisms (including Pacific and Olympia oysters, bay mussels, and pteropods) that were deployed in mesocosms inside and outside the kelp farm. Inside the kelp farm, we found reduced shell dissolution in all of the examined species. Two oyster species (Pacific and Olympia oysters) showed faster growth inside the kelp farm. It is important to note that the improved benefits are likely due to multiple factors; i.e. more favorable carbonate chemistry conditions, food availability, and energy trade-offs.

We investigated possible drivers of the field results with subsequent laboratory experiments with juvenile Pacific and Olympia oysters. Our laboratory results demonstrated that both oyster species can grow faster and have significantly less dissolution under experimental conditions of higher pH mean and frequency of variability. The amplitude of pH variation in the treatment was 0.2, equating to around 0.7 aragonite saturation state. These results are consistent with the findings of previous investigations. The difference between the laboratory treatments was much greater than observed or predicted effects of the kelp farm. The laboratory results indicated that benefits to oysters are observed after two to four weeks of exposure in the experimental conditions, indicating the beneficial effect of cumulative exposure over time.

Our field results suggest that association with kelp may locally benefit shellfish and other calcifiers, while our laboratory results confirm that Pacific and Olympia oysters benefit from improved pH conditions.

Key Finding 4. Model simulations of the Hood Head kelp farm indicated slightly reduced concentrations of dissolved inorganic carbon.

A key component of this project was the creation of a kelp model to explore phytoremediation effects under varied carbonate chemistry and nutrient (nitrogen) conditions. Field data collected during the two-year field investigation (flow conditions, temperature, salinity, stratification, chemistry, biology, kelp production) were used to drive model calculations. In simulations of farm dynamics during the spring and summer of 2017 and 2018, the largest decreases in dissolved inorganic carbon (DIC) and increases in aragonite saturation were found in the middle of the farm during periods of weak currents.

Although changes to seawater were too small to be measured *in situ*, model simulations showed a very small increase in aragonite saturation (maximum increase was 0.025). Laboratory studies have not demonstrated that changes at this scale have biological effects.

Key Finding 5. The simulated effect of kelp farms on local acidification conditions depends on current velocity, kelp density, and farm size.

An important finding of this investigation was determining more precisely the conditions under which seaweed farming *could* significantly affect seawater chemistry locally. *The Hood Head seaweed farm did not measurably change the seawater chemistry at the site.* However, modeling results suggest that under the right conditions, including current speed, nutrient availability, kelp density, and farm size, seaweed farms could measurably affect seawater chemistry locally. As we populate our toolkit for adapting to or mitigating acidified conditions, it is critical to understand the limits, potential, and correct application of each tool. Our experience also underscores that assessment and modeling are important in designing

future kelp farming operations, if one of the intended purposes is nutrient and carbon uptake in the environment.

Key Finding 6. There may be benefits to growing kelp in Puget Sound.

Based on our investigation at Hood Head, we demonstrated that seaweeds can be cultured in Puget Sound at a commercial scale, and that there is strong interest among growers and others for producing food-grade kelp. There is also growing interest among organic farmers in late season kelp biomass for soil enrichment. While limited, biological assessments suggest that growing seaweed in proximity to shellfish may make a positive difference for calcifiers, including oysters. To be clear, seaweed farming will not solve basin-wide acidification problems. Additional research needs to be conducted to determine whether seaweed farming in Puget Sound could improve local conditions at shellfish farms and provide an adaptation strategy that would assist in growing shellfish under increasingly acidifying conditions. (See Future Research section.)

Key Finding 7. Model simulations suggest that kelp farms could be engineered and sited to achieve larger effects on local acidification conditions.

The model proved to be the best vehicle for defining the conditions under which seaweed cultivation could exert a detectable effect on seawater chemistry. In the model, inputs included the seeding density of the kelp, water temperature, solar irradiance, current velocity, ambient nutrient concentrations, and carbonate chemistry variables. The model simulation calculated growth, photosynthetic and respiration rates of the kelp, and the impacts of kelp growth and metabolism on nutrient, oxygen, and DIC concentrations in seawater flowing through the farm. Modeling results indicate that the Hood Head site – an area of relatively fast-flowing currents with average speed of ~10-15 centimeters/second (cm/sec) at a depth of 3 meters – is a suboptimal location for siting kelp farms if a major objective is to locally reduce dissolved inorganic carbon and counter acidification. However, model simulations indicated that sites with lower current speeds, higher kelp density, and a larger growing area may have a greater local effect on seawater chemistry. In model simulations, the sweet spot that yielded the largest kelp effect occurred when flow rates were 10% of ambient flow observed at the Hood Head site. However, these optimal flow conditions may not exist in Puget Sound, and other complexities (e.g., respiration of detritus, self-shading, flow blocking) require further investigation. The sweet spot will also depend upon having sufficient light intensity and nutrient availability, which are both high at Hood Head. Sensitivity analyses with the model clearly showed that much larger decreases in DIC occurred in simulations where farm size or kelp density were significantly increased. For example, the maximum drawdown of DIC increased from approximately 1 $\mu\text{mol/kg}$ to 35 $\mu\text{mol/kg}$ when kelp densities increased tenfold. For context, the area at the Hood Head farm devoted to kelp cultivation was about 2.5 acres (1 hectare), which was composed of eighteen 500 foot growlines, with ten feet of separation between adjacent lines. The density of kelp grown at Hood Head in 2017 and 2018 was relatively low compared to commercial densities elsewhere in the world, especially in Asia. Therefore, increasing densities at kelp farms in Puget Sound should be feasible.

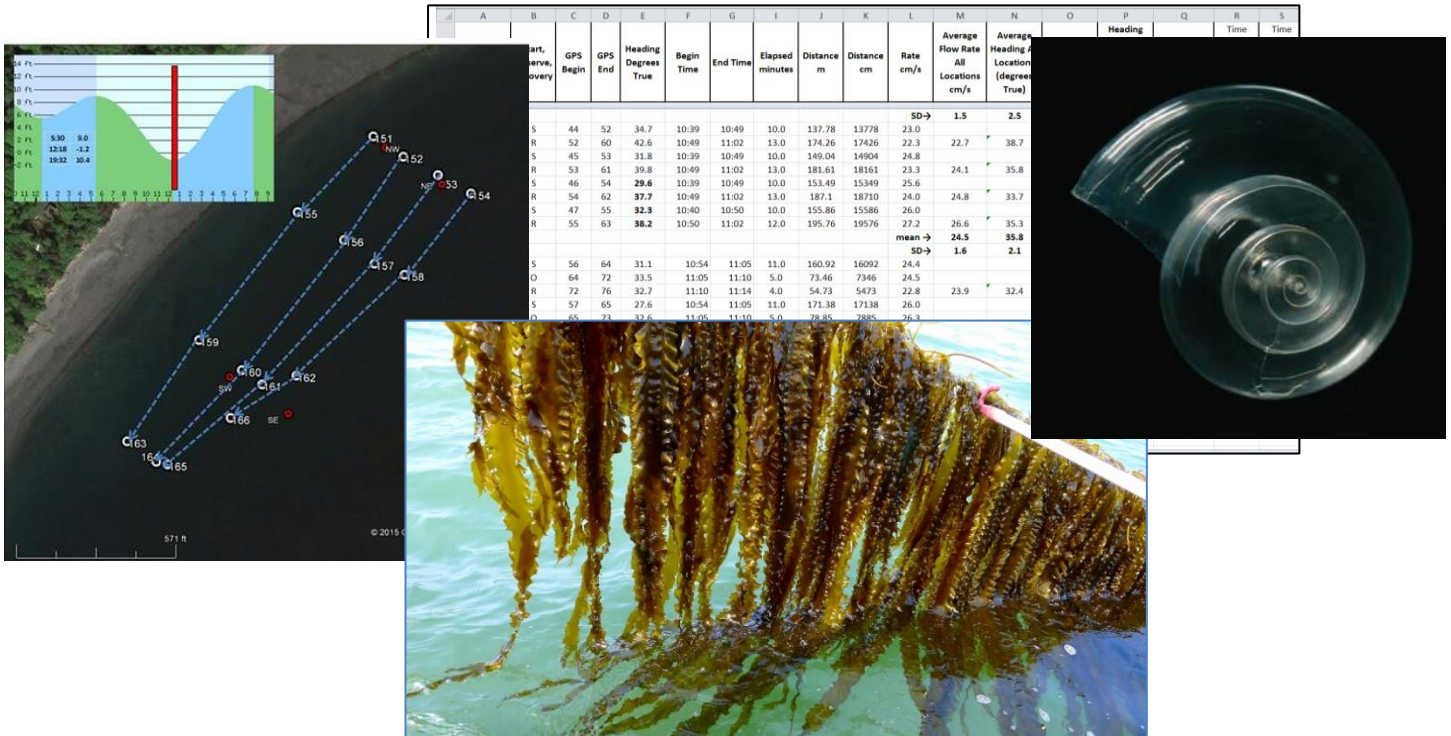
Key Finding 8. Outreach and publicity associated with this project stimulated new interest in kelp farming in Washington State.

The Hood Head investigation garnered significant publicity and attention. The coupling of multiple project elements – including kelp cultivation, chemical and biological assessment, and modeling – created a unique platform for building interest in actions that can potentially deliver multiple benefits. Seaweed farming workshops hosted by Washington Sea Grant and other partners in 2019 and 2020 attest to this growing interest.

APPENDIX A

Report entitled **Preliminary Assessment of Seawater Circulation near Hood Head, Hood Canal, Washington for Seaweed Cultivation Ocean Acidification Refugium Evaluation** authored by Dr. Jack Rensel (Rensel Associates Aquatic Sciences), reviewed by PSRF and submitted to Vulcan Philanthropy on August 31, 2015.

Preliminary Assessment of Seawater Circulation near Hood Head, Hood Canal, Washington for Seaweed Cultivation – Ocean Acidification Refugium Evaluation



Prepared for:
Puget Sound Restoration Fund
Betsy Peabody and Joth Davis
382 Wyatt Way NE
Bainbridge Island, WA 98110

Prepared by:
Jack Rensel Ph.D.
Rensel Associates Aquatic Sciences
4209 234th Street NE
Arlington WA 98223 USA

7 September 2015

Contents

Introduction	5
Background	5
Objectives	6
Site Location and General Characteristics.....	7
Methods	10
Results.....	12
Visual Drogue Distribution Plots	12
Tabular Data and Calculations	17
Flow Direction and Velocity	22
Summary and Conclusions	29
References Cited	31
Appendix	33

List of Figures

Figure 1. Project vicinity map	7
Figure 2. Project near-vicinity map.	8
Figure 3. Example possible seaweed array as yellow colored lines within the aquatic lease area in green background color.....	9
Figure 4. Windowshade drogue and marker float as described in the text.....	10
Figure 5. Generalized summary of flow directions for daytime ebb and flood of July 17, 2015. 12	
Figure 6. Generalized summary of flow directions for daytime ebb and flood of July 17, 2015. .13	
Figure 7. Generalized summary of flow directions for daytime ebb and flood of July 17, 2015. .13	
Figure 8. Generalized summary of flow directions for daytime ebb and flood of July 17, 2015. 14	
Figure 9. Generalized summary of flow directions for daytime ebb and flood of July 17, 2015. 14	
Figure 10. Generalized summary of flow directions for daytime ebb and flood of August 21, 2015, sets 1-5 left and sets 6-10 right.....	15
Figure 11. Generalized summary of flow directions for daytime ebb and flood of August 21, 2015, set 11 left and set 12 right.	15
Figure 12. Generalized summary of flow directions for daytime ebb and flood of August 21, 2015, set 13 left and set 15 right. Sets 14 and 16 not shown for brevity.	16
Figure 13. Generalized summary of flow directions for daytime ebb and flood of August 21, 2015, set 17 left and set 20 right.	16

Figure 14. Generalized summary of flow directions for daytime ebb and flood of August 21, 2015, sets 21-23.....	17
Appendix Figure 15. Ebb tide July 17, 2015.....	33
Appendix Figure 16. Ebb tide July 17, 2015.....	34
Appendix Figure 17 Ebb tide July 17, 2015	34
Appendix Figure 18 Ebb tide July 17, 2015	35
Appendix Figure 19 Ebb tide July 17, 2015	35
Appendix Figure 20. Ebb tide July 17, 2015	36
Appendix Figure 21. Ebb tide July 17, 2015	36
Appendix Figure 22. Change of tide, July 17, 2015.....	37
Appendix Figure 23. Flood tide July 17, 2015.....	37
Appendix Figure 24. Flood tide July 17, 2015.....	38
Appendix Figure 25. Flood tide July 17, 2015.....	38
Appendix Figure 26. Flood tide July 17, 2015.....	39
Appendix Figure 27. Flood tide July 17, 2015.....	39
Appendix Figure 28. Flood tide July 17, 2015.....	40
Appendix Figure 29. Flood tide July 17, 2015.....	40
Appendix Figure 30. Flood tide July 17, 2015.....	41
Appendix Figure 31. Flood tide July 17, 2015.....	41
Appendix Figure 32. Flood tide July 17, 2015.....	42
Appendix Figure 33. Flood tide July 17, 2015.....	42
Appendix Figure 34. Flood tide July 17, 2015.....	43
Appendix Figure 35. Last plot for July 17, 2015 survey.....	43
Appendix Figure 36. Begin August 21, 2015 ebb tide.	44
Appendix Figure 37. August 21, 2015 ebb tide	44
Appendix Figure 38. August 21, 2015 ebb tide	45
Appendix Figure 39. August 21, 2015 ebb tide	45
Appendix Figure 40. August 21, 2015 ebb tide	46
Appendix Figure 41. August 21, 2015 ebb tide	46
Appendix Figure 42. August 21, 2015 ebb tide	47
Appendix Figure 43. August 21, 2015 ebb tide	47
Appendix Figure 44. August 21, 2015 ebb tide	48
Appendix Figure 45. August 21, 2015 ebb tide	48
Appendix Figure 46. August 21, 2015 ebb tide	49
Appendix Figure 47. August 21, 2015 ebb tide	49
Appendix Figure 48. August 21, 2015 ebb tide	50
Appendix Figure 49. August 21, 2015 ebb tide	50
Appendix Figure 50. August 21, 2015 ebb tide	51
Appendix Figure 51. August 21, 2015 ebb tide	51
Appendix Figure 52. August 21, 2015 flood tide	52

Appendix Figure 53. August 21, 2015 flood tide	52
Appendix Figure 54. August 21, 2015 flood tide	53
Appendix Figure 55. August 21, 2015 flood tide	53
Appendix Figure 56. August 21, 2015 flood tide	54
Appendix Figure 57. August 21, 2015 flood tide	54
Appendix Figure 58. End August 21 2015 survey.	55

List of Tables

Table 1. Field survey timing and concurrent predicted tidal and wind conditions.	11
Table 2. Drogue survey data and calculations 27 July 2015.....	18
Table 3. Drogue survey data and calculations 21 August 2015.....	22
Table 4. Summary statistics for sampling times by location and tide.	26
Table 5. Parsing of summary data into tidal stage for sampling times and variation from straight through flow within the lease area.....	27
Table 6. Summary of flow velocity statistics from Hood Head drogue survey.	28

Acknowledgements

This report was prepared with funding provided by the Paul Allen Family Foundation to the Puget Sound Restoration Fund and a subcontract to Rensel Associates Aquatic Sciences..

Dr. Joth Davis provided the assistance in completing the field work at the Hood Head site including provision of the sampling vessel.

Cover photos from this report except:

Pteropod photo from: Washington State Blue Ribbon Panel on Ocean Acidification (2012): *Ocean Acidification: From Knowledge to Action, Washington State's Strategic Response*. H. Adelman and L. Whitely Binder (eds). Washington Department of Ecology, Olympia, Washington. Publication no. 12-01-015.

Seaweed photo credit: Thimble Island Oyster Company

Citation

This technical report may be cited as:

Rensel, J.E. 2015. Preliminary Assessment of Seawater Circulation near Hood Head, Hood Canal, Washington for Seaweed Cultivation – Ocean Acidification Refugium Evaluation. Prepared by Rensel Associates Aquatic Sciences for Puget Sound Restoration Fund and Paul Allen Family Foundation. 55 p.

Introduction

Background

Seaweed cultivation known as “marine agronomy” and wild seaweed harvest occurs in many countries for human food and animal feed. In Japan and Asia alone, the production is worth many billions of US dollars.

Increasingly there is interest in seaweed cultivation for concurrent other purposes too. These include removal of excess nutrients such as dissolved inorganic nitrogen from coastal areas with eutrophication issues, as fuel stock for alternative energy production, for aquatic habitat conservation or restoration and for pharmaceutical and chemical extraction.

The subject of a project spearheaded by the Puget Sound Restoration Fund (PSRF) is another purpose: seaweed for creation of refugia for sensitive species being adversely affected by the increasingly acidic marine waters. The concept is simple: seaweed removes carbonates from seawater and results in less acidity but quantifying the effect is far from simple. PSRF and their partner organizations propose creation and documentation of economically self-sustaining refugia where seaweed is harvested to cover the costs of production while providing the benefit of sweetening the water, i.e., increasing pH and aragonite saturation, the latter an important factor in maintaining shell-forming marine species that are increasingly threatened.

However, adequate data or validated models of marine agronomy as a means to mitigate ocean acidification (OA) are scarce or non-existent, although they are the subject of publications, discussion and theoretical modeling. OA mitigation is sometimes considered a qualitative side-benefit of marine agronomy and it may be modeled in terms of theoretical carbon removal and effects on carbonate chemistry. However, ocean acidification in coastal areas remains difficult to measure versus background variation related to mixing and transport. OA determination in coastal areas especially requires the use of sensitive and accurate measuring equipment for pH and the related parameters of carbonate chemistry that are only now being developed. The PSRF project will include use of state-of-the-art seawater chemical measurement moorings that will be arrayed up and downstream of a large seaweed farm. By estimating seaweed biomass and growth and comparing the water chemistry effects, a real-world evaluation of such a system can be quantitatively measured and compared to existing models and projections commonly used.

This report includes preliminary data and analysis of water circulation at a seaweed project in Washington State that is intended to provide proof of concept for creation of ocean acidification refugia. This report is a minor step in the process of planning, building and operating the seaweed-OA refugium but necessary to begin to understand how to place carbonate chemistry, current meters and other moorings around the facility.

The approach to be taken with the refugium planning involves measuring background conditions upstream of the seaweed array and the effects of the seaweed downstream after the water passes through all of the seaweed. When the tide changes, the downstream

becomes upstream but the problem is that flows are often in different directions so the fixed moorings downstream will sometimes only be measuring part of the effect of the entire seaweed array. Determining about how often that sometimes occurs was a goal of this small study.

Upstream/downstream aquatic measurements are commonly used in marine ecology studies and regulatory monitoring. I have used it to measure fecal coliform production of seabirds and gull in the Dungeness River and Bay (Rensel 2003) and nutrient production by aquaculture facilities on numerous occasions (Nash 2001). It has been used for Washington Departments of Fish and Wildlife, Natural Resources and Ecology for required monitoring of floating aquaculture in the past. Its use yielded reasonably accurate results compared to widely accepted laboratory data when conducted appropriately, as I reported in the State's programmatic EIS for marine fish culture (Parametrix et al. 1990). I also used the approach for stable isotope studies of aquaculture and IMTA effects in Puget Sound (Rensel et al. 2011) and the nutrient depleted mid-Columbia River (Rensel 2010).

When seaweed production is underway at the Hood Head facility, current meters will be positioned up and downstream of the seaweed and possibly within the culture area to provide physical transport velocity and direction (vector) data. However, it is very difficult to estimate the actual rates of the seaweed effects unless the water is flowing like a pipeline through the facility, i.e., straight through and parallel with the long axis of the facility. This will not occur regularly, but should several times daily for long enough periods to collect reasonably accurate data. When the water flows tangentially, some unknown amount of the effect will escape monitoring. All of this assumes a uniform downstream effects field unless several downstream instrument moorings can be use. Some minor variation of flow direction will have to be accepted, say five compass degrees, or 2.8% of the possible 180 compass degrees of a 360-degree compass rose. Elapsed time of flow through must also be considered to measure the effects of the entire facility.

Objectives

In order to measure the effects of the seaweed array upon water carbonate chemistry, it is essential that the hydrodynamics of the site be understood before final design of the sampling strategy and monitoring equipment placement. The process initiated with this survey will involve additional study and planning by the project team that includes many other participants.

The primary objective of the drogue (i.e., drifter) studies reported herein was to document the frequency with which water flows directly through the project site. This is the first step in a process of deciding where the water chemistry moorings will be placed and how it is to be operated. A companion objective was to collect concurrent drogue velocity information. More accurate effects measurements will likely occur when flows are modestly slow and dilution of effect is minimized. Velocity measurement can more accurately be done by current meters and will commence in the winter of 2015-2016. However, the drogue data gives some first insight into the range of expected velocity that will be found as this study was conducted on both large and small tidal exchange days.

Although perhaps obvious to some readers, drogue tracking provides valuable wide-area information not provided by current meter moorings that focus on a single point (i.e., Lagrangian vs. Eulerian measurements). The drogues follow the pathway of water movement throughout a monitored area and several can be set at once and followed concurrently. By repeatedly placing, tracking with GPS, recapturing and replacing the drogues upstream of the project area an estimate of the pathways taken and variation from straight through flow was made in this survey. Such data could also be made by placing current meters at both ends of the facility, but directional transport in the area between them would remain unknown and speculative. Drogue data may also be useful to determine if there is a need to build a seaweed array within the aquatic lease area that is angled to match some dominant flow direction, although this may be technically difficult.

A third intangible but important objective I have found with all drogue surveys is to simply be on the site of a marine project or study area to observe conditions, birds and marine mammals, use by humans, wind waves, etc. In the present case, we had discussions with several local boaters including residents of Hood Head and we felt these contacts to be valuable and all those who came by voiced strong support for the project. Remote sensing is a wonderful thing, but on-site human observation and contact with local residents is an important factor in the success of any project.

Site Location and General Characteristics

The study site is located in Western Washington State near the entry to a long, narrow and deep fjord known as Hood Canal northwest of Seattle (Figure 1). Located in the North Hood Canal region, the general area is known for a long floating bridge (Figure 2) and is just north of the U.S. Navy's Trident submarine base.



Figure 1. Project vicinity map

Seawater from Admiralty Inlet in the main basin of Puget Sound flows into the area during mixed semidiurnal tidal flows. The orientation of Hood Canal from southwest to northeast and surrounding topography allows for orographic channeling of prevailing southwest winter winds to northerly winds in the summer. Hood Canal's southern and central regions have been the subject of increasing concern due to seasonal deep-water hypoxia and vertical stratification-turnover events that cause marine fish and invertebrate kills and other adverse conditions. However, the project site is within a subarea of northern Hood Canal area that is subject to very active vertical mixing that prevents such problems.

North Hood Canal is relatively deep with depths to approximately 175 meters, but the project is located nearshore adjacent to Hood Head in less than 20 m depth. Hood Head is an island along the west shore of Hood Canal that is lightly populated with residential or seasonal occupied cabins.

The seaweed project site has previously been leased for longline shellfish aquaculture from the Washington Department of Natural Resources and is presently having a permit modification to allow for seaweed aquaculture. As shown in Figure 2, the lease area is located on the west side of Hood Canal and the east side of Hood Head Island (or peninsula, depending on tidal height). It is protected from north winds by a sand spit (Hannon Point) to the north and to some extent by the Hood Canal floating bridge to the south.

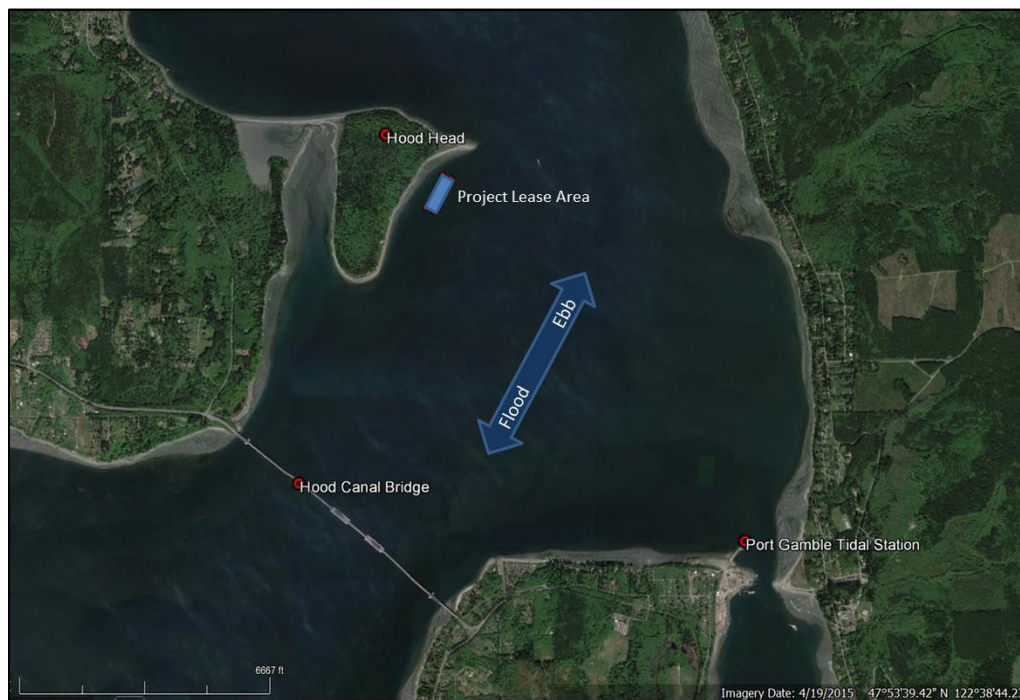


Figure 2. Project near-vicinity map.

The Hood Head aquatic lease area corners are located as follows:

NE Corner: 47°52'58.7" N; 122°36'54.3" W

NW Corner: 47°52'57.6" N; 122° 36' 51.0" W

SE Corner: 47°53' 07.4" N; 122 ° 36' 47.3" W

SW Corner: 47°53' 06.3" N; 122° 36' 44.1" W

The project lease area measures 1000' (304.9 m) north to south and 250' (76.2 m) east to west. The lease area is 5.74 acres (250,000 ft² or 2.32 hectares). The seaweed array final size and orientation is not yet determined but may be approximately 500 ft. long by 250 ft. wide (152.4 m x 76.2 m) or 125,000 ft² (11,612 m² or 0.0116 km²). An example layout with the seaweed longlines oriented longitudinally is shown as Figure 3. Small yellow dots indicate possible current meter locations, although more than one current meter may be placed at each end to provide a more accurate measure of flow direction and velocity.



Figure 3. Example possible seaweed array as yellow colored lines within the aquatic lease area in green background color.

Source: Puget Sound Restoration Fund unpublished proposal.

Methods

Water circulation studies were conducted using “windowshade drogues” that were nylon, underwater sails attached by a 1/16th inch line to a surface float (Figure 4). The underwater sails were 1 x 0.75 meter dimension (0.75 m²) and set to operate at an average depth of 2.0 m below the surface. The surface floats were 10” bullet shaped commercial trawl buoys with a ¾-inch diameter schedule 90 PVC conduit of 1.5 m length placed through them. The conduit provides enhanced visibility for locating and as a means to attach the thin line to the underwater windowshade sail. Each drogue was numbered on the float as well as having stripes on the pole for distant identification.



Figure 4. Windowshade drogue and marker float as described in the text.

Windowshade drogues were deployed in various locations and patterns depending on conditions and tidal stage but mostly in an array of four drogues, spaced in equal distances and a perpendicular array in relation to the shoreline. During northward flowing conditions, the drogues were placed along such a transect parallel to south end of the array. During southward flows, the drogues were placed along the north end of the lease area.

GPS locations of the drogues were logged by use of a Garmin GPSmap 60CSx geographic positioning unit operated with WAAS enabled. The GPS antenna was held immediately over each drogue as the boat navigated by and the location recorded. Given the short distances involved in this survey, at least three locations were logged for each drogue within the lease area, with more recorded if the flows were slow. As the drogues passed the midway north to south part of the lease area, their location was recorded and another set of drogues were placed upstream. In this manner, usually eight drogues were deployed at any given time. Winds were not a factor in these surveys (Table 1) and GPS accuracy was acceptable, but not as good as normally experienced in Puget Sound.

Table 1. Field survey timing and concurrent predicted tidal and wind conditions.

Date	Time	Predicted Tidal Height(ft)	Predicted Tidal Change (ft)	High/Low Tide	Wind Velocity Range (mph)	Wind Velocity Average (mph)	GPS 95% confidence Interval
7/17/2015	5:30 AM	9.0'	3.4'	H	--	--	
7/17/2015	12:18 PM	-1.2'	10.2'	L	0 – 7	4.0	3.2 m
7/17/2015	19:32 PM	10.4'	11.6'	H	2 - 10	6.0	3.4 m
8/21/2015	10:13AM	7.7	5.7'	H	--	--	
8/21/2015	15:45 PM	4.9	2.8'	L	0 - 2	1.0	3.6 m
8/21/2015	21:55 PM	9.2	4.3'	H	0 - 2	0.5	3.4 m

The first survey day had both a large ebb and flood tidal exchange (10.2 and 11.6 ft respectively), while the second survey day was picked to be modestly low (2.8 and 4.3 respectively). These predictions were for the tidal station in Hood Canal near the entry to Port Gamble that is across the water body to the east.

For comparison, the mean tidal range at this station is 6.7' and spring tides for this station are defined as 10.3' elevation change. Thus, we sampled nearly matched large ebb and flood tides on the first sampling day and small ebb and flood tides on the second sampling day and bracketed the mean tidal amplitude values.

Results

Visual Drogue Distribution Plots

Detailed drogue tracks from both days surveys are included in this report's appendix. Figures 5 through 14 below condense and summarize the results for the general direction of most drogues during each indicated tidal period. Raw data with some data reduction are shown in Table 2 and 3 after the generalized drogue path charts.

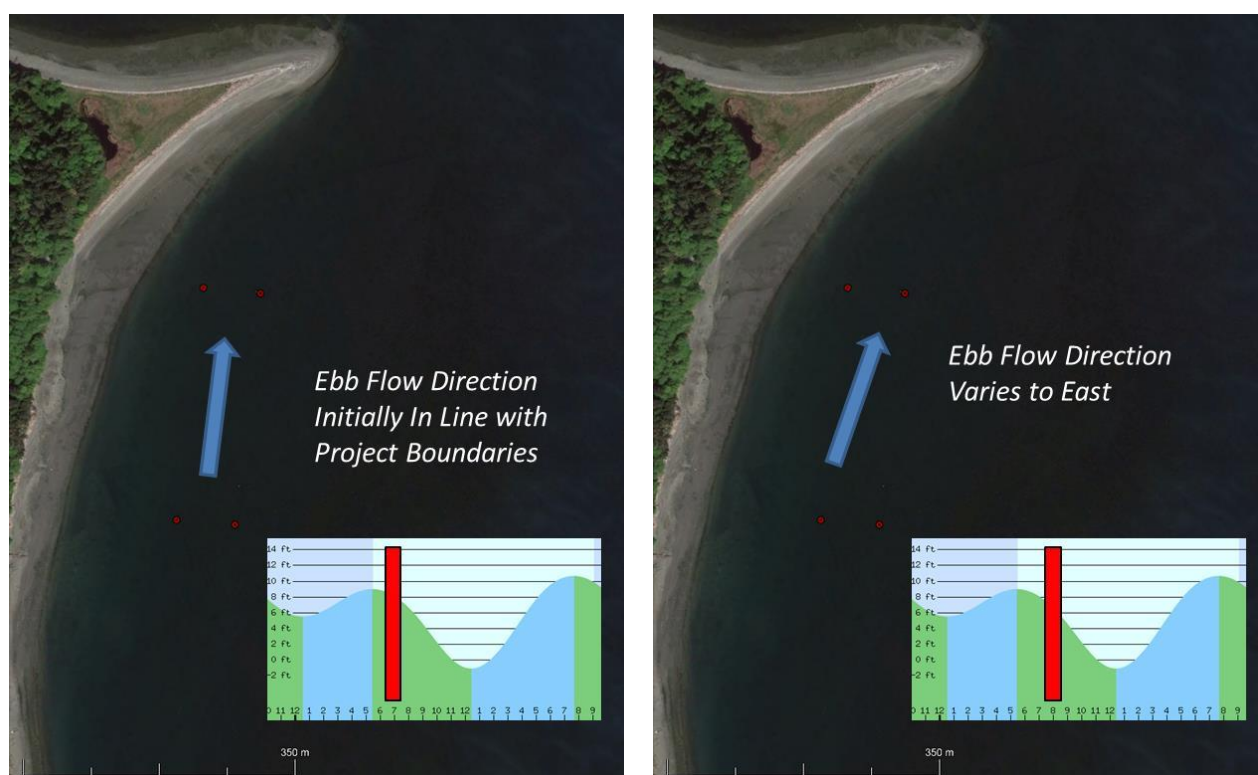


Figure 5. Generalized summary of flow directions for daytime ebb and flood of July 17, 2015.

Small red circles represent the four corners of the WDNR lease area for this project. Predicted tidal chart for Port Gamble Entry Tidal Station shown in lower right of each figure. Time of drogue monitoring represented for each figure indicated by the red vertical bar in the tidal chart. See appendix for more detailed plots of each drogue path used to make these generalized plots.

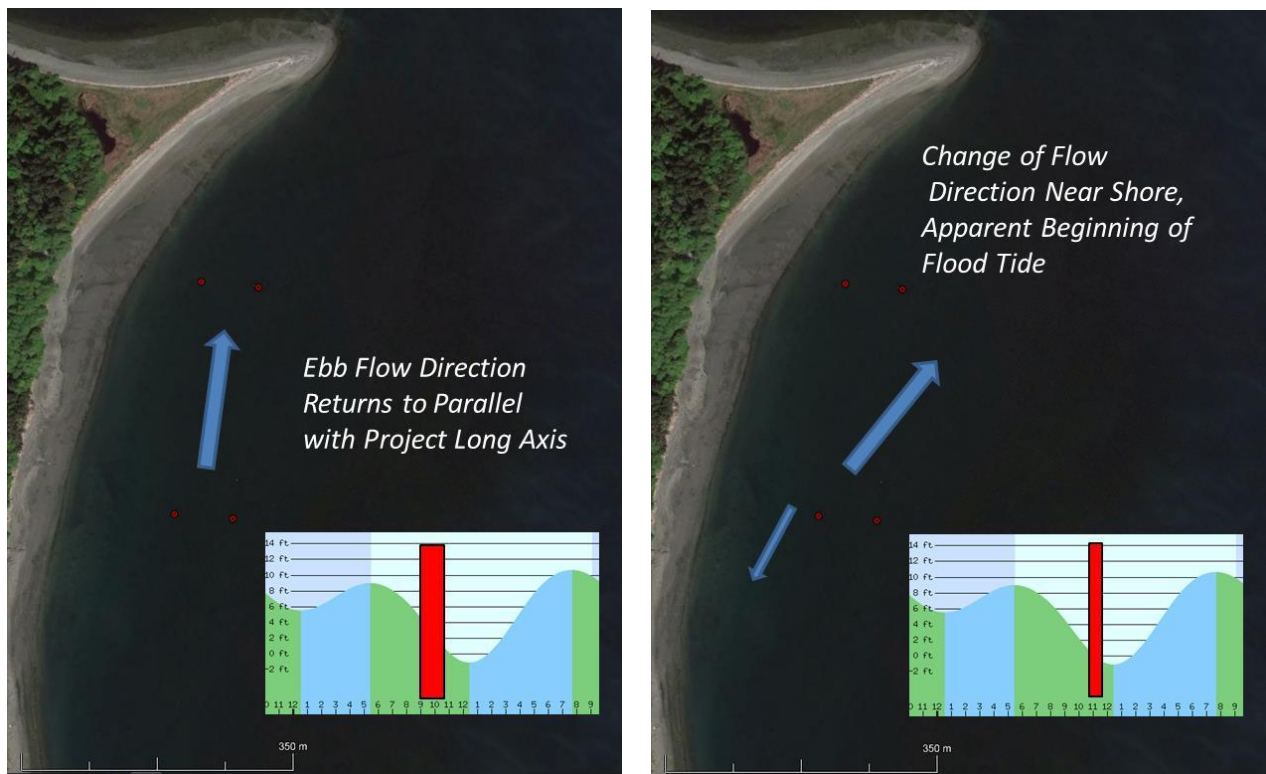


Figure 6. Generalized summary of flow directions for daytime ebb and flood of July 17, 2015.

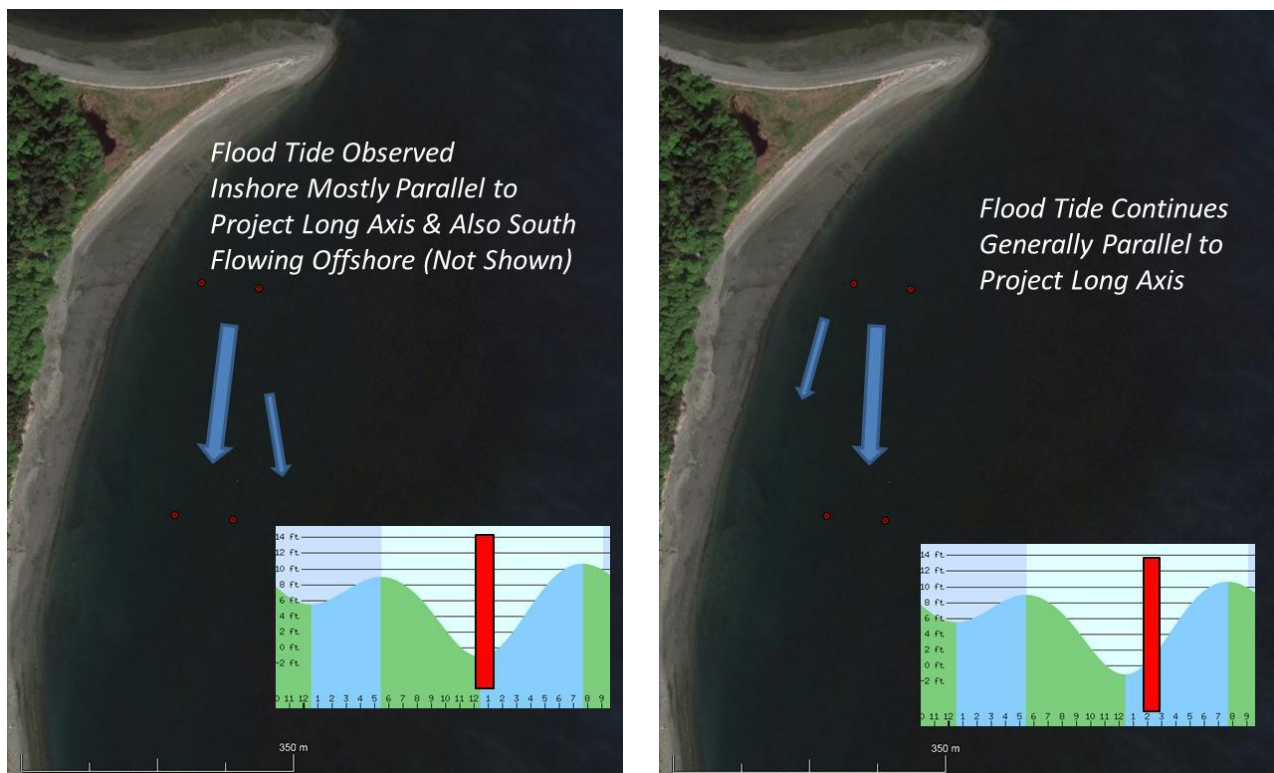


Figure 7. Generalized summary of flow directions for daytime ebb and flood of July 17, 2015.

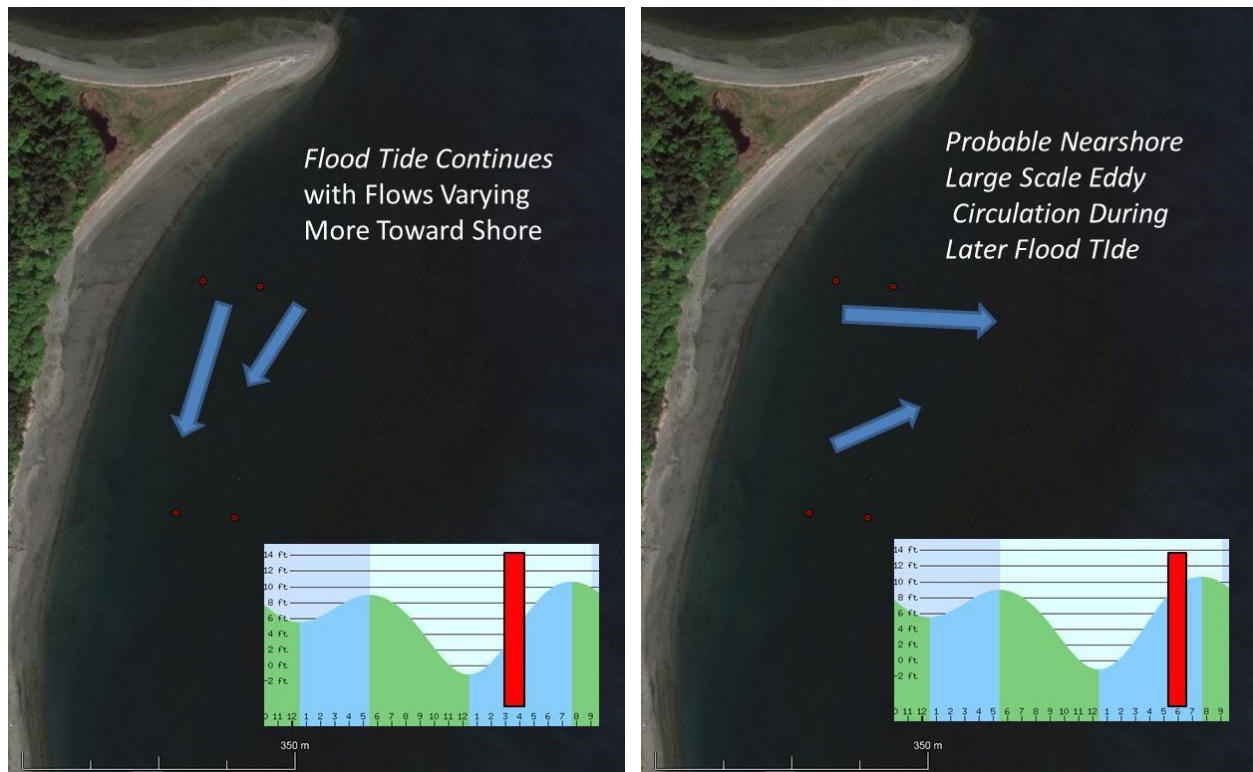


Figure 8. Generalized summary of flow directions for daytime ebb and flood of July 17, 2015.

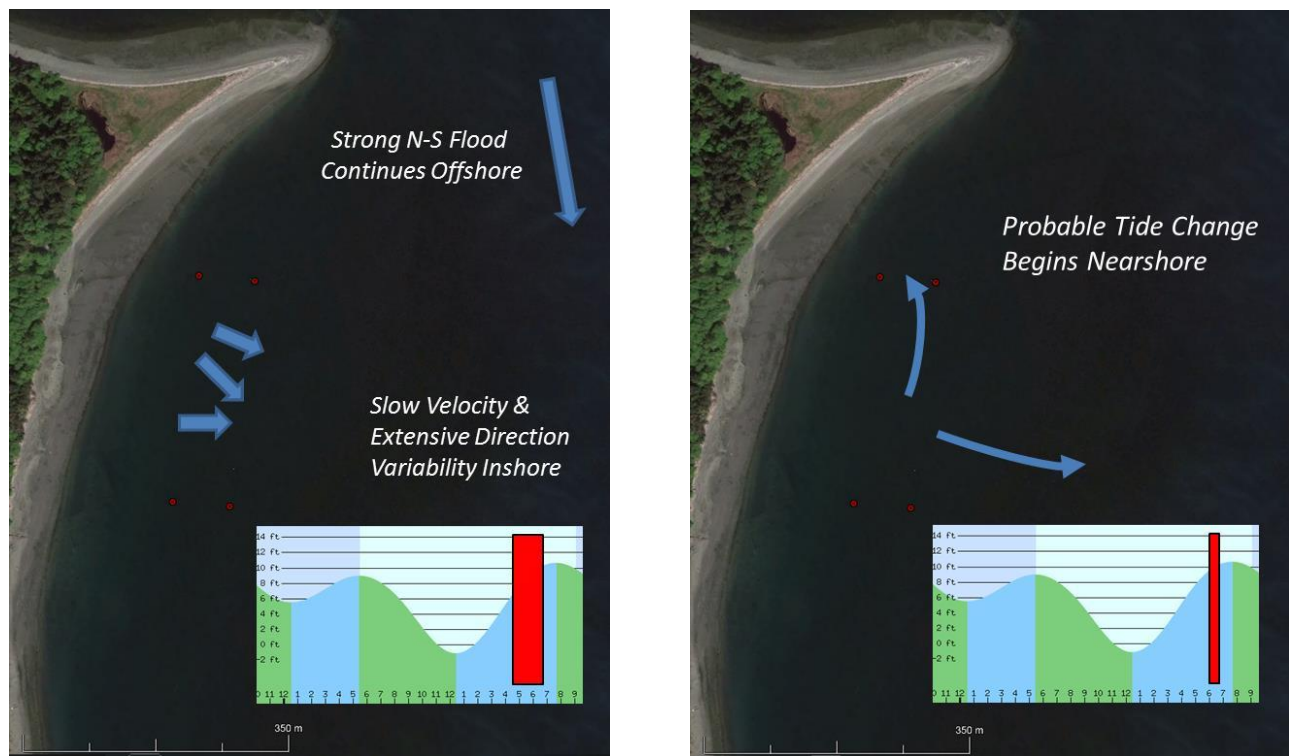


Figure 9. Generalized summary of flow directions for daytime ebb and flood of July 17, 2015.

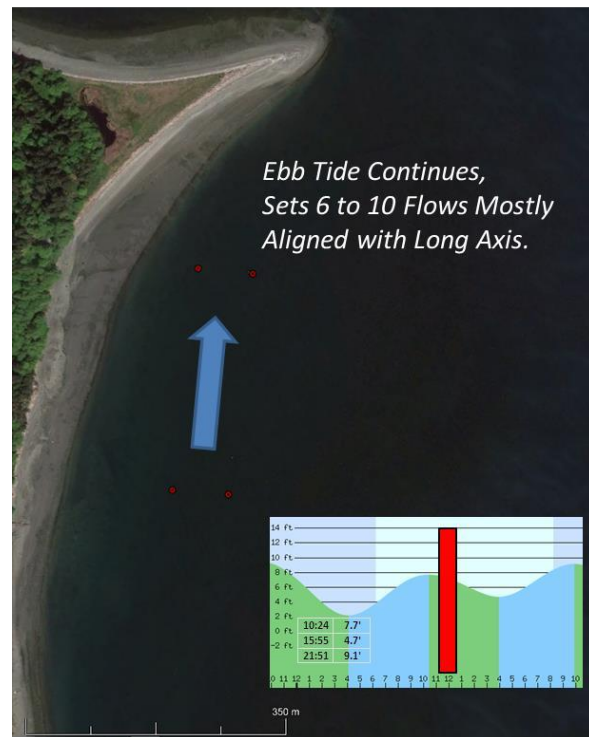
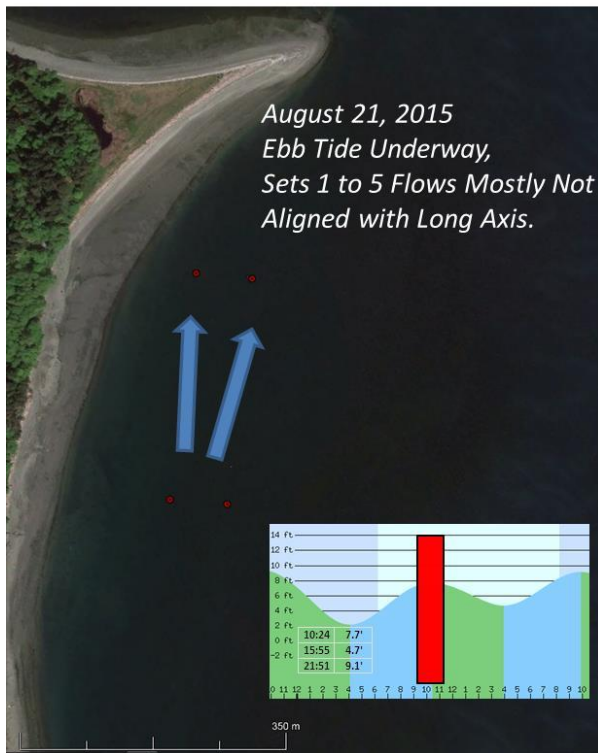


Figure 10. Generalized summary of flow directions for daytime ebb and flood of August 21, 2015, sets 1-5 left and sets 6-10 right.

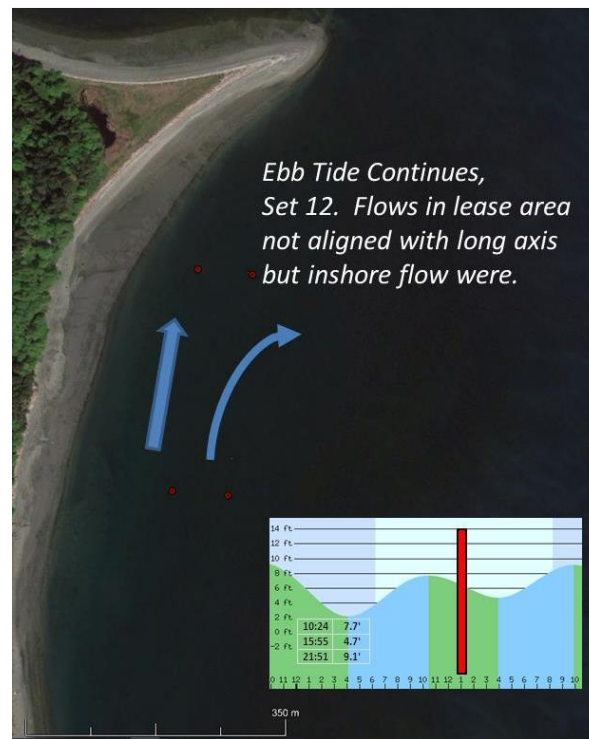
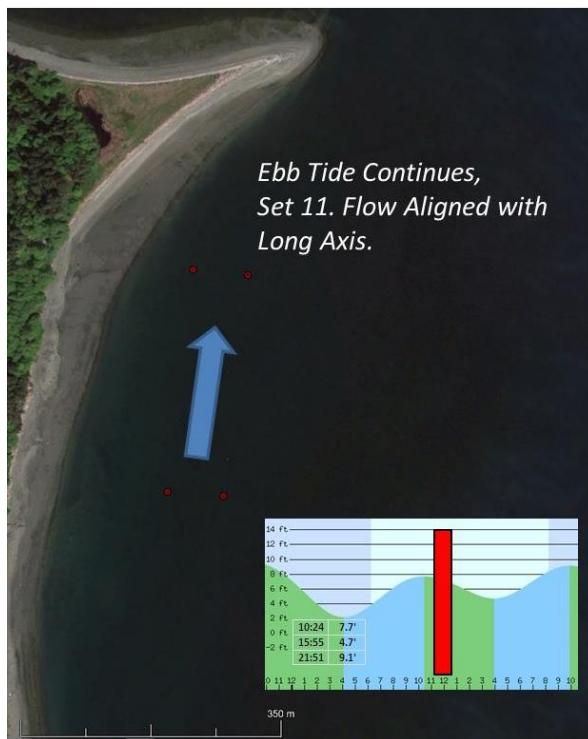


Figure 11. Generalized summary of flow directions for daytime ebb and flood of August 21, 2015, set 11 left and set 12 right.

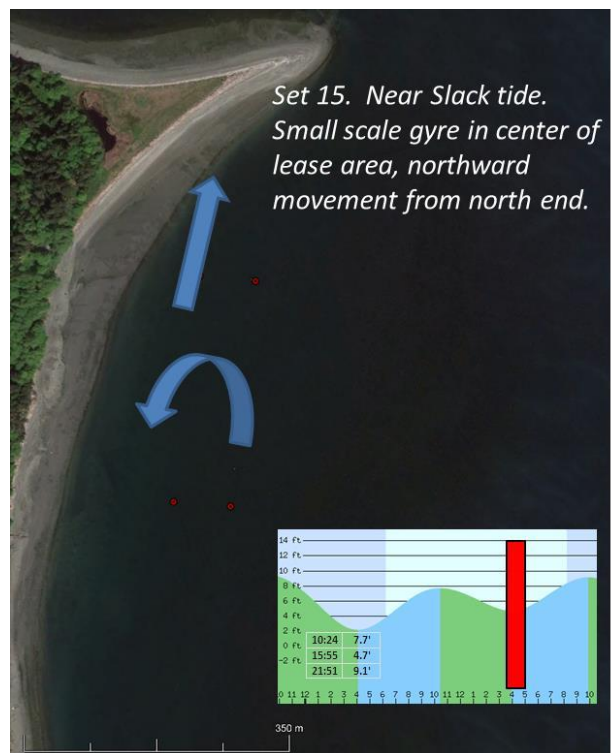
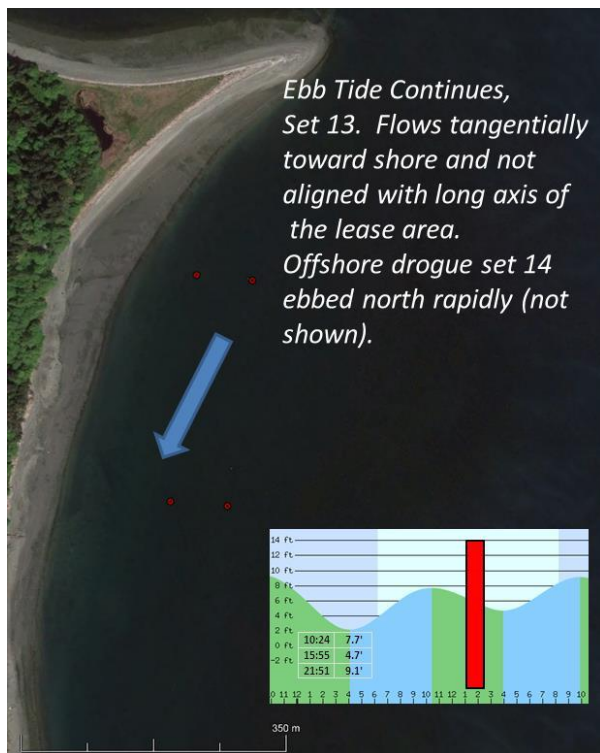


Figure 12. Generalized summary of flow directions for daytime ebb and flood of August 21, 2015, set 13 left and set 15 right. Sets 14 and 16 not shown for brevity.

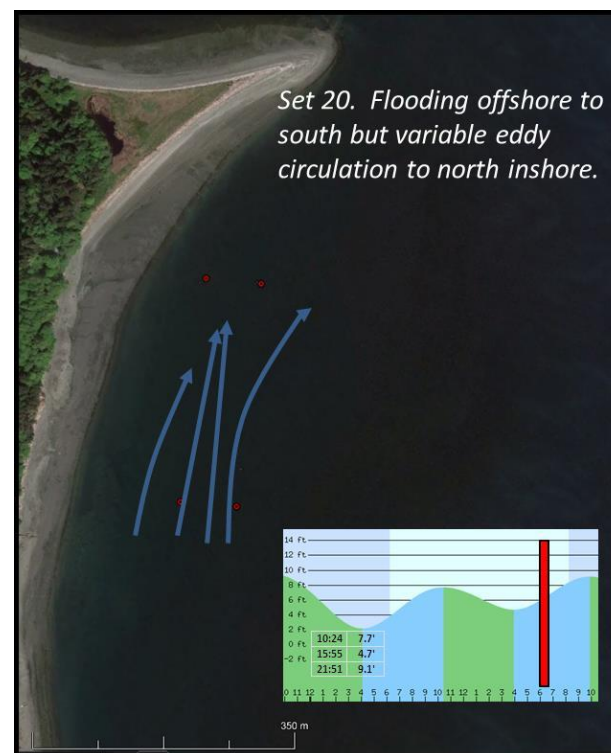
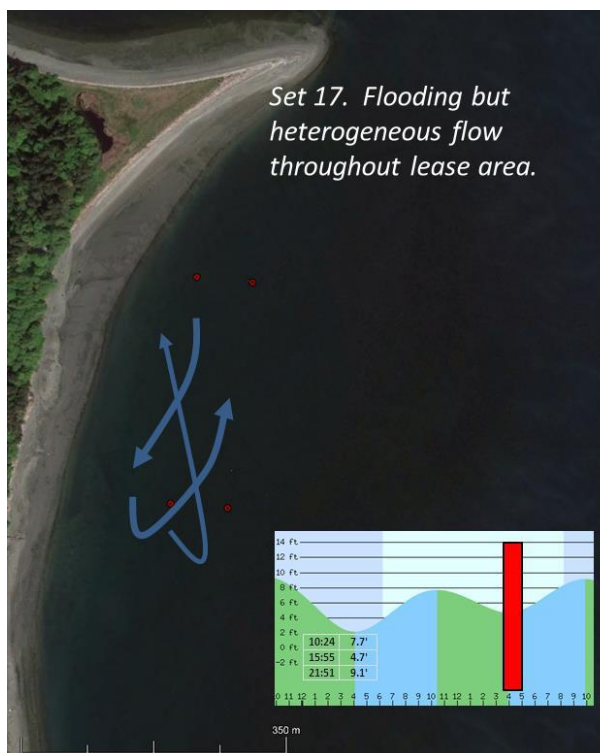


Figure 13. Generalized summary of flow directions for daytime ebb and flood of August 21, 2015, set 17 left and set 20 right.

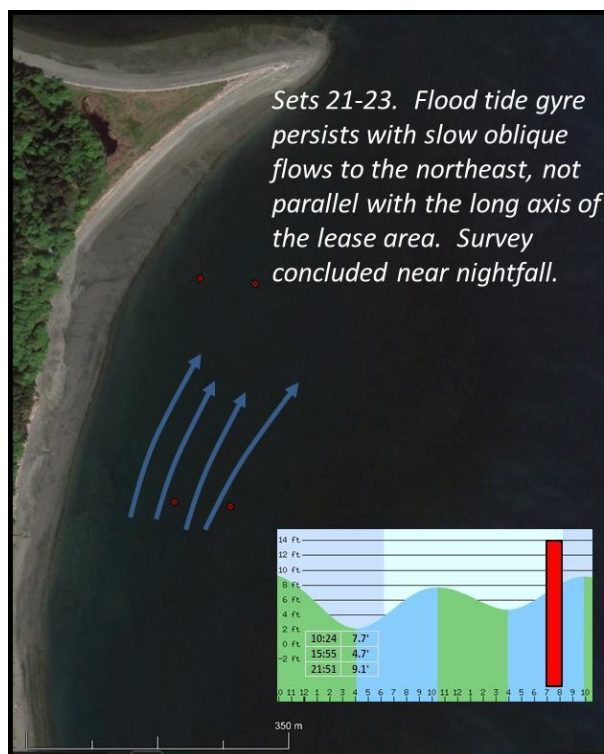


Figure 14. Generalized summary of flow directions for daytime ebb and flood of August 21, 2015, sets 21-23.

Tabular Data and Calculations

In this section data tables for all observations, inside and outside the lease area are reported in spreadsheet form. Several pages of this table follow. Important results are the five right columns indicating conditions in within the lease area only and periods of minimal direction variation from “straight through” the lease area flow. Bold entries in the “heading degrees True) column indicate measurements completely within the lease area only. These data are addressed in the next section of this report. These data are available to project team members in Excel format.

With regard to quality assurance: I inspected for outliers and improbable results and in two drogue tracks, I found to contain an error that were based on 10-minute time recording errors from my entries in the field. These errors were apparent by checking immediately prior and later entries in clusters of drogues released or measured at the same time so the corrections were obvious. In addition, a technician coded some of the first day’s compass direction in either direction, inducing 180-degree errors. Every one of those data entries was replotted and checked by a separate worker to insure accuracy. All of the original data were correct, but some entries were 180 degrees incorrect by using the measuring tool in Google Earth in the wrong direction.

Table 2. Drogue survey data and calculations 27 July 2015.

27 July 15 Drogue No.	Start, Observe, Recovery	GPS Begin	GPS End	Heading Degrees True*	Begin Time	End Time	Elapsed minutes	Distance m	Rate cm/s	Average Flow Rate All Locations cm/s	Average Heading All Locations (Degrees T)	Observed Flow in Lease Area cm/s	Heading Deviation from Straight Through (Degrees T)	Minutes Sampled Within Lease Area	Elapsed Time < 10 degrees Variation	Elapsed Time < 5 degrees Variation
Set No. 1 Ebb																
1	S	21	25	39.4	6:49	6:59	10.0	233.1	38.9							
1	R	25	32	51.5	6:59	7:12	13.0	197.0	25.3	32.1	45.5					
2	S	22	26	40.0	6:49	7:00	11.0	276.8	41.9			41.9	12.0	11		
2	R	26	31	51.0	7:00	7:12	12.0	251.5	34.9	38.4	45.5					
3	S	23	27	36.4	6:52	7:00	10.0	321.2	53.5							
3	R	27	30	44.4	7:00	7:11	11.0	312.5	47.3	50.4	40.4					
4	S	24	28	39.2	6:52	7:01	11.0	348.6	52.8							
4	R	28	29	41.7	7:01	7:10	9.0	356.6	66.0	59.4	40.5					
									mean →	45.1	43.0	41.9	12.0			
									SD →	12.2	2.9	NA	NA			
Set No.2 Ebb																
3	S	33	38	33.4	7:15	7:23	8.0	227.8	47.5			47.5	5.4	8	8	
3	R	38	43	52.9	7:23	7:41	18.0	488.3	45.2	46.3	43.2					
4	S	34	39	33.3	7:15	7:23	8.0	249.4	52.0			52.0	5.3	8	8	
4	R	39	42	44.4	7:23	7:40	17.0	532.5	52.2	52.1	38.9					
5	S	35	40	40.1	7:15	7:24	9.0	265.1	49.1							
5	O	40	41	40.4	7:24	7:39	15.0	568.6	63.2	56.1	40.3					
									mean →	51.5	40.8	49.7	5.4			
									SD →	4.9	2.2	3.2	0.1			
Set No.3 Ebb																
1	S	47	51	33.9	8:10	8:19	9.0	148.8	27.6			27.6	28.0	9		
1	R	51	55	48.7	8:19	8:30	11.0	209.7	31.8	29.7	41.3	31.8	5.9	11	11	
2	S	48	52	39.1	8:11	8:19	8.0	173.0	36.0			36.0	20.7	8		
2	O	52	56	44.6	8:19	8:30	11.0	231.1	35.0							
2	R	56	61	31.9	8:30	8:47	17.0	471.3	46.2	39.1	38.5					
3	S	49	53	38.6	8:11	8:20	9.0	183.2	33.9							
3	O	53	57	43.2	8:20	8:31	11.0	252.6	38.3							
3	R	57	60	29.0	8:31	8:46	15.0	525.9	58.4	43.5	36.9					
4	S	52	54	34.2	8:12	8:20	8.0	199.7	41.6							
4	O	54	58	39.9	8:20	8:31	11.0	279.3	42.3							
4	R	58	59	14.3	8:31	8:45	14.0	483.4	57.6	47.2	29.5					
									mean →	39.9	36.6	31.8	18.2			
									SD →	7.6	5.1	4.2	11.3			
Set No.4 Ebb																
1	S	63	67	343.3	8:53	9:07	14.0	48.0	5.7							
1	R	67	82	201.9	9:07	9:31	24.0	38.5	2.7	4.2	272.6					
2	S	64	68	7.8	8:54	9:08	14.0	106.7	12.7							
2	R	68	81	298.6	9:08	9:30	22.0	52.3	4.0	8.3	153.2					
3	S	65	69	19.4	8:55	9:09	14.0	365.0	43.5							
3	O	69	80	32.8	9:09	9:28	19.0	407.2	35.7			35.71	4.8	19	19	19
3	R	80	83	32.2	9:28	9:36	8.0	92.3	19.2	32.8	28.1					
4	S	66	70	25.4	8:55	9:10	15.0	518.6	57.6							
4	R	70	79	34.7	9:10	9:26	16.0	660.9	68.8	63.2	30.1					
									mean →	27.1	121.0	20.0	8.0			
									SD →	27.2	116.8	22.3	4.6			
Set No.5 Ebb																
5	S	71	75	29.8	9:14	9:24	10.0	191.3	31.9				1.8	10	10	10
5	R	75	84	44.9	9:24	9:37	13.0	297.9	38.2	35.0	37.4					
6	S	72	76	30.0	9:15	9:24	9.0	287.6	53.3				2.0	9	9	9
6	R	76	85	45.7	9:24	9:38	14.0	264.3	31.5	42.4	37.9					
7	S	73	77	27.3	9:15	9:25	10.0	309.6	51.6				0.7	10	10	10
7	R	77	86	42.3	9:25	9:40	15.0	466.8	51.9	51.7	34.8					
8	S	74	78	28.6	9:15	9:25	10.0	339.0	56.5							
8	R	78	87	29.6	9:25	9:41	16.0	620.0	64.6	60.5	29.1					
									mean →	47.4	34.8	21.1	3.4			
									SD →	11.1	4.0	1.6	2.9			
Set No.6 Ebb																
1	S	88	92	22.2	9:53	10:00	7.0	77.3	18.4			18.4	5.8	7	7	
1	O	92	96	41.5	10:00	10:11	11.0	75.5	11.4			11.4	13.5	11		
1	O	96	103	79.2	10:11	10:27	16.0	131.7	13.7			13.7	51.2	16		
1	R	103	105	28.7	10:27	10:42	15.0	255.3	28.4	18.0	42.9					
2	S	89	93	25.1	9:53	10:01	8.0	147.3	30.7			30.7	2.9	8	8	8
2	O	93	97	49.5	10:01	10:12	11.0	152.8	23.2							
2	O	97	102	20.8	10:12	10:26	14.0	115.3	13.7							
2	R	102	104	230.1	10:26	10:40	14.0	98.0	11.7	19.8	81.4					
3	S	90	94	26.3	9:54	10:01	7.0	184.7	44.0							
3	O	94	98	30.3	10:01	10:12	11.0	189.3	28.7							
3	O	98	101	44.1	10:12	10:25	13.0	101.6	13.0							
3	R	101	106	27.8	10:25	10:43	18.0	11.4	1.1	21.7	32.1					
4	S	91	95	30.0	9:54	10:02	8.0	221.5	46.1			46.1	2.0	8	8	8
4	O	95	99	38.4	10:02	10:13	11.0	277.9	42.1							
4	R	99	100	19.6	10:13	10:24	11.0	344.7	52.2	46.8	29.3					
									mean →	26.6	46.4	38.4	2.5			
									SD →	13.6	24.0	10.9	0.6			

27 July 15 Drogue No.	Start, Observe, Recovery	GPS Begin	GPS End	Heading Degrees True*	Begin Time	End Time	Elapsed minutes	Distance m	Rate cm/s	Average Flow Rate All Locations cm/s	Average Heading All Locations (Degrees T)	Observed Flow in Lease Area cm/s	Heading Deviation from Straight Through (Degrees T)	Minutes Sampled Within Lease Area	Elapsed Time < 10 degrees Variation	Elapsed Time < 5 degrees Variation
Set No.7 Ebb																
1	S	107	114	211.2	10:48	11:02	14.0	6.7	0.8							
1	R	114	118	217.9	11:02	11:17	15.0	144.0	16.0	8.4	214.5					
2	S	108	113	49.5	10:49	11:01	12.0	101.5	14.1			14.1	21.5	12		
2	R	113	117	53.0	11:01	11:15	14.0	336.0	40.0	27.0	51.3					
3	S	109	112	46.4	10:52	11:00	10.0	230.5	38.4			38.4	18.4	10		
3	R	112	116	12.9	11:00	11:14	14.0	212.9	25.3	31.9	29.7					
4	S	110	111	37.9	10:52	10:59	9.0	284.2	52.6							
4	R	111	115	28.8	10:59	11:13	14.0	259.3	30.9	41.7	33.4					
									mean →	27.3	82.2	25.5	10.7			
									SD →	14.0	88.7	15.0	10.7			
Set No.8 Near Slack																
1	S	119	123	208.9	11:20	11:23	3.0	40.0	22.2							
1	O	123	127	232.4	11:23	11:29	6.0	56.2	15.6							
1	O	127	131	244.3	11:29	11:35	6.0	44.9	12.5							
1	R	131	135	218.2	11:35	11:47	12.0	154.4	21.4	17.9	226.0					
2	S	120	124	172.3	11:20	11:24	4.0	37.2	15.5			15.5	35.7	4		
2	O	124	128	85.8	11:24	11:29	5.0	48.9	16.3							
2	O	128	132	52.2	11:29	11:36	7.0	67.2	16.0							
2	R	132	136	41.5	11:36	11:52	14.0	56.3	6.7	13.6	88.0					
3	S	121	125	106.7	11:21	11:24	3.0	32.9	18.3							
3	O	125	129	47.9	11:24	11:30	6.0	95.0	26.4							
3	O	129	133	23.6	11:30	11:36	6.0	52.8	14.7							
3	R	133	137	302.3	11:36	11:51	15.0	25.8	2.9	15.6	120.1					
4	S	122	126	23.7	11:21	11:25	4.0	94.7	39.5							
4	O	126	130	344.6	11:25	11:30	5.0	37.3	12.4							
4	O	130	134	216.4	11:30	11:37	7.0	78.4	18.7							
4	R	134	138	198.7	11:37	11:51	14.0	92.8	11.0	20.4	195.8					
									mean →	16.9	157.5	15.5	35.7			
									SD →	2.9	64.3	NA	NA			
Set No.9 Flood Begins																
1	S	139	143	206.6	11:53	12:03	10.0	152.1	25.4			25.4	1.4	10	10	
1	R	143	147	212.4	12:03	12:11	8.0	136.4	28.4	26.9	209.5					
2	S	140	144	202.4	11:54	12:04	10.0	146.4	24.4			24.4	5.6	10	10	
2	R	144	148	218.0	12:04	12:12	8.0	65.4	13.6	19.0	210.2					
3	S	141	145	215.0	11:54	12:04	10.0	104.4	17.4			17.4	7.0	10	10	
3	R	145	149	229.2	12:04	12:13	9.0	105.3	19.5	18.5	222.1					
4	S	142	146	170.0	11:55	12:05	10.0	27.1	4.5							
4	R	146	152	145.9	12:05	12:14	9.0	12.1	2.2	3.4	158.0					
									mean →	16.9	199.9	20.7	12.4			
									SD →	9.8	28.6	4.9	15.7			
Set No.10 Begin Flood																
1	S	151	155	219.4	12:21	12:29	8.0	116.7	24.3							
1	O	155	159	212.0	12:29	12:41	12.0	178.3	24.8							
1	R	159	163	214.5	12:41	12:48	7.0	136.6	32.5	27.2	215.3					
2	S	152	156	209.9	12:22	12:30	8.0	113.0	23.6			23.6	1.9	8	8	8
2	O	156	160	212.3	12:30	12:41	11.0	182.3	27.6			27.6	4.3	11		11
2	R	160	164	212.2	12:41	12:48	7.0	138.9	33.1	28.1	211.5					
3	S	153	157	209.8	12:22	12:31	9.0	120.1	22.2			22.2	1.8	9	9	9
3	O	157	161	217.3	12:31	12:41	10.0	182.4	30.4			30.4	9.3	10	10	
3	R	161	165	223.8	12:41	12:48	7.0	136.5	32.5	28.4	217.0					
4	S	154	158	213.7	12:22	12:31	9.0	115.7	21.4							
4	O	158	162	221.0	12:31	12:42	11.0	163.0	24.7							
4	R	162	166	231.4	12:42	12:49	7.0	86.4	20.6	22.2	222.0					
									mean →	26.5	216.4	26.0	4.3			
									SD →	2.9	4.4	3.7	3.5			
Set No.11 Flood																
1	S	167	171	224.2	13:03	13:12	9.0	137.1	25.4							
1	R	171	175	216.1	13:12	13:20	8.0	124.2	25.9	25.6	220.2					
2	S	168	172	217.5	13:03	13:13	10.0	196.1	32.7			32.7	9.5	10	10	
2	R	172	176	208.1	13:13	13:21	8.0	209.1	43.6	38.1	212.8	43.6	0.1	8	8	8
3	S	169	173	217.9	13:04	13:13	9.0	220.2	40.8			40.8	9.9	9	9	
3	R	173	177	218.5	13:13	13:21	8.0	191.7	39.9	40.4	218.2	39.9	10.5	8		
4	S	170	174	221.2	13:04	13:14	10.0	199.2	33.2							
4	R	174	178	223.7	13:14	13:22	8.0	160.7	33.5	33.3	222.5					
									mean →	34.4	218.4	39.2	7.5			
									SD →	6.5	4.1	4.6	5.0			
Set No.12 Flood																
1	S	179	183	205.7	13:32	13:43	11.0	207.5	31.4							
1	R	183	187	233.7	13:43	13:51	8.0	130.3	27.2	29.3	219.7					
2	S	180	184	214.8	13:32	13:44	12.0	214.3	29.8			29.8	6.8	12	12	
2	R	184	188	210.9	13:44	13:52	8.0	164.9	34.3	32.1	212.9	34.3	2.9	8	8	8
3	S	181	185	208.4	13:32	13:44	12.0	232.9	32.3			32.3	0.4	12	12	12
3	R	185	189	210.3	13:44	13:52	8.0	155.8	43.0	34.8	189.5	43.0	8.2	7	7	7
4	S	182	186	123.0	13:33	13:45	12.0	151.2	21.0			21.0	85.0	12		
4	R	186	190	216.2	13:45	13:52	7.0	180.4	43.0	32.0	169.6					
									mean →	32.0	197.9	32.1	20.7			
									SD →	2.3	22.9	7.9	36.1			

27 July 15 Drogue No.	Start, Observe, Recovery	GPS Begin	GPS End	Heading Degrees True*	Begin Time	End Time	Elapsed minutes	Distance m	Rate cm/s	Average Flow Rate All Locations cm/s	Average Heading All Locations (Degrees T)	Observed Flow in Lease Area cm/s	Heading Deviation from Straight Through (Degrees T)	Minutes Sampled Within Lease Area
Set No.13 Flood														
1	S	191	195	216.0	14:07	14:15	8.0	64.1	13.4					
1	O	195	199	219.5	14:15	14:24	9.0	35.3	6.5					
1	R	199	203	258.0	14:24	14:33	9.0	11.4	2.1	7.3	231.2			
2	S	192	196	217.5	14:07	14:16	9.0	72.1	13.3			13.3	9.5	9
2	O	196	200	235.2	14:16	14:24	8.0	58.7	12.2			12.2	27.2	8
2	R	200	204	277.6	14:24	14:34	10.0	26.6	4.4	10.0	243.4			
3	S	193	197	228.1	14:07	14:16	9.0	58.7	10.9			10.9	20.1	9
3	O	197	201	246.6	14:16	14:26	10.0	66.0	11.0			11.0	38.6	10
3	R	201	205	271.5	14:26	14:34	8.0	42.8	8.9	10.3	248.7			
4	S	194	198	242.6	14:07	14:16	9.0	92.0	17.0					
4	O	198	202	253.4	14:16	14:26	10.0	94.1	15.7					
4	R	202	206	261.6	14:26	14:35	9.0	47.4	8.8	13.8	252.5			
									mean →	10.4	244.0	11.9	23.9	
									SD→	2.7	9.3	1.2	12.2	
Set No.14 Flood														
1	S	207	211	212.5	14:52	14:59	9.0	16.7	3.1					
1	O	211	215	218.1	14:59	15:13	14.0	222.8	26.5					
1	R	215	219	214.3	15:13	15:20	7.0	105.7	25.2	18.9	215.0			
2	S	208	212	180.0	14:52	14:59	9.0	26.4	4.9			4.9	28.0	9
2	O	212	216	209.8	14:59	15:14	15.0	225.0	25.0			25.0	1.8	15
2	R	216	220	213.8	15:14	15:21	7.0	123.2	29.3	21.3	201.2	29.3	5.8	7
3	S	209	213	189.5	14:51	15:00	9.0	52.1	9.6			9.6	18.5	9
3	O	213	217	212.0	15:00	15:14	14.0	210.9	25.1			25.1	4.0	14
3	R	217	221	220.8	15:14	15:22	8.0	122.3	25.5	22.0	207.4	25.5	12.8	8
4	S	210	214	205.7	14:51	15:00	9.0	83.9	15.5					
4	O	214	218	215.4	15:00	15:14	14.0	216.4	25.8					
4	R	218	222	223.4	15:14	15:22	8.0	117.2	24.4	25.1	214.8			
									mean →	21.8	209.6	19.9	11.8	
									SD→	2.6	6.6	10.0	10.1	
Set No.15 Ebb														
1	S	223	227	21.2	15:29	15:40	11.0	29.0	4.4					
1	R	227	235	74.4	15:40	15:56	16.0	90.4	9.4	6.9	47.8			
2	S	224	228	81.9	15:30	15:41	11.0	31.4	4.8			4.8	53.9	11
2	R	228	236	97.1	15:41	15:57	16.0	130.5	13.6	9.2	89.5			
3	S	225	229	89.0	15:30	15:41	11.0	30.8	4.7			4.7	61.0	11
3	R	229	237	103.0	15:41	15:57	16.0	137.3	14.3	9.5	96.0			
									mean →	8.5	77.8	4.7	57.5	
									SD→	1.4	26.2	0.1	5.0	
Set No.16 Ebb														
5	S	226	231	93.1	15:38	15:43	5.0	10.1	3.4					
5	R	231	240	65.5	15:43	16:03	20.0	129.1	10.8	7.1	79.3			
6	S/R	232	239	96.3	15:45	16:01	16.0	155.2	16.2	16.2	85.0	16.2	68.3	16
7	S/R	233	241	77.7	15:45	16:04	19.0	120.5	10.6	10.6	83.2	10.6	49.7	19
8	S/R	234	241*	48.9	15:46	16:05	19.0	98.0	8.6	8.6	72.1	8.6	20.9	19
									mean →	10.6	79.9	11.8	46.3	
									SD→	4.0	5.7	3.9	23.9	
Set No.17 Ebb														
1	S	242	251	48.7	16:06	16:28	22.0	176.9	13.4			13.4	20.7	22
1	R	251	256	73.7	16:28	16:33	5.0	46.1	15.4	14.4	61.2	15.4	45.7	5
2	S	243	252	56.5	16:07	16:29	22.0	208.4	15.8			15.8	28.5	22
2	R	252	257	74.1	16:29	16:33	4.0	26.6	11.1	13.4	65.3	11.1	46.1	4
3	S	244	247	53.4	16:08	16:17	9.0	92.3	17.1			17.1	25.4	9
3	O	247	253	67.0	16:17	16:29	12.0	127.1	17.7					
3	R	253	258	167.4	16:29	16:34	5.0	5.0	1.7	11.8	95.9			
4	S	245	254	60.1	16:08	16:29	21.0	202.2	16.0					
4	R	254	259	213.3	16:29	16:34	5.0	15.2	5.1	10.6	136.7			
7	S/R	249	252	208.3	16:21	16:26	5.0	59.1	19.7	19.7	162.3			
8	S	246	248	49.3	16:11	16:19	8.0	65.8	13.7					
8	R	248	255	112.3	16:19	16:30	11.0	74.9	11.3	12.5	80.8			
									mean →	13.7	100.4	14.5	33.3	
									SD→	3.2	40.8	2.3	11.9	

27 July 15 Drogue No.	Start, Observe, Recovery	GPS Begin	GPS End	Heading Degrees True*	Begin Time	End Time	Elapsed minutes	Distance m	Rate cm/s	Average Flow Rate All Locations cm/s	Average Heading All Locations (Degrees T)	Observed Flow in Lease Area cm/s	Heading Deviation from Straight Through (Degrees T)	Minutes Sampled Within Lease Area	Elapsed Time < 10 degrees Variation	Elapsed Time < 5 degrees Variation
Set No.18 Ebb																
1	S	260	264	66.4	16:43	16:53	10.0	63.1	10.5			10.5	38.4	10		
1	O	264	269	184.6	16:53	17:03	10.0	54.5	9.1							
1	O	269	274	169.1	17:03	17:20	17.0	30.8	3.0							
1	R	274	283	132.9	17:20	17:34	14.0	56.4	6.7	7.3	138.3					
2	S	261	265	98.5	16:43	16:53	10.0	47.7	8.0			8.0	70.5	10		
2	O	265	270	169.3	16:53	17:03	10.0	30.2	5.0							
2	O	270	275	149.4	17:03	17:20	17.0	72.1	7.1							
2	R	275	284	129.2	17:20	17:35	15.0	93.4	10.4	7.6	136.6					
3	S	262	266	135.1	16:44	16:54	10.0	23.4	3.9			3.9	72.9	10		
3	O	266	271	229.8	16:54	17:04	10.0	32.7	5.4							
3	O	271	276	181.4	17:04	17:21	17.0	52.3	5.1							
3	R	276	285	92.5	17:21	17:35	14.0	73.0	8.7	5.8	159.7					
4	S	263	267	193.5	16:44	16:54	10.0	42.9	7.1			7.1	14.5	10		
4	O	267	272	201.1	16:54	17:04	10.0	47.1	7.8							
4	O	272	277	207.9	17:04	17:21	17.0	75.5	7.4							
4	R	277	286	72.9	17:21	17:36	15.0	80.5	8.9	7.8	168.8					
8	S	268	273	157.2	16:59	17:06	7.0	110.8	26.4							
8	O	273	278	163.5	17:06	17:23	17.0	327.1	32.1							
8	R	278	291	170.0	17:23	17:45	22.0	316.7	24.0	28.0	163.6					
									mean →	11.3	153.4	7.4	49.1			
									SD→	9.4	14.9	2.7	27.9			
Set No.19 Ebb																
1	S	287	292	116.7	17:41	17:55	14.0	29.8	3.5			3.5	88.7	14		
1	R	292	296	84.5	17:55	18:10	15.0	28.3	3.1	3.3	100.6					
2	S	288	293	110.0	17:41	17:55	14.0	39.8	4.7			4.7	82.0	14		
2	R	293	297	78.9	17:55	18:11	16.0	7.5	0.8	2.8	94.5					
3	S	289	294	141.8	17:41	17:56	15.0	46.5	5.2			5.2	113.8	15		
3	R	294	298	14.0	17:56	18:11	15.0	13.1	1.5	3.3	77.9					
4	S	290	295	166.1	17:42	17:56	14.0	52.3	6.2							
4	R	295	299	140.1	17:56	18:12	16.0	39.5	4.1	5.2	153.1					
									mean →	3.6	106.5	4.5	94.8			
									SD→	1.1	32.5	0.8	16.8			
Set No.19 Ebb																
1	S	300	304	43.4	18:14	18:25	11.0	33.1	5.0			5.0	15.4	11		
1	O	304	309	18.5	18:25	18:29	4.0	42.4	17.7			17.7	9.5	4	4	
1	R	309	315	77.5	18:29	18:53	24.0	16.1	1.1	8.5	46.5	1.1	49.5	24		
2	S	301	305	86.0	18:14	18:26	12.0	47.2	6.6			6.6	58.0	12		
2	O	305	310	8.8	18:26	18:40	14.0	79.3	9.4			9.4	19.2	14		
2	R	310	316	178.5	18:40	18:54	14.0	64.3	7.7	7.3	91.1					
3	S	302	306	78.3	18:15	18:27	12.0	33.8	4.7			4.7	50.3	12		
3	O	306	311	47.5	18:27	18:40	13.0	57.9	7.4							
3	R	311	314	18.3	18:40	18:52	12.0	46.4	6.4	6.4	48.0					
4	S	303	307	127.7	18:15	18:27	12.0	39.4	5.5							
4	O	307	308	97.2	18:27	18:34	7.0	35.3	8.4							
4	O	308	312	93.6	18:34	18:41	7.0	72.4	17.2							
4	R	312	313	94.7	18:41	18:52	9.0	127.1	23.5	13.7	103.3					
									mean →	9.0	72.2	7.4	33.7			
									SD→	3.2	29.3	5.7	21.2			

Table 3. Drogue survey data and calculations 21 August 2015

21 Aug. 15 Drogue No.	Start, Observe, Recovery	GPS Begin	GPS End	Heading Degrees True*	Begin Time	End Time	Elapsed minutes	Distance m	Rate cm/s	Average Flow Rate All Locations cm/s	Average Heading All Locations (Degrees T)	Observed Flow in Lease Area cm/s	Heading Deviation from Straight Through (Degrees T)	Minutes Sampled Within Lease Area	Elapsed Time < 10 degrees Variation	Elapsed Time < 5 degrees Variation
Set No. 1 Ebb																
1	S	1	5	30.2	9:18	9:27	9.0	61.92	11.5							
1	R	5	15	28.8	9:27	9:52	25.0	234.89	15.7	13.6	29.5					
2	S	2	6	22.5	9:18	9:27	9.0	79.98	14.8							
2	R	6	16	26.3	9:27	9:53	26.0	225.64	14.5	14.6	24.4					
3	S	3	7	23.7	9:19	9:28	9.0	97.33	18.0							
3	R	7	17	25.4	9:28	9:54	26.0	241.72	15.5	16.8	24.6					
4	S	4	8	18.0	9:19	9:28	9.0	101.82	18.9			18.9	10.0	9	9	
4	R	8	18	24.1	9:28	9:54	26.0	246.89	15.8	17.3	21.0	24.1	3.91	26	26	26
									mean →	15.6	24.9	21.5	7.0			
									SD →	1.8	3.5	3.7	4.3			
Set No. 2 Ebb																
5	S	11	23	37.8	9:50	10:14	24.0	226.24	15.7							
5	R	23	35	44.8	10:14	10:29	15.0	155.24	17.2	16.5	41.3					
6	S	12	24	42.9	9:50	10:15	25.0	264.51	17.6							
6	R	24	40	46.2	10:15	10:30	15.0	181.93	20.2	18.9	44.5					
7	S	13	25	41.5	9:50	10:15	25.0	282.14	18.8			9.2	13.5	25		
7	R	25	37	44.3	10:15	10:31	16.0	171.3	17.8	18.3	42.9	10.2	16.3	16		
8	S	14	26	41.2	9:51	10:15	24.0	294.94	20.5			7.5	13.2	24		
8	R	26	38	43.8	10:15	10:31	16.0	202.13	21.1	20.8	42.5	6.9	15.8	16		
									mean →	18.6	42.8	8.5	14.7			
									SD →	1.8	1.3	1.5	1.6			
Set No. 3 Ebb																
1	S	27	31	40.3	10:18	10:27	9.0	119.82	22.2							
1	O	31	39	41.4	10:27	10:33	6.0	78.91	21.9							
1	R	39	48	47.2	10:33	10:44	11.0	112.33	17.0	20.4	43.0					
2	S	28	32	40.6	10:18	10:27	9.0	114.31	21.2							
2	O	32	40	40.4	10:27	10:34	7.0	79.71	19.0							
2	R	40	49	43.4	10:34	10:44	10.0	146.85	24.5	21.5	41.5					
3	S	29	33	35.3	10:19	10:27	8.0	119.83	25.0			3.0	7.3	8	8	
3	O	33	41	38.4	10:27	10:34	7.0	84.42	20.1			7.9	10.4	7		
3	R	41	50	42.9	10:34	10:45	11.0	147.81	22.4	22.5	38.9	5.6	14.9	11		
4	S	30	34	31.1	10:19	10:27	8.0	128.32	26.7			1.3	3.1	8	8	
4	O	34	42	38.3	10:27	10:34	10.0	89.45	23.0			5.0	6.7	10	10	
4	R	42	51	42.9	10:34	10:45	11.0	145	22.0	23.9	37.4	6.0	14.9	11		
									mean →	22.1	40.2	4.8	9.6			
									SD →	1.5	2.5	2.3	4.7			
Set No. 4 Ebb																
5	S	44	52	34.7	10:39	10:49	10.0	137.78	23.0							
5	R	52	60	42.6	10:49	11:02	13.0	174.26	22.3	22.7	38.7					
6	S	45	53	31.8	10:39	10:49	10.0	149.04	24.8							
6	R	53	61	39.8	10:49	11:02	13.0	181.61	23.3	24.1	35.8					
7	S	46	54	29.6	10:39	10:49	10.0	153.49	25.6			2.4	1.6	10	10	10
7	R	54	62	37.7	10:49	11:02	13.0	187.1	24.0	24.8	33.7	4.0	9.7	13	13	
8	S	47	55	32.3	10:40	10:50	10.0	155.86	26.0			2.0	4.3	10	10	10
8	R	55	63	38.2	10:50	11:02	12.0	195.76	27.2	26.6	35.3	0.8	10.2	12		
									mean →	24.5	35.8	2.3	6.5			
									SD →	1.6	2.1	1.3	4.2			
Set No. 5 Ebb																
1	S	56	64	31.1	10:54	11:05	11.0	160.92	24.4							
1	O	64	72	33.5	11:05	11:10	5.0	73.46	24.5							
1	R	72	76	32.7	11:10	11:14	4.0	54.73	22.8	23.9	32.4					
2	S	57	65	27.6	10:54	11:05	11.0	171.38	26.0							
2	O	65	73	32.6	11:05	11:10	5.0	78.85	26.3							
2	R	73	77	35.1	11:10	11:14	4.0	58.73	24.5	25.6	31.8					
3	S	58	66	27.7	10:54	11:06	12.0	185.44	25.8			2.2	0.3	12	12	12
3	O	66	74	31.1	11:06	11:11	5.0	78.7	26.2			1.8	3.1	5	5	5
3	R	74	78	40.5	11:11	11:15	4.0	66.91	27.9	26.6	33.1	0.1	12.5	4		
4	S	59	67	29.7	10:55	11:06	11.0	199.3	30.2			2.2	1.7	11	11	11
4	O	67	75	33.7	11:06	11:11	5.0	89.03	29.7			1.7	5.7	5	5	
4	R	75	79	35.7	11:11	11:15	4.0	70.97	29.6	29.8	33.0	1.6	7.7	4	4	4
									mean →	26.5	32.6	1.6	5.2			
									SD →	2.5	0.6	0.8	4.5			

21 Aug. 15 Drogue No.	Start, Observe, Recovery	GPS Begin	GPS End	Heading Degrees True*	Begin Time	End Time	Elapsed minutes	Distance m	Rate cm/s	Average Flow Rate All Locations cm/s	Average Heading All Locations (Degrees T)	Observed Flow in Lease Area cm/s	Heading Deviation from Straight Through (Degrees T)	Minutes Sampled Within Lease Area	Elapsed Time < 10 degrees Variation	Elapsed Time < 5 degrees Variation
Set no. 6 Ebb																
5	S	68	80	30.5	11:07	11:18	11.0	170.91	25.9							
5	R	80	88	30.1	11:18	11:24	6.0	111.86	31.1	28.5	30.3					
6	S	69	81	26.2	11:08	11:18	10.0	177.11	29.5							
6	R	81	89	27.2	11:18	11:25	7.0	124.83	29.7	29.6	26.7					
7	S	70	82	25.9	11:08	11:18	10.0	196.95	32.8			4.8	2.1	10	10	10
7	R	82	90	35.8	11:18	11:25	7.0	120.51	28.7	30.8	30.8	0.7	7.8	7	7	
8	S	71	83	26.5	11:08	11:18	10.0	207.8	34.6			6.6	1.5	10	10	10
8	R	83	91	30.3	11:18	11:25	7.0	131.87	31.4	33.0	28.4	3.4	2.3	7	7	7
									mean →	30.5	29.1	3.9	3.4			
									SD→	1.9	1.9	2.5	2.9			
Set No.7 Ebb																
1	S	84	92	28.0	11:20	11:30	10.0	182.9	30.5							
1	R	92	100	32.9	11:30	11:40	10.0	106.39	17.7	24.1	30.4					
2	S	85	93	23.3	11:20	11:30	10.0	190.28	31.7							
2	R	93	101	31.5	11:30	11:37	7.0	111.76	26.6	29.2	27.4					
3	S	86	94	25.7	11:21	11:31	10.0	206.57	34.4			6.4	2.3	10	10	10
3	R	94	102	34.3	11:31	11:37	6.0	129.71	36.0	35.2	30.0	8.0	6.3	6	6	
4	S	87	95	30.5	11:21	11:31	10.0	218.34	36.4			8.4	2.5	10	10	10
4	R	95	103	33.3	11:31	11:37	6.0	128.21	35.6	36.0	31.9	7.6	5.3	6	10	
									mean →	31.1	29.9	7.6	4.1			
									SD→	5.6	1.9	0.9	2.0			
Set No. 8 Ebb																
5	S	96	104	20.3	11:33	11:40	7.0	150.31	35.8							
5	R	104	112	27.6	11:40	11:47	7.0	100.34	23.9	29.8	23.9					
6	S	97	105	22.5	11:34	11:41	7.0	160.63	38.2							
6	R	105	113	29.0	11:41	11:47	6.0	105.74	29.4	33.8	25.7					
7	S	98	106	21.7	11:34	11:42	8.0	181.57	37.8							
7	R	106	114	32.2	11:42	11:47	5.0	118.07	39.4	38.6	26.9					
8	S	99	107	25.5	11:34	11:42	8.0	189.11	39.4			11.4	2.5	8	8	8
8	R	107	115	30.3	11:42	11:48	6.0	110.41	30.7	35.0	27.9	2.7	2.3	6	6	6
									mean →	34.3	26.1	7.0	2.4			
									SD→	3.6	1.7	6.2	0.2			
Set No.9 Ebb																
1	S	108	116	24.1	11:44	11:59	15.0	258.35	28.7							
1	R	116	120	26.6	11:59	12:04	5.0	67.79	22.6	25.7	25.3					
2	S	109	117	26.5	11:45	11:59	14.0	256.85	30.6							
2	R	117	121	30.6	11:59	12:04	5.0	63.19	21.1	25.8	28.5					
3	S	110	118	29.6	11:45	12:00	15.0	289.54	32.2			4.2	1.6	15	15	15
3	R	118	122	35.2	12:00	12:05	5.0	81.92	27.3	29.7	32.4	0.7	7.2	5	5	
4	S	111	119	29.4	11:45	12:00	15.0	302.5	33.6			5.6	1.4	15	15	15
4	R	119	123	42.2	12:00	12:05	5.0	90.33	30.1	31.9	35.8	2.1				
									mean →	28.3	30.5	3.1	3.4			
									SD→	3.1	4.6	2.2	3.3			
Set No. 10 Ebb																
1	S	124	128	30.3	12:09	12:12	12.5	173	23.1							
1	R	128	146	31.0	12:12	12:27	15.0	72.49	8.1	15.6	30.6					
2	S	125	129	27.5	12:10	12:22	12.0	198.7	27.6							
2	R	129	137	26.5	12:22	12:27	5.0	79.31	26.4	27.0	27.0					
3	S	124	130	24.3	12:10	12:22	12.0	223.95	31.1							
3	R	130	138	27.7	12:22	12:27	5.0	75.58	25.2	28.1	26.0					
4	S	127	131	27.6	12:10	12:23	13.0	232.56	29.8			1.8	0.4	13	13	13
4	R	131	139	32.4	12:23	12:27	4.0	78.29	32.6	31.2	30.0	4.6	4.4	4	4	4
									mean →	25.5	28.4	3.2	2.4			
									SD→	6.9	2.2	2.0	2.8			
Set No.11 Ebb																
5	S	132	146	24.6	12:25	12:39	14.0	144.63	17.2							
5	R	146	148	43.2	12:39	12:50	11.0	76.51	11.6	14.4	33.9					
6	S	133	141	26.0	12:25	12:39	14.0	158.98	18.9							
6	R	141	149	40.4	12:39	12:51	12.0	97.05	13.5	16.2	33.2					
7	S	136	142	27.2	12:25	12:39	14.0	185.02	22.0			6.0	0.8	14	14	14
7	R	142	150	31.9	12:39	12:51	12.0	115.33	16.0	19.0	29.5	12.0	3.9	12	12	12
8	S	135	143	28.4	12:26	12:40	14.0	201.1	23.9			4.1	0.4	14	14	14
8	R	143	151	37.1	12:40	12:51	11.0	151.28	22.9	23.4	32.8	5.1	9.1	11	11	
									mean →	18.3	32.4	6.8	3.6			
									SD→	3.9	1.9	3.6	4.0			

21 Aug. 15 Drogue No.	Start, Observe, Recovery	GPS Begin	GPS End	Heading Degrees True*	Begin Time	End Time	Elapsed minutes	Distance m	Rate cm/s	Average Flow Rate All Locations cm/s	Average Heading All Locations (Degrees T)	Observed Flow in Lease Area cm/s	Heading Deviation from Straight Through (Degrees T)	Minutes Sampled Within Lease Area	Elapsed Time < 10 degrees Variation	Elapsed Time < 5 degrees Variation
Set No. 12 Ebb																
1	S	144	152	20.3	12:41	12:57	16.0	96.43	10.0							
1	R	152	156	38.7	12:57	13:09	12.0	181.08	25.1	17.6	29.5					
2	S	145	153	31.7	12:42	12:57	16.0	132.34	10.0							
2	R	153	157	32.8	12:57	13:09	12.0	176.47	24.5	17.4	30.9					
3	S	146	154	32.4	12:42	12:58	16.0	169.09	17.6			10.4	4.4	16	16	6
3	O	154	160	52.5	12:53	13:12	19.0	95.46	8.4			19.6	24.5	19		
3	R	160	164	74.3	13:12	13:23	11.0	52.1	7.9	11.3	53.1	20.1	46.3	11		
4	S	147	155	40.5	12:42	12:58	16.0	197.17	20.5			7.5	12.5	16		
4	O	155	161	57.6	12:58	13:12	14.0	128.25	15.3			12.7	29.6	14		
4	R	161	165	79.8	13:12	13:23	11.0	79.5	12.0	16.0	59.3					
										mean →	15.6	43.2	14.1	23.4		
										SD→	2.9	15.2	5.6	16.1		
Set No. 13 Ebb																
1	S	158	162	168.5	13:11	13:22	11.0	19.15	23.9							
1	O	162	168	247.4	13:22	13:37	15.0	25.57	2.8							
1	O	168	171	217.9	13:37	14:25	48.0	89.8	3.1							
1	R	171	174	142.5	14:25	15:15	50.0	155.84	5.2	11.7	176.5	22.8	65.6	50		
2	S	159	163	180.1	13:11	13:22	11.0	12.81	23.9							
2	O	163	167	239.4	13:22	13:40	18.0	25.17	2.3							
2	O	167	170	241.2	13:40	14:23	43.0	171.76	6.7							
2	R	170	173	216.3	14:23	15:14	51.0	245.93	8.0	16.0	127.9					
										mean →	13.8	152.2	22.8	65.6		
										SD→	3.0	34.3	NA	NA		
Set No. 14 Ebb																
3	S	166	169	39.6	13:29	13:40	11.0	157.86	23.9							
3	R	169	172	25.1	13:40	14:40	60.0	842.52	23.4	23.7	32.3					
										mean →	23.7	32.3	NA	NA		
										SD→	NA	NA	NA	NA		
Set No. 15 Near Slack																
1	S	175	181	324.5	15:17	15:30	13.0	11.07	1.4							
1	O	181	181	261.2	15:30	15:45	15.0	20.46	2.3							
1	R	181	184	198.5	15:45	15:51	6.0	7.71	2.1	1.9	261.4					
2	S	176	179	19.3	15:18	15:31	13.0	73.91	9.5			18.5	8.7	13	13	
2	O	179	182	17.9	15:31	15:46	15.0	52.69	5.9							
2	O	182	187	295.7	15:46	16:07	21.0	48.57	3.9			24.1	87.7	21		
2	R	187	192	240.1	16:07	16:30	23.0	146.52	10.6	7.5	143.2					
3	S	177	180	28.5	15:18	15:32	14.0	84.77	10.1							
3	R	180	183	29.1	15:32	15:47	15.0	64.85	7.2	8.6	28.8					
										mean →	6.0	144.5	21.3	48.2		
										SD→	3.6	116.3	4.0	55.8		
Set No. 16 Flood																
1	S	185	189	308.1	15:52	16:05	13.0	20.1	2.6							
1	R	189	193	248.4	16:05	16:31	26.0	4.07	0.3	1.4	278.2					
3	R	188	191	23.1	16:10	16:29	19.0	240.6	21.1	21.1	23.1					
4	R	189	190	33.3	16:21	16:26	5.0	11.6	3.9	3.9	33.3					
										mean →	8.8	111.5	NA	NA		
										SD→	10.7	144.5	NA	NA		
Set No. 17 Flood																
1	S	194	198	165.3	16:53	16:58	5.0	35.11	11.7							
1	O	198	203	138.9	16:58	17:17	19.0	33.42	2.9							
1	O	203	211	355.2	17:17	17:32	15.0	91.78	10.2							
1	R	211	221	2.2	17:32	17:57	25.0	189.14	12.6	9.4	165.4					
2	S	195	199	200.3	16:53	16:59	6.0	29.45	8.2			19.8	7.7	6	6	
2	O	199	205	205.6	16:59	17:10	11.0	110.38	16.7			11.3	2.4	11	11	11
2	O	205	213	267.9	17:10	17:33	23.0	29.88	2.2							
2	R	213	218	332.1	17:33	17:54	21.0	46.62	3.7	7.7	251.5					
3	S	197	200	223.5	16:54	16:59	5.0	13	4.3			23.7	15.5	5		
3	O	200	207	212.4	16:59	17:20	21.0	76.38	6.1							
3	O	207	210	231.7	17:20	17:31	11.0	56.45	8.6							
3	R	210	219	240.1	17:31	17:55	15.0	80.43	10.3	7.9	218.5					
										mean →	8.3	211.8	18.3	8.6		
										SD→	0.9	43.4	6.3	6.6		
Set No. 18 Flood																
4	S	201	204	184.7	17:03	17:18	15.0	92.4	10.3							
4	O	204	212	331.9	17:18	17:32	14.0	30.98	3.7							
4	R	212	222	30.0	17:32	17:57	25.0	280.4	18.7	10.9	182.2					
5	S	202	206	209.9	17:04	17:19	15.0	75.7	8.4			19.6	1.9	15	15	15
5	O	206	214	221.9	17:19	17:34	15.0	63.83	7.1							
5	R	214	217	272.1	17:34	17:54	10.0	26.1	6.8	7.3	236.0					
										mean →	9.1	209.1	19.6	1.9		
										SD→	2.6	38.0	NA	NA		

21 Aug. 15 Drogue No.	Start, Observe, Recovery	GPS Begin	GPS End	Heading Degrees True*	Begin Time	End Time	Elapsed minutes	Distance m	Rate cm/s	Average Flow Rate All Locations cm/s	Average Heading All Locations (Degrees T)	Observed Flow in Lease Area cm/s	Heading Deviation from Straight Through (Degrees T)	Minutes Sampled Within Lease Area	Elapsed Time < 10 degrees Variation
Set No. 19 Flood															
6	S	208	209	240.0	17:20	17:30	10.0	40.52	6.8						
6	R	209	220	260.6	17:30	17:56	26.0	116.04	7.4	7.1	250.3				
7	R	215	216	11.7	17:46	17:50	4.0	70.32	29.3	29.3	11.7				
									mean →	18.2	131.0	NA	NA		
									SD→	15.7	168.7	NA	NA		
Set No.20 Flood															
1	S	223	227	38.4	18:00	18:10	10.0	88.45	14.7						
1	R	227	235	49.8	18:10	18:21	11.0	146.42	22.2	18.5	44.1				
2	S	224	228	39.6	18:00	18:10	10.0	129.6	21.6						
2	R	228	240	39.5	18:10	18:22	12.0	152.92	21.2	21.4	39.6				
3	S	225	229	34.3	18:01	18:11	10.0	138.72	23.1			4.9	6.3	10	10
3	R	229	237	31.5	18:11	18:22	11.0	155.28	23.5	23.3	32.9	4.5	3.5	11	11
4	S	226	230	40.4	18:01	18:11	10.0	151.76	25.3			2.7	12.4	10	
4	R	230	238	48.6	18:11	18:22	11.0	162.62	24.6	25.0	44.5	3.4	20.6	11	
									mean →	22.0	40.3	3.9	10.7		
									SD→	2.8	5.4	1.0	7.6		
Set No. 21 Flood															
5	S	231	239	38.6	18:18	18:30	12.0	88.1	12.2						
5	O	239	247	65.3	18:30	18:40	10.0	96.68	16.1						
5	R	247	255	65.2	18:40	18:56	16.0	125.29	13.1	13.8	56.4				
6	S	232	240	40.5	18:18	18:30	12.0	98.64	13.7						
6	O	240	248	52.1	18:30	18:41	11.0	98.25	14.9						
6	R	248	256	60.3	18:41	18:57	16.0	155.04	16.2	14.9	51.0				
7	S	233	241	56.9	18:18	18:30	12.0	100.89	14.0			14.0	28.9	12	
7	O	241	249	57.3	18:30	18:41	11.0	91.61	13.9			14.1	29.3	11	
7	R	249	257	63.8	18:41	18:57	16.0	108.77	11.3	13.1	59.4				
8	S	234	242	49.7	18:19	18:31	12.0	113.24	15.7			12.3	21.7	12	
8	O	242	250	56.9	18:31	18:42	11.0	103.34	15.7			12.3	28.9	11	
8	R	250	258	63.3	18:42	18:58	16.0	125.71	13.1	14.8	56.6				
									mean →	14.2	55.8	13.2	27.2		
									SD→	0.9	3.5	1.0	3.7		
Set No. 22 Flood															
1	S	243	251	38.7	18:37	18:54	17.0	130.13	12.8						
1	R	251	267	55.7	18:54	19:16	22.0	151.81	11.5	12.1	47.2				
2	S	244	252	42.7	18:38	18:54	16.0	102.6	10.7						
2	R	252	268	56.1	18:54	19:16	22.0	130.9	9.9	10.3	49.4				
3	S	245	253	44.5	18:38	18:54	16.0	122.5	12.8			15.2	16.5	16	
3	R	253	269	55.8	18:54	19:16	22.0	119.4	9.0	10.9	50.1	19.0	27.8	22	
4	S	246	254	56.6	18:38	18:55	17.0	135.68	13.3			14.7	28.6	17	
4	R	254	270	61.3	18:55	19:17	22.0	163.6	12.4	12.8	59.0	15.6	33.3	22	
									mean →	11.5	51.4	16.1	26.5		
									SD→	1.2	5.2	1.9	7.2		
Set No. 23 Flood															
5	S	259	263	39.1	19:04	19:14	10.0	72.29	12.0						
5	R	263	271	51.2	19:14	19:37	23.0	127.4	9.2	10.6	45.1				
6	S	260	264	35.7	19:04	19:14	10.0	61.67	10.3						
6	R	264	272	45.6	19:14	19:38	24.0	121.85	8.5	9.4	40.7				
7	S	261	265	44.0	19:04	19:14	10.0	70.93	11.8						
7	R	265	273	42.9	19:14	19:38	24.0	135.79	9.4	10.6	43.5	18.6	14.9	24	
8	S	262	266	47.0	19:05	19:15	10.0	73.48	12.2						
8	R	266	274	43.5	19:15	19:40	25.0	143.46	9.6	10.9	45.3	18.4	15.5		
									mean →	10.4	43.6	18.5	15.2		
									SD→	0.7	2.1	0.1	0.4		

Flow Direction and Velocity

Flow direction determination was a primary goal of this brief study. Summary statistics (Table 4) and a more detailed data parsing into components (Table 5) are presented here.

Approximately equal sampling time occurred on both sampling days (Table 4). Day one had less ebb tide sampling by a 16% margin compared to day two. Drogues remained in the lease area at nearly the same fraction (32% and 33% of each day respectively). In these regards, the sampling was fairly balanced between days.

Table 4. Summary statistics for sampling times by location and tide.

Day 1 July 27, 2015	Minutes	Percent
Total drogue sampling time	2293	100%
All ebb tide sampling	997	43%
All flood tide sampling	1190	52%
All slack tide sampling	106	5%
Drogue sampling in lease area	729	32%
Drogue sampling outside lease area	1564	68%
Day 2 August 21, 2015	Minutes	Percent
Total drogue sampling time	2529	100%
All ebb tide sampling	1490	59%
All flood tide sampling	904	36%
All slack tide sampling	135	5%
Drogue sampling in lease area	826	33%
Drogue sampling outside lease area	1703	67%

Table 5 illustrates the breakout of results by tidal period and consistency of flow through that was parallel to the long axis of the lease area to within > 10 and >5 degree variations. Some data from Table 4 are intentionally repeated in Table 5.

Slack tide in terms of no water motion was actually not observed at any time during these surveys, Drogue kept moving at all times but the slowest movement period on day one was designated as slack tide. On day two, a very long period of minimal motion occurred in the middle of the predicted afternoon flood tide period while water motion offshore remained robust. Offshore motion was determined by occasionally setting drogues offshore and quickly recovering them once direction and velocity were determined.

As an important aside, the water flooded southward offshore while this sluggish northward inshore circulation occurred. Drogue movement slowed to a very slow rate as they reached shallow region north of the lease area and just south of Hannon Point, but they did not contact

the sea bottom. I speculate that at such times when the seaweed is present, the refuge effect of the seaweed project may become greatest, as dilution of the seaweed effects will be minimal. However, straight through flow occurred infrequently on the small flood of day two (4% of the entire ebb, Table 5) thus measurement of the effect may often be qualitative as flux calculations or algorithms may not be useful a large percentage of the time. Nevertheless, this may be an important goal to measure.

The ebb tide was marginally best for day one versus the flood and much better than the flood for day two in terms of consistency of flow parallel to the lease long axis. Fully 16% of the entire ebb tide sampled was within 5 degrees of parallel to lease area long axis on day two.

Table 5. Parsing of summary data into tidal stage for sampling times and variation from straight through flow within the lease area.

	Ebb		Flood		"Slack"	
	Minutes	Percent of Ebb	Minutes	Percent of Flood	Minutes	Percent of Slack
Day 1 July 27, 2015						
Total drogue sampling time	997	43%	1190	52%	106	5%
Drogue sampling time in lease area	209	29%	482	66%	38	5%
> 10 degree variation from long axis for total sampling time by tide	128	13%	115	10%	38	36%
> 5 degree variation from long axis for total sampling time by time	64	6%	64	5%	28	26%
	Ebb		Flood		"Slack"	
	Minutes	Percent of Ebb	Minutes	Percent of Flood	Minutes	Percent of Slack
Day 2 August 21, 2015						
Total drogue sampling time	1490	59%	904	36%	135	5%
Drogue sampling time in lease area	566	38%	226	25%	34	25%
> 10 degree variation from long axis for total sampling time by tide	334	22%	53	6%	13	10%
> 5 degree variation from long axis for total sampling time by time	232	16%	37	4%	0	0%

Flow velocity and its interrelation with direction are also important to this project. Due to time limitations for preparing this report, only the basic velocity data are reported here. Table 6 illustrates that overall stronger flows occurred for both tides on the Day one, large tidal amplitude day in July 2015 for all drogue locations. That is not surprising but the small tidal amplitude day was relatively strong too, only 17% (3.8 cm/s) less average velocity. This was obvious when at the site and making these measurements.

Within the lease area only mean ebb velocity exceeded mean flood velocity on day one. On day two, the flood was approximately twice as strong despite the long quiescent period mentioned

above. To some extent, the data are biased because of increased monitoring during active periods of drogue movement and this was evident in the velocity data.

Large standard deviations relative to the means indicate large variation in flow. Maximum calculated velocities within the lease area were 52 cm/s on day one for all locations and 24.1 cm/s on day two. Maximum velocity was not much different on ebb versus flood on both days. Larger tides will occur at this site during seaweed production. Current meters will provide a better view of velocity at the site. That data will be scrutinized for several factors including peak velocity and percentile velocity distribution. The observed velocities from this survey are not known to be destructive to sugar kelp (*Saccharina latissima*) or bull kelp (*Nereocystis luetkeana*) survival and in fact, these grow in much higher velocity conditions in the Strait of Juan de Fuca and the San Juan Islands. High rates of flow will reduce the seawater chemistry signal produced by the seaweed culture array. The data herein could be further used to estimate the probable seawater effects once seaweed biomass and timing projects are made.

Table 6. Summary of flow velocity statistics from Hood Head drogue survey.

All Drogue Locations	Velocity cm/s	Ebb only cm/s	Flood Only cm/s
Day 1 Mean	22.4	30.9	14.6
Day 1 SD	16.2	17.8	11.0
Day 2 Mean	18.6	23.0	12.2
Day 2 SD	9.4	8.2	6.2
Inside lease area only	Velocity cm/s	Ebb only cm/s	Flood Only cm/s
Day 1 Mean	18.6	25.9	14.5
Day 1 SD	13.5	14.0	12.1
Day 2 Mean	8.2	6.3	11.8
Day 2 SD	6.9	5.9	7.0

Summary and Conclusions

Shallow seawater circulation surveys were conducted near Hood Head in Northern Hood Canal, Washington State using drift objects (drogues) tracked with a GPS receiver during warm weather with light winds. An existing Washington Department of Natural Resources aquatic land leased area in this location will be the site to study the effects of a seaweed aquaculture on ocean acidification. The concept being tested is creation of seawater habitat and refugia for aquatic species such as wild and cultured shell-forming organisms that are especially sensitive to increasing ocean acidification (OA). The growth and timely harvest of seaweed will remove excess carbon and nutrients from surrounding seawater and the PAFF project is being designed to document these benefits quantitatively.

The main objective of the brief field surveys reported herein was to begin to understand the flow patterns through the seaweed project area and near vicinity. Extensive and high quality instrumentation will be located “upstream and downstream” of the seaweed and this survey by the University of Washington Applied Physics Laboratory and NOAA Pacific Marine Environmental Laboratory staff and others. This preliminary survey was intended to help inform on optimum location of the moorings and the suitability of the site for calculating net change of seawater carbonate chemistry, dissolved oxygen and dissolved nutrients conditions. At this point, the site appears to be suitable for the task but more study with current meters and other approaches are planned.

A probable sampling strategy for quantifying seawater effect of the seaweed will involve measuring results when water passes directly through the seaweed array, in line with the long axis of the seaweed longlines like a pipeline effect. Models of seaweed physiology and growth can be applied or adapted to the region, but without quality field data, validation of models is not possible and the chance for error in estimating effects high.

The study days included daylight ebb and flood tides that were much larger and smaller than the mean tidal amplitude for the subject area. As expected from the bathymetry and surrounding shoreline topography, ebb tide in a northerly direction produced the optimum conditions for measurement with 16% of the observations within 5 degrees of straight through. This occurred on day two of sampling is especially good as flow velocity was less that day than on the large tidal day one. Lower flow rates allow better signal to background noise determination, as dilution is less. Evidence of gyre circulation was apparent during much of the flood tide due to the presence of Hannon Point just north of the lease area. Nevertheless, reverse flow patterns resulting from gyre circulation during flood tide approximated “straight through” flow that could be useful for monitoring, particularly as flow velocity at such times was also reduced.

Although more study with current meters are necessary, it is apparent that the Hood Head site should perform admirably in terms of having regular flows of seawater to provide dissolved

growth nutrients while not exceeding flow rate thresholds known to produce damage to the seaweed or the mooring facility.

North Hood Canal has much higher near surface concentrations of dissolved inorganic nitrogen than South Hood Canal in general (Paulson et al. 2007) even in summer months. South Hood Canal has long periods of nutrient depletion in surface waters during summer months that would preclude seaweed culture (EPA 1991). Deepwater hypoxia and abrupt vertical turn over events have caused fish and invertebrate kills and habitat stress for many years (e.g., Newton et al. 1995)

The Hood Head site maximum flow rates on a large tidal exchange day peaked near 50 cm/s in this drogue study. Allowing for storm driven conditions on spring tidal days for worst-case, maximum flow rate conditions, I would expect maximum ebb flows to reach rates of 60 to 75 cm/s but we will know more after current meters are deployed in the winter of 2015-2016. The effects of sustained southerly winds on surface flow in Hood Canal could be significant at the Hood Head site. That can be evaluated during the winter while current meters are deployed. Exposure to larger wind waves may affect kelp morphology (Fowler-Walker 2006) and thus economic value but the North Hood Canal Floating Bridge acts as a breakwater to significantly reduce wind distance fetch and risks from wind waves.

Sugar kelp (*Saccharina latissima*) to be grown at the Hood Head site are known to produce only very modest drag forces on long line mooring facilities at rates below 100 to 150 cm/s in engineering studies reported by Olanrewaju et al. (2014). This species and related species of seaweed are common on central and north Puget Sound aquaculture floats (Rensel and Forster 2007) including those at Deepwater Bay, Cypress Island that have flow rates that exceed the probable peak rates expected at the Hood Head seaweed refugium site. To optimize year-round production, other species of seaweed will be required for summer and fall periods. Drogue data herein and current meter data will be useful in choosing the species and culture practices.

References Cited

- Folwer-Walker, M.J., T Wernberg and S.D. Connell.2006. [Differences in kelp morphology between wave sheltered and exposed localities: morphologically plastic or fixed traits?](#) Marine Biology 148:755-767.
- Nash, C.E. (editor). 2001. [The net-pen salmon farming Industry in the Pacific Northwest.](#) NOAA Tech. Memo. NMFS-NWFSC-49, 125 p.
- Newton, J.A., A.L. Thomson, L.B. Eisner, G.A. Hannach, and S.L. Albertson. 1995. Dissolved oxygen concentrations in Hood Canal: Are conditions different than forty years ago? In Puget Sound Research '95 Proceedings, Puget Sound Water Quality Authority, Olympia, WA, pp. 1002-1008.
- Olanrewaju, et al. 2014 [Advances in environmental engineering and green technologies. \(AEEGT\) book series.](#) Information Science Reference. Hershey, Pennsylvania (701 E. Chocolate Ave., Hershey, PA, 17033) : IGI Global.
- Paulson, A.J., Konrad, D.P., Frans, L.M., Noble, M., Kendall, C., Joshberger, E.G., Juffman, R.L., and T.D. Olsen. 2006. [Freshwater and saline loads of dissolved inorganic nutrients to Hood Canal and Lynch Cove, western Washington.](#) U.S. Geological Survey Scientific Investigations Report. 2006-5106. 92 p.
- Parametrix, Battelle Northwest Laboratories and Rensel Associates. 1990. [Programmatic Environmental Impact Statement: Fish culture in floating net-pens.](#) Prepared for the Washington Department of Fisheries and other resource agencies. 161 pp.
- Rensel Associates and PTI Environmental Services. 1991. [Nutrients and Phytoplankton in Puget Sound.](#) Peer reviewed monograph prepared for U.S. Environmental Protection Agency, Puget Sound Estuary Program. Region 10, Seattle. Report 910/9-91-002. 130 pp.
- Rensel, J.E. 2003. [Dungeness Bay Bathymetry, Circulation and Fecal Coliform Studies. Phase 2.](#) Prepared by Rensel Associates Aquatic Science Consultants, Arlington, Washington for the Jamestown S’Klallam Tribe, Sequim Washington and the U.S. Environmental Protection Agency, Seattle, Washington. 94 p.
- Rensel, J.E. 2010. [Tracing of fish farm effects on sediment and food web of Rufus Wood Lake, Columbia River, 2009 Results.](#) Prepared by Rensel Associates Aquatic Sciences, Arlington WA for Pacific Aquaculture Inc. and the Colville Confederated Tribes, Nespelem, Washington. 38 pp
- Rensel, J.E. and J.R.M. Forster. 2007. [Beneficial environmental effects of marine net pen aquaculture.](#) Rensel Associates Aquatic Sciences Technical Report prepared for NOAA Office of Atmospheric and Oceanic Research. 57 pp.

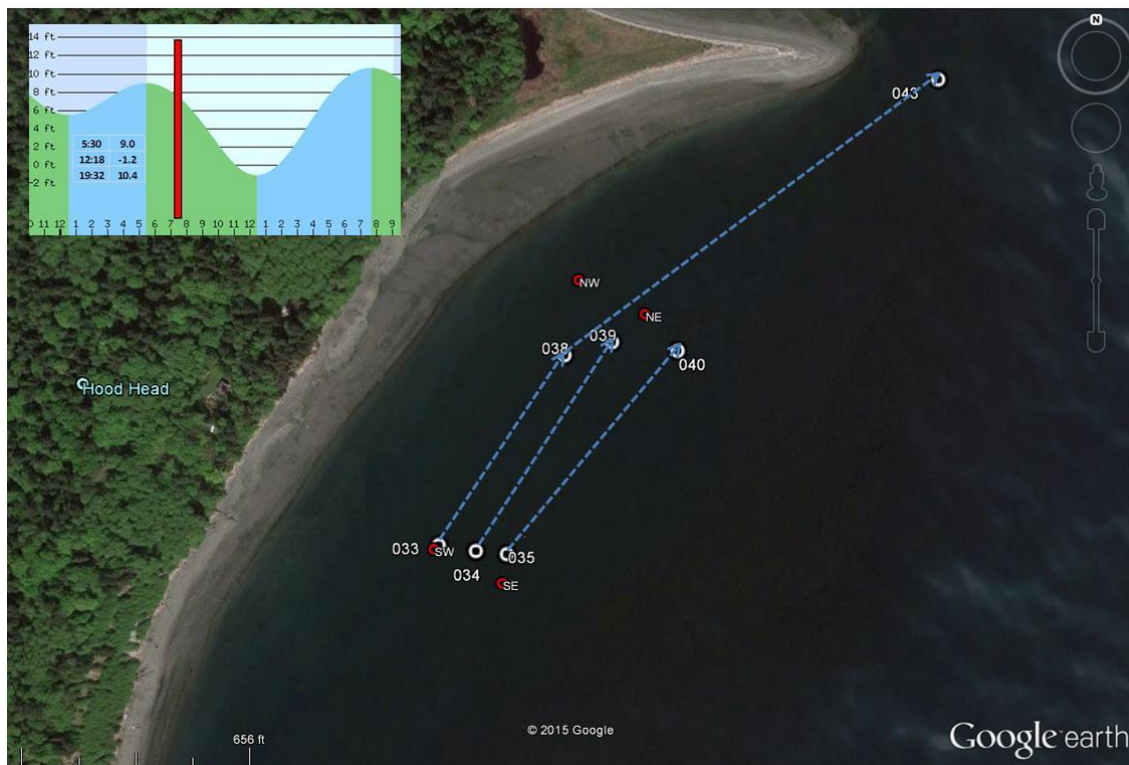
Rensel, J.E., K. Bright and Z. Siegrist. 2011 "[Integrated fish-shellfish mariculture in Puget Sound](#)" Final Report for NOAA Award – NA080AR4170860. NOAA National Marine Aquaculture Initiative. Rensel Associates, Arlington WA in association with American Gold Seafoods and Taylor Shellfish Inc. 82 p.

Washington State Blue Ribbon Panel on Ocean Acidification (2012): [*Ocean Acidification: From Knowledge to Action, Washington State's Strategic Response*](#). H. Adelsman and L. Whitely Binder (eds). Washington Department of Ecology, Olympia, Washington. Publication no. 12-01-015

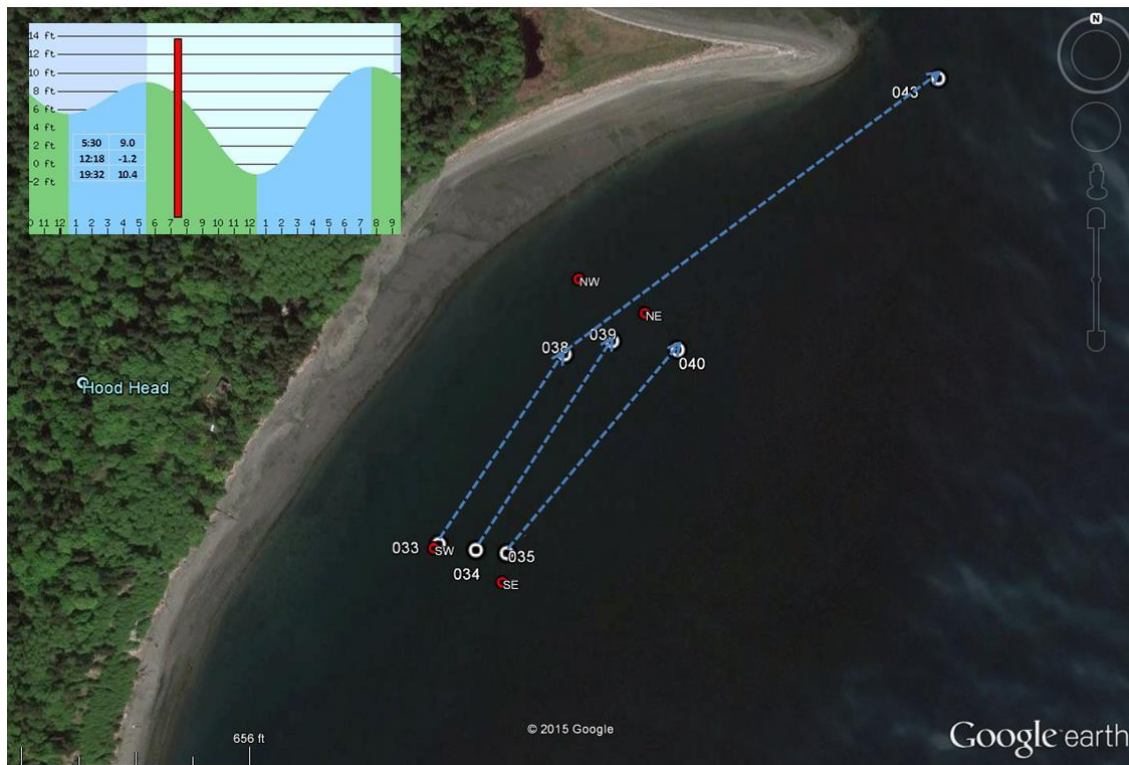
Appendix

The following images indicate the aquatic lease area corners (small red circles with NW, NE, SW or SE corner labels). Plots of all of the drogue tracks collected nearshore near and within the lease area are indicated by the blue dotted line drawn to connect measured GPS locations indicated as white circles and associated GPS codes.

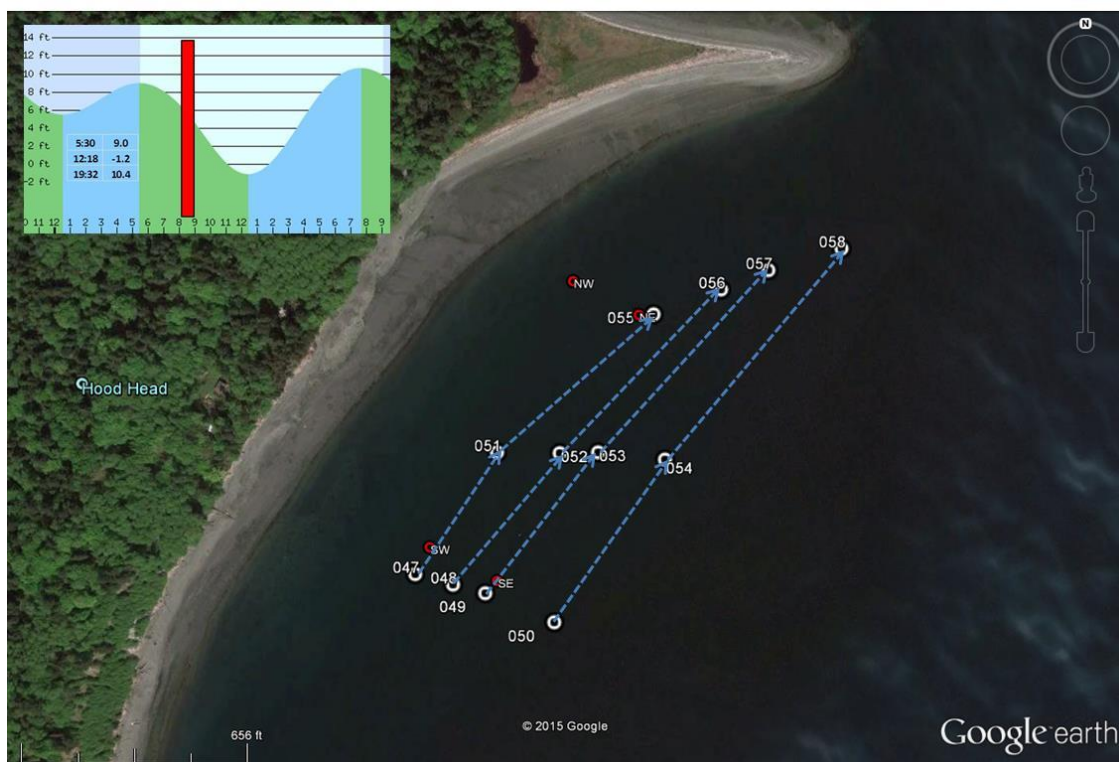
Some drogue surveys use attached GPS recorders, but this was not necessary for this survey, as the distance between recordings was very small and the time intervals short. Thus, it is highly unlikely that any of the drogues deviated significantly from the reported pathways herein.



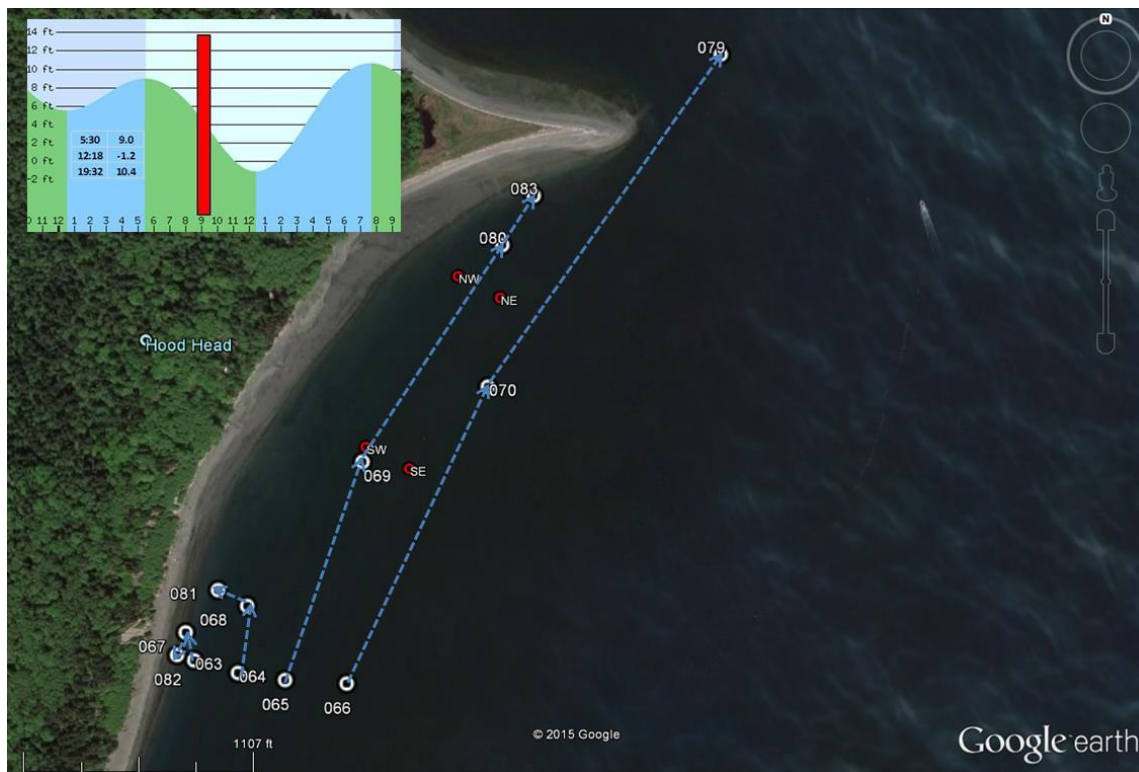
Appendix Figure 15. Ebb tide July 17, 2015.



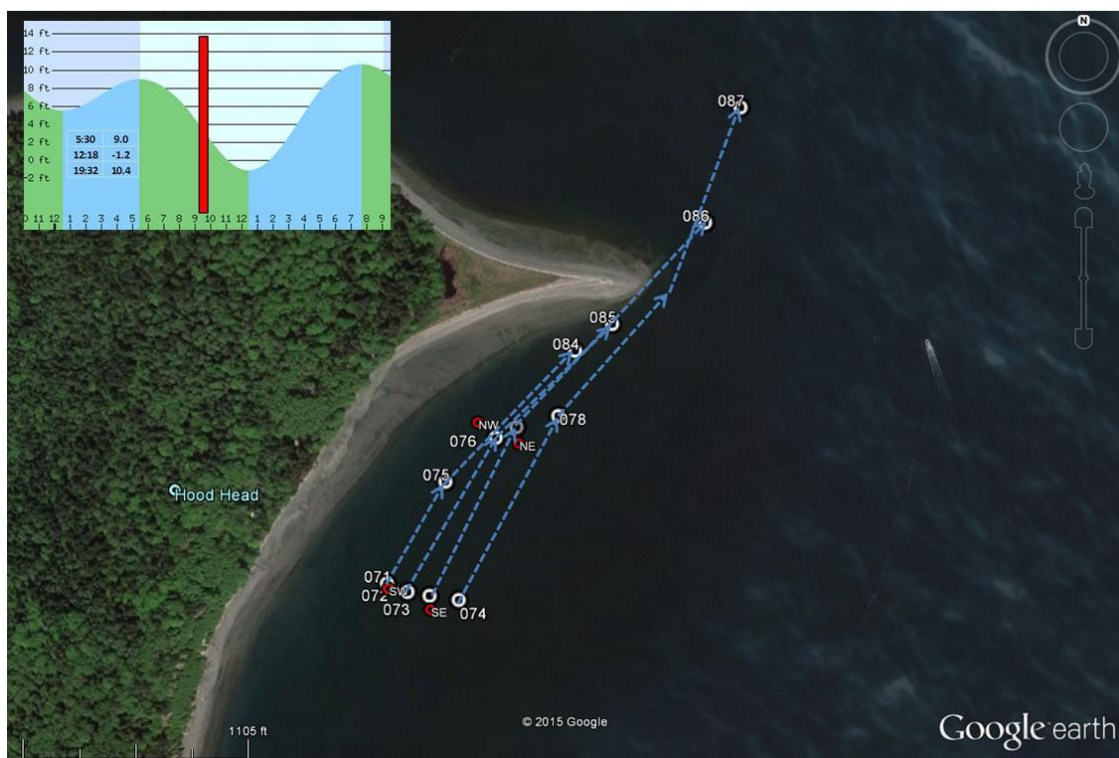
Appendix Figure 16. Ebb tide July 17, 2015



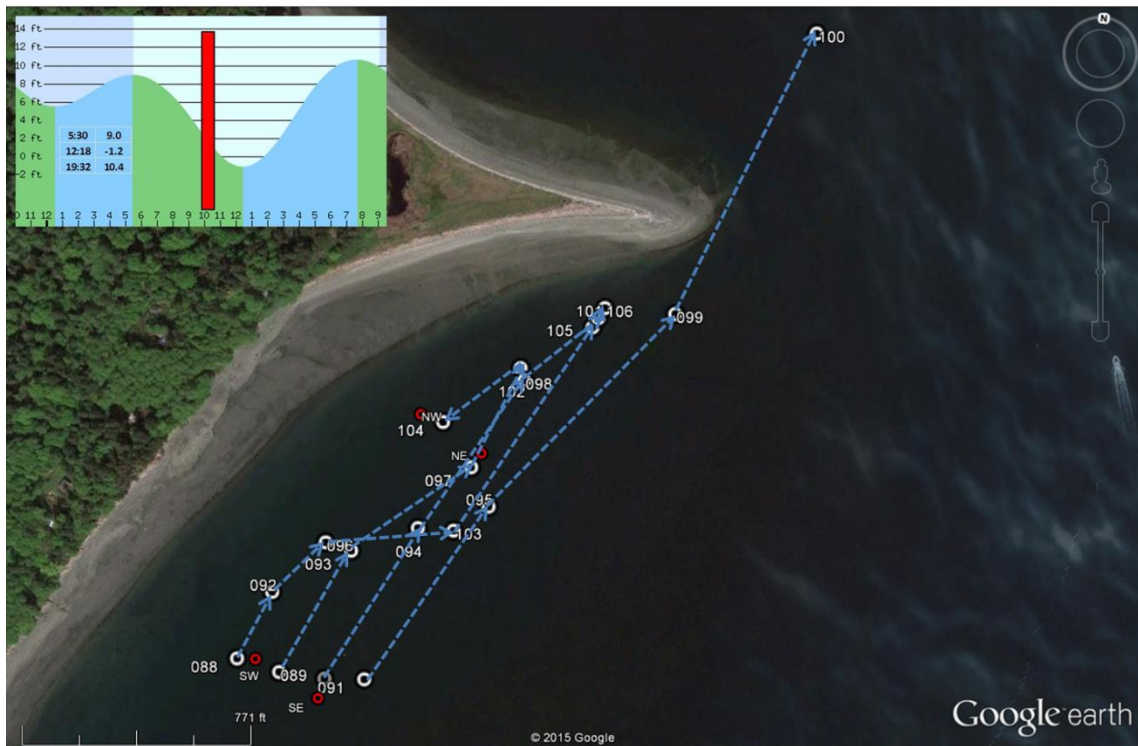
Appendix Figure 17 Ebb tide July 17, 2015



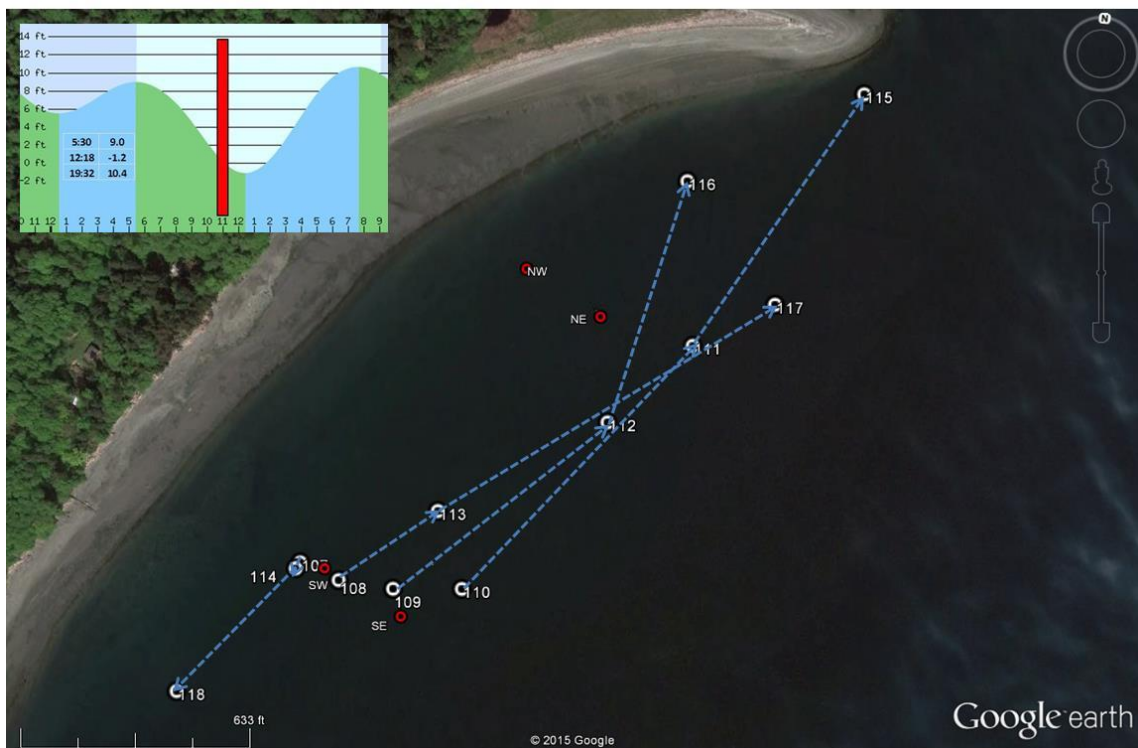
Appendix Figure 18 Ebb tide July 17, 2015



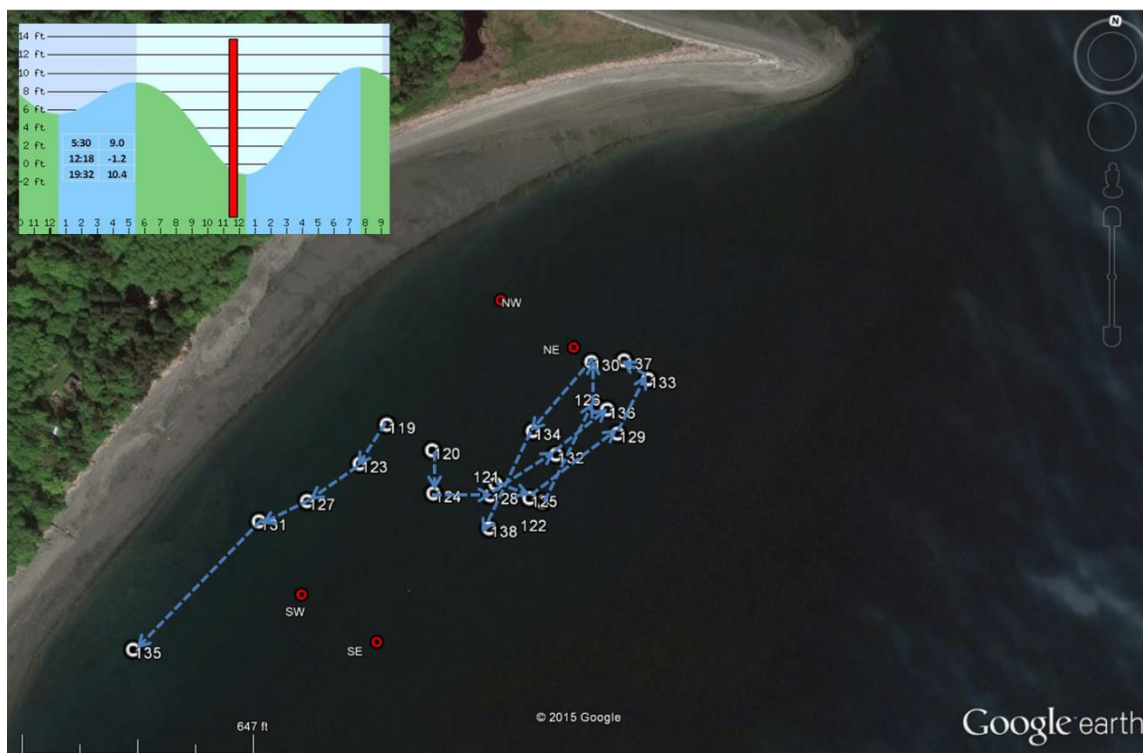
Appendix Figure 19 Ebb tide July 17, 2015



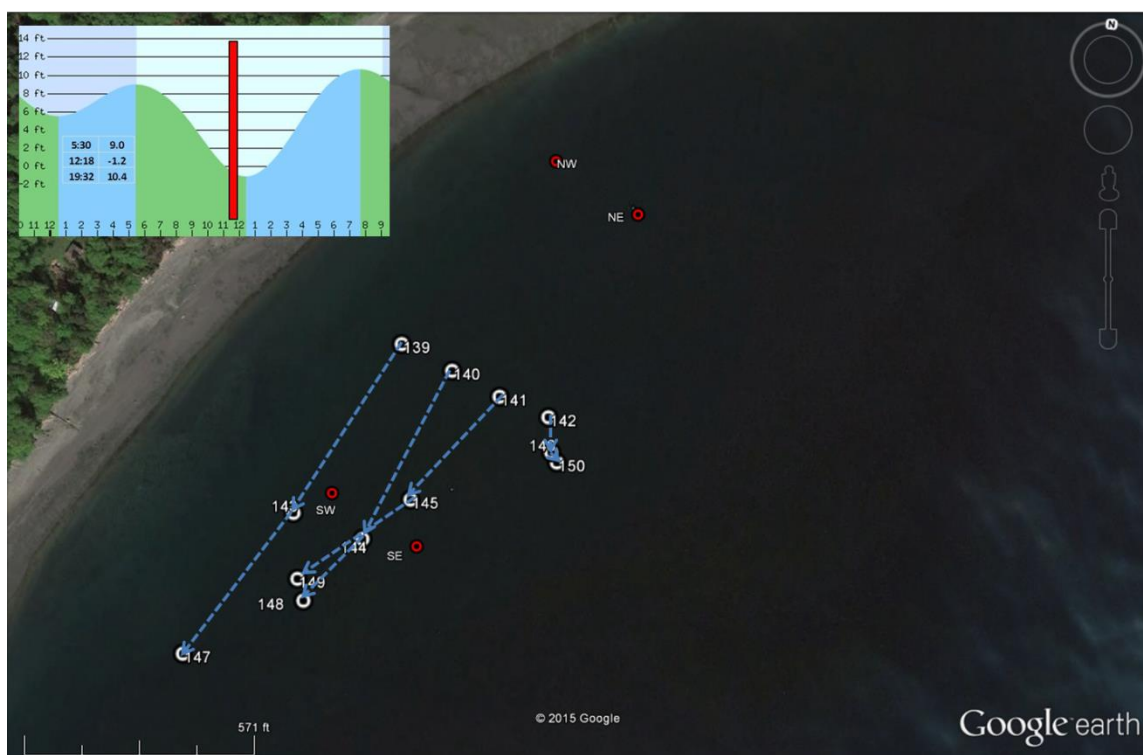
Appendix Figure 20. Ebb tide July 17, 2015



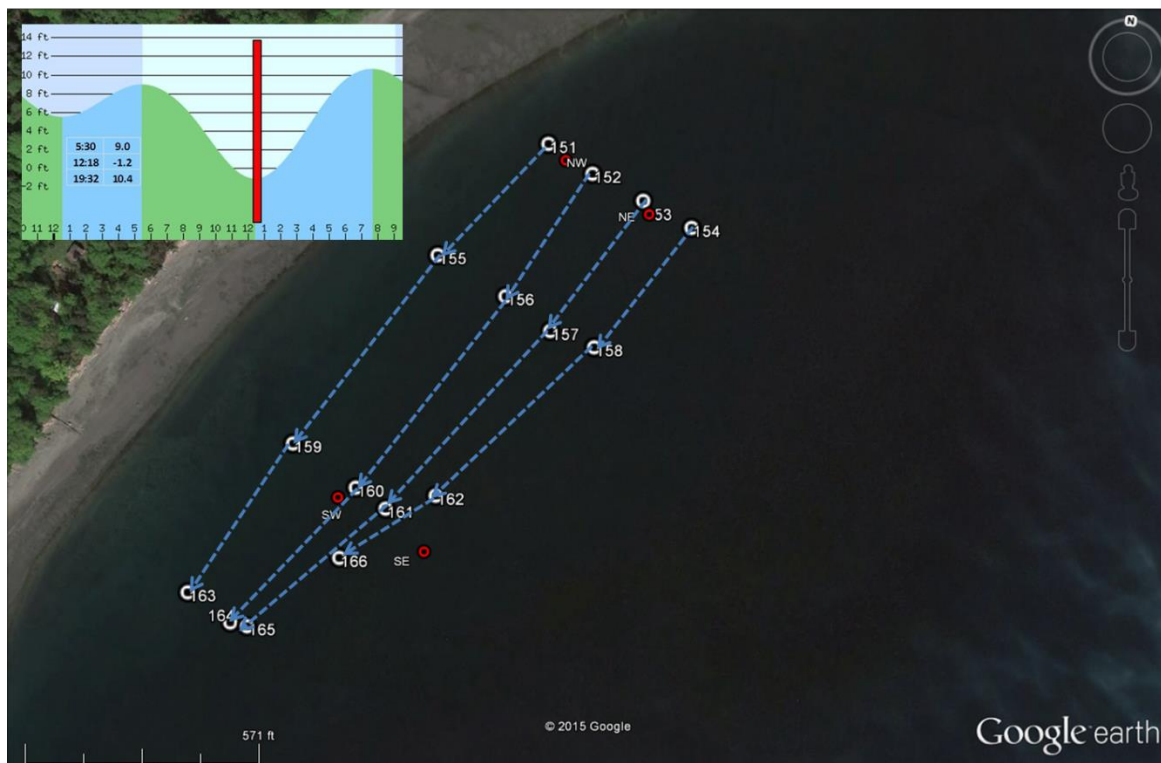
Appendix Figure 21. Ebb tide July 17, 2015



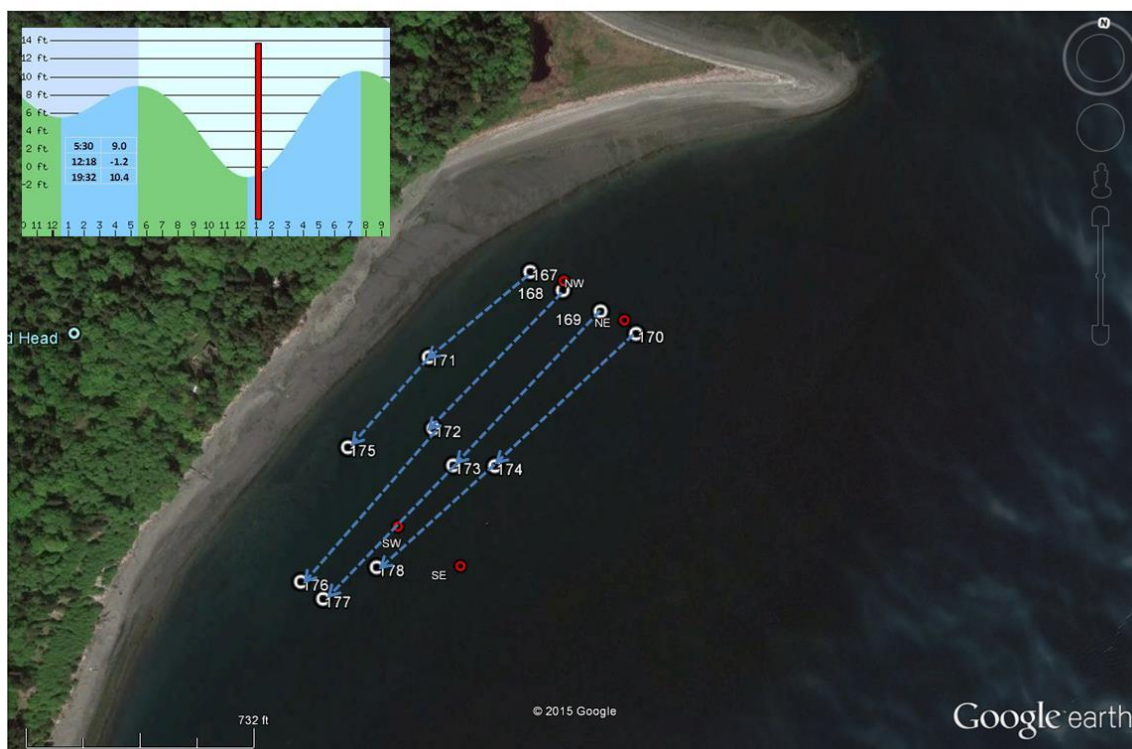
Appendix Figure 22. Change of tide, July 17, 2015



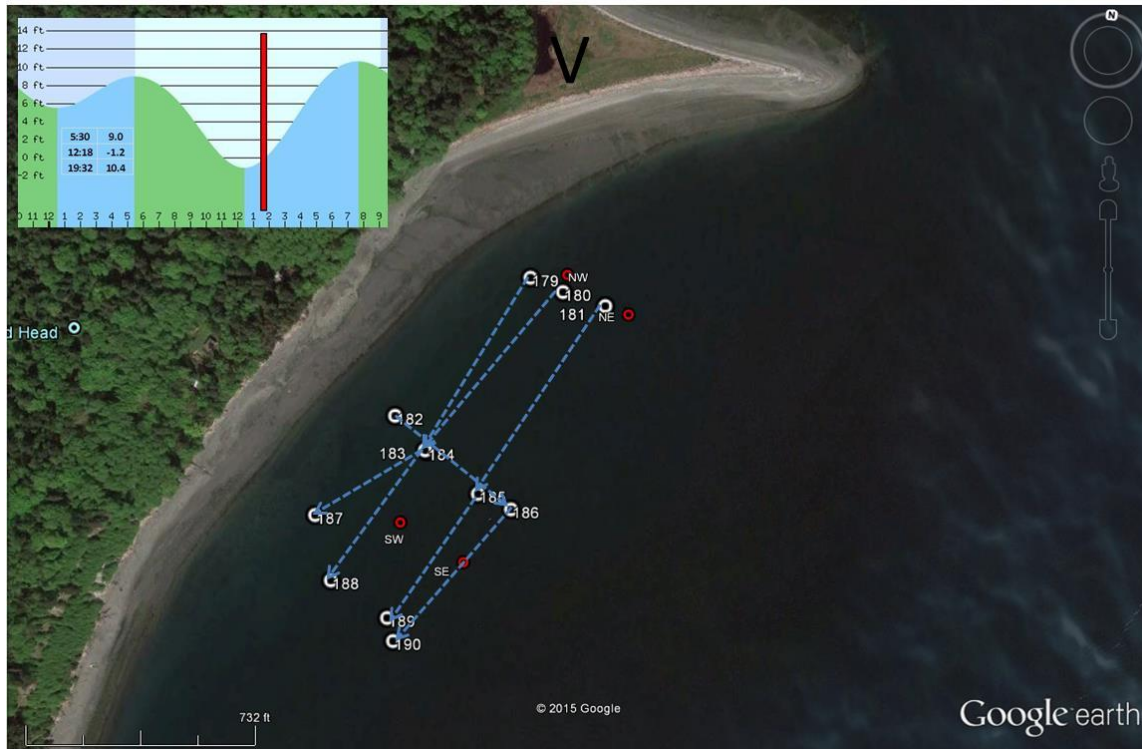
Appendix Figure 23. Flood tide July 17, 2015



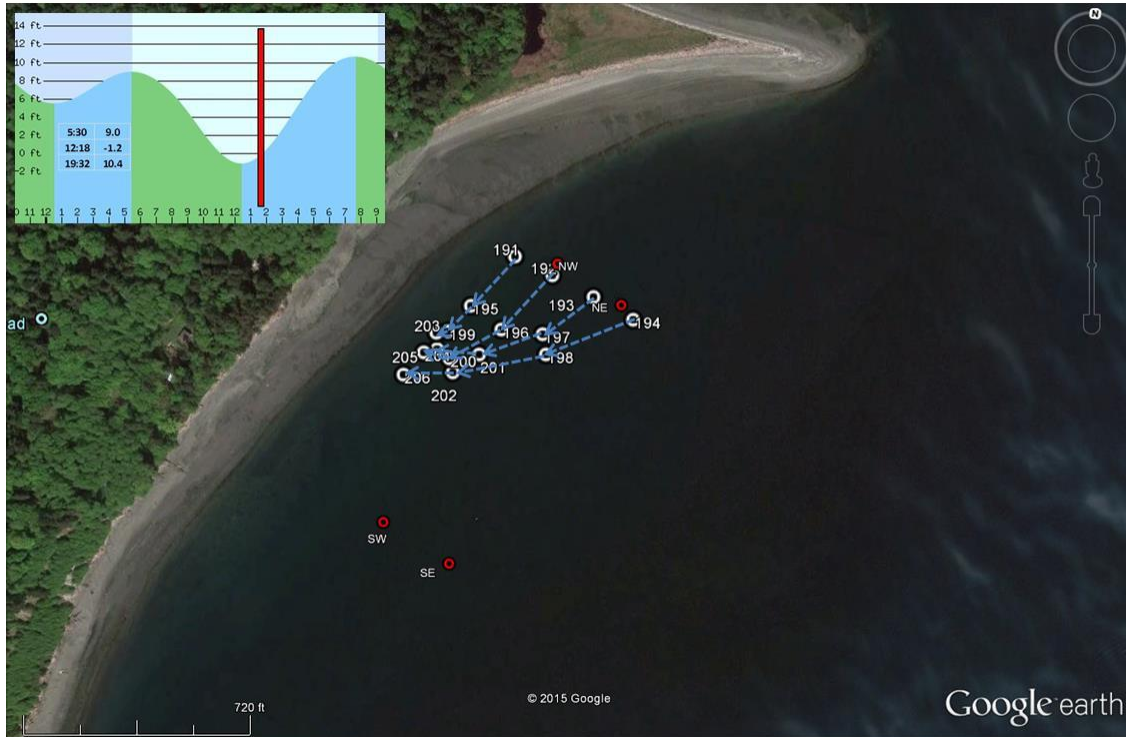
Appendix Figure 24. Flood tide July 17, 2015



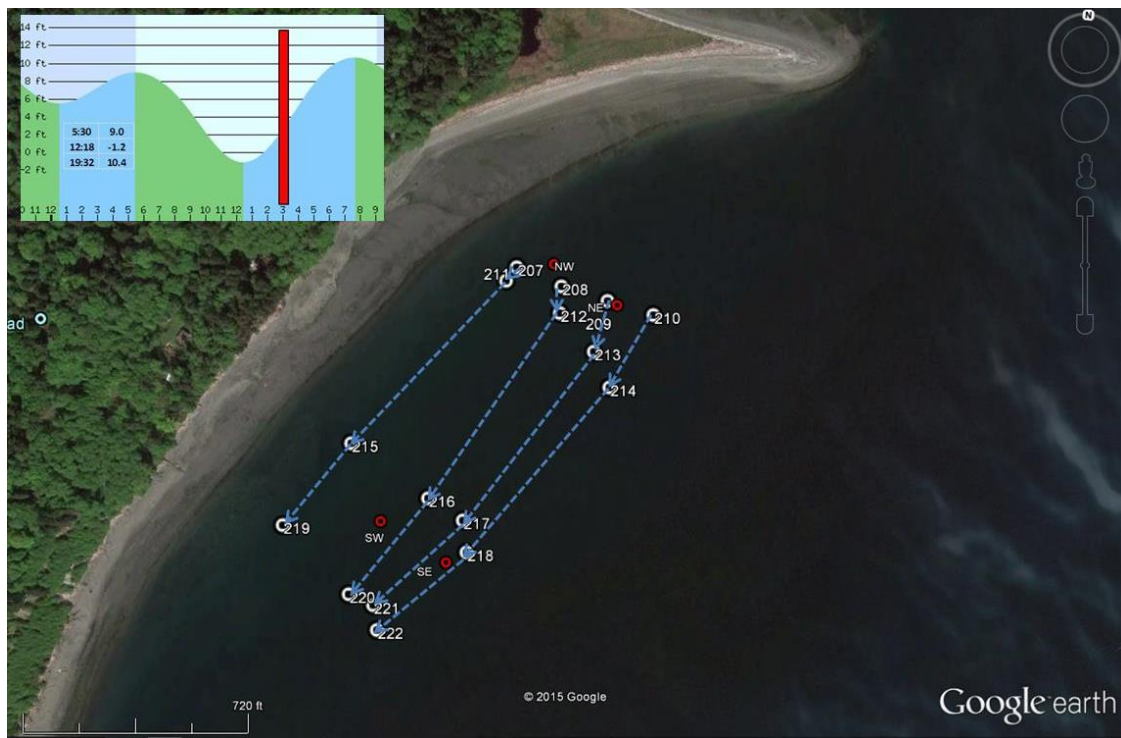
Appendix Figure 25. Flood tide July 17, 2015



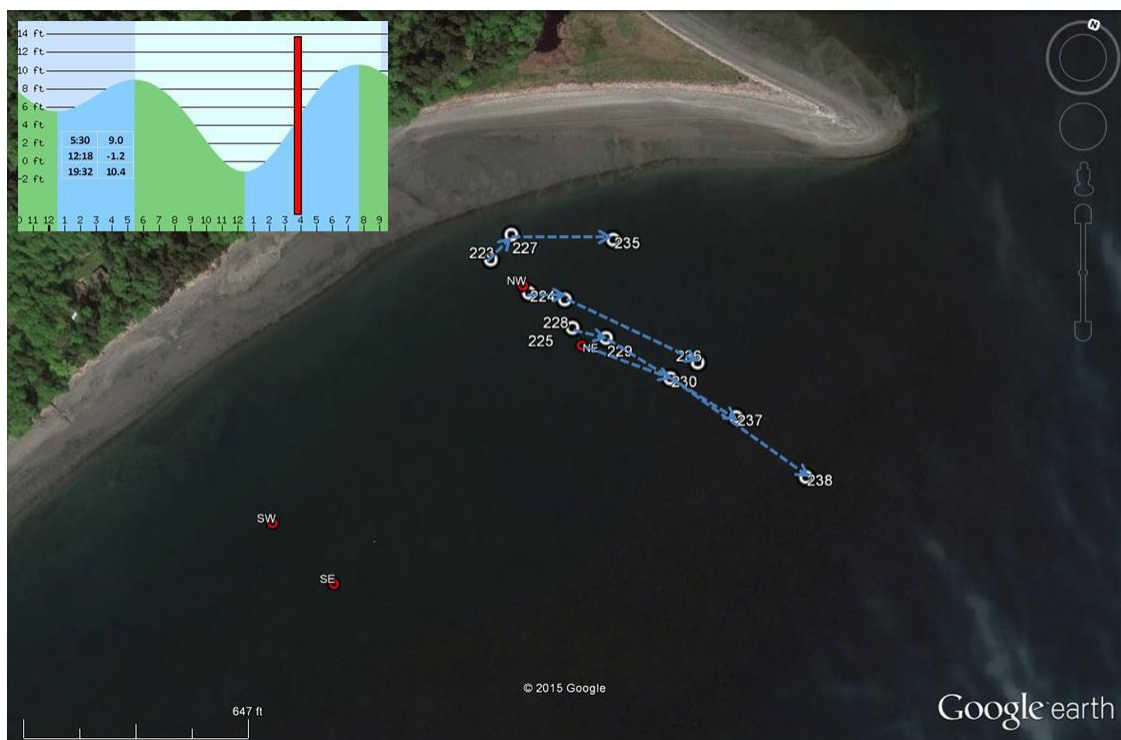
Appendix Figure 26. Flood tide July 17, 2015



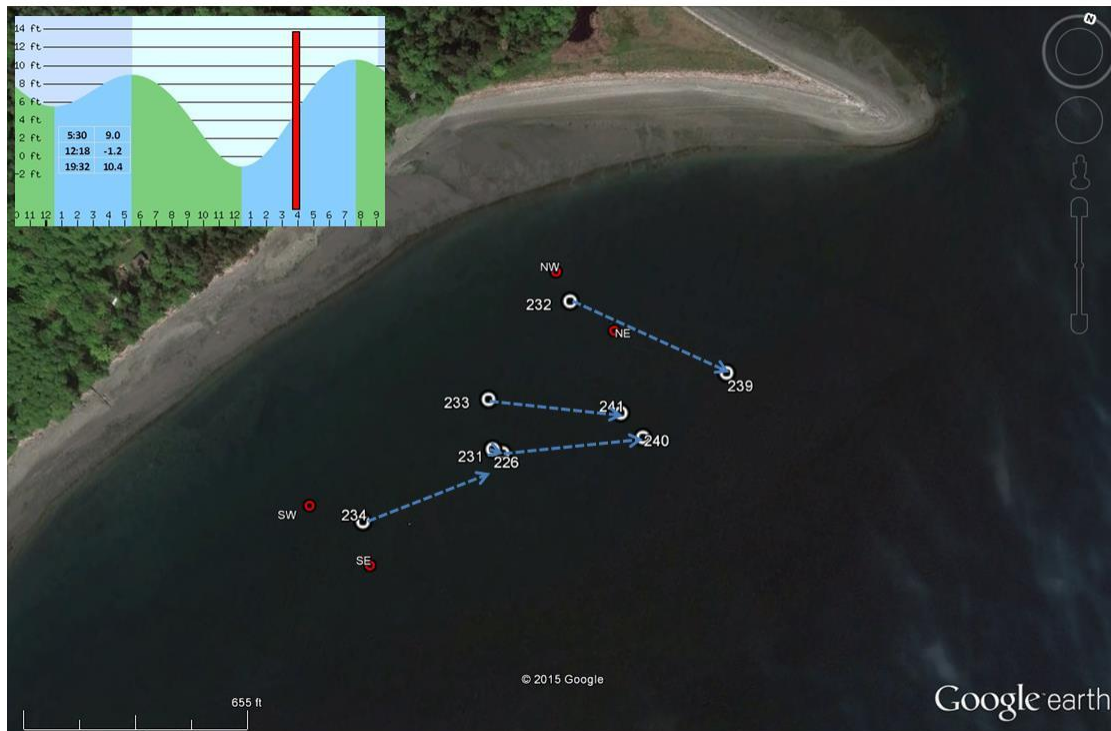
Appendix Figure 27. Flood tide July 17, 2015



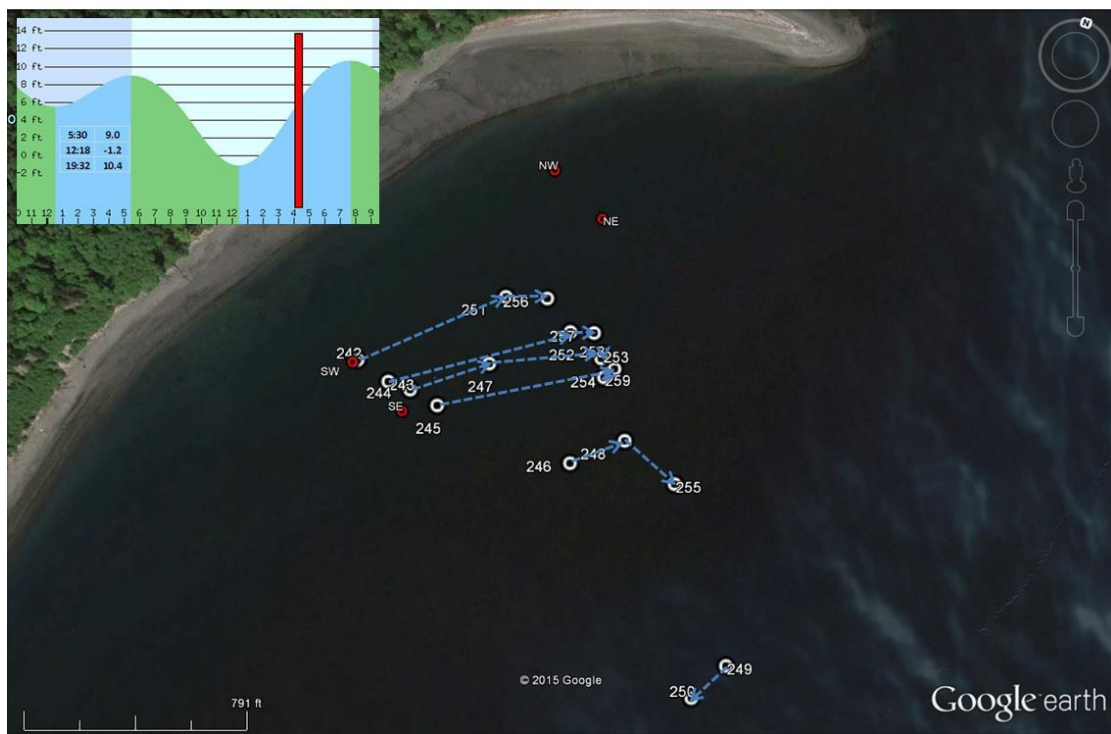
Appendix Figure 28. Flood tide July 17, 2015



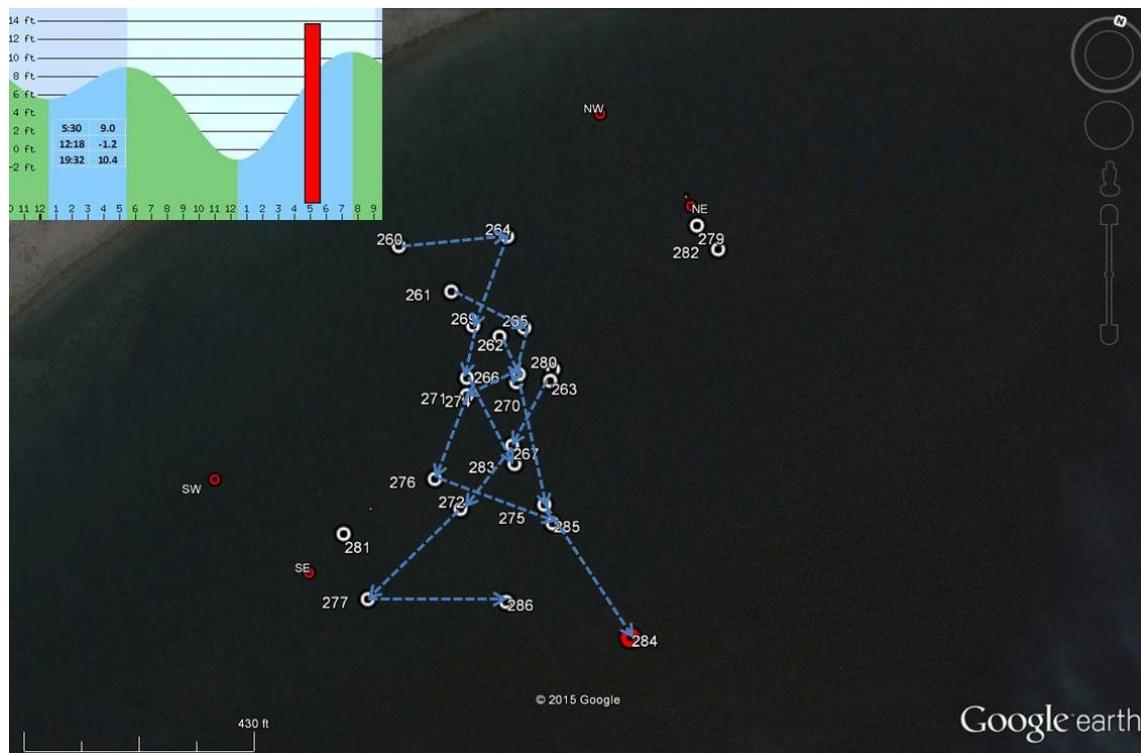
Appendix Figure 29. Flood tide July 17, 2015



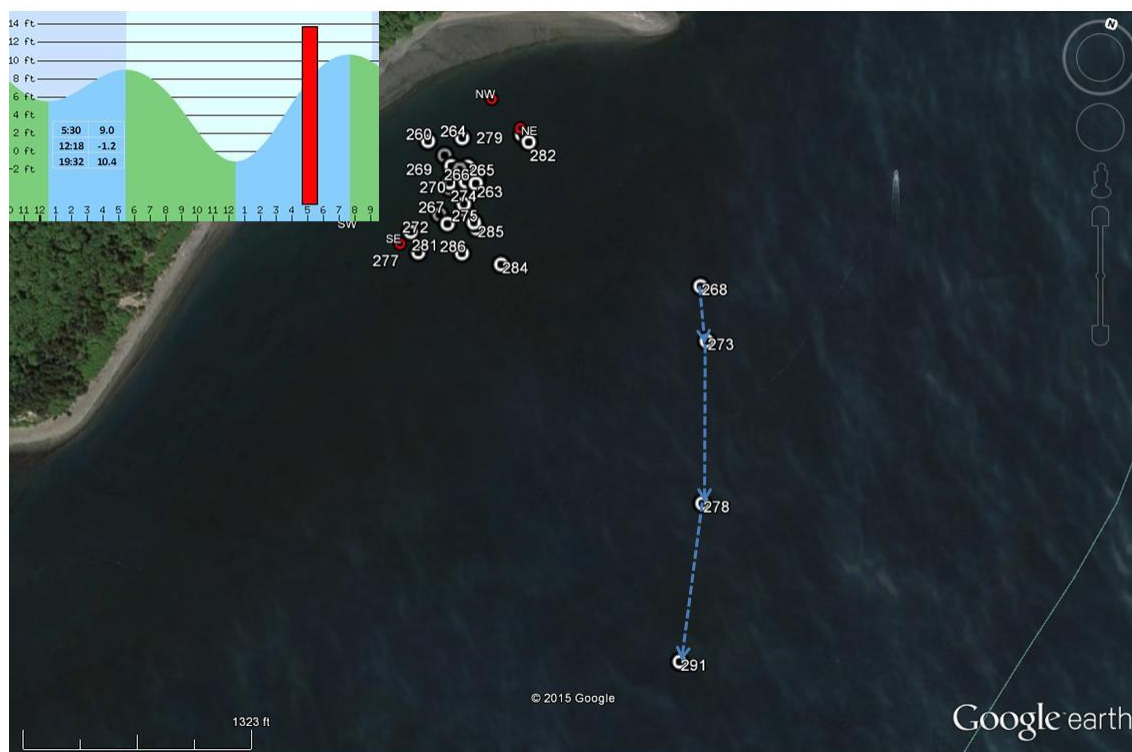
Appendix Figure 30. Flood tide July 17, 2015

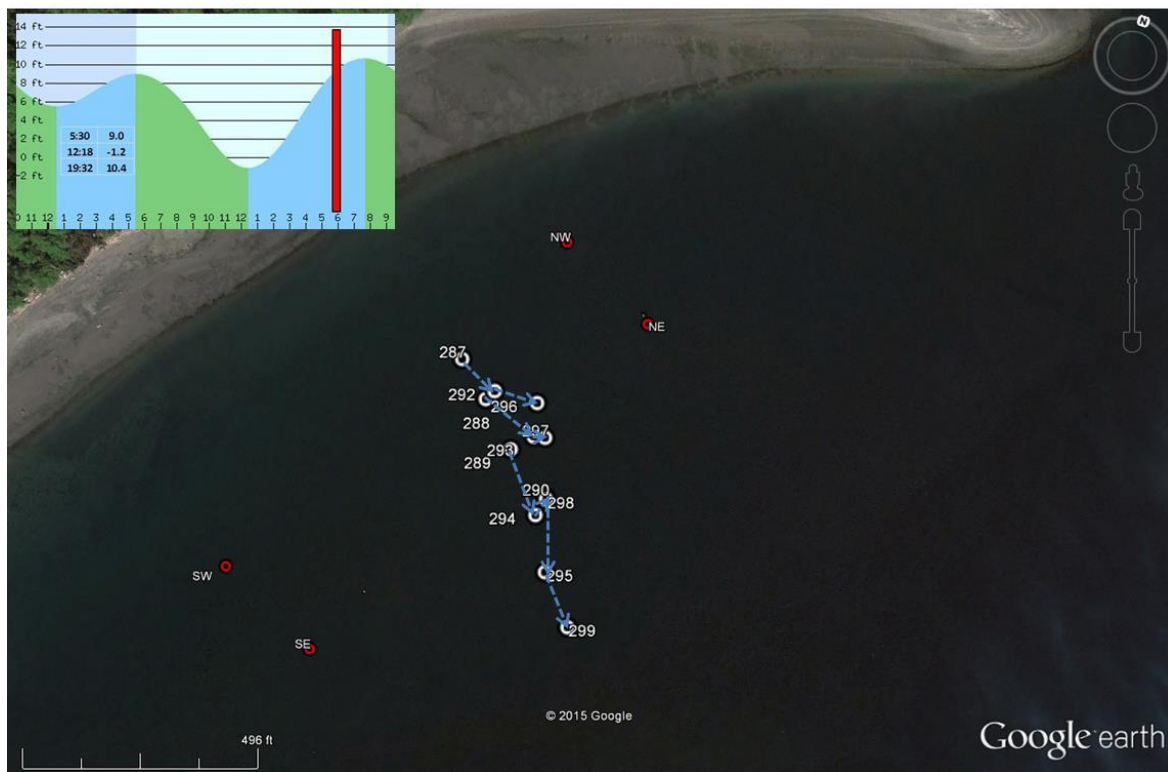


Appendix Figure 31. Flood tide July 17, 2015

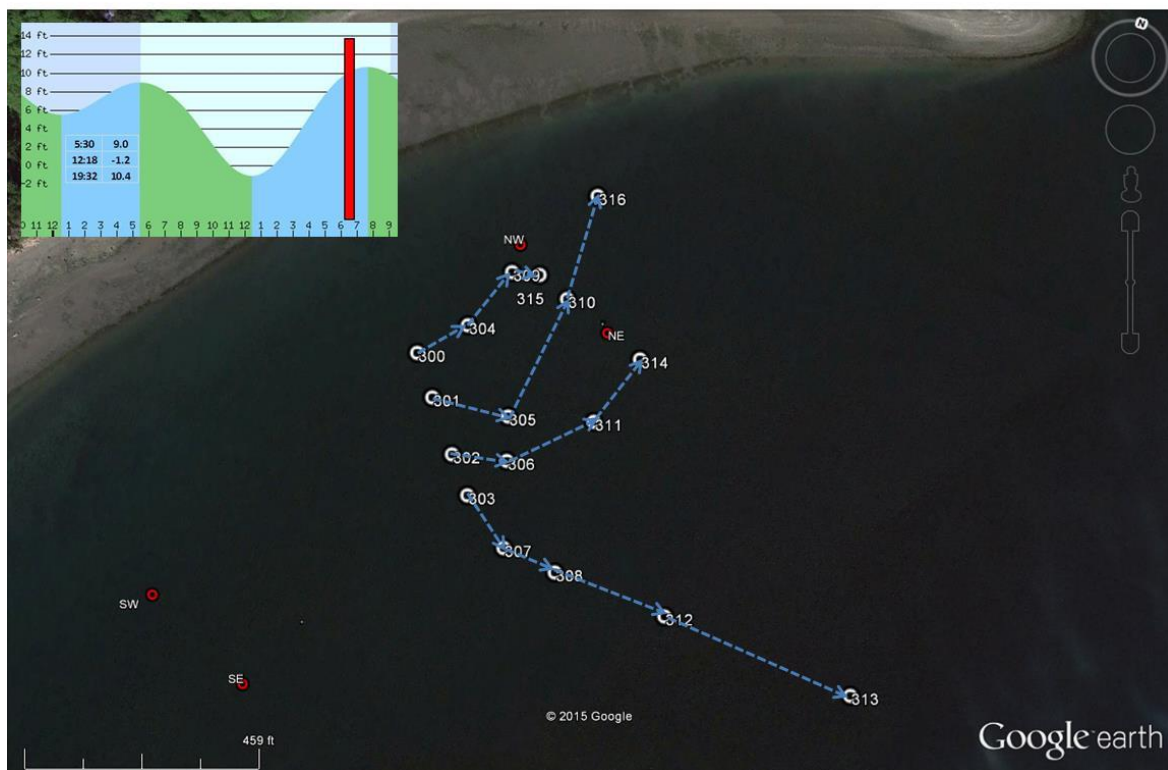


Appendix Figure 32. Flood tide July 17, 2015

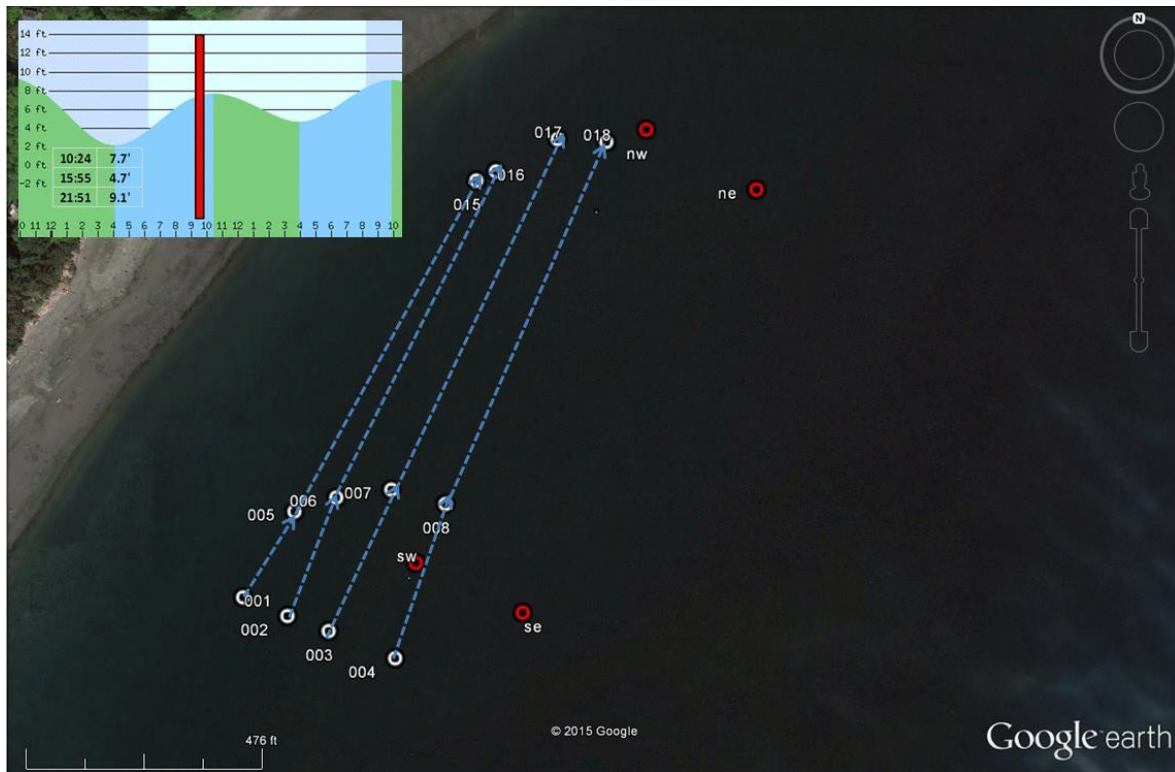




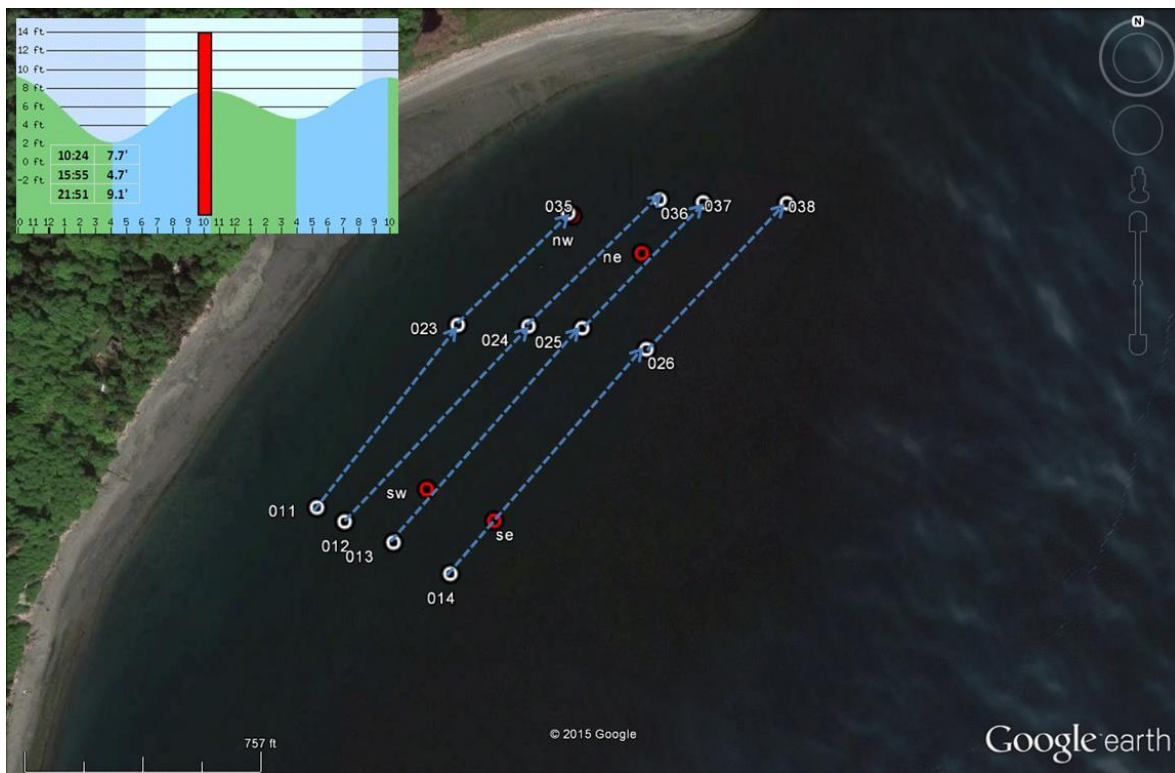
Appendix Figure 34. Flood tide July 17, 2015



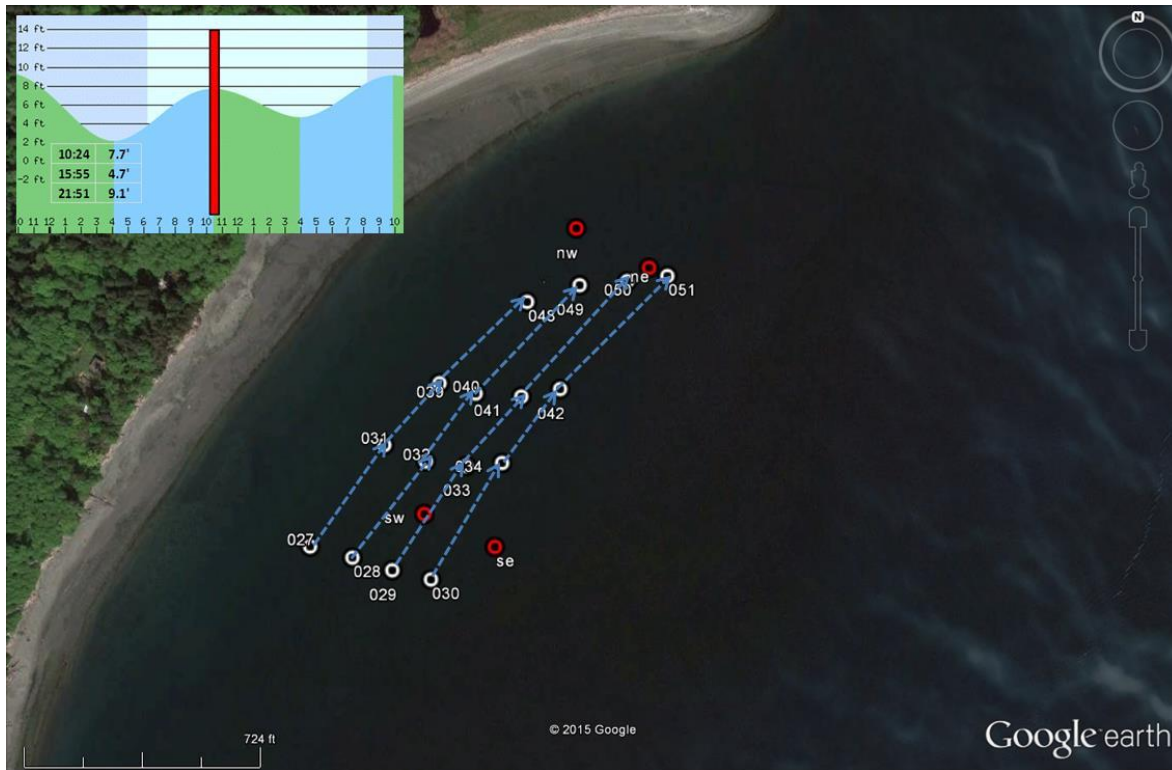
Appendix Figure 35. Last plot for July 17, 2015 survey.



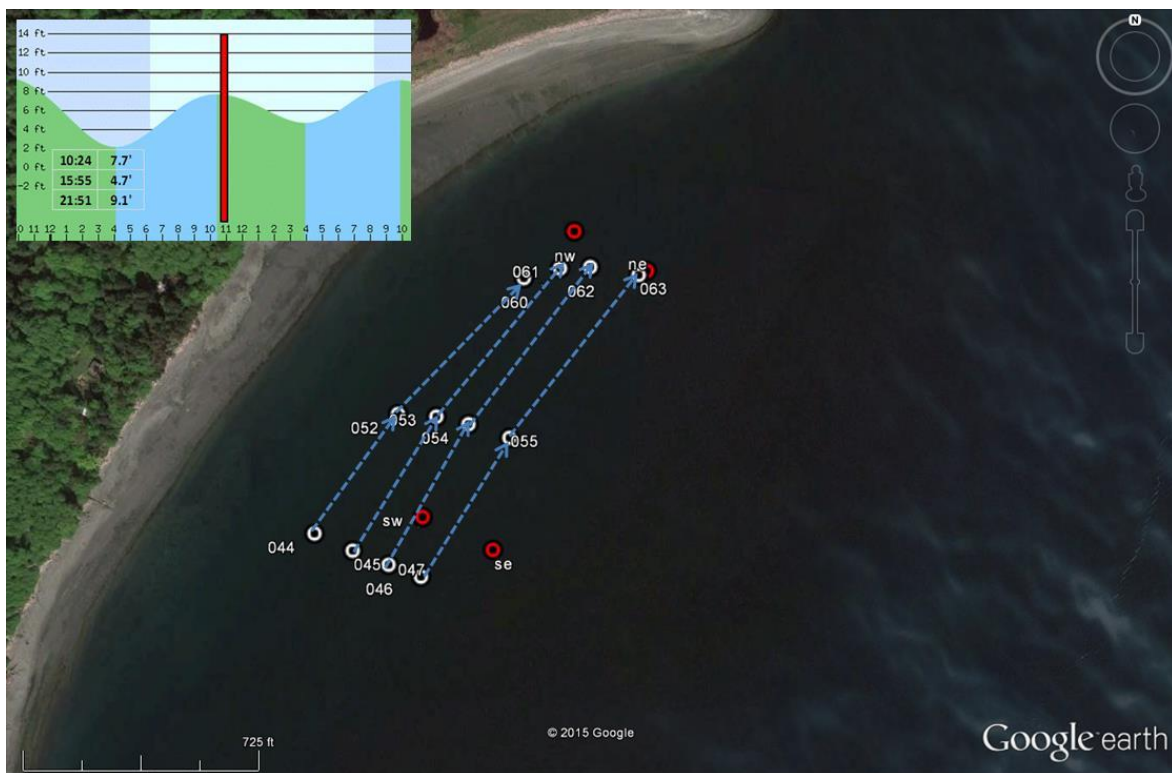
Appendix Figure 36. Begin August 21, 2015 ebb tide.



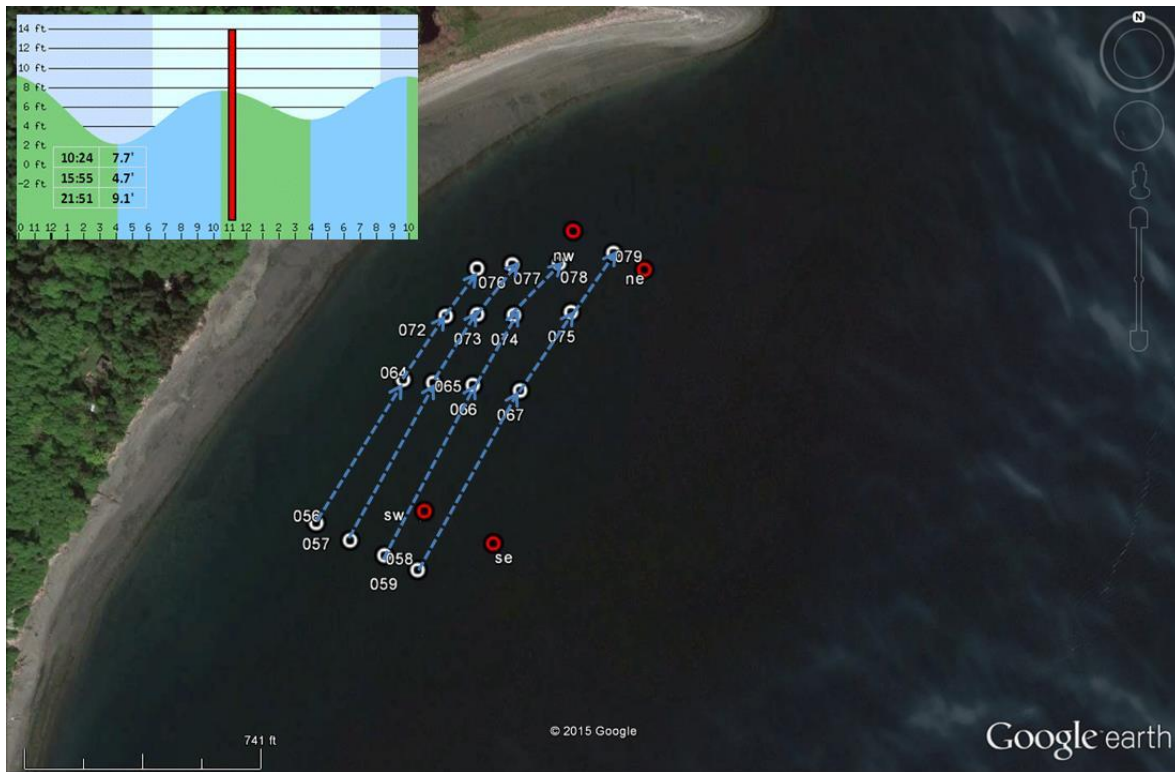
Appendix Figure 37. August 21, 2015 ebb tide



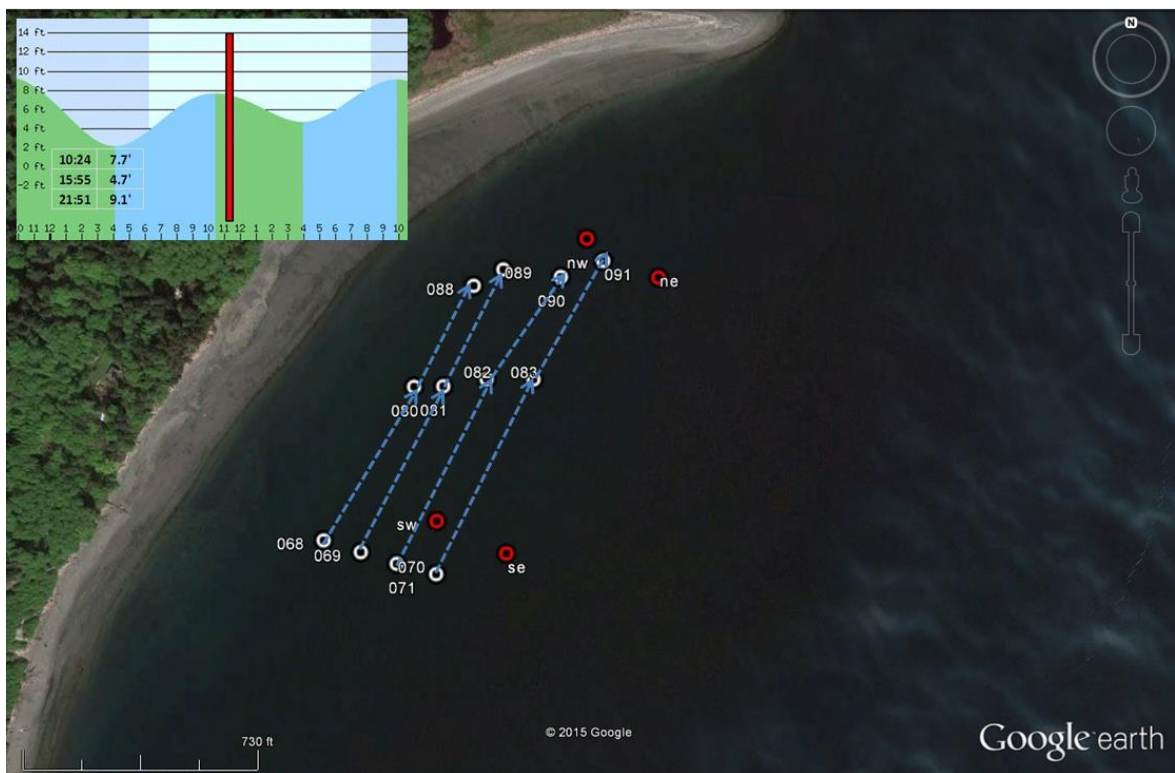
Appendix Figure 38. August 21, 2015 ebb tide



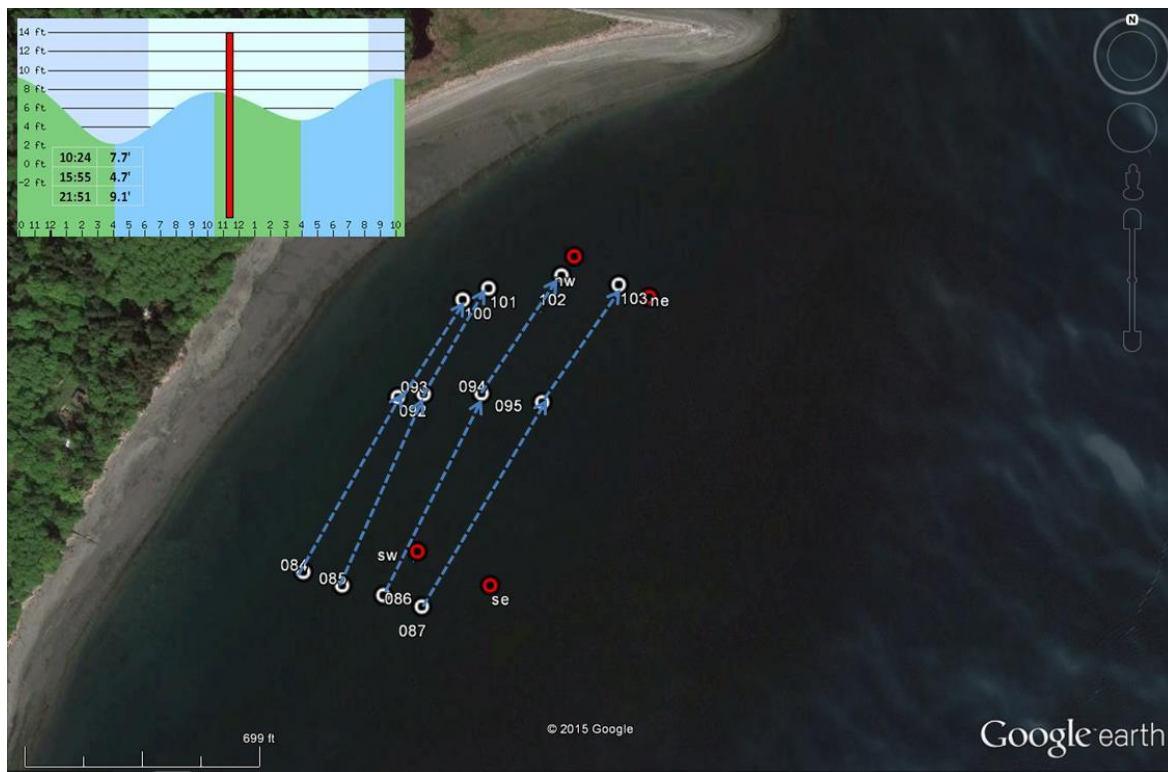
Appendix Figure 39. August 21, 2015 ebb tide



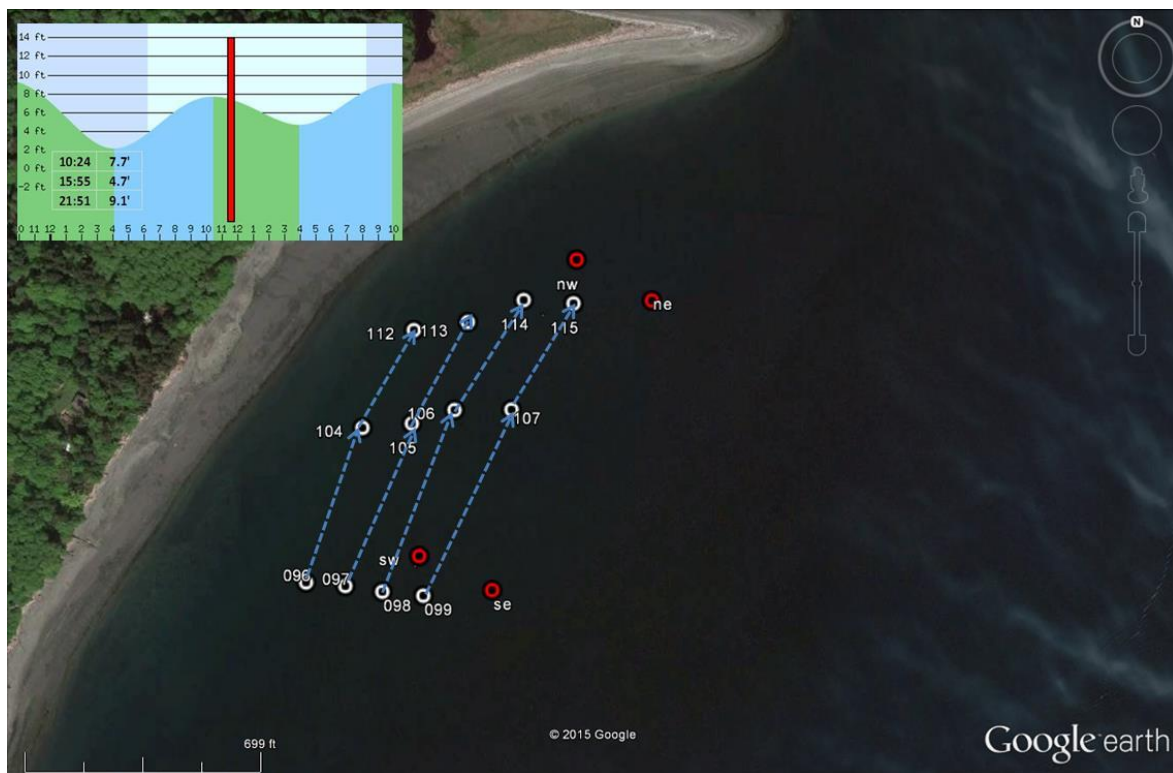
Appendix Figure 40. August 21, 2015 ebb tide



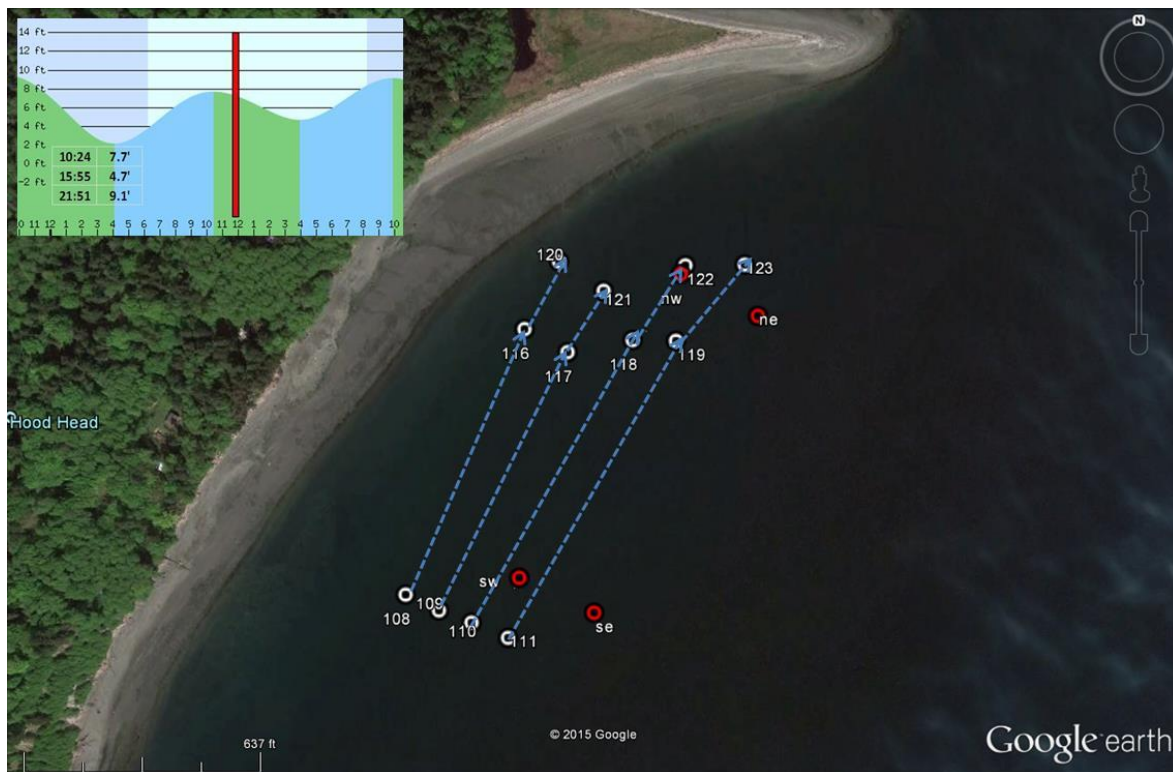
Appendix Figure 41. August 21, 2015 ebb tide



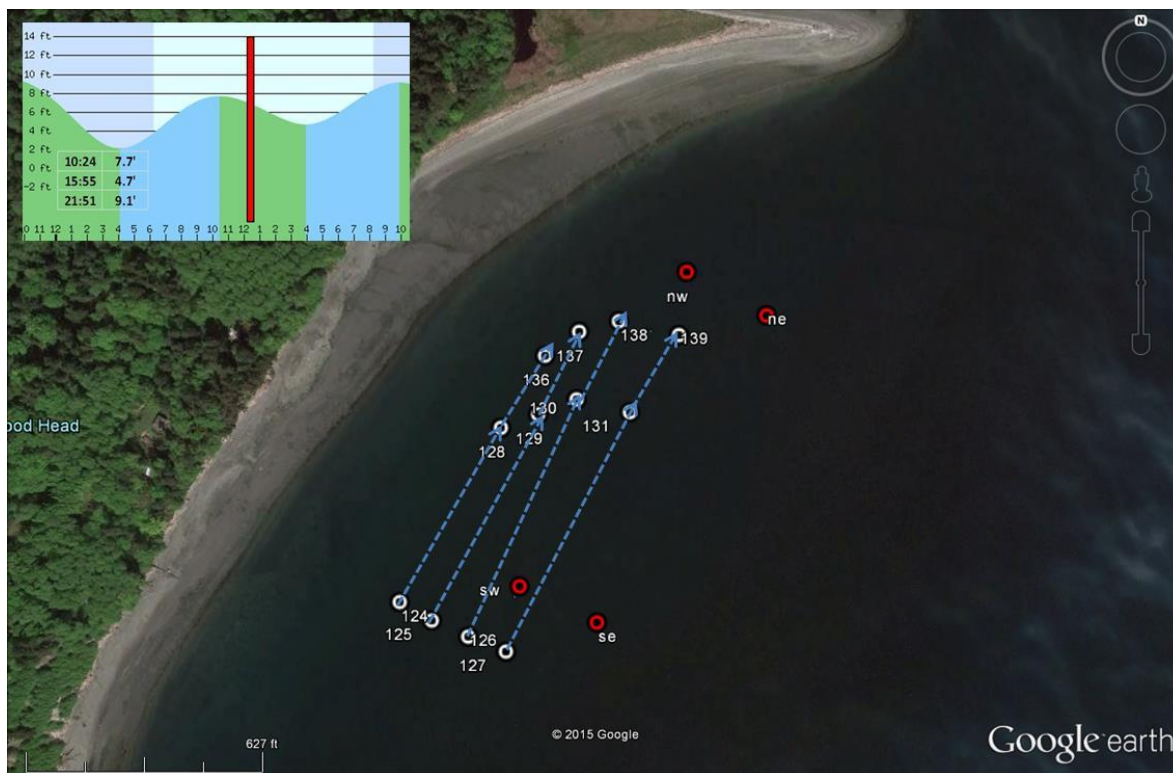
Appendix Figure 42. August 21, 2015 ebb tide



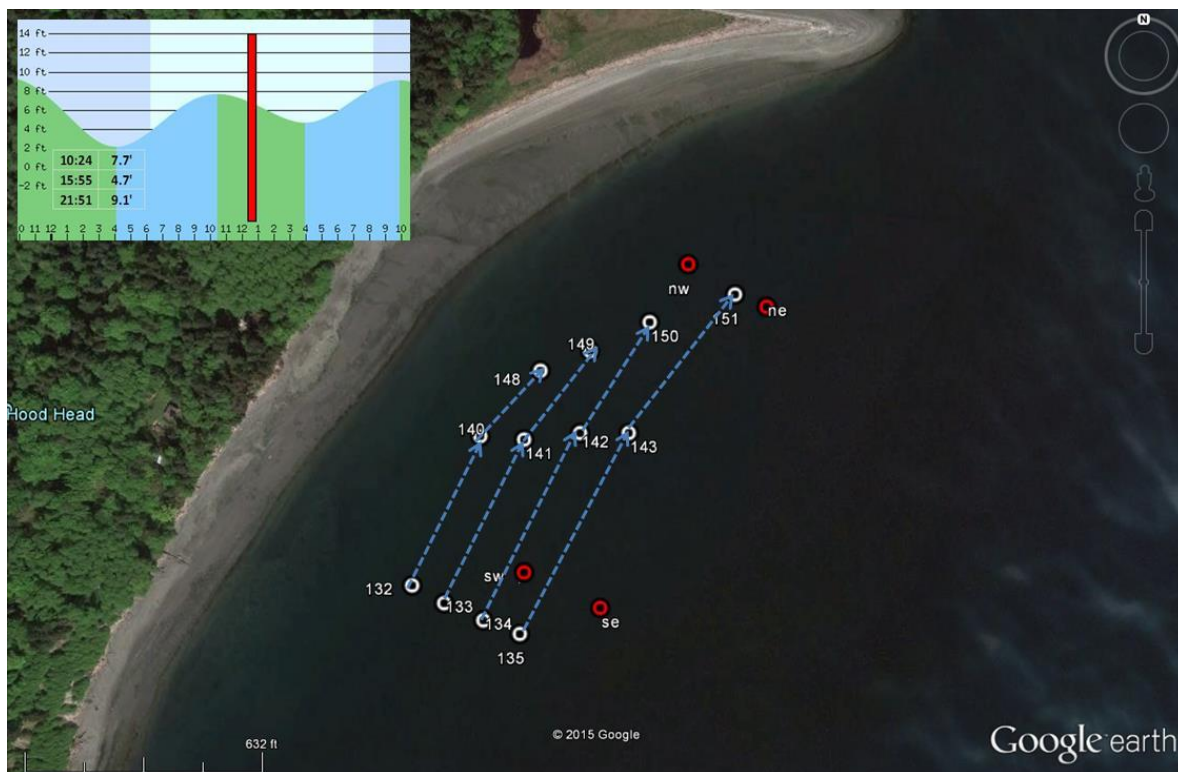
Appendix Figure 43. August 21, 2015 ebb tide



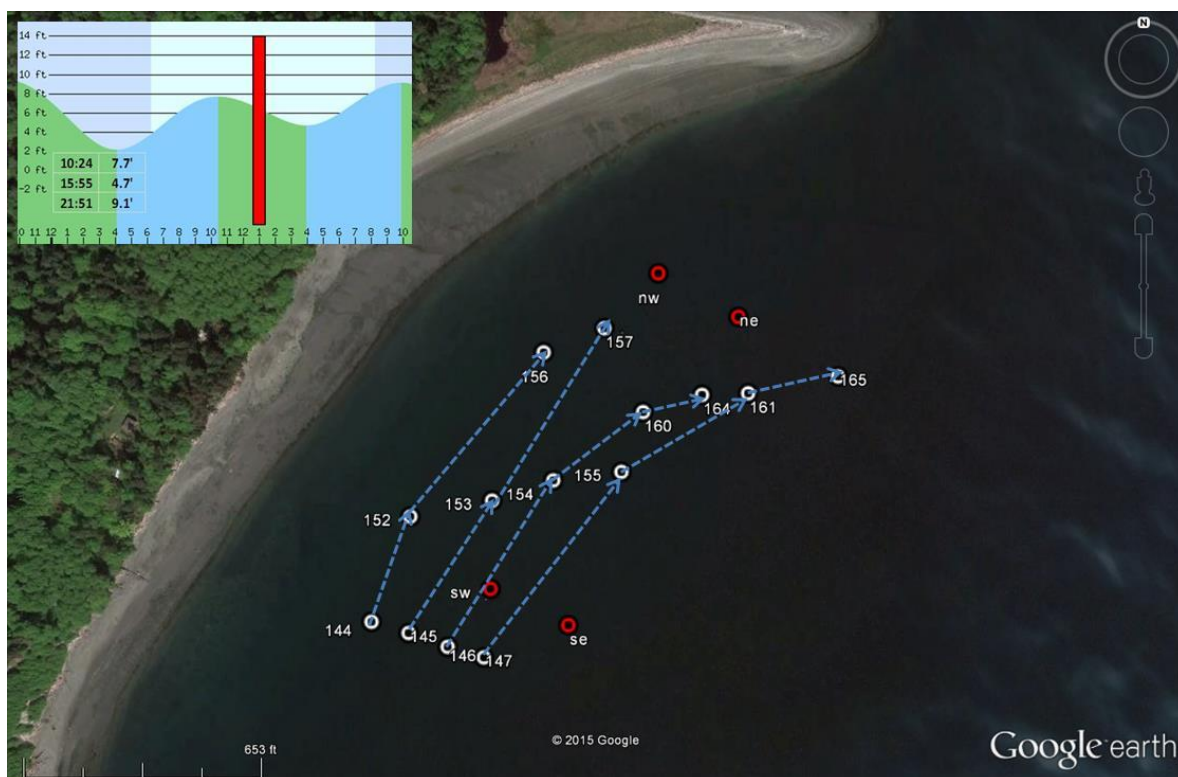
Appendix Figure 44. August 21, 2015 ebb tide



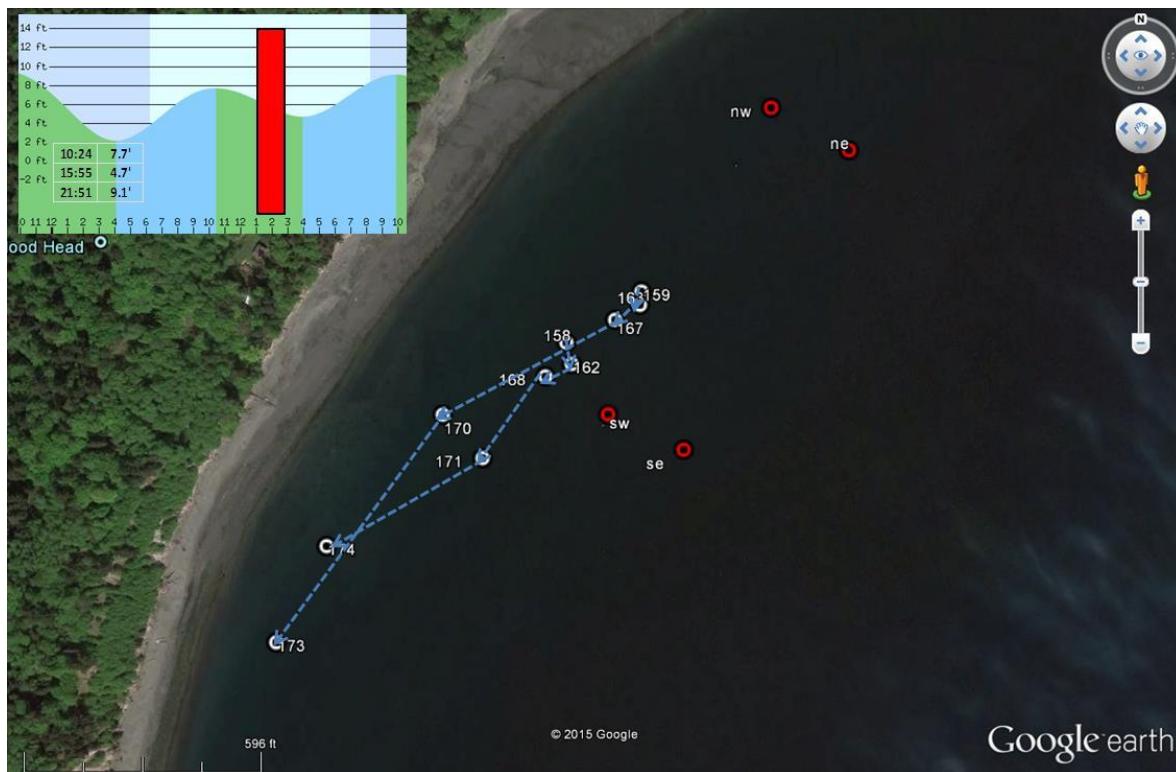
Appendix Figure 45. August 21, 2015 ebb tide



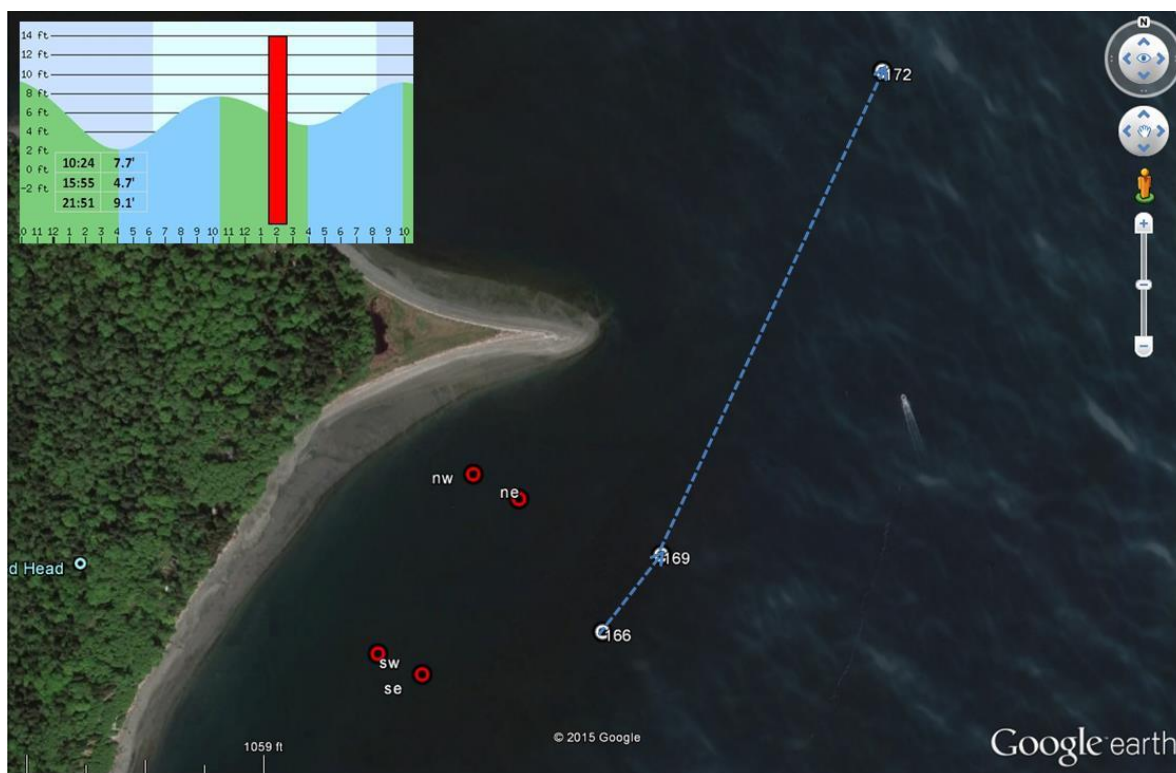
Appendix Figure 46. August 21, 2015 ebb tide



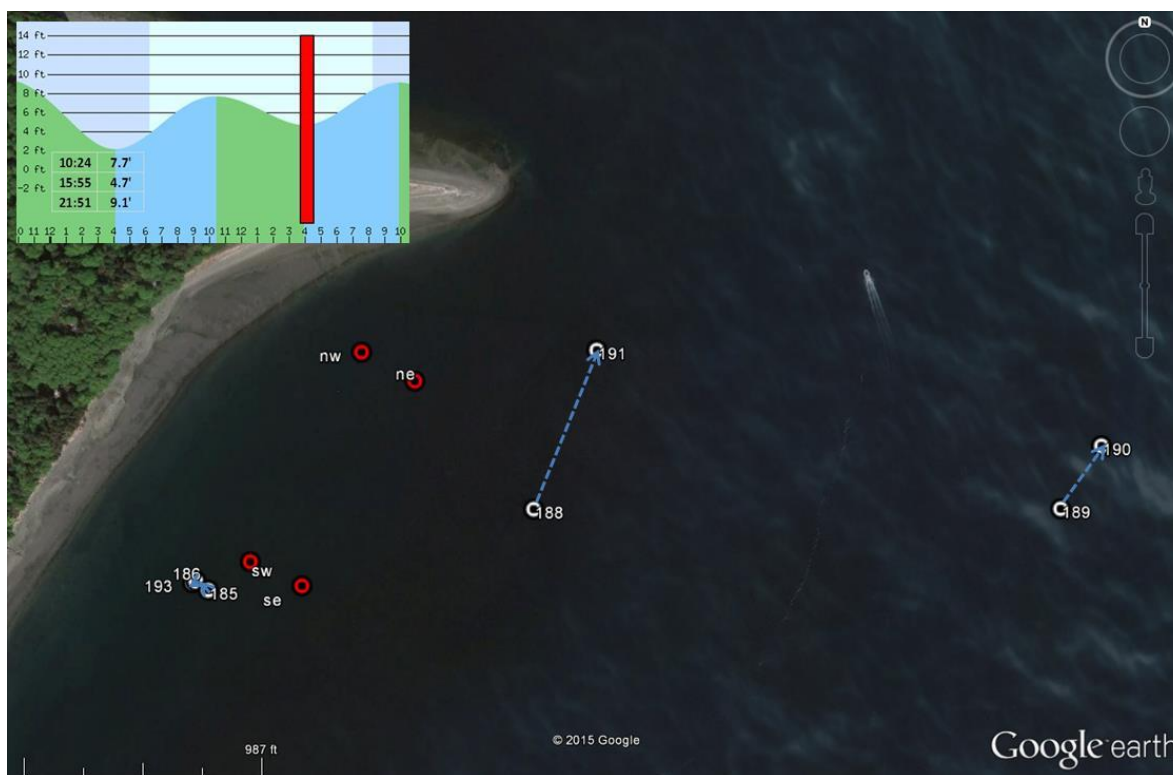
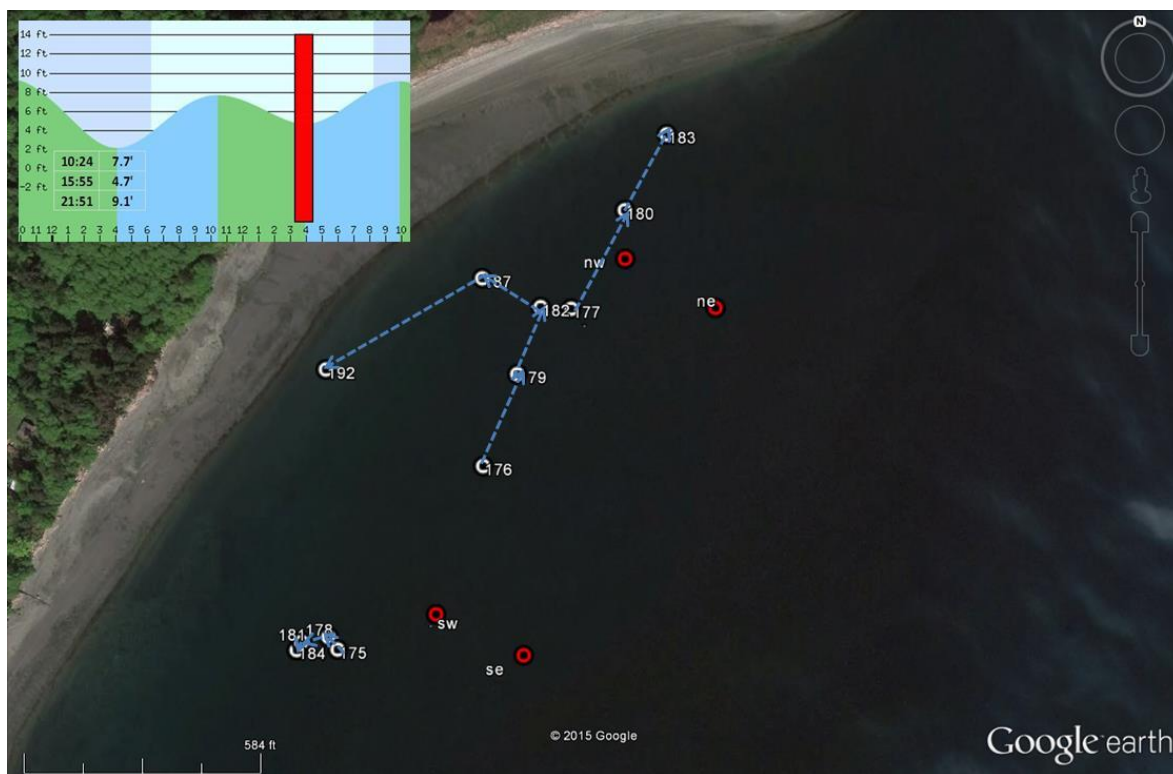
Appendix Figure 47. August 21, 2015 ebb tide

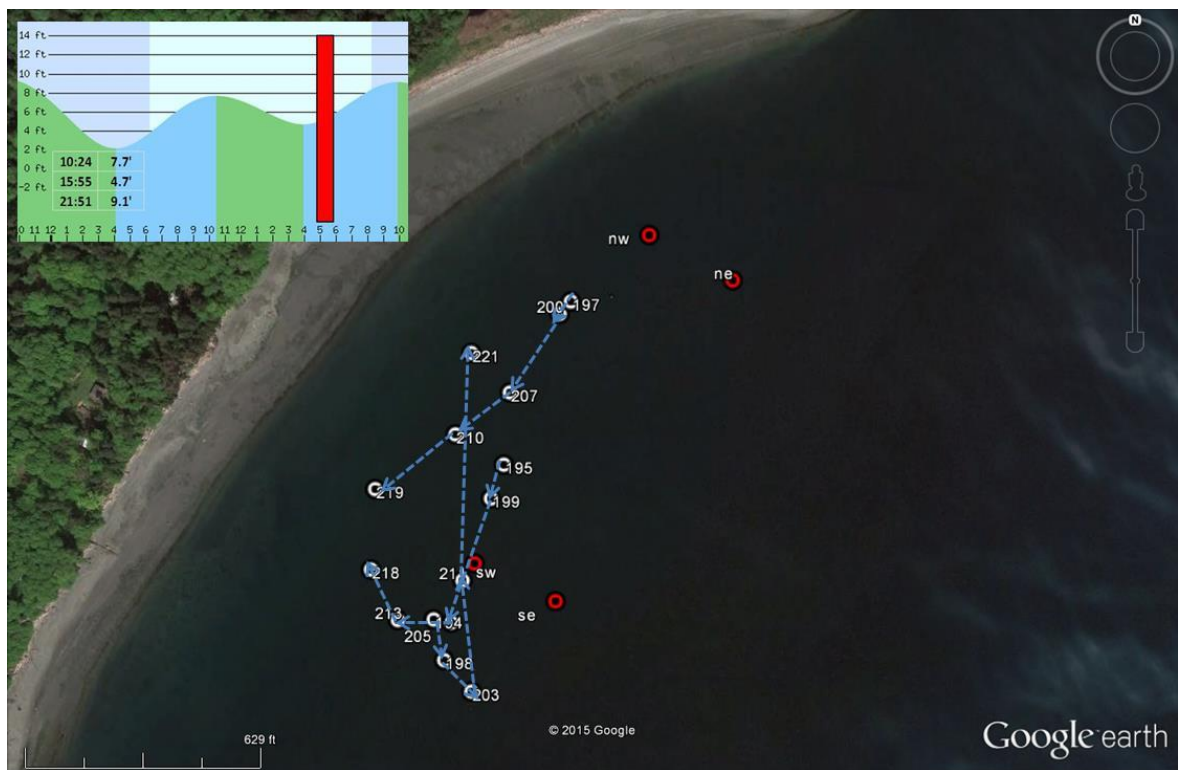


Appendix Figure 48. August 21, 2015 ebb tide

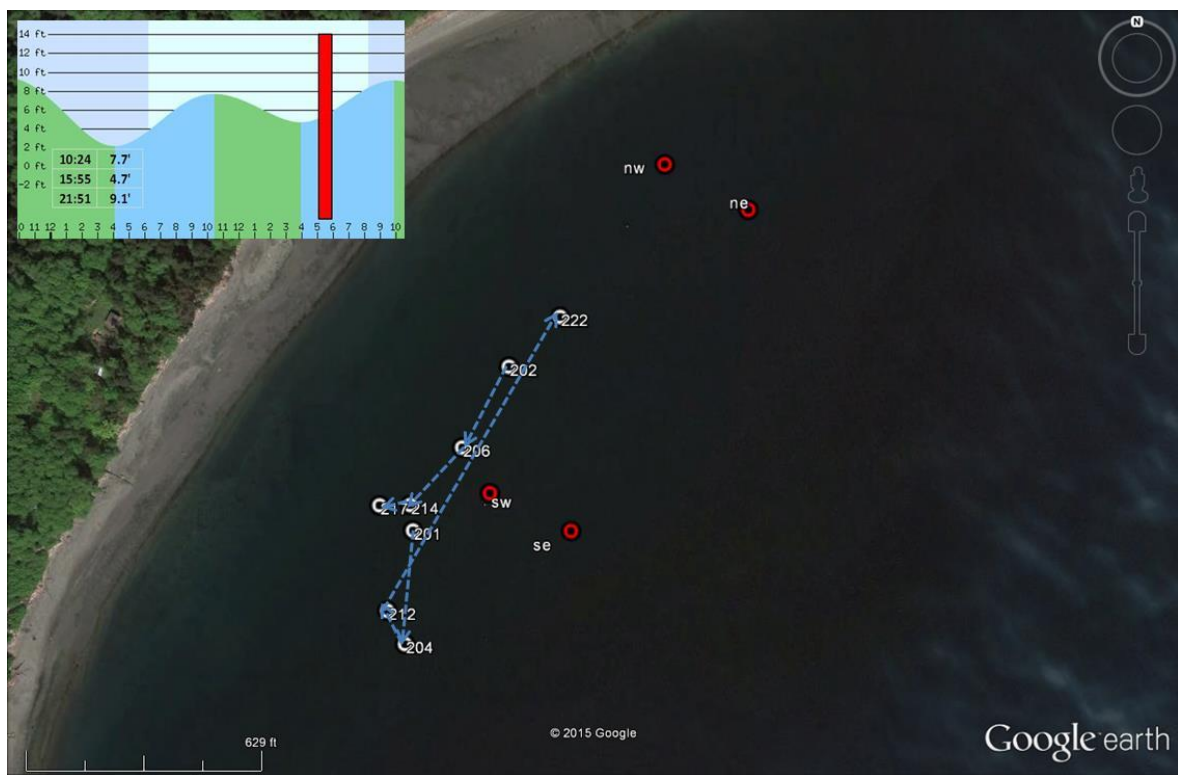


Appendix Figure 49. August 21, 2015 ebb tide

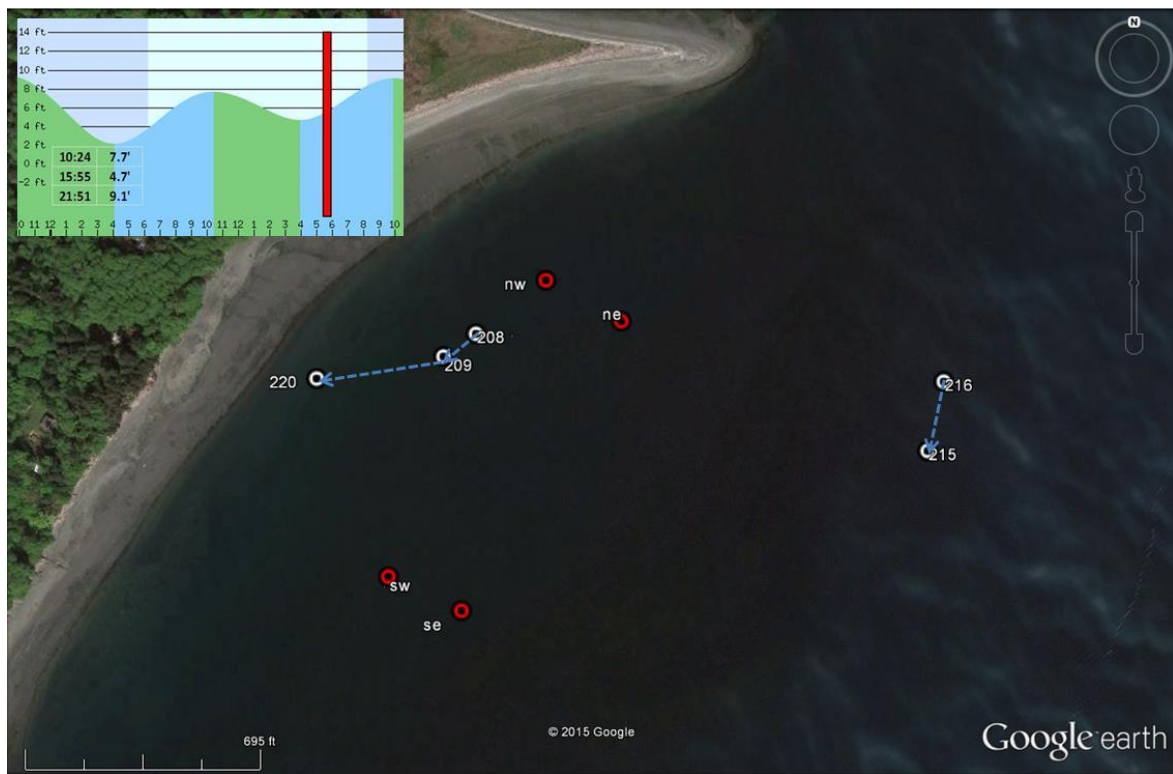




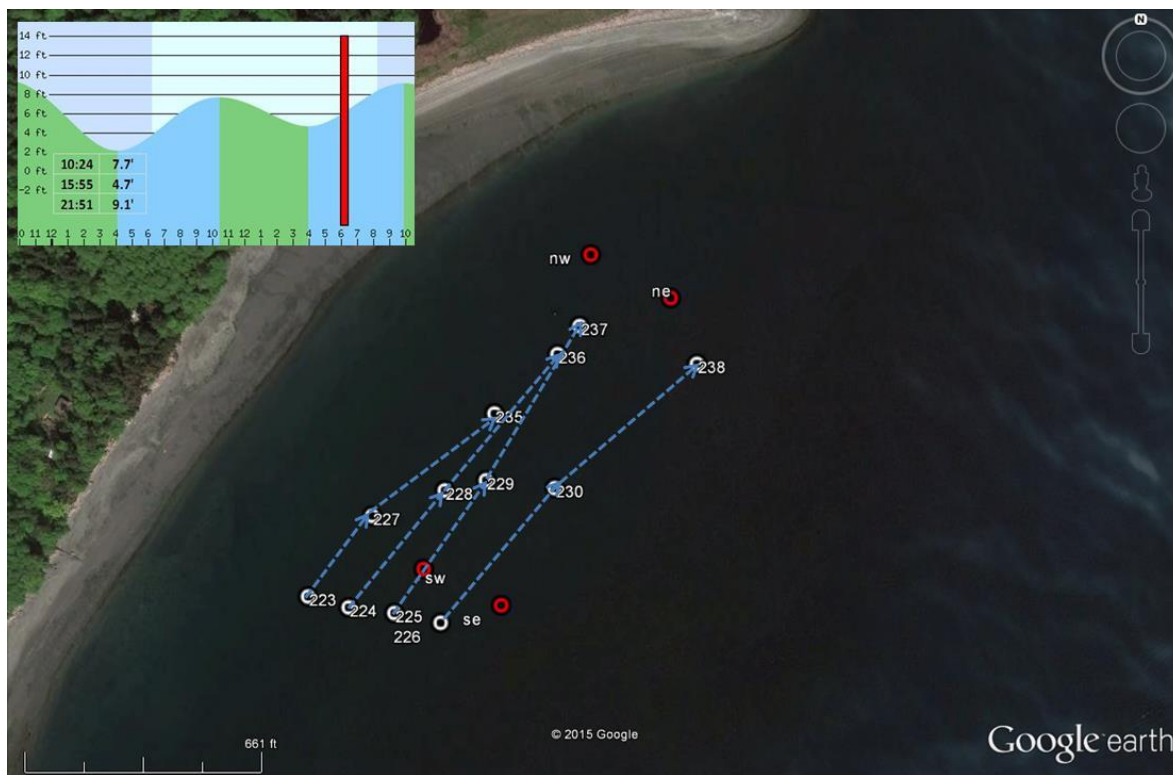
Appendix Figure 52. August 21, 2015 flood tide



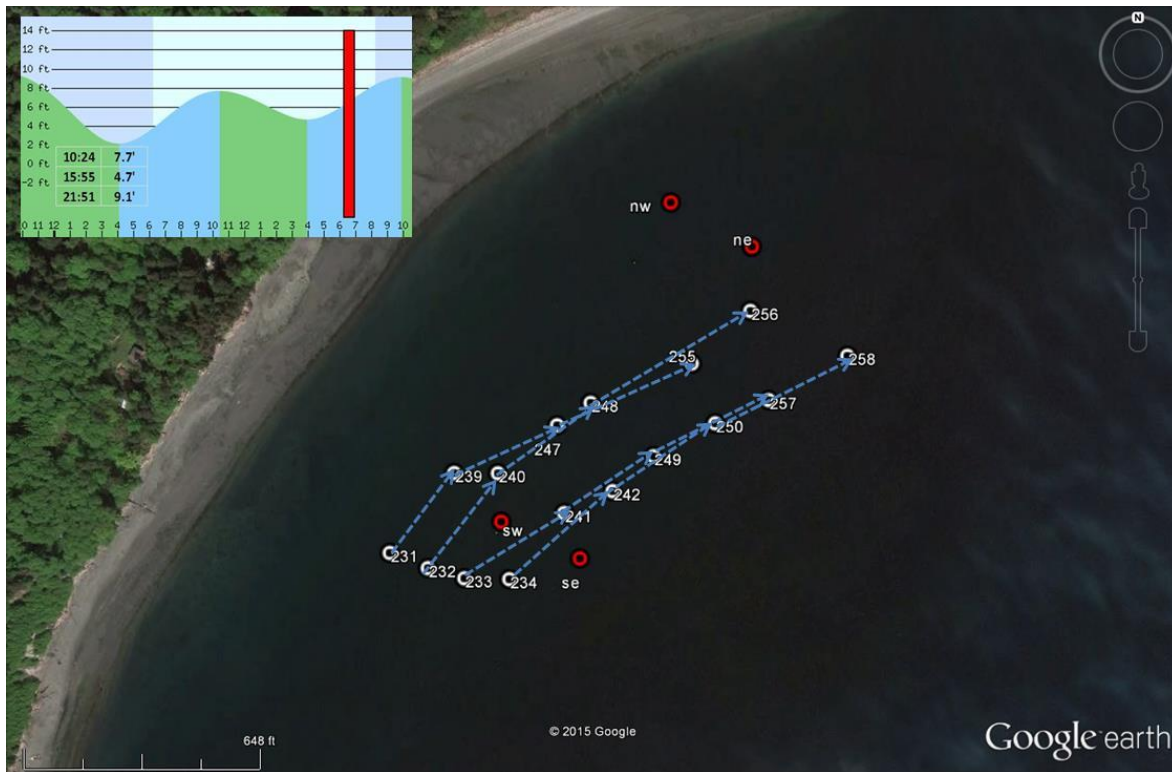
Appendix Figure 53. August 21, 2015 flood tide



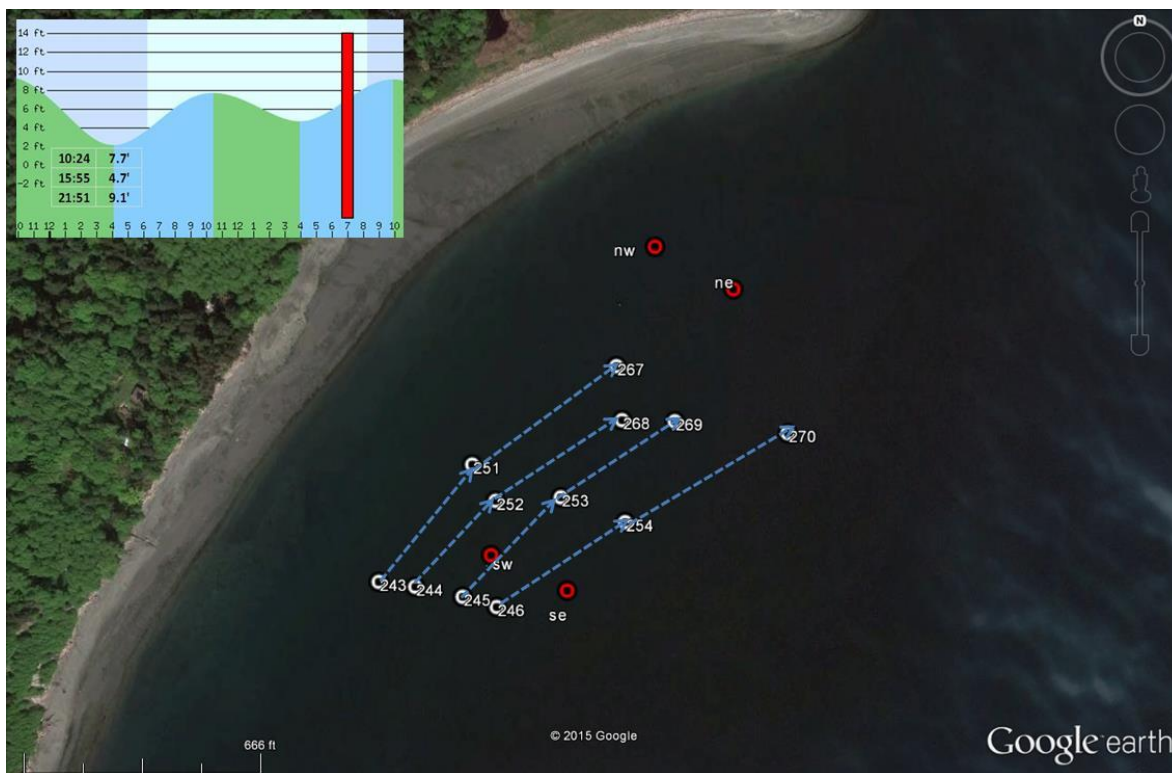
Appendix Figure 54. August 21, 2015 flood tide



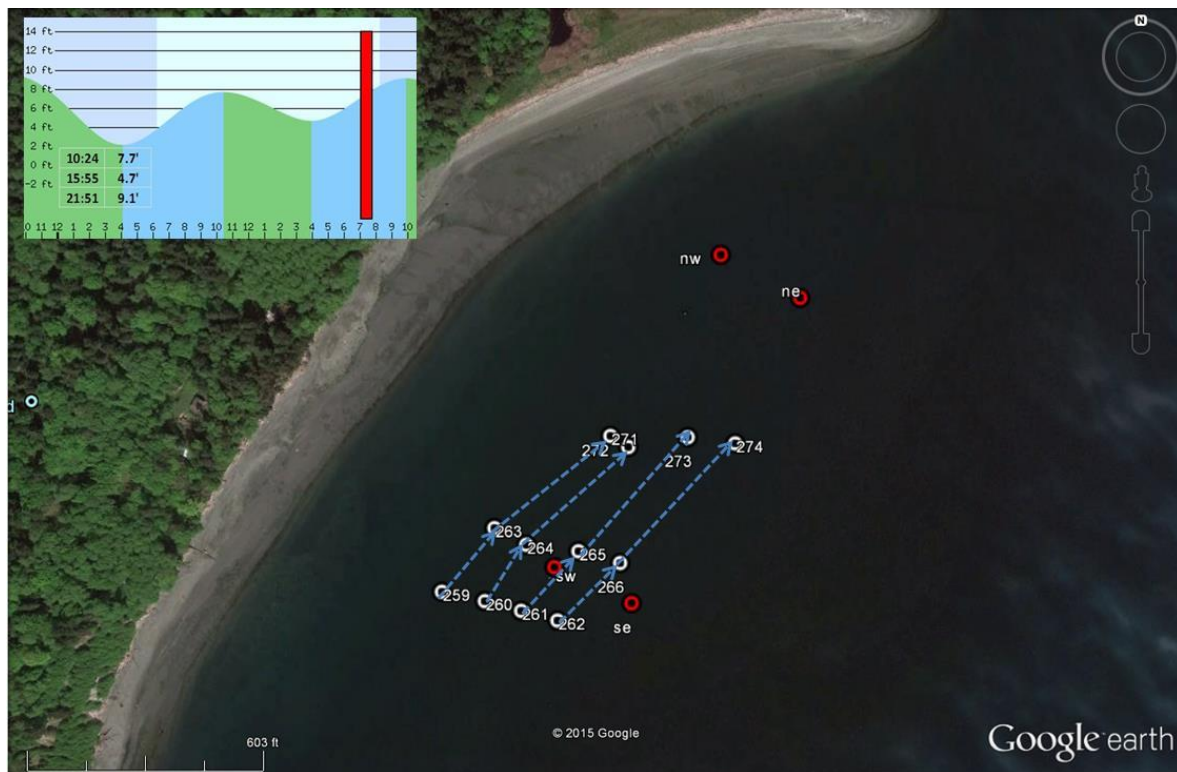
Appendix Figure 55. August 21, 2015 flood tide



Appendix Figure 56. August 21, 2015 flood tide



Appendix Figure 57. August 21, 2015 flood tide



Appendix Figure 58. End August 21 2015 survey.